JOURNAL OF THE MYANMAR ACADEMY OF ARTS AND SCIENCE

Chemistry, Industrial Chemistry

Journal of the Myanmar Academy of Arts and Science, 2026, **Vol. XXIII, No.1B**

Published in August, 2026, Chemistry, Industrial Chemistry

Myanmar Academy of Arts and Science

Edition

2026, August, 275 Copies

Published by

Dr Maung Kyaw (00322) Vice-President,

Myanmar Academy of Arts and Science

ISSN 2520-0186

LCCN 2003-323143

Printed by

U Tin Soe (00171), Manager

Universities Press, Yangon, Myanmar

FOREWORD

On 26 February 2026, the Myanmar Academy of Arts and Science (MAAS) was reconstituted to accelerate the implementation of four different strategies:

(a) encouraging universities and colleges to engage in more research activities
(b) organizing domestic and international research conferences
(c) publishing research journals and proceedings, and
(d) fostering research collaboration among local and international universities

Since the year 2001, the MAAS has been making every effort to fulfil these important functions in collaboration with universities and colleges across the country. As a result, the MAAS has published research papers in 23 volumes on diverse academic disciplines in the Journal of the Myanmar Academy of Arts and Science. It is a great honor to say that the 24th research conference was successfully held at the University of Yangon on 9–11 March 2024. The theme of this conference is *'Research and Innovation for Peace, Prosperity and Sustainability'*. A total of 369 research papers presented by both faculty and postgraduates at the conference have been published in Volume XXIII as follows:

Vol. XXIII, No. 1A	Chemistry
Vol. XXIII, No. 1B	Chemistry, Industrial Chemistry
Vol. XXIII, No. 2	Physics, Mathematics and Computer Studies
Vol. XXIII, No. 3	Zoology, Marine Science, Environment and Water Studies
Vol. XXIII, No. 4	Botany, Geology
Vol. XXIII, No. 5	English, History, Philosophy, Geography, Psychology, International Relations, Oriental Studies
Vol. XXIII, No. 6	Myanmar
Vol. XXIII, No. 7	Law, Library and Information Studies, Archaeology, Anthropology, Language and Linguistics
Vol. XXIII, No. 8	Applied Statistics, Management Studies, Statistics, Commerce, Economics, Journalism and Tourism
Vol. XXIII, No. 9A	Educational Theory and Management, Curriculum and Methodology
Vol. XXIII, No. 9B	Educational Psychology

I firmly believe that the empirical research findings from these papers will provide practical assistance for research candidates and those who are interested in research work. I am also hopeful that these findings will significantly contribute to the well-being of the community at large as well as the State's socio-economic development.

On behalf of the members of the MAAS, I would like to offer my special gratitude and thanks to those who have contributed their research papers to this journal. I also do appreciate the editing work done by senior professors and scholars of high standing as well as the members of the MAAS Editorial Board. Finally, my heartfelt thanks go to the members of the Publication Committee and the Department of Higher Education for their great dedication to the success of this journal.

Dr. Soe Win
President
Myanmar Academy of Arts and Science

Journal of the Myanmar Academy of Arts and Science

Vol. XXIII. No.1B

Contents

Section (i) Chemistry

Section (ii) Industrial Chemistry

INVESTIGATION OF SOME BIOLOGICAL ACTIVITIES OF *DIOSCOREA WALLICHII* HOOK. F. (KADAT) TUBER

Su Hnin Wai[1], Prema[2], Thandar Aung[3], Ni Ni Than[4]

Abstract

This study investigates the antimicrobial, antioxidant, cytotoxic, and anti-arthritic activities of *Dioscorea wallichii* Hook. L. (Kadat) tuber. The antimicrobial activity was screened using the agar well diffusion method on 95 % ethanol, watery, ethyl acetate, and pet-ether extracts. The results indicated that the watery extract exhibited the highest antimicrobial potency among the tested extracts. The *in vitro* antioxidant activity was assessed using the DPPH free radical scavenging assay, yielding IC_{50} values of 26.21 µg/mL for the watery extract and 13.62 µg/mL for the 95 % ethanol extract, indicating a stronger antioxidant effect from the ethanol extract. The anti-arthritic activity was evaluated by the egg albumin denaturation method, revealing that the 95% ethanol extract (IC_{50} = 6.77 µg/mL) exhibited more effective anti-arthritic activity than the watery extract (IC_{50} = 13.07 µg/mL). Cytotoxicity was assessed using a brine shrimp lethality bioassay, which demonstrated that both watery and 95 % ethanol extracts were free from toxicity at concentrations up to 1000 µg/mL, with LC_{50} values indicating no harmful effects.

Keywords: *Dioscorea wallichii* Hook. f. (Kadat) tuber, antimicrobial activity, antioxidant activity, anti-arthritic activity, cytotoxicity

Introduction

The genus *Dioscorea* L., within the family Dioscoreaceae, encompasses approximately 600 species distributed primarily across tropical and subtropical regions in Africa, Asia, and the Americas. Known for its ecological adaptability, Dioscorea includes herbaceous monocotyledonous plants, many of which are cultivated for their tubers, a major carbohydrate source in traditional diets. These tubers, rich in starch, play an essential role in providing daily caloric intake for communities in Africa and Asia and hold considerable economic significance (Ayensu & Coursey, 1972; Paul *et al*., 2017). Dioscorea plants, including commonly known yams, also contribute to the pharmaceutical and cosmetics industries, notably as a source of diosgenin, a steroidal sapogenin used in the synthesis of steroid drugs. Distinctive for their twining, climbing stems, which may coil in either direction, Dioscorea species exhibit alternate or occasionally opposite leaves, often cordate with prominent venation. Species such as *D. wallichi*i, distributed throughout regions like Bangladesh, China, and Southeast Asia, are prized not only as food but also for their therapeutic properties. Indigenous communities have long valued Dioscorea for traditional medicine, with uses ranging from pain relief and treatment of dysentery to skin ailments and rheumatism, though comprehensive documentation of these practices remains limited (Kumar *et al*., 2017). Bioactive compounds found in Dioscorea spp., such as alkaloids, flavonoids, saponins, and phenols, contribute to a wide range of health benefits, including antioxidant, anti-inflammatory, antimicrobial, and antiviral effects (Salehi *et al*., 2019). Specifically, steroidal saponins in Dioscorea have shown potential in cancer prevention and immune support (Patel *et al*., 2012).

[1] Department of Chemistry, University of Bago
[2] Department of Chemistry, University of Yangon
[3] Department of Chemistry, University of Yangon
[4] Department of Chemistry, University of Yangon

The therapeutic potential of *D. wallichii*, particularly due to compounds like diosgenin, has drawn interest in reproductive health applications and hormone therapy (Che *et al*., 2014). Dioscorea is important in nutrition and medicine, making it a valuable subject of ethnobotanical and pharmacological research as both a cultural staple and a promising health resource.

Materials and Methods

Plant Materials

Kadat tubers were collected from July to August 2024 in Taikkyi Township, Yangon Region, Myanmar. (Figure 1) The collected sample was identified as *Dioscorea wallichii* Hook. L. (Kadat) tuber at the Botany Department, University of Yangon. The sample was cleaned thoroughly with water. Then the fresh tuber was cut into small pieces and air-dried at room temperature. The dried samples were ground into powder by a grinding machine, sieved and stored in an airtight container for further use.

Figure 1. Photographs of plant and tuber of *D. wallichii*

Preparation of Crude Extracts for Biological Activities

Approximately 20 g of dried powdered sample was extracted three times with 95% ethanol for 6 h, then filtered, and the volume was reduced using a rotary evaporator to obtain the ethanol extract. For the water extract, 20 g of dried powdered sample was boiled in 100 mL of distilled water, then filtered, and the solvent was concentrated by evaporation in a water bath. This produced the water extract. Other crude extracts were prepared following the same procedure as for the 95% ethanol extract. All crude extracts were dried and stored in a refrigerator for future use.

Determination of Antimicrobial Activity by Agar Well Diffusion Method

For antimicrobial activity screening by the agar well diffusion method, 0.5 g of peptone and 0.25 g of sodium chloride were dissolved in distilled water, and the solution was made up to 100 mL with additional distilled water. The pH of this solution was adjusted to 7.2 using 0.1 M sodium hydroxide, and 1.5 g of agar was added. The nutrient agar was then boiled, and 20–25 mL of the medium was poured into a test tube, plugged with cotton wool, and autoclaved at 121 °C for 15 min. The tubes were subsequently cooled to 60 °C, and the medium was poured into sterilized Petri dishes, followed by the addition of 0.1 mL of spore suspension. The agar was

allowed to set for 30 min, after which a 10 mm agar well was made using a sterilized cork borer. Next, approximately 0.1 mL of the sample was introduced into the agar well, and the plates were incubated at 37 °C for 24 h. The antimicrobial activity of ethanol, water, ethyl acetate, and petroleum ether extracts of Kadat tuber was screened using the agar well diffusion method. The appearance of an inhibition zone around the agar well indicated the presence of antimicrobial activity.

Determination of Antioxidant Activity by DPPH Free Radical Scavenging Assay

The DPPH free radical scavenging activity of 95% ethanol and water extracts of Kadat tuber was determined using a UV-visible spectrophotometric method. The control solution was prepared by mixing 1.5 mL of 20 µM DPPH solution with 1.5 mL of 95% ethanol in brown bottles, using a shaker. The blank solution was prepared by mixing 1.5 mL of the test sample solution with 1.5 mL of 95% ethanol. The sample solutions were prepared by thoroughly mixing 1.5 mL of 20 µM DPPH solution with 1.5 mL of various concentrations of test sample solution (3.91, 7.81, 15.63, 31.25, 62.50, and 125.00 µg/mL). These solutions were incubated at room temperature and shaken for 30 min. The absorbance of each solution was then measured at 517 nm using a UV-visible spectrophotometer (Irulandi *et al*., 2016). The absorbance measurements were performed in triplicate for each concentration.

Determination of Cytotoxicity by Brine Shrimp Lethality Bioassay

The brine shrimp (*Artemia salina*) were used in this study for a cytotoxicity bioassay. Artificial seawater [3.8% (w/v) NaCl] was prepared by dissolving 38 g of sodium chloride in 1 L of distilled water. Brine shrimp cysts (0.25 g) were put into 500 mL of artificial seawater in a separating funnel. This funnel was placed near a lamp. Light is essential for the cysts to hatch. Brine shrimp cysts are required to hatch with constant supplied oxygen and 24 h incubation at room temperature. 9 mL of artificial seawater and 1 mL of different concentrations of samples (1000, 100, 10, 1 µg/mL) and standard solutions were added to each chamber. Alive brine shrimp (10 nauplii) were then taken with a Pasteur pipette and placed into each chamber. They were incubated at room temperature for about 24 h. After 24 h, the number of dead and surviving brine shrimp was counted, and cytotoxicity was estimated using the 50 % lethal concentration (LC_{50}) (Singh *et al*., 2015). The control solution was prepared following the same procedure, using distilled water instead of the sample solution.

Determination of Anti-arthritic Activity by Egg Albumin Method

The reaction mixture (5 mL) consisted of 0.2 mL of egg albumin (from a fresh hen's egg), 2.8 mL of phosphate-buffered saline (PBS, pH 6.4), and 2 mL of varying concentrations of crude Kadat tuber extracts (95 % ethanol and watery extracts) to achieve final concentrations of 100, 200, 400, 800, and 1000 µg/mL. A similar volume of double-distilled water was used as the control. The mixtures were then incubated at 37°C for 15 min, followed by heating at 70 °C for 5 min. After cooling, the absorbance was measured at 660 nm. Diclofenac sodium was used as the standard drug (Sunmathi *et al*., 2016).

Results and Discussion

Antimicrobial Activity of Extracts of Kadat Tuber by Agar Well Diffusion Method

The antimicrobial activity of four crude extracts: petroleum ether, ethyl acetate, 95% ethanol, and water, derived from *Dioscorea wallichii* Hook. f. (Kadat) tuber was assessed by using the agar well diffusion method against a panel of eight microorganisms: *Agrobacterium tumefaciens*, *Bacillus pumilus*, *Bacillus subtilis*, *Candida albicans*, *Escherichia coli*, *Micrococcus luteus*, *Pseudomonas aeruginosa*, and *Staphylococcus aureus*. This method, which measures the diameter of inhibition zones around each well, is an established technique for evaluating antimicrobial potency; a larger zone of inhibition indicates stronger antimicrobial activity. The study results, summarized in Table 1 and illustrated in Figure 2, revealed that among the extracts tested, the water extract demonstrated the highest antimicrobial efficacy across the tested microorganisms. The superior activity of the water extract could be attributed to its ability to concentrate polar bioactive compounds, which are more soluble in aqueous media and may include antimicrobial phytochemicals such as saponins, tannins, or glycosides commonly found in *Dioscorea* species. The extracts of ethanol, ethyl acetate, and petroleum ether showed moderate to low antimicrobial activity, varying due to their solubility of active constituents in solvents of varying polarities.

Table 1. Inhibition Zone Diameter of Crude Extracts from *D. wallichii* Tuber by Agar Well Diffusion Method

Microorganisms	Diameter of inhibition zone (mm)				
	PE	**EtOAc**	**EtOH**	**H_2O**	***STD**
A. tumefaciens	15	16	19	21	27
B. pumilus	16	16	19	21	27
B. subtilis	15	16	19	22	27
C. albicans	15	16	19	21	27
E. coli	16	16	19	22	27
M. luteus	15	16	19	22	28
P. fluorescens	16	16	20	22	28
S. aureus	15	16	19	21	28

For Bacterial *STD = Chloramphenicol
For Fungus *STD = Nystatin

Agar well diameter – 10 mm
10 mm – 14 mm = weak activity
15 mm – 19 mm = moderate activity
20 mm and above = potent activity

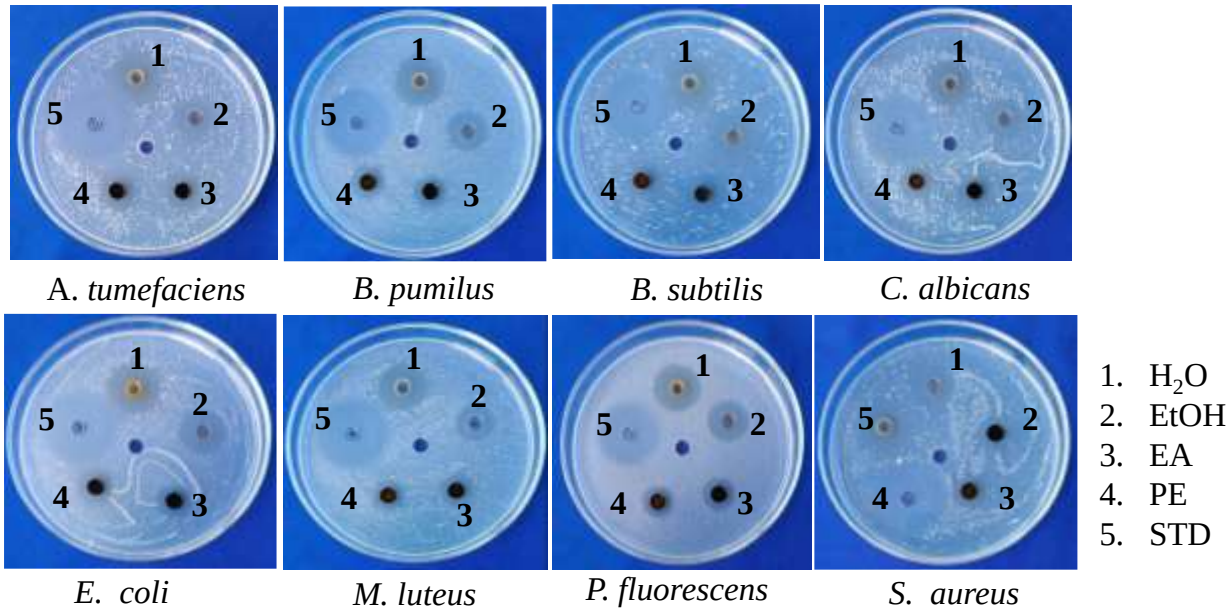

Figure 2. Antimicrobial activity of various crude extracts from the tuber of *D. wallichii* (Kadat) on eight microorganisms

Antioxidant Activity of Extracts of Kadat Tuber by DPPH Free Radical Scavenging Assay

The antioxidant activity of ethanol and watery extracts from the Kadat tuber was evaluated using the DPPH free radical scavenging assay, with ascorbic acid serving as the standard reference. The extracts were tested with six different concentrations: 3.91, 7.81, 15.63, 31.25, 62.5, and 125 µg/mL. The absorbance was measured at 517 nm using a UV-visible spectrophotometer. The results indicated that the IC_{50} values for the ethanol extract, aqueous extract, and ascorbic acid were 13.62 µg/mL, 26.21 µg/mL, and 4.68 µg/mL, respectively. This suggests that the ethanol extract exhibited a more potent antioxidant activity compared to the watery extract. However, both crude extracts demonstrated lower antioxidant activity than the standard ascorbic acid. Overall, the findings indicate that the Kadat tuber possesses significant free radical scavenging activity, suggesting its potential as an alternative source for cancer treatment. Detailed results can be found in Table 2 and illustrated in Figures 3 and 4.

Table 2. Average % Inhibition and IC_{50} Values of Crude Extracts of Kadat Tuber

Extract	% RSA ± SD at different concentrations (µg/mL)						IC_{50} (µg/mL)
	3.91	7.81	15.62	31.25	62.5	125	
ethanol	35.5 ± 0.44	42.12 ± 0.48	52.72 ± 0.42	65.69 ± 0.00	71.97 ± 0.75	78.24 ± 0.55	13.62
watery	23.78 ± 0.44	29.92 ± 0.96	44.00 ± 0.74	52.86 ± 0.53	59.07 ± 1.03	66.53 ± 1.16	26.21
std. Ascorbic acid	48.99 ± 0.53	54.09 ± 1.36	56.64 ± 0.44	63.83 ± 1.06	66.61 ± 0.35	87.13 ± 0.76	4.68

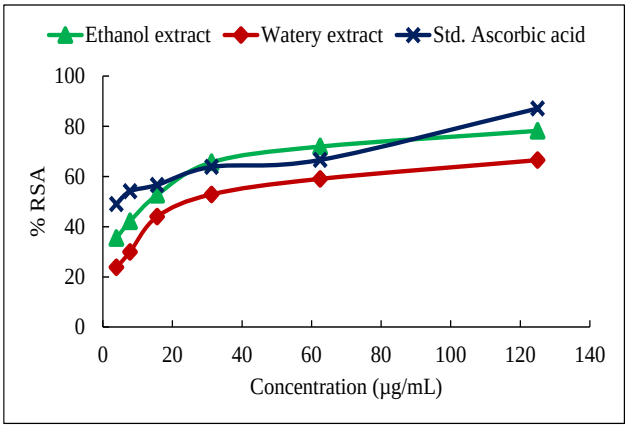

Figure 3. A plot of % RSA of different concentrations of crude extracts of Kadat tuber

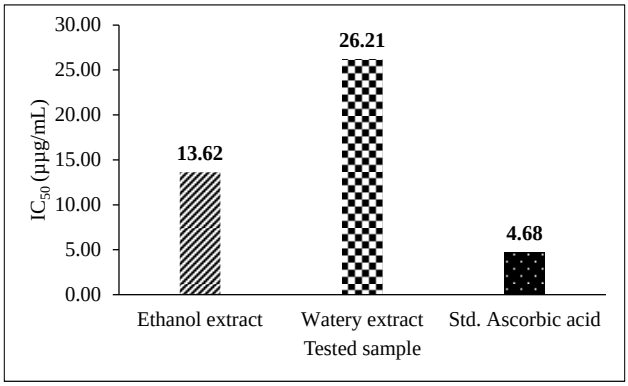

Figure 4. A bar graph of IC_{50} values of crude extract of Kadat tuber and standard ascorbic acid

Anti-arthritic Activity of Crude Extracts of Kadat Tuber

Arthritis, a chronic inflammatory disorder, often results from the denaturation of proteins, which triggers immune responses and leads to symptoms such as joint pain, swelling, and stiffness. The anti-arthritic potential of natural products, particularly plant extracts, is commonly evaluated by measuring their ability to inhibit protein denaturation, which serves as an indicator of their anti-inflammatory and immunomodulatory effects. In this study, the anti-arthritic activity of ethanol and water extracts of Kadat tuber was assessed *in vitro* using the protein denaturation inhibition method with egg albumin as a model protein.

The inhibitory concentration (IC_{50}) values of the ethanol and water extracts against protein denaturation were 6.77 µg/mL and 13.07 µg/mL, respectively (Table 3). These values represent the concentrations required to inhibit 50% of protein denaturation and serve as a quantitative measure of the effectiveness of extract. A lower IC_{50} value indicates a higher potency in inhibiting protein denaturation. Consequently, the ethanol extract of Kadat tuber, with its lower IC_{50}, demonstrates ~~superior~~ anti-arthritic activity compared to the standard and the water extract (Figures 5 and 6). This enhanced efficacy of the ethanol extract could be attributed to its potential to dissolve and concentrate more bioactive compounds that may be responsible for reducing protein denaturation.

Table 3. Average % Protein Denaturation and IC_{50} Values of Crude Extracts of Kadat Tuber

Extract	% Protein denaturation at different concentrations (µg/mL)						IC_{50} (µg/mL)
	3.91	7.81	15.62	31.25	62.5	125	
Ethanol	34.34 ± 9.50	55.68 ± 0.59	76.54 ± 0.39	80.66 ± 0.10	86.38 ± 0.10	89.64 ± 0.18	6.77
Watery	30.52 ± 2.86	41.97 ± 0.93	53.9 ± 2.37	65.73 ± 1.64	74.92 ± 0.12	84.84 ± 0.14	13.07
std. diclofenac	8.41 ± 1.93	45.69 ± 0.85	53.23 ± 0.00	60.26 ± 0.66	70.28 ± 1.14	79.39 ± 0.75	12.28

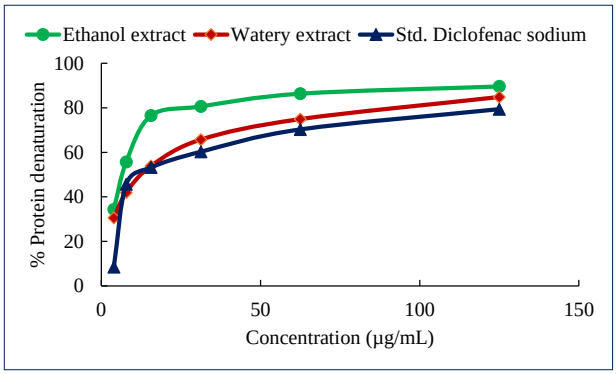

Figure 5. A plot of % protein denaturation versus concentrations of crude extracts of Kadat tuber and standard diclofenac sodium

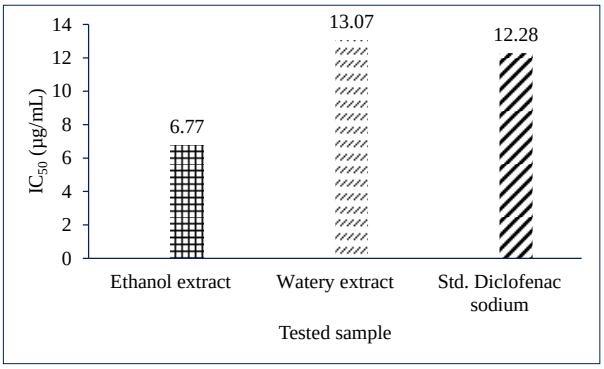

Figure 6. A bar graph of IC_{50} values of crude extracts of Kadat tuber and standard diclofenac sodium

Cytotoxicity of Crude Extracts of Kadat Tuber

The cytotoxicity of the water and ethanol extracts of *D. wallichii* Hook. f. (Kadat) tuber was evaluated using the brine shrimp lethality bioassay, a well-established preliminary screening method to assess potential toxicity. In this assay, brine shrimp (*Artemia salina*) larvae are exposed to varying concentrations of crude extracts to determine their lethal concentration (LC_{50}). LC_{50} values below 1000 µg/mL are considered toxic (active), while values above 1000 µg/mL indicate non-toxic (inactive) extracts. According to the results summarized in Table 4, the LC_{50} values of both the water and ethanol extracts were greater than 1000 µg/mL, suggesting that neither extract exhibited cytotoxic effects under the conditions tested. These findings indicate that both extracts of Kadat tuber are likely safe and non-toxic at the concentrations used in the assay. The absence of cytotoxicity in the brine shrimp lethality bioassay suggests that the water and ethanol extracts of Kadat tuber may be safe for further development and use, particularly in applications involving food or medicinal formulations. However, while the brine shrimp assay provides an initial indication of cytotoxicity, further *in vitro* and *in vivo* cytotoxicity studies on human cell lines would be necessary to comprehensively evaluate the safety profile of these extracts for potential therapeutic or dietary use.

Table 4. Cytotoxicity of Different Concentrations of Crude Extracts of Kadat Tuber Against *Artemia salina* (Brine Shrimp)

Extract	Dead % by using different concentrations (µg/mL) of samples (Mean ± SEM)				LC_{50} (µg/mL)
	1	10	100	1000	
Ethanol	30 ± 0.00	40 ± 0.00	40 ± 0.00	47 ± 0.00	> 1000
Watery	33 ± 0.00	37 ± 1.53	40 ± 0.71	40 ± 0.00	> 1000
$K_2Cr_2O_7$	7 ± 1.00	20 ± 3.01	100 ± 0.00	100 ± 0.00	43.75
Caffeine	0 ± 0.00	23 ± 1.20	30 ± 0.58	40 ± 1.16	> 1000

Conclusion

The present research investigates various biological activities of the Kadat tuber, focusing on its antimicrobial, antioxidant, anti-arthritic, and cytotoxicity effects. The watery extract exhibited potent antimicrobial activity, with inhibition zone diameters exceeding 20 mm while the ethanol, ethyl acetate, and pet-ether extracts showed moderate activity, with inhibition zones ranging from 15 to 19 mm. The antioxidant activity in terms of IC_{50} values is 13.62 µg/mL for ethanol, 26.21 µg/mL for watery extract and 4.68 µg/mL for ascorbic acid. The ethanol extract exhibited higher antioxidant activity than the watery extract indicating its free radical scavenging properties. In the anti-arthritic activity, the ethanol extract (IC_{50} = 6.77 µg/mL) was more effective than the aqueous extract (IC_{50} = 13.07 µg/mL). Regarding cytotoxicity, both ethanol and watery extracts of the Kadat tuber showed no cytotoxic effects on brine shrimp at concentrations up to 1000 µg/mL. The findings of this research highlight the significant biological activities of the Kadat tuber, particularly its potent antimicrobial and anti-arthritic properties. The ethanol extract emerged as the most effective in both antioxidant and anti-arthritic activities, while the aqueous extract showed promising antimicrobial effects. In experiments, neither extract was harmful to cells at the concentrations tested, which suggests they might be safe for further applications. Overall, the Kadat tuber represents a valuable natural resource with potential therapeutic investigation to explore its full range of bioactive compounds.

Acknowledgements

The authors would like to express their profound gratitude to Professor Dr Thandar Aung, Professor and Head, Dr Ni Ni Than, Department of Chemistry, University of Yangon, for supervising this research.

References

Ayensu, E. S., and D. G. Coursey, (1972). *Yam: Dioscorea spp. (Dioscoreaceae)*. In *The Wealth of India Raw Materials* vol. **6** CSIR.

Che, C. T., H. Zhang, K. Plant and Y. Zhou. (2014). "Chemical Constituents of *Dioscorea* Species". *Food Chemistry*, vol. **151**, pp. 345–352.

Irulandi, K., S. Geetha and P. Mehalingam. (2016). "Antioxidant, Antimicrobial Activities and Phytochemical Analysis of Leaves Extracts of *Dioscorea wallich*ii Hook. f.". *Journal of Applied Pharmaceutical Science*, vol. 6 (11), pp. 70–74.

Kumar, S., P. Mahanti, N. R. Singh, S. K. Rath, P. K. Jena and J. K. Patra. (2017). "Antioxidant Activity, Antibacterial Potential and Characterization of Active Fraction of *Dioscorea pentaphylla* L. Tuber Extract Collected from Similipal Biosphere Reserve, Odisha, India". *Brazilian Journal of Pharmaceutical Sciences*, vol. **53** (4), e17006.

Patel, S., P. Patel, A. Gupta and R. Nair. (2012). "Pharmacognostic Studies of the Plant *Dioscorea bulbifera*". *Asian Pacific Journal of Tropical Disease*, vol. **2** (3), pp. S1–S4.

Paul C., A. Debnath, R. Chanda and B. Debnath. (2017). "Taxonomical Note, New Distributional Record and Traditional Use for *Dioscorea wallichii* Hook. f. (Dioscoreaceae) of TripuraNorth-East India". *Annals of Plant Sciences*. vol. **6** (12), p.1868.

Salehi, B., A. P. Mishra, I. Shukla, M. Sharifi-Rad, M. D. M. Contreras and A. Segura-Carretero. (2019). "Dioscorea Plants: A Genus Rich in Vital Nutrients and Bioactive Phytochemicals". *Applied Sciences*, vol. **9** (11), p. 2233.

Salehi, B., B. Sener, M. Kilic, J. Sharifi-Rad, R. Naz, Z. Yousaf, F. N. Mudau, P. V. T. Fokou, S. M. Ezzat, M. H. EI Bishbishy, Y. Taheri, G. Lucariello, A. Durazzo, M. Lucarini, H. A. R. Suleria and A. Santini. (2019).

"Dioscorea Plants: A Genus Rich in Vital Nutra-pharmaceuticals - *A Review*". *Iranian Journal of Pharmaceutical Research*, vol. **18**, pp. 68–89.

Singh, M. P., J. S. D. Singh and R. Rajesh. (2015). "Brine Shrimp Cytotoxic Assay for Polyherbal Formulation of *Moringa oleifera, Viola odorata, Allium sativum*." *International Journal of Innovative Pharmaceutical Sciences and Research*, vol. **3** (12), pp. 1639–1643.

Sunmathi, D., R. Sivakumar and K. Ravikumar. (2016). "*In vitro* Anti-inflammatory and Antiarthritic Activity of Ethanolic Leaf Extract of *Alternanthera sessilis* (L.) R.BR. exDC and *Alternanthera philoxeroides* (Mart.) Griseb." *International Journal of Advances in Pharmacy, Biology and Chemistry*, vol. **5** (2), pp. 109–115.

SOME BIOLOGICAL ASSESSMENT OF *PLUCHEA INDICA* (L.) LESS ROOT (YAY-KHAYU) FROM THE TANINTHARYI REGION

Hein Htet Soe[1], Prema[2], Nway Shwan Oo[3], Ni Ni Than[4]

Abstract

Pluchea indica (L.) Less is naturally grown in mangroves along the Tanintharyi Coastal Region. It is locally known as "Yay-Khayu" and has been utilised as a source of food and medicine and for making herbal tea. This research has been carried out to investigates the total phenolic and flavonoid contents, antimicrobial, antioxidant, cytotoxicity, and anti-arthritic activities collected of *P.indica* root collected from the Tanintharyi Coastal Region. The total phenolic and flavonoid contents of ethanol and watery extracts from *P. indica* root were determined by the Folin-Ciocalteu Reagent (FCR) and aluminium chloride colourimetric methods. In addition, the antimicrobial efficacy of watery, ethanol, ethyl acetate, and petroleum ether crude extracts from *Pluchea indica* root samples was evaluated against eight microorganisms using the agar well diffusion method. The tested microorganisms included *Agrobacterium tumefaciens*, *Bacillus pumilus*, *Bacillus subtilis*, *Candida albicans*, *Escherichia coli*, *Micrococcus luteus*, *Pseudomonas fluorescens*, and *Staphylococcus aureus*. According to the analysis, all the crude extracts from the root sample exhibit significant antimicrobial activity on most of the microorganisms. The cytotoxicity of ethanol and watery extracts from the *P. indica* root sample was evaluated using the *Artemia salina* (brine shrimp) bioassay. The obtained results showed that neither the ethanol nor the watery extract of the root sample exhibited significant toxicity to a maximum dose of 1000 µg/mL. The antioxidant potential of the ethanolic and watery extracts from the root sample was assessed using the DPPH free radical scavenging assay. The antioxidant activity of the ethanol extract was found to be higher than that of the watery extract from the root sample. Furthermore, the egg albumin denaturation method was used to evaluate the anti-arthritic properties of both ethanol and watery extracts from the root sample. It was found that the ethanol extract showed significantly higher anti-arthritic activity than the watery extract of the root sample.

Keywords: *Pluchea indica* (L.) Less, antimicrobial activity, cytotoxicity, antioxidant activity, anti-arthritic activity

Introduction

The medicinal plants are vital species that, based on traditional medicine and modern scientific research, offer valuable health benefits and aid in treating various diseases. They are considered abundant sources of compounds that can be utilized in developing and producing pharmaceutical drugs to enhance human health (Oladeji *et al*., 2019).

Antioxidants are compounds that reduce oxidative damage to biological processes by donating electrons to free radicals, rendering them harmless. Free radicals are closely linked to oxidative stress, which occurs when oxygen interacts with certain chemicals, leading to the formation of free radicals. Once these are produced, the potential risk lies in the damage they may cause by interacting with vital cellular components such as DNA, proteins, and cell membranes. Among the numerous naturally occurring antioxidants, ascorbic acid, carotenoids, and phenolic compounds are more effective (Duh *et al*., 1999).

Arthritis includes various types of joint disorders, such as rheumatoid arthritis (RA) and osteoarthritis (OA), which can affect either a single joint or multiple joints. The typical signs of arthritis include joint swelling, tenderness, and stiffness, often accompanied by a reduced range of motion. These symptoms can vary in intensity, from mild discomfort to severe impairment. (Lespasio *et al*., 2017).

[1] Department of Chemistry, University of Yangon
[2] Department of Chemistry, University of Yangon
[3] Department of Chemistry, Myeik University
[4] Department of Chemistry, University of Yangon

P. indica known as Yay-Khayu in Myanmar, is a member of the *Asteraceae* family and a well-known medicinal plant that grows naturally in many Asian countries. It could be found in Thailand, India, China, the Philippines, Malaysia, and Myanmar (Wang *et al*., 2008; Panda and Luyten, 2018). It contains various biochemical compounds, including sesquiterpenes, flavonoids, tannins, saponins, sterols, alkaloids, and thiophenes (Ruan *et al*., 2018). It is also used to treat a wide range of conditions, including lumbago, kidney stones, leucorrhea, inflammation, gangrenous and atonic ulcers, haemorrhoids, dysentery, eye disorders, itchy skin, acid stomach, dysuria, abdominal pain, scabies, fever, muscle soreness, diabetes, and rheumatism, among others (Sabrin *et al*., 2022).

Therefore, the total phenolic and total flavonoid contents, antimicrobial activity, cytotoxic effects, antioxidant properties, and anti-arthritic potential of *P. indica* (Yay-Khayu) root extract were evaluated in this study.

Materials and Methods

Location of Sampling Sites

P. indica is one of the coastal flowering plants in Tanintharyi Coastal Region. It is an evergreen shrub and is found abundantly in salt marshes and mangrove swamps with a 1 to 2 m height. It plays a significant part in preserving the ecological balance along the Tanintharyi coastal areas. The selected sample also occurred in Palaw Township, Tanintharyi Region of Myanmar. For the current study, a *P. indica* root sample was chosen. The location of the sampling site and the collected root sample are illustrated in Figure 1.

Figure 1. Map showing the collection site of *P. indica* root (Yay-Khayu) in Palaw Township, Tanintharyi Region

Collection and Preparation of Sample

P. indica root sample was collected from Palaw Township during June 2024. This sample was identified by an authorized botanist in the Department of Botany, at Myeik University. The root sample was cleaned with tap water and then distilled water to remove the dirt on the surface of the root, and air-dried. The air-dried sample was made into powder with an electric grinder and stored in airtight containers to prevent moisture changes and other contamination.

Determination of Total Phenol Contents (TPC) as Gallic Acid Equivalent

The total phenolic content was determined by the Folin-Ciocalteu method (Saxena *et al*., 2013). Each extracted sample solution (0.5 mL) was added into 5 mL of FC reagent (1:10) and incubated for 5 min. To each tube, 4 mL of 1 M sodium carbonate solution was added, the tubes were kept at room temperature for 15 min, and the UV absorbance of the reaction mixture was read at λ_{max} 765 nm. Total phenolic content was estimated as micrograms of gallic acid equivalent per milligram (μg GAE/mg) of crude extract.

Determination of Total Flavonoid Contents (TFC) by Aluminium Chloride Colorimetric (ACC) Assay

The total flavonoid content was determined using an aluminium chloride colorimetric assay (Basma *et al*., 2011). Each extracted sample solution (0.5 mL) was mixed with 1.5 mL of methanol, 0.1 mL of 1 % aluminium chloride solution, 0.1 mL of 1 M potassium acetate and 2.8 mL of distilled water, the tubes were allowed to stand for 30 min at room temperature. The absorbance of the solution was measured at 415 nm using a UV spectrophotometer. Results were expressed as milligrams of quercetin equivalents (QE) per gram of extract (mg QE/g extract).

Determination of Antimicrobial Efficacy

The antimicrobial efficacy of watery, ethanol, ethyl acetate, and pet-ether extracts of *P. indica* root was investigated by using the agar well diffusion method at the Department of Botany, Pathein University.

Evaluation of Cytotoxicity Bioassay

Preparation of artificial seawater: Artificial seawater (3.8 % (w/v) NaCl) was prepared by dissolving (38 g) of sodium chloride in 1 L of distilled water.

Hatching of brine shrimp (*Artemia salina*): Brine shrimp cysts (0.5 g) were put into 1 L of artificial seawater in a bottle. This bottle was placed near a lamp. Light is essential for the cysts to hatch. Brine shrimp cysts are required to hatch with constant supplied oxygen and 24 h incubation at room temperature.

Determination of cytotoxicity test: The cytotoxicity test of crude extracts was assessed by using brine shrimp lethality bioassay. The sample solution was prepared with 9 mL of artificial seawater, 1 mL of various concentrations of samples, and alive brine shrimp (10 nauplii) with a Pasteur pipette. Potassium dichromate was used as a standard positive control and caffeine was also used as a standard negative control. They were incubated at room temperature for 24 h. After 24 h, the number of survivals of nauplii was counted and the percentage of mortality was determined using the following equation (Singh *et al*., 2015).

% mortality = (no. of dead nauplii/initial no. of live nauplii) × 100

Determination of Antioxidant Capacity by DPPH Free Radical Scavenging Assay

The effect on DPPH radical was determined using the method by Hishamuddin *et al*. (2020). Antioxidant activities of 95 % ethanol and watery extracts were carried out in a DPPH free radical scavenging assay, and the absorbance of these solutions was measured at 517 nm by using a UV-visible spectrophotometer. Absorbance measurements were done in triplicate for each solution, and then the mean values obtained were used to calculate the percent inhibition of oxidation by the following formula. Then, IC_{50} (50 % inhibitory concentration) values were also calculated by a linear regressive Excel program.

$$\% \text{ Inhibition} = [A_{control} - (A_{sample} - A_{blank}) / A_{control}] \times 100$$

where, $A_{control}$ = absorbance of DPPH in EtOH solution

A_{sample} = absorbance of the test sample and DPPH solution

A_{blank} = absorbance of the test sample and EtOH solution

Screening of Anti-arthritic Activity

The anti-arthritic activity was evaluated using the egg albumin denaturation method by Madhuranga (2023)**.** Diclofenac sodium was used as the standard drug. The control solution was created by 2 mL of distilled water, 0.2 mL of 1 % egg albumin, and 2.8 mL of phosphate-buffered saline (pH 7.4). The sample solution was also prepared with 0.2 mL of 1 % egg albumin, 2.8 mL of phosphate-buffered saline (PBS, pH 6.4), and 2 mL of different concentrations of crude extracts of root. Then the mixtures were incubated at 37 °C in an incubator for 15 min and then heated at 70 °C for 5 min. After cooling, their absorbance was measured at 280 nm by a UV-visible spectrophotometer. The whole test procedure was done in triplicate.

Results and Discussion

Total Phenolic Contents of Crude Extracts Root of *P. indica* (Yay-Khayu)

In the present investigation, the total phenolic contents of the *P. indica* root sample were estimated by the Folin-Ciocalteu method. Gallic acid (3, 4, 5-trihydraxybenzoic acid) was used to construct a standard calibration curve for total phenol estimation. Total phenolic content (TPC) was expressed as micrograms of gallic acid equivalent (GAE) per milligram of crude extract (µg GAE/mg) (Table 1 and Figure 2). According to the results, the total phenolic content was found to be ethanol extract (104.69 mg) of GAE/g which is higher than the watery extract (52.86 mg) of GAE/g of the extract (Table 2 and Figure 3).

Table 1. The absorbance of Different Concentrations of Standard Gallic Acid at λ_{max} 765 nm

Concentration (µg/mL)	Absorbance (mean value)
0.625	0.094
1.25	0.105
2.5	0.134
5	0.183
10	0.283
20	0.472

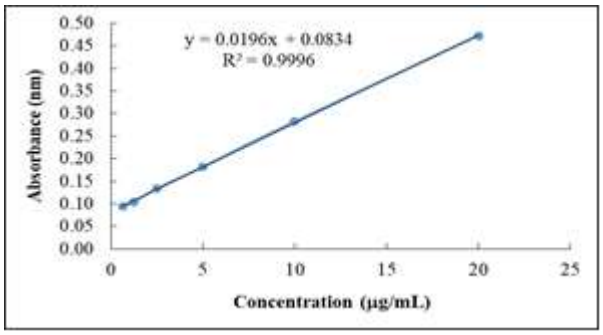

Figure 2. Calibration curve of standard gallic acid at 765 nm

Table 2. Total Phenolic Contents of Crude Extracts of the Root of *P. indica*

Extracts	TPC (mg GAE/g ± SD)
Ethanol	104.69 ± 0.001
Watery	52.86 ± 0.003

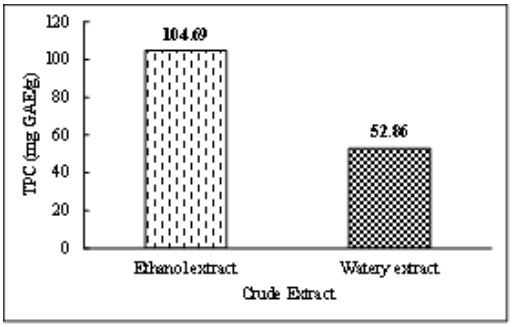

Figure 3. A bar graph of total phenolic contents of crude extracts of the root of *P. indica*

Total Flavonoid Contents of Crude extracts Root of *P. indica* (Yay-Khayu)

The total flavonoid contents of the *P. indica* root sample were investigated by the aluminium chloride colourimetric method. Quercetin was used as a standard compound for the

quantification of the standard calibration curve for total flavonoid estimation as shown in Table 3 and Figure 4. The total flavonoid contents (TFC) were expressed as micrograms of quercetin equivalent (QE) per milligram of crude extract (µg QE/mg). From the results, the total flavonoid contents in ethanol and ethanol extracts were found to be 24.36 and 13.45 mg QE/g, respectively. (Table 4 and Figure 5).

Table 3. The absorbance of Different Concentrations of Standard Quercetin at λ_{max} 415 nm

Concentration (µg/mL)	Absorbance (mean value)
0.625	0.003
1.25	0.006
2.5	0.013
5	0.027
10	0.057
20	0.111

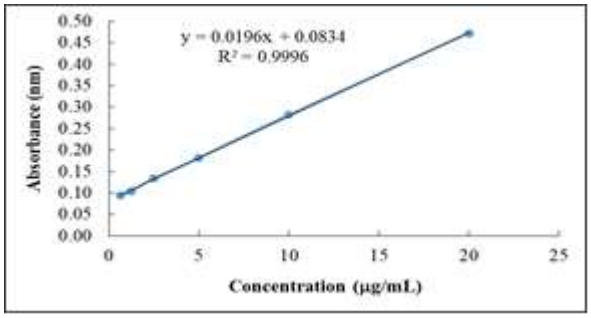

Figure 4. Calibration curve of standard quercetin at 415 nm

Table 4. Total Flavonoid Contents of Crude Extracts of the Root of *P. indica*

Extracts	TFC (mg QE/g ± SD)
Ethanol	45.00 ± 0.014
Watery	23.57 ± 0.001

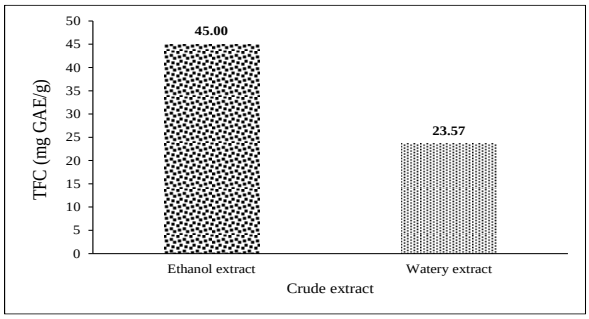

Figure 5. A bar graph of total flavonoid contents of crude extracts of the root of P. indica

Antimicrobial Efficacy of *P. indica* Root (Yay-Khayu) Sample

The antimicrobial efficacy was determined by the agar well diffusion method. The antimicrobial efficacy of the different extracts (watery, ethanol, ethyl acetate, and pet-ether) against eight microorganisms such as *Agrobacterium tumefaciens, Bacillus pumilus, Bacillus subtilis, Candida albicans, Escherichia coli, Staphylococcus aureus, Micrococcus luteus,* and *Pseudomonas fluorescens* are listed in Table 5 and Figure 6.

A larger inhibition zone indicates stronger antimicrobial activity of the tested substances. Based on these findings, all crude extracts from root samples demonstrated significant antimicrobial effects against most microorganisms. Among them, the ethyl acetate extracts showed the highest antimicrobial activity against all tested microorganisms, with inhibition zones measuring between 19 mm and 23 mm, followed by ethanol, watery, and pet-ether extracts. Moreover, ethanol extract has higher antimicrobial activity than watery and pet-ether extract within inhibition zones ranging from 17 mm to 18 mm. While the watery extract had weaker antimicrobial activity compared to ethyl acetate and ethanol extracts, it was more effective than the pet-ether extract, with inhibition zones from 15 mm to 17 mm. Among all extracts, the pet-ether extract displayed the weakest antimicrobial activity against both bacterial and fungal pathogens. From

overall observation, the root extracts may be applied in the development of antimicrobial agents, especially in the treatment of infections caused by both gram-positive and gram-negative bacteria, as well as fungal pathogens.

Table 5. Antimicrobial Efficacy of *P. indica* Root (Yay-Khayu) Sample

Test organisms	Inhibition zone diameter (mm)				
	Watery extract	Ethanol extract	Ethyl acetate extract	Pet-ether extract	Standard
A. tumefaciens	17	18	23	12	27
B. pumilus	16	18	19	12	27
B. subtilis	16	17	19	12	27
C. albicans	16	18	20	11	27
E. coli	15	17	19	11	27
M. luteus	16	17	20	11	28
P. fluorescens	16	17	19	11	28
S. aureus	16	17	19	11	28

For bacteria*STD = Chloramphenicol
For fungus *STD = Nystatin

10-12 mm = weak activity, 13-18 mm = moderate activity, > 18 mm = high activity; well size = 8 mm

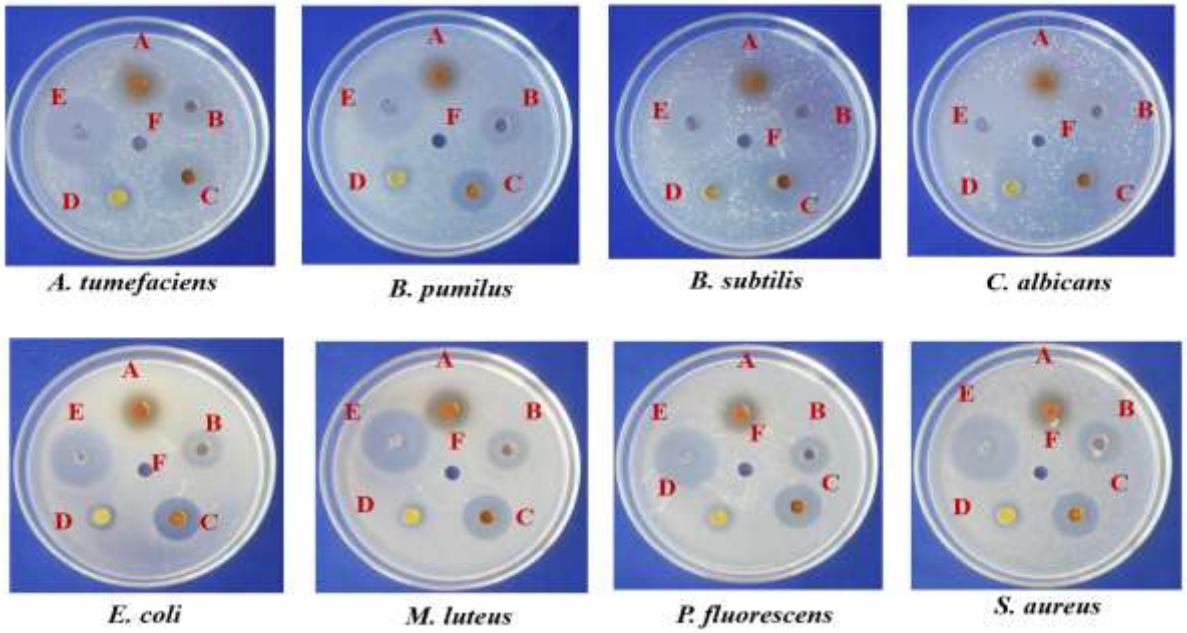

Figure 6. Inhibition well diameters of *P. indica* (Yay-Khayu) root against eight microorganisms (A) Watery extract, (B) 95 % Ethanol extract, (C) Ethyl acetate extract (D) Pet-ether extract, (E) Standard (F) Control

Cytotoxicity of Watery and Ethanol Extracts of *P. indica* Root (Yay-Khayu) Sample

A brine shrimp lethality bioassay, using the *Artemia salina* (Brine shrimp), was a simple and cost-effective bioassay that was used to assess the cytotoxic effects of the watery and ethanol extracts of the root sample. The cytotoxicity was expressed as 50 % lethal dose concentration LC_{50}. A lower LC_{50} value indicates greater toxicity, while a higher LC_{50} indicates that the substance is

less toxic or non-toxic. Substances with LC_{50} values below 1000 µg/mL are typically regarded as cytotoxic. Watery and ethanol extracts of the *P. indica* (Yay-Kha-Yu) root sample were dissolved in distilled water to get 2000 µg/mL concentrations, used as a stock solution, and then it was diluted with 9 mL of artificial seawater and alive brine shrimp (10 nauplii) to obtain 1000, 100, 10, and 1 µg/mL concentrations. In this experiment, potassium dichromate was used as a cytotoxic agent and effectively induced mortality in the brine shrimp, serving as the standard positive control. In contrast, caffeine served as the standard negative control and demonstrated no cytotoxicity. The results of the cytotoxicity test for watery and ethanol extracts of *P. indica* (Yay-Khayu) root are shown in Table 6.

Both the watery and ethanol extracts of *P. indica* root showed LC_{50} values of 1000 µg/mL, indicating that these extracts are non-toxic at the tested concentration of 1000 µg/mL. Overall, the findings suggest that *P. indica* root extracts are non-toxic at the tested dosages, which could be indicative of their potential safety in further biological application.

Table 6. Results of Cytotoxicity Test for Four Different Doses of Watery and Ethanol Extracts of *P. indica* Root (Yay-Khayu) Sample

Tested sample	Extracts	% of Dead Brine Shrimp (Mean ± SEM) in Various Concentrations (µg/mL)				LC_{50} (µg/ mL)
		1	10	100	1000	
Root	watery	10 ± 1.00	20 ± 0.00	23 ± 0.58	33 ± 0.58	>1000
	ethanol	13 ± 0.57	23 ± 0.57	33 ± 0.58	50 ± 1.15	1000
standard	$K_2Cr_2O_7$	7 ± 1.00	20 ± 0.00	100 ± 0.00	100 ± 0.00	43.75
	caffeine	0 ± 0.00	23 ± 1.20	30 ± 0.58	40 ± 1.16	>1000

Antioxidant Activity of Watery and Ethanol Extracts from *P. indica* Root (Yay-Khayu) Sample

The present work shows the antioxidant activity of watery and ethanol extracts from *P. indica* (Yay-Khayu) root was studied by the DPPH assay. The antioxidant activity was expressed as 50 % oxidative inhibitory concentration IC_{50}. The DPPH assay acts as a free radical scavenger or hydrogen donor to evaluate antioxidant capacity. Watery and ethanol extracts of the selected *P. indica* (L.) Less. (Yay-Khayu) root samples were dissolved in ethanol and then it was diluted with ethanol to obtain 125, 62.5, 31.3, 15.62, 7.81, and 3.91 µg/mL concentrations. After mixing these solutions with DPPH solution, their absorbance was measured at 517 nm. Ascorbic acid was used as a standard reference in this experiment. The IC_{50} values for each sample were determined using a linear regression analysis in Excel. The results are described in Table 7 and Figures 7 and 8.

The results of this experiment showed that IC_{50} was 42.46 µg/mL for watery extract and 26.27 µg/mL for ethanol extract. Since the lower the IC_{50} values, the higher the free radical scavenging activity, i.e., the higher the antioxidant capacity, the antioxidant activity of ethanol extract (IC_{50} = 20.67 µg/mL) was found to be higher than that of watery extract (IC_{50} = 42.46 µg/mL) in the root sample. Compared to the standard ascorbic acid (IC_{50} = 4.68 µg/mL), all crude extracts of the root samples demonstrated less potent antioxidant activity. Thus, the high content of antioxidants in the ethanol extract from the Yay-Khayu root sample suggested its potential as a strong antioxidant material and its ability to neutralize and reduce many oxidizing compounds.

Table 7. Oxidative Percent Inhibitions and IC_{50} Values of Ethanol and Watery Extract of *P. indica* Root (Yay-Khayu) Sample and Standard Ascorbic Acid

Tested sample	Extracts	% Inhibitions (Means ± SD) in various concentrations (µg/mL)						IC_{50} (µg/mL)
		3.91	7.81	15.625	31.25	62.5	125	
Root	ethanol	12.63 ± 0.20	22.85 ± 2.28	44.69 ± 0.40	61.12 ± 0.00	72.95 ± 0.40	87.58 ± 0.53	20.67
	watery	34.94 ± 0.12	38.41 ± 0.50	40.81 ± 0.95	47.03 ± 0.70	55.31 ± 0.40	63.19 ± 0.12	42.46
Standard	ascorbic acid	48.99 ± 0.53	54.09 ± 1.36	56.64 ± 0.44	63.83 ± 1.06	66.61 ± 0.35	87.13 ± 0.76	4.68

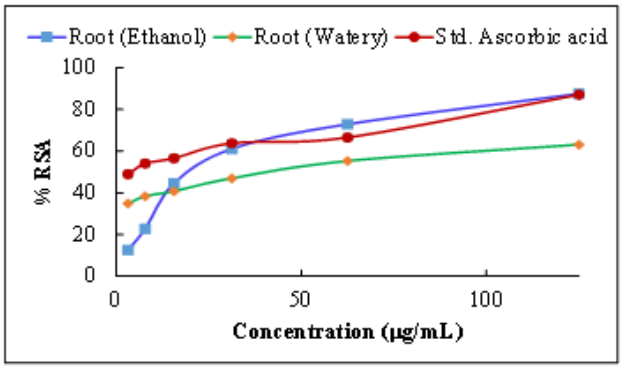

Figure 7. A plot of % RSA vs concentration of crude extracts of *P. indica* root and standard ascorbic acid

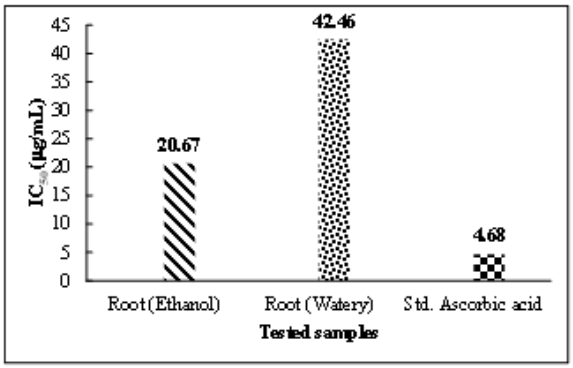

Figure 8. A bar graph of IC_{50} values of crude extracts of *P. indica* root and standard ascorbic acid

Anti-arthritic Activity of *P. indica* Root (Yay-Khayu) Sample

This study investigates the anti-arthritic properties of watery and ethanol extracts from the root of *P. indica* (L.) Less. (Yay-Khayu) using the egg albumin denaturation assay. Protein denaturation is linked to inflammation. A substance's potential anti-arthritic action is demonstrated by its capacity to prevent protein denaturation. Using a fresh hen's egg, the *in vitro* egg albumin denaturation method is used to screen for anti-arthritic properties. In this experimental work, diclofenac sodium was used as a standard. Watery and ethanol extracts from the root sample of the selected *P. indica* (Yay-Khayu) were dissolved in water and used as a stock solution. These were then further diluted with water to get concentrations of 500, 250, 125, 62.5, 31.3, 15.62, and 7.81 µg/mL. Afterward, each solution was mixed with 1 % egg albumin and phosphate-buffered saline (pH 6.4), and their absorbance was measured at 280 nm. Based on absorbance values, the obtained results of % inhibition of each sample in different concentrations were calculated and tabulated in Table 8, Figures 9 and 10.

In conditions like rheumatoid arthritis, cancer, and diabetes, which involve inflammation, protein denaturation leads to the formation of autoantigens. Therefore, by preventing protein denaturation, it is possible to reduce inflammatory activity. In the investigation of anti-arthritic

properties using the egg albumin denaturation method on *P. indica* (Yay-Khayu) root from Palaw Township, the IC_{50} values were determined to be 34.00 µg/mL for the watery extract and 25.35 µg/mL for the ethanol extract. From the experimental work, all the crude extracts from the root sample exhibited weaker anti-arthritic activity compared to the standard diclofenac sodium, which has an IC_{50} value of 18.39 µg/mL. The results show that the IC_{50} value of the ethanol extract from the root sample is lower than that of the watery extract. Since a lower IC_{50} value indicates greater anti-arthritic activity, this suggests that the ethanol extract has a stronger anti-arthritic potential compared to the watery extract. Thus, the ethanol extract of the Yay-Khayu root sample can serve as an anti-arthritic agent to reduce inflammation, joint pain, and the progression of arthritis symptoms.

Table 8. Results of Anti-arthritic Activity of Ethanol and Watery Extracts of *P. indica* Root (Yay-Khayu) Sample and Standard Diclofenac Sodium

Tested sample	Extracts	% Inhibition (Mean ± SD) in different concentrations (µg/mL)						IC_{50} (µg/ mL)
		15.62	31.3	62.5	125	250	500	
Root	ethanol	15.92 ± 0.00	70.67 ± 1.96	79.67 ± 0.44	83.21 ± 1.73	88.32 ± 0.48	93.04 ± 0.49	25.35
	watery	14.88 ± 1.33	49.43 ± 0.49	55.89 ± 1.62	76.01 ± 0.69	77.28 ± 0.56	87.14 ± 0.13	34.00
Standard	diclofenac sodium	46.36 ± 0.00	66.93 ± 1.45	78.20 ± 0.84	84.88 ± 0.55	89.70 ± 0.18	93.60 ± 0.12	18.39

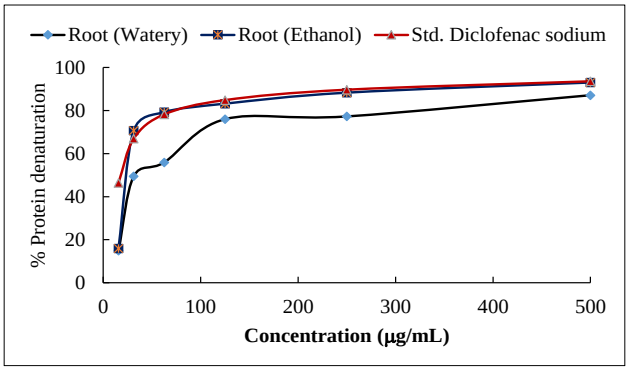

Figure 9. A plot of % protein denaturation vs concentration of crude extracts of *P. indica* root and standard diclofenac sodium

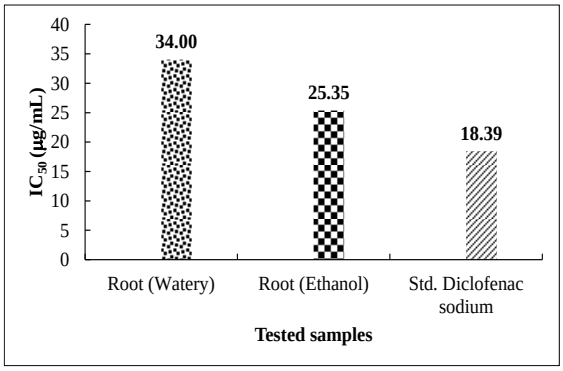

Figure 10. A bar graph of IC_{50} values of crude extracts of *P. indica* root and standard diclofenac sodium

Conclusion

The key objectives of this study were to evaluate the total phenolic and flavonoid contents, antimicrobial efficacy, cytotoxicity, antioxidant capacity, and anti-arthritic activity of *P. indica* (Yay-Khayu) root sample from the Palaw Township, Tanintharyi Region. Based on the data, the ethanol extract of *P. indica* root was observed to contain higher phenol and flavonoid contents than the watery extract. The finding suggests that *P. indica* root extracts, particularly the ethanol and ethyl acetate extracts, may serve as effective antimicrobial agents against bacterial and fungal pathogens. The toxicity assessment showed that both watery and ethanol extracts had LC_{50} values of 1000 µg/mL, indicating that they are non-toxic at this concentration. Therefore, *P. indica* root extracts are safe for potential biological applications at the tested doses, making them suitable for further research and development in therapeutic applications. The antioxidant potential of the root extracts was evaluated based on free radical scavenging activity, with lower IC_{50} values indicating stronger antioxidant capacity. The ethanol extract showed high antioxidant activity (IC_{50} = 20.67 µg/mL) compared to the watery extract (IC_{50} = 42.46 µg/mL). This highlights the ethanol extract as a potency antioxidant agent, which may protect against oxidative damage. This study demonstrated that both the watery and ethanol extracts of *P. indica* root have significant anti-arthritic potential, as indicated by their ability to prevent protein denaturation such as rheumatoid arthritis.

The IC_{50} value for the ethanol extract (25.35 µg/mL) was lower than that of the watery extract (34.00 µg/mL), suggesting that the ethanol extract has stronger anti-arthritic activity. This indicates that ethanol extract can be more effective in reducing inflammation, joint pain, and the progression of arthritis symptoms. Thus, the overall findings indicate that *P. indica* root extract samples have significant potential as antimicrobial agents, antioxidants, and anti-arthritic for the treatment of microbial infections, oxidative stress, and inflammation-related diseases.

Acknowledgement

The author would like to express our sincere thanks to Professor Dr Ni Ni Than allowing us to present this research topic.

References

Basma, A. A., Z. Zakaria, L. Y. Latha, and S. Sasidharan. (2011). "Antioxidant Activity and Phytochemicals Screening of the Methanol Extracts of *Euphorbia hirta* L". *Asia Pacific Journal of Tropical Medicine*, vol. **4**(5), pp. 386-390.

Duh, P. D., Y. Y. Tu, and G. C. Yen. (1999). "Antioxidants Activity of Aqueous Extract Harnjyur (*Chrysanthemum morifolium* Ramat)". *Lebensmwiss Technol*., vol. **32**, pp. 269-277.

Hishamuddin, S. N. A., Q. Q. Amir, A. H. Mohamed and N. R. Said. (2020). "Extraction of Bioactive Compounds from Longan Peel by Using Solvent Extraction Method and its Antioxidant Activity". *ASM Science journal*, vol. **13**(6), pp. 60-65.

Lespasio, M. J., N. S. Piuzzi, M. E. Husni, G. F. Muschler, A. Guarino, and M. A. Mont. (2017). "Knee Osteoarthritis: a primer". *Perm J*, vol. **21**, pp. 1-7.

Madhuranga, H. D. T. and D. N. A. W. Samarakoon. (2023). "*In vitro* Anti-inflammatory Egg Albumin Denaturation Assay: An Enhanced Approach". *Journal of Natural & Ayurvedic Medicine,* vol. **7**(3), pp. 1-6.

Oladeji, O. S., K. A., Odelade, and K. Oloke. (2019). "Phytochemical Screening and Anti-microbial Investigation of *Moringa oleifera* Leaf Extract". *African Journal of Science and Technology, Innovation, and Development,* vol. **12**(1), pp. 79-84.

Panda, S. K. and W. Luyten. (2018). "Antiparasitic Activity in Asteraceae with Special Attention to Ethnobotanical Use by the Tribes of Odisha, India". *Parasite*, vol. **25**, pp. 10-25.

Ruan, J., Z. Li, J. Yan, P. Huang, H. Yu, and L. Han. (2018)."Bioactive Constituents from the Aerial Parts of *Pluchea indica* Less." *Molecules*, vol. **23**, pp. 1-11.

Sabrin, R., M. Ibrahim, A. A. Bagalagel, M. R. Diri, A. O. Noor, H. T. Bakhsh, and G. A. Mohamed. (2022). "Phytoconstituents and Pharmacological Activities of Indian Camphorweed (*Pluchea indica*): A Multi-Potential Medicinal Plant of Nutritional and Ethnomedicinal Importance". *Molecules*, vol. **27**, pp. 1-49.

Saxena, M., J. Saxena, R. Nema, D. Singh, and A. Gupta. (2013). "Phytochemistry of Medicinal Plants". *Journal of Pharmacognosy and Phytochemistry*, vol. **1**(6), pp. 168-172.

Singh, M. P., J. Singh S. D., and R. Rajesh. (2015). "Brine Shrimp Cytotoxic Assay for Polyherbal Formulation of *Moringa oleifera, Viola odorata, Allium sativum*". *International Journal of Innovative Pharmaceutical Sciences and Research*, vol. **3**(12), pp. 1639-1643.

Wang, J., Y. H. Pei, W. H. Lin, Z. W. Deng, and L. Qiao. (2008). "Chemical Constituents from the Stems and Leaves of Marine Mangrove Plant *Pluchea indica* (L.) Less". *Shenyang Yaoke Daxue Xuebao*, vol. **25**, pp. 960-963.

INVESTIGATION OF SOME BIOACTIVITIES OF *CURCUMA PETIOLATA* ROXB. (MALAR) RHIZOME

Kay Thi[1], Prema[2], Thandar Aung[3], Ni Ni Than[4]

Abstract

Curcuma petiolata, also known as the petiole turmeric and as referred to as Malar in Myanmar is primarily used in traditional medicine for its anti-inflammatory and antioxidant properties. Additionally, its rhizome is utilised as a culinary spice in various Southeast Asian dishes, adding flavour and colour. This study aims to explore the preliminary phytochemical tests, soluble matter content, antimicrobial, antioxidant, cytotoxic, and anti-arthritic properties of the rhizome of *C. petiolata*. In this study, the preliminary phytochemical investigation, it was found that alkaloids, flavonoids, glycosides, saponins, tannins, α-amino acids, carbohydrates, phenolic compounds, reducing sugars, organic acids, steroids, and terpenoids were present in the rhizome of *C. petiolata*. The extractable matter contents of the sample were determined by the WHO method with different solvents such as water, ethanol, methanol, chloroform, ethyl acetate, and petroleum ether. The resultant data indicated that the selected sample is more soluble in water. Additionally, the antimicrobial activity of crude extracts such as petroleum ether, ethyl acetate, ethanol, and watery extracts of *C. petiolata* was tested on eight microorganisms by agar well diffusion method. The antioxidant activity of ethanol and watery extracts of *C. petiolata* rhizome was evaluated by the 2,2-diphenyl-1-picrylhydrazyl (DPPH) free radical scavenging assay. A brine shrimp lethality bioassay investigated the cytotoxicity of the watery and ethanol extracts. The egg albumin denaturation method performed the anti-arthritic activity of watery and ethanol extracts. As a result, *C. petiolata* contains biologically active compounds and exhibits medicinal properties.

Keywords: *Curcuma petiolata*, antimicrobial activity, antioxidant activity, cytotoxicity, anti-arthritic activity

Introduction

Medicinal plants have been utilised for thousands of years in various cultures worldwide for their therapeutic properties. These plants contain bioactive compounds that can promote health and treat diseases, making them a cornerstone of traditional medicine (Wagner and Ulrich-Merzenich, 2009). Recent studies have highlighted the importance of these plants in modern pharmacology, with many contemporary drugs derived from their natural compounds (Newman and Cragg, 2016). Today, there is increasing scientific interest in exploring these plants for new medicines and treatments. Understanding their potential benefits helps researchers develop effective healthcare solutions. *Curcuma petiolata*, commonly known as a species of turmeric and referred to as Malar in Myanmar, is a flowering plant belonging to the ginger family, Zingiberaceae. This plant is native to the tropical regions of Southeast Asia, particularly found in countries like Thailand and Malaysia. It is recognised for its distinctive foliage and vibrant yellow flowers, contributing to its popularity in ornamental horticulture (Kress *et al*., 2002). *C. petiolata* rhizome is a botanical specimen renowned in traditional medicine for its diverse biological activities and phytochemical compositions. *C. petiolata* has been historically valued for its medicinal properties, including antioxidant (Jayaprakash *et al*., 2006), anti-inflammatory (Ammon *et al*., 1992), anticancer (Hatcher *et al*., 2008) and antimicrobial effects (Haddad *et al.*, 2011). This research aims to further explore its health benefits and potential applications in healthcare and drug development.

[1] Department of Chemistry, Taunggyi University
[2] Department of Chemistry, University of Yangon
[3] Department of Chemistry, University of Yangon
[4] Department of Chemistry, University of Yangon

Materials and Methods

Collection and Preparation of Plant Sample

The sample was collected from Inn Pyin Village, Kalaw Township, Southern Shan State in Myanmar. The selected sample was identified as *Curcuma petiolata* Roxb. (Malar) at the Botany Department of the University of Yangon. After collection, the rhizome was thoroughly washed with water to remove impurities. Then, it was sliced into smaller pieces and air-dried at room temperature. After drying, the sample was ground into a fine powder using a grinding machine, then sieved and stored in an airtight container for future use.

Preliminary Phytochemical Investigation of *C. petiolata* (Malar) Rhizome

A preliminary phytochemical analysis was carried out on a dried powdered sample of *C. petiolata* (Malar) rhizome using the appropriate reported methods. The aim was to determine the presence or absence of various phytochemicals such as alkaloids, α-amino acids, carbohydrates, cyanogenic glycosides, organic acids, flavonoids, glycosides, phenolic compounds, reducing sugars, saponins, steroids, tannins, starch, and terpenoids.

Determination of the Soluble Matter Contents

The soluble matter content of the sample in various organic solvents, including petroleum ether, ethyl acetate, chloroform, methanol, ethanol, and water, was determined using the method outlined by the WHO.

Preparation of Crude Extracts for Biological Activities

Approximately 20 g of dried powder was subjected to successive extractions with 95 % ethanol for six hours, followed by filtration. The filtrate was then concentrated using a rotary evaporator to obtain the ethanol extract. For the watery extract, another 20 g of dried powder was boiled in 100 mL of distilled water and filtered. The resulting solution was concentrated by evaporating the water using a water bath to yield the watery extract. Both crude extracts were subsequently dried and stored in a refrigerator for a few weeks.

Determination of Antimicrobial Activity by Agar Well Diffusion Method

The antimicrobial activity of various crude extracts, such as ethanol, petroleum ether, ethyl acetate, and watery extract, was investigated by the agar-well diffusion method at the Department of Chemistry, Pathein University. Chloramphenicol and nystatin were used as positive controls for antibacterial and antifungal tests, respectively. Test organisms are *Escherichia coli*, *Micrococcus luteus*, *Bacillus subtilis*, *Bacillus pumilus*, *Staphylococcus aureus*, *Pseudomonas fluorescens*, *Agrobacterium tumefaciens*, and *Candida albicans*.

The test agar plates containing test organisms (0.1 mL) were punched to make the wells (10 mm in diameter) using a sterilised cork borer and filled with the extract solutions (0.1 mL). Then these plates were incubated at 37 °C for 24 h. After incubation, the diameters of the growth inhibition zones surrounding the agar wells were measured in mm. These zones indicated the presence of antimicrobial activities, selectively inhibiting the growth of test organisms.

Determination of Antioxidant Activity by DPPH Free Radical Scavenging Assay

The antioxidant activity of *C. petiolata* extracts was investigated using the DPPH free radical scavenging assay with a spectrophotometric method. For the control solution, 1.5 mL of

DPPH solution was combined with 1.5 mL of ethanol in the brown bottles. The sample solutions were prepared by thoroughly mixing 1.5 mL of DPPH solution with 1.5 mL of various concentrations of the tested sample (3.91, 7.81, 15.63, 31.25, 62.50, and 125.00 µg/mL). These mixtures were incubated at room temperature and shaken on a shaker for 30 minutes. Following this incubation period, the absorbance of each solution was measured at 517 nm using a spectrophotometer (Baliyan *et al*., 2022). Absorbance measurements were conducted in triplicate for each solution, and the percent radical scavenging activity was calculated according to the following equation:

$$\% \text{ RSA} = \frac{A_{control} - (A_{sample} - A_{blank})}{A_{control}} \times 100$$

where, % RSA = percent radical scavenging activity
$A_{control}$ = absorbance of DPPH in EtOH solution
A_{sample} = absorbance of tested sample + DPPH solution
A_{blank} = absorbance of tested sample + EtOH solution

Cytotoxicity Determination Using the Brine Shrimp Lethality Bioassay

In this study, brine shrimp (*Artemia salina*) was utilised for a cytotoxicity bioassay. Artificial seawater was prepared by dissolving 38 grams of sodium chloride in 1 litre of distilled water. Brine shrimp cysts (0.5 grams) were added to 1 litre of artificial seawater in a bottle and were then placed under a lamp to provide the light necessary for hatching. The cysts required a constant oxygen supply and were incubated at room temperature for 24 h. Next, 9 mL of artificial seawater and 1 mL of sample solutions at different concentrations (1000, 100, 10, and 1 µg/mL) were added to individual chambers. Using a Pasteur pipette, 10 live brine shrimp nauplii were transferred into each chamber. They were incubated at room temperature for approximately 24 h. After this period, the number of dead or surviving brine shrimps was counted to determine cytotoxicity, and the 50 % lethal concentration (LC_{50}) was calculated as described by Baravalia *et al*. (2012). The control solution was prepared similarly, using distilled water instead of the sample solution. Caffeine and potassium dichromate were used as standards.

Determination of Anti-arthritic Activity by Egg Albumin Method

The reaction mixture (5 mL) consisted of 0.2 mL of egg albumin, 2.8 mL of phosphate-buffered saline (PBS, pH 6.4), and 2 mL of various concentrations of crude extracts from Malar rhizome, resulting in final concentrations of 7.81, 15.62, 31.25, 62.5, and 125 µg/mL. A similar volume of double-distilled water was used as a control. The mixtures were incubated at 37 °C for 15 minutes, followed by heating at 70 °C for 5 minutes. After cooling, the absorbance was measured at 660 nm. Diclofenac sodium was used as a reference drug (Sunmathi *et al*., 2016).

$$\% \text{ Protein denaturation} = \frac{A_{sample} - A_{control}}{A_{sample}} \times 100$$

$A_{control}$ = absorbance of control solution
A_{sample} = absorbance of tested sample solution

Results and Discussion

Phytochemicals Present in *C. petiolata* (Malar) Rhizome

To know the types of phytoorganic constituents present in the rhizome of *C. petiolata* (Malar), the phytochemical investigation was preliminarily carried out according to conventional methods. The results obtained from these experiments are summarised in Table 1. The

phytochemical tests revealed the presence of secondary metabolites such as alkaloids, *α*-amino acids, carbohydrates, glycosides, organic acids, reducing sugars, saponins, phenolic compounds, flavonoids, tannins, steroids, starch, and terpenoids in the sample except cyanogenic glycosides.

The main constituents of *C. petiolata* such as phenolic compounds, tannins, flavonoids, and steroids, may contribute to its bioactivities, including antimicrobial, antioxidant, and antiarthritic properties.

Table 1. Preliminary Phytochemical Screening Results of *C. petiolata* Rhizome

Tests	Extract	Reagent used	Observation	Remarks
		Dragendorff's reagent	orange ppt.	+
alkaloids	1 % HCl	Wagner's reagent	reddish brown ppt.	+
		sodium picrate	yellow ppt.	+
flavonoids	EtOH	conc. HCl and Mg ribbon	pale yellow	+
terpenoids	$CHCl_3$	acetic anhydride and conc. H_2SO_4	yellow	+
steroids	PE	acetic anhydride and conc. H_2SO_4	green	+
α-amino acids	H_2O	ninhydrin reagent	purple	+
glycosides	H_2O	10 % lead acetate	white ppt.	+
saponins	H_2O	H_2O	frothing	+
tannins	EtOH	1 % gelatin and 1 % $FeCl_3$	brown ppt.	+
carbohydrates	H_2O	5 % *α*-naphthol and conc: H_2SO_4	reddish brown ppt.	+
phenolic compounds	H_2O	10 % $FeCl_3$	deep blue ppt.	+
starch	H_2O	I_2, KI	dark-blue ppt.	+
reducing sugars	H_2O	Benedict's solution	brick-red	+
organic acids	H_2O	bromocresol green	green	+
cyanogenic glycosides	H_2O	conc. H_2SO_4, sodium picrate paper	no brick red	-

(+) = presence (-) = absence (ppt.) = precipitate

The Soluble Matter Contents of *C. petiolata* Rhizome

The soluble matter contents in some organic solvents and water were determined by the WHO method. In these experiments, the organic solvents used were ethanol, methanol, ethyl acetate, chloroform, and pet-ether. In the determination of water-soluble matter, the addition of a small amount of chloroform was necessary to prevent the fermentation of the extract. The soluble matter contents in some organic solvents such as PE, $CHCl_3$, EtOAc, EtOH, MeOH, and water calculated on dried weight of the samples were found to be 5.73 %, 2.68 %, 3.42 %, 2.83 %, 3.16

%, and 18.85 % (w/w) in rhizome, respectively (Table 2). The resulting data suggested that the soluble matter contents increase with increasing polarity of the solvents. It also indicated that the sample may contain more polar compounds.

Table 2. Soluble Matter Contents of *C. petiolata* Rhizome

Solvent	Soluble matter contents (%)
petroleum ether	5.73
chloroform	2.68
ethyl acetate	3.42
ethanol	2.83
methanol	3.16
water	18.85

Antimicrobial Activity of Crude Extracts of Malar Rhizome

The assessment of antimicrobial activity using the agar well diffusion method involves measuring the clear zone diameter around the wells. This diameter, which includes the size of the well, indicates the degree of antimicrobial activity. The results of antimicrobial activity are shown in Table 3 and Figure 1. It was found that all crude extracts have antimicrobial activity. All extracts of Malar rhizome exhibited potent activity against all tested microorganisms with inhibition zones ranging from 20 mm and above. Therefore, Malar rhizomes can be effective against a variety of diseases caused by bacteria, viruses, fungi, and parasites. Moreover, it can be used in natural medicine, food preservation, and as an environmentally friendly alternative to synthetic antibiotics.

Table 3. Inhibition Zone Diameter of Crude Extracts from *C. petiolata* by Agar Well Diffusion Method

Microorganisms	Diameter of inhibition zone (mm)				
	Watery extract	Ethanol extract	Pet-ether extract	Ethyl acetate extract	*STD
A. tumefaciens	37	28	21	20	27
B. pumilus	37	29	21	21	27
B. subtilis	38	28	21	21	27
C. albicans	38	28	21	20	27
E. coli	37	29	20	20	27
M. luteus	37	29	21	21	28
P. fluorescens	38	28	20	20	28
S. aureus	37	28	20	20	28

*STD = Chloramphenicol (for bacteria) and Nystatin (for fungus)

Agar well diameter = 8 mm 10–14 mm = weak activity

15–19 mm = moderate activity 20 mm and above = high activity

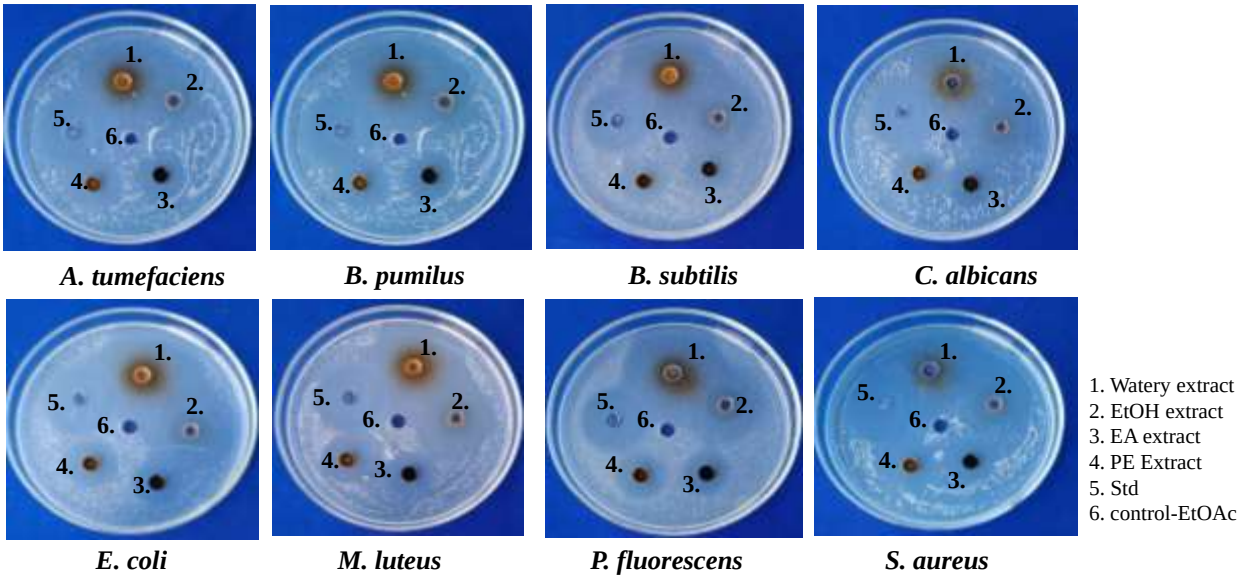

Figure 1. Effect of watery, ethanol, petroleum ether, and ethyl acetate extracts from Malar rhizome on some microorganisms

Antioxidant Activity of Extracts of *C. petiolata* Rhizome by DPPH Free Radical Scavenging Assay

The antioxidant activity of ethanol and watery extracts of the Malar rhizome was assessed by the DPPH free radical scavenging assay. DPPH is a stable free radical, which has been widely accepted as a tool for estimating the free radical-scavenging activities of antioxidants. It was found that the larger % RSA indicates the higher antioxidant activity. In contrast, the lower IC_{50} value indicates the more effective antioxidant activity. The inhibition percentage of DPPH in the presence of watery and ethanol extracts of *C. petiolata* and their IC_{50} values are shown in Table 4 and Figure 2. The IC_{50} values were observed to be 8.89 µg/mL for the watery extract and 18.34 µg/mL for ethanol extract. The watery extract was found to have higher antioxidant activity than the ethanol extract but lower than the positive control ascorbic acid (IC_{50} = 4.68 µg/mL) (Figure 3). The watery extract of *C. petiolata* has potent activity. Therefore, Malar rhizome could be used for the treatment of many diseases caused by oxidative stress.

Table 4. Average % Inhibition and IC_{50} Values of Crude Extracts of Malar Rhizome

Tested samples	% RSA ± SD of different concentrations (µg/mL)						IC_{50}
	3.91	7.81	15.63	31.25	62.5	125	(µg/mL)
watery extract	44.91 ± 0.44	49.37 ± 0.21	53.91 ± 0.53	59.62 ± 0.42	67.71 ± 0.60	71.76 ± 0.42	8.89
ethanol extract	37.59 ± 1.78	41.21 ± 1.04	47.42 ± 1.78	62.27 ± 1.92	77.55 ± 0.09	86.33 ± 0.32	18.34
Std. ascorbic acid	48.99 ± 0.53	54.03 ± 1.36	56.64 ± 0.44	63.83 ± 1.06	66.61 ± 0.35	87.13 ± 0.76	4.68

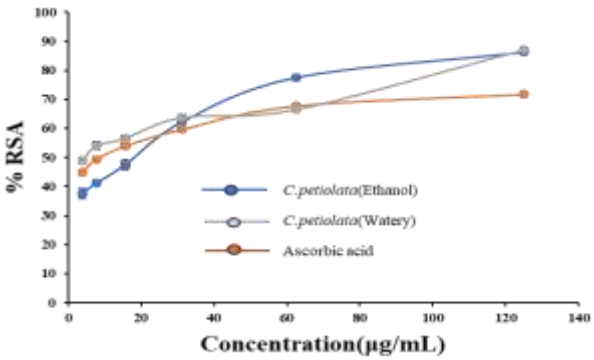

Figure 2. A plot of % RSA of different concentrations of crude extracts from *C. petiolata* rhizome

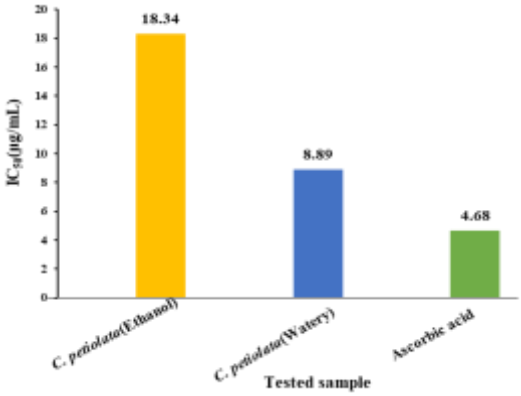

Figure 3. A bar graph of IC_{50} of crude extracts from *C. petiolata* rhizome

Cytotoxicity of Crude Extracts of Malar Rhizome

While certain plants exhibit beneficial biological properties, they can also pose risks to human health. A cytotoxicity test determines whether a product or compound will have any toxic effect on living cells. The brine shrimp lethality bioassay investigated the cytotoxicity of watery and ethanol extracts of Malar rhizome, and the results are shown in Table 5. From the results, the LC_{50} values of watery and ethanol extracts were found to be greater than 1000 µg/mL. If the LC_{50} values of samples are less than 1000 µg/mL these samples are toxic (active) and greater than 1000 µg/mL are non-toxic (inactive). The positive control ($K_2Cr_2O_7$) exhibited a significantly lower LC_{50} value of 43.75 µg/mL, classifying it as highly toxic. The negative control (caffeine) also showed an LC_{50} value greater than 1000 µg/mL, confirming no inherent cytotoxicity. Since the LC_{50} values of watery and ethanol extracts are less than 1000 µg/mL they have no cytotoxic effects and therefore, Malar is safe for use in various purposes.

Table 5. Cytotoxicity of Different Concentrations of Crude Extracts of Malar Rhizome against *Artemia salina* (Brine Shrimp)

Tested samples	% of dead brine shrimp in different concentrations of sample (µg/mL)				LC_{50} (µg/mL)
	1	10	100	1000	
watery extract	30 ± 0.00	30 ± 1.41	35 ± 2.12	35 ± 0.71	> 1000
ethanol extract	20 ± 1.41	30 ± 1.41	40 ± 1.41	47 ± 0.71	> 1000
Std. $K_2Cr_2O_7$	7 ± 1.00	20 ± 0.00	100 ± 0.00	100 ± 0.00	43.75
Std. caffeine	0 ± 0.00	23 ± 1.20	30 ± 0.58	40 ± 1.16	>1000

(caffeine – negative control and $K_2Cr_2O_7$ - positive control)

Anti-arthritic Activity of Crude Extracts of Malar Rhizome

Anti-arthritic activity of crude extracts of Malar rhizome was determined by the protein denaturation method. The effect of watery and ethanol extracts of the Malar rhizome was evaluated against denaturation of egg albumin and showed 12.73 µg/mL and 19.18 µg/mL (Table 6 and Figure 4), respectively. From the results shown in Figure 5, the IC_{50} value of the ethanol extract of the malar rhizome is lower than that of the watery extract. The IC_{50} value of the watery extract is close to standard and it has more anti-arthritic potency than the ethanol extract since the lower the IC_{50} value, the higher the anti-arthritic activity. So, the watery extract of malar rhizome can serve as a potent anti-arthritic agent and it could be used for treatments such as skin inflammation, gout, osteoarthritis, and rheumatoid arthritis.

Table 6. Average % Protein Denaturation and IC_{50} Values of Crude Extracts of Malar Rhizome

Tested samples	% protein denaturation ± SD of different concentrations (µg/mL)						IC_{50} (µg/mL)
	7.81	15.62	31.25	62.5	125	250	
watery extract	38.95 ± 0.40	56.55 ± 1.34	64.81 ± 0.35	74.28 ± 0.13	79.26 ± 0.10	85.30 ± 0.18	12.73
ethanol extract	7.64 ± 0.00	20.83 ± 0.00	52.64 ± 0.64	64.80 ± 0.89	69.59 ± 0.75	79.18 ± 0.21	19.18
St. diclofenac sodium	45.69 ± 0.85	53.23 ± 0.00	60.26 ± 0.66	70.28 ± 1.14	79.39 ± 0.75	85.96 ± 0.24	12.28

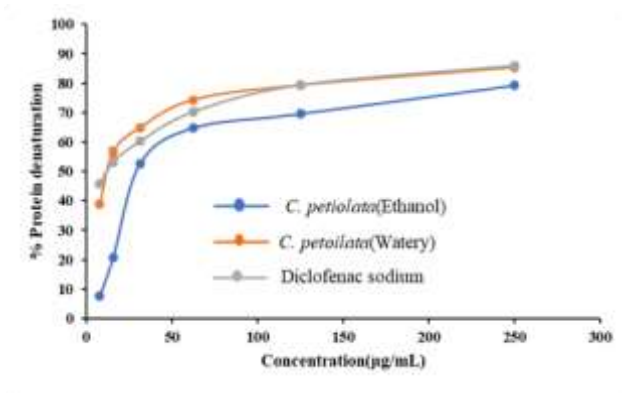

Figure 4. A plot of % protein denaturation of different concentrations of crude extracts from *C. petiolata* rhizome

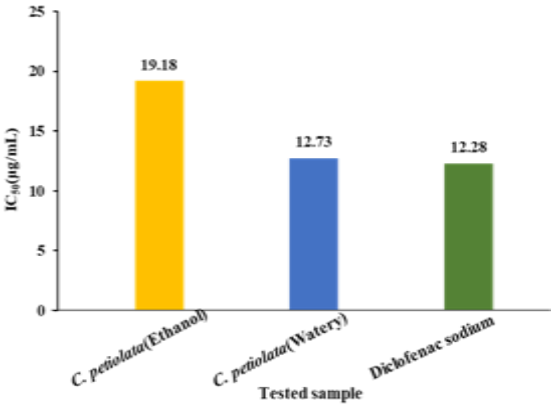

Figure 5. A bar graph of IC_{50} of crude extracts from *C. petiolata* rhizome

Conclusion

From the research on the bioactivity of *Curcuma petiolata* (Malar) rhizome, the inferences could be deduced as follows. Based on the data, the antimicrobial activity of watery and ethanol extracts is potent. The antioxidant activity of the watery extract (IC_{50} = 8.89 μg/mL) is more effective than that of the watery extract (IC_{50} = 18.34 μg/mL). According to the cytotoxic effect, ethanol and watery extracts from the *C. petiolata* rhizome were observed to be free from toxic effects up to 1000 μg/mL. In terms of anti-arthritic activity, the ethanol extract (IC_{50} = 12.7 μg/mL) was more effective than the watery extract (IC_{50} = 19.18 μg/mL). Malar rhizome reveals its significant potential as a natural therapeutic agent, showing strong antioxidant properties that may help migrate oxidative stress-related diseases. Its antimicrobial effect indicates against bacterial and fungal infections. Cytotoxicity results exhibit further safety evaluation, and its anti-arthritic activity highlights its potential for managing inflammatory conditions. Studying the biological activities of *C. petiolata* helps us understand its traditional medicinal uses and highlights its potential as a source of new medicines.

Acknowledgements

The author wish to extend their heartfelt thanks to Drs Prema, Thandar Aung for Supervision of this Research.

References

Ammon, H. P., M. I. Anazodo, H. Safayhi, B. N. Dhawan, and R. C. Srimal. (1992). "Curcumin: A Potent Inhibitor of Leukotriene B4 Formation in Rat Peritoneal Polymorphonuclear Neutrophils (PMNL)". *Planta Med.*, vol. **58** (2), pp. 226–228.

Baliyan, S., R. Mukherjee, A. Priyadarshini, A. Vibhuti, A. Gupta, R. P. Pandey, and C. M. Chang. (2022). "Determination of Antioxidants by DPPH Radical Scavenging Activity and Quantitative Phytochemical Analysis of *Ficus religiosa*". *Molecules*, vol. **27**, pp. 1–19.

Baravalia, Y., Y. Vaghasiya, and S. Chanda. (2012). "Brine Shrimp Cytotoxicity, Anti-inflammatory and Analgesic Properties of *Woodfordia fruticosa* Kurz Flowers". *Iranian Journal of Pharmaceutical Research*, vol. **11** (3), pp. 851–861.

Haddad, M., M. Sauvain, and E. Deharo. (2011). "*Curcuma* as a Parasiticidal Agent: A Review". *Planta Med.*, vol.**77** (6), pp. 672–678.

Hatcher, H., R. Planalp, J. Cho, F. M. Torti, and S. V. Torti. (2008). "Curcumin: from Ancient Medicine to Current Clinical Trials". *Cell Mol. Life Sci.*, vol. **65** (11), pp. 1631–1652.

Jayaprakasha, G. K., L. J. Rao, and K. K. Sakariah. (2006). "Antioxidant Activities of Curcumin, Demethoxycurcumin and Bisdemethoxycurcumin". *Food Chem.*, vol. **98** (4), pp. 720–724.

Kress W.J., L.M. Prince, and K.J. Williams. (2002). "The Phylogeny and a New Classification of the Gingers (Zingiberaceae): Evidence from Molecular Data". *American Journal of Botany*, vol. **89**, pp. 1682–1696.

Newman, D. J. and G. M. Cragg. (2016). "Natural Products as Sources of New Drugs over the 30 years from 1981 to 2014". *Journal of Natural Products*, vol. **79** (3), pp. 629–661.

Sunmathi, D., R. Sivakumar, and K. Ravikumar. (2016). "*In vitro* Anti-inflammatory and Antiarthritic Activity of Ethanolic Leaf Extract of *Alternanthera sessilis* (L.) R.BR. ex DC and *Alternanthera philoxeroides* (Mart.) Griseb". *Int. J. Adv. Phar., Biol. and Chem.*, vol. **5** (2), pp. 109–115.

Wagner, H. and G. Ulrich-Merzenich. (2009). "Synergy Research: Approaching a New Generation of Phytopharmaceuticals". *Phytomedicine*, vol. **16** (2-3), pp. 97–110.

INVESTIGATION OF ACUTE TOXICITY, ANTIMICROBIAL ACTIVITY, ANTIOXIDANT ACTIVITY OF THE STEM BARK OF *Dalbergia cultrata* Graham Ex Benth. (Yin Daik)

May Theint[1], Kay Khaing Win[2], Tin Myo Thant[3], Myo Thida Chit[4]

Abstract

One of Myanmar's medicinal plant, *Dalbergia cultrata* Graham Ex Benth. was selected for chemical investigation and partial structure elucidation. Firstly, the phytochemical screening of the stem bark of *D. cultrata* was performed by standard method, indicating the presence of α-amino acids, carbohydrates, flavonoids, glycosides, phenolic compounds, reducing sugars, saponins, tannins, steroids and terpenoids. In addition, the OECD Guidelines of Limit Test (425) examined the acute oral toxicity test to determine a test sample's median lethal dose (LD_{50}). Based on the result, a 2000 mg/kg ethanol extract dose showed no signs of acute toxicity in all the experimental mice. However, one animal died at a dose of 5000 mg/kg, indicating that this dosage is approaching or surpassing the LD_{50} threshold. The administration of 2000 mg/kg ethanol extract to the test animals showed the results of normal to significant weight gain in all the animals. However, at 5000 mg/kg, animal 3 showed considerable weight loss, which showed that the dose may have caused adverse effects in some individuals. The Agar well diffusion method evaluated the antimicrobial activity of *n*-hexane, dichloromethane, ethyl acetate, watery, and ethanol extracts. It was found that ethanol and ethyl acetate extracts showed high activity on all organisms except *Bacillus substilis* and *Escherichia coli.* The antioxidant activity of ethyl acetate and ethanol extracts was evaluated using the DPPH assay method. It was found that ethyl acetate extract showed higher antioxidant activity than ethanol extract.

Keywords: *Dalbergia cultrata*, acute toxicity, antimicrobial activity, antioxidant activity, phytochemical

Introduction

Dalbergia is a large genus of trees, shrubs, lianas, and woody climbers in the pea family, the Fabaceae, consisting of approximately 274 accepted species widely distributed in the tropical and subtropical regions of the world, such as South Africa and India, Laos, Myanmar, Thailand and Vietnam in Asia (Aye *et al*., 2019). Members of the genus enjoy several traditional uses all over the world. Various species are widely used in the treatment of different ailments like aphthae, bleeding piles, cough, diarrhoea, dysentery, dyspepsia, epigastric, epistaxis, gonorrhoea, haemorrhages, leprosy, malaria, rheumatism, scabies, scalding urine, stomach ache, syphilis, traumatic injuries, and ulcers, etc. (Saha *et al.*, 2013). Species are also used for their analgesic, anthelmintic, anti-inflammatory, antimicrobial, antipyretic, anti-spermicidal, anti-ulcerogenic, aphrodisiac, astringent, expectorant, and larvicidal activities in traditional medicine (Bekker *et al*., 2002). Some species are validated through pharmacological investigations, while others require scientific investigations to rationalise their traditional uses. The plant family is known to contain isoflavonoids and neoflavonoids (Chan *et al*., 1997). Several phytochemical constituents like isoflavonoids, neoflavonoids, glycosides, cinnamyl phenols, quinones, and furans have been isolated from different species of *Dalbergia* (Innocent, 2012).

D. cultrata was selected for chemical and pharmacological activity analyses in this research work. The present research aims to investigate the acute toxicity, antimicrobial activity, and antioxidant activity of various crude extracts of the stem bark of *D. cultrata*.

[1] Department of Chemistry, Yadanabon University
[2] Department of Chemistry, University of Mandalay
[3] Department of Chemistry, University of Mandalay
[4] Department of Chemistry, University of Mandalay

Family - Fabaceae

Scientific name - *Dalbergia cultrata* Graham Ex Bentham

English name - Rosewood

Common name - Yin daik

Part used - Stem bark

Medicinal uses - Leishmania diseases and cancer diseases

The trunk and leaves of *Dalbergia cultrata* Grahm Ex Benth. are described in Figure 1.

Botanical description of *D. cultrata*

Figure 1. Trunk and Leaves of *Dalbergia cultrata* Grahm Ex Benth.

Materials and Methods

Collection and Preparation of Samples

The stem bark of *D. cultrata* was collected from Pyin Oo Lwin Township, Mandalay Region. Firstly, the collected bark sample was cleaned, then chopped into small pieces and allowed to air dry in the ventilated room for about two weeks. This air-dry sample was kept in a glass bottle with a stopper and it was used throughout the experiment.

Phytochemical Investigation of the Stem Bark of *D. cultrata*

Phytochemical investigation of the stem bark of *D. cultrata* was performed by the standard method (Harborne, 1998).

Extraction of Crude Extracts from the Stem Bark of *D. cultrata*

About 2.2 kg of airdried sample was percolated with 6.5 L of 95 % ethanol thrice for four days. The obtained solution was filtered and the filtrate was removed by a rotatory evaporator then this extract sample was evaporated at room temperature and the ethanol crude extract was obtained. The obtained ethanol crude extract was dissolved by (1:1) v/v of ethanol and *n*-hexane and then stirred using a magnetic stirrer. The obtained solution was partitioned with 200 mL *n*-hexane, with a solution of 200 mL H_2O and 200 mL dichloromethane, and with 200 mL ethyl acetate by using a separating funnel three times for each respectively. Then 10.50 g of *n*-hexane extract, 10.36 g of dichloromethane extract, 3.99 g of ethyl acetate extract, and 10.50 g of watery extract were obtained.

Determination of Acute Toxicity of Ethanol Extract from the Stem Bark of *D. cultrata*

The acute toxicity of an ethanolic extract of *D. cultrata* stem bark was determined using the OECD Guidelines of Limit Test (425) in an in vivo mouse model. This experiment was done at the Department of Biotechnology of Mandalay Technological University in the Mandalay Region.

In this study, the acute oral toxicity test followed the OECD Guidelines of Limit Test (425) which aims to determine the median lethal dose (LD_{50}) of a test substance. The test involved administering two different doses of *D. cultrata* ethanol extract (2000 mg/kg and 5000 mg/kg) to the tested mice and monitoring for signs of mortality and clinical symptoms over a specific observation period. A control group was also included, receiving 2 mL of 20 % ethanol.

Procedure: The study begins with the determination of a starting dose, often chosen based on existing information or estimates. Alternatively, a limit test may be conducted when the LD_{50} is assumed to be higher than the limit dose (e.g., 2000 mg/kg). The first animal is administered the test substance at the chosen dose level (e.g., 2000 mg/kg) and observed for toxicity or death. After administering the dose, the animal is monitored for signs of toxicity over 48 h. Observations include behavioural changes, weight loss, or death. If no lethal effects are observed, another animal is tested at a higher dose to determine the threshold of toxicity. If lethal effects are observed, the dose is adjusted downward for the next animal. If toxicity is observed at either a dose of 2000 mg/kg or 5000 mg/kg, the dose is reduced for the next animal, and the process continues following the "Up-and-Down" method. The process of dosing and observation continues, with doses increased or decreased based on the response of the animals. More animals are tested following the up-and-down procedure to narrow down the LD_{50} estimate.

The study is concluded when sufficient data is gathered to make a reliable estimate of the LD_{50} (the dose at which 50 % of the animals die) or to classify the test substance based on its toxicity. The results are analyzed, and the LD_{50} is determined based on the cumulative data. This information helps to assess the substance's acute toxicity classification. This method minimizes the number of animals used while ensuring a precise estimate of the test substance’s toxicity.

Determination of Antimicrobial Activity of the Stem Bark of *D. cultrata*

The antimicrobial activity of *n*-hexane, dichloromethane, ethyl acetate, watery, and ethanol extracts of the stem bark of *D. cultrata* was determined by applying the agar well diffusion method in the Department of Chemistry, University of Mandalay. The test microorganisms used for the antibacterial activity screening were *Agrobacterium tumerfaciens, Bacillus substilis, Micrococcus luteus, Pseudomonas fluorescens, Escherichia coli, Salmonella typhi.*

Procedure: The crude extract ($20\ \mu L$) was used to check the antimicrobial activity against test organisms by the agar well diffusion method. Well, having an 8 mm diameter was utilised for antimicrobial assay. The assay medium was prepared with 1 % glucose, 0.3 % polypeptone, 0.1 % KNO_3, 1.8 % agar, and 100 mL distilled water at pH 6.5 was used for the antimicrobial activity test. One percent of the test organism was added to the assay medium and then poured into plates. After solidification, wells impregnated with sample (crude extract) were filled on the agar plates and were incubated for 24 – 36 hours at room temperature. Clear zones (inhibitory zones) surrounding the test well indicate the presence of bioactive metabolites which inhibit the growth of test organisms (Collins *et al*., 2004).

Determination of Antioxidant Activity of Crude Extracts of the Stem Bark of *D. cultrata* by DPPH Assay Method

In this present research work, the determination of the antioxidant activity of ethanol extract and ethyl acetate extract of the stem bark of *D. cultrata* was performed by the DPPH Assay method at the Department of Chemistry, University of Mandalay.

Procedure: DPPH radical scavenging activity was determined by the UV-visible spectrophotometric method. The control solution was prepared by mixing 0.002 % DPPH solution (2 mL) and 70 % ethanol (2 mL). The sample solution was prepared by thoroughly mixing 0.002 % (w/v) DPPH solution (2 mL) and the test sample solution (2 mL). The solution was allowed to stand at room temperature for 30 minutes. Absorbance of the solution was measured at 517 mm by using a spectrophotometer and percent inhibition was calculated by using the following equation:

$$\% \text{ Inhibition} = \left[\frac{A_{DPPH} - (A_{Sample} - A_{Blank})}{A_{DPPH}}\right] x\ 100$$

where, % Inhibition = percent inhibition of test sample

A_{DDPH} = absorbance of DPPH in EtOH solution,

A_{Sample} = absorbance of sample and DPPH solution,

A_{Blank} = absorbance of sample and EtOH solution

Results and Discussion

Phytochemicals of the Stem Bark of *D. cultrata*

Preliminary phytochemical analysis of the bark of *D. cultrata* detected the presence of flavonoids, glycosides, phenolic compounds, saponins, α-amino acids, reducing sugars, tannins, steroids, and terpenoids, and the absence of alkaloids. These results are shown in Table 1.

Table 1. Results of Phytochemical Screening of the Stem Bark of *Dalbergia cultrata*

No.	Constituents	Extract	Reagents used	Observation	Results
1	alkaloids	1% HCl	Dragendorff's Wagner's Mayer's	no orange ppt no reddish brown ppt no white ppt	-
2	α-amino acids	DW	Ninhydrin	violet colour spot	+
3	flavonoids	EtOH	Mg turning and conc. H_2SO_4	red colour solution	+
4	glycosides	EtOH	10% lead acetate	yellow ppt	+
5	phenolic	EtOH	10% $FeCl_3$	brown colour ppt	+
6	reducing sugars	DW	Benedict's solution	brick red ppt	+
7	saponins	DW	distilled water	frothing solution	+
8	steroids	Pet-ether	acetic anhydride and conc: H_2SO_4	green colour solution	+
9	tannins	EtOH	10% $FeCl_3$ and conc. H_2SO_4	white ppt	+
10	terpenoids	EtOH	$CHCl_3$, acetic anhydride and conc. H_2SO_4	red ppt	+

(+) = presence, (-) = absence, ppt = precipitate

Acute Toxicity of the Ethanol Extract from the Stem Bark of *D. cultrata*

The acute oral toxicity test followed the OECD Guidelines of Limit Test (425), which aims to determine the median lethal dose (LD_{50}). The test involved administering two doses of *D. cultrata* ethanol extract (2000 mg/kg and 5000 mg/kg) to the tested mice and monitoring for signs of mortality and clinical symptoms over a specific observation period. A control group was also included, receiving 2 mL of 20 % ethanol. These results are shown in Table 2.

Table 2. Observations of Acute Oral Toxicity in Different Dosages of Ethanol Extract of *D. cultrata* Compared with the Control Group

Dose of sample (mg/kg)	Total mice	Observation	Number of mice alive/dead on day by day									
			1	**2**	**3**	**4**	**5**	**6**	**7**	**8**	**9**	**10**
2000	5	alive	5	5	5	5	5	5	5	5	5	5
		dead	0	0	0	0	0	0	0	0	0	0
5000	5	alive	4	4	4	4	4	4	4	4	4	4
		dead	1	1	1	1	1	1	1	1	1	1
20 % ethanol 2 mL (control)	5	alive	5	5	5	5	5	5	5	5	5	5
	5	dead	0	0	0	0	0	0	0	0	0	0

The data suggests that *D. cultrata* extract at 2000 mg/kg does not exhibit acute toxicity, as no mortality was observed in this group. However, at 5000 mg/kg, one subject died, indicating that this dosage is close to or exceeds the LD_{50} threshold. The single mortality at 5000 mg/kg could indicate inter-individual variability in response to the extract. The control group experienced no mortality or adverse effects, confirming the non-toxicity of the 20 % ethanol solution.

Table 3. Observations of Individual Body Weight Data after Treatment of Ethanol Extract of *D. cultrata* (2000 mg/kg)

Animal	Body weight (g) before and after treating with ethanol extract		
	Day 0	**Day 7**	**Day 14**
1	25.73	26.10	26.62
2	25.76	27.7	28.69
3	25.61	25.83	28.3
4	26. 3	27. 93	28. 61
5	26.1	26.37	29.31

The individual body weight (g) of the tested mice after administering 2000 mg/kg ethanol extract of *D. cultrata*. It was observed that normal to significant weight gain in all animals is shown, indicating that the dose may have no adverse effect. This result is shown in Table 3.

Table 4. Observations of Individual Body Weight Data after Treatment of Ethanol Extract of *D. cultrata* (5000 mg/kg)

Animal	Body weight (g) before and after treating with ethanol extract		
	Day 0	Day 7	Day 14
1	27.01	-	-
2	27.13	27.3	27.8
3	27.04	24.9	24.9
4	27.90	29.83	30.61
5	27.43	31.59	32.1

The individual body weight (g) of the tested mice after administering 5000 mg/kg ethanol extract of *D. cultrata*. It was found that animal 3 showed significant weight loss, indicating that the dose may have adverse effects in some individuals. This result is shown in Table 4.

Antimicrobial Activity of the Stem Bark of *D. cultrata*

The antimicrobial activity of *n*-hexane, dichloromethane, ethyl acetate, watery and ethanol extracts of the stem bark of *D. cultrata* was determined by applying the agar well diffusion method on six selected organisms (*Agrobacterium tumerfaciens, Bacillus substilis, Micrococcus luteus, Pseudomonas fluorescens, Escherichia coli, Salmonella typhi)*). The results are shown in Table 5 and Figure 2.

Table 5. Antimicrobial Activity of the Stem Bark of *D. cultrata*

Extracts	Inhibition zone diameters (mm)					
	I	II	III	IV	V	VI
n-Hexane	-	-	-	-	-	-
DCM	-	12 (+)	-	26 (+++)	18 (++)	-
EtOAc	20 (+++)	-	23 (+++)	21 (+++)	-	18 (++)
Watery	-	-	-	23 (+++)	-	23 (+++)
EtOH	24 (+++)	-	23 (+++)	23 (+++)	-	24 (+++)

I – *A. tumerfaciens,* II - *B. substilis*
III - *M. luteus,* IV- *P. fluorescens*
V - *E. coli,* VI- *S. typhi*

Agar well diameter		8 mm
< 12 mm	(-)	no activity
13 mm -15 mm	(+)	low activity
16 mm - 20 mm	(++)	high activity
> 21 mm	(+++)	very high activity

The antimicrobial activity of the crude extracts is shown in Table 5. According to this table, *n*-hexane extract did not show antimicrobial activity on all tested organisms. Furthermore, dichloromethane extract showed very high activity on *Pseudomonas fluorescens*, medium activity on *Escherichia coli*, and low activity on *Bacillus substilis* but had no activity on other test organisms. Moreover, the ethanol and ethyl acetate extract showed very high activity on all tested organisms except *Bacillus substilis* and *Escherichia coli.* Watery extract had very high activity on *Pseudomonas fluorescens* and *Salmonella typhi* but no activity on other test organisms.

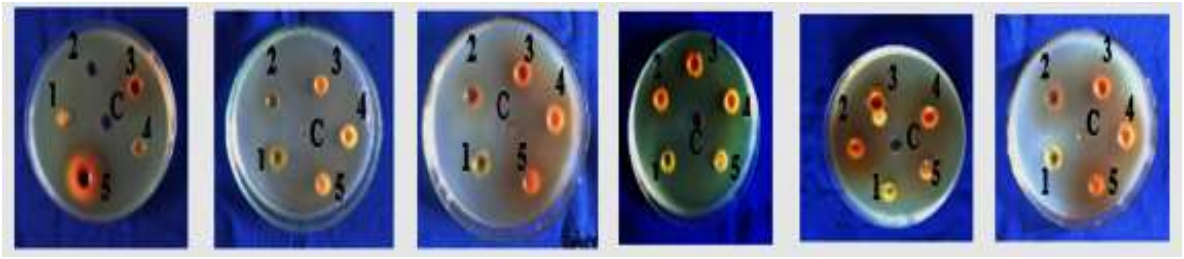

Pseudomonas fluorescens | *Salmonella typhi* | *Micrococcus luteus* | *Agrobacterium tumerfaciens* | *Bacillus substili* | *Escherichia coli*

1. *n*-hexane extract 2. DCM extract 3. EtOAc extract

4. Watery extract 5. EtOH extract C. Control

Figure 2. Inhibition zones of the antimicrobial activity of various extracts from the stem bark *D. cultrata*

The inhibition zones of the antimicrobial activity of various extracts are shown in Figure 2. Zone of inhibition (ZOI) is used to determine if the tested organism is susceptible (ZOI produced), intermediate (small ZOI produced), or resistant (no ZOI produced) to the antimicrobial agent. According to these results, *n*-hexane extract showed no ZOI in all the bacterial plates, indicating that it has no activity on all the tested bacteria. DCM extract showed large ZOI in *P. fluorescens*, medium in *E. coli*, small in *B. substilis*, and no ZOI in *A. tumerfaciens, M. luteus, S. typhi*, resulting that DCM extract had very high activity on *P.fluroenscens*, high activity on *E.coli*, low activity on *B. substilis* and no activity on *A. tumerfaciens, M. luteus, S. typhi.* The EtOAc extract had large ZOI in *A. tumerfaciens, M. luteus, P. fluorescens*, medium in *S. typhi*, and no ZOI in *B. substilis* and *E. coli*, indicating that very high activity on *A. tumerfaciens, M. luteus, P. fluorescens*, and high activity on *S. typhi*, and no activity on *B. substilis* and *E. coli*. The watery extract had large ZOI in *P. fluorescens* and *S. typhi*, and no ZOI in *A. tumerfaciens, B. substilis, M. luteus*, and *E. coli*, indicating that watery extract showed very high activity on *P. fluorescens* and *S. typhi*, and no activity on *A. tumerfaciens, B. substilis, M. luteus*, and *E. coli*. The EtOH extract had large ZOI in *A. tumerfaciens, M. luteus, P. fluorescens*, and *S. typhi*, and no ZOI in *B. substilis* and *E. coli*, indicating that very large activity on *A. tumerfaciens, M. luteus, P. fluorescens*, and *S. typhi*, and no activity on *B. substilis* and *E. coli.* According to the results, EtOAc and EtOH extracts have very high and high antimicrobial activity on the tested microorganisms except *B. substilis* and *E. coli*, and *n*-hexane extract has no activity on all tested microorganisms.

Antioxidant Activity of the Stem Bark of *D. cultrata*

IC_{50} values of ethyl acetate extract and ethanol extract from the stem bark of *D. cultrata* were observed to be 10.14 µg / mL and 98.71 µg /mL, respectively. The antioxidant activity of *D. cultrata was* lower than standard ascorbic acid with an IC_{50} value of 5.23 µg /mL. These results are shown in Tables 6, 7, and 8 and in Figures 3, 4, and 5.

Table 6. Antioxidant Activity of Ethyl Acetate Extract of *D. cultrata*

No.	Sample concentration (µg/mL)	Absorbance	(%) Inhibition	IC_{50} (µg/mL)
1	6.25	0.301	43.95	10.14
2	12.5	0.253	52.89	
3	25	0.212	60.52	
4	50	0.158	70.58	
5	100	0.027	94.97	

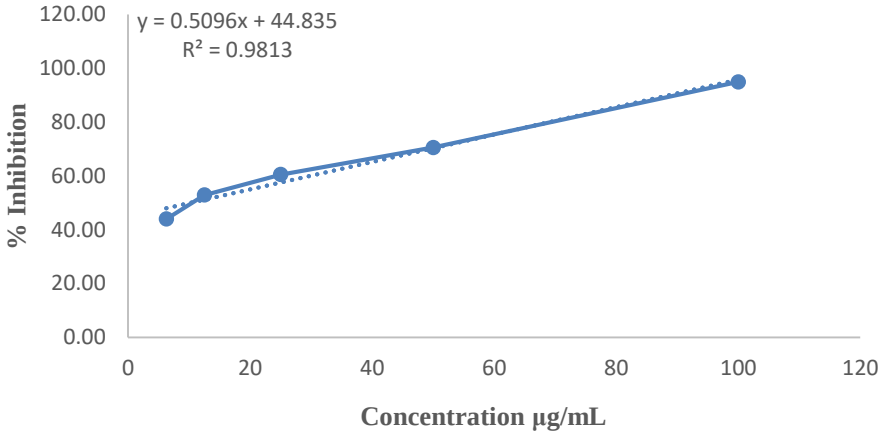

Figure 3. Percent inhibition of ethyl acetate in various concentrations

Table 7. Antioxidant Activity of Ethanol Extract of *D. cultrata*

No.	Sample concentration (µg/mL)	Absorbance	(%) Inhibition	IC_{50} (µg/mL)
1	25	0.341	36.50	98.71
2	50	0.315	41.34	
3	100	0.256	52.33	
4	200	0.171	68.16	
5	400	0.023	95.72	

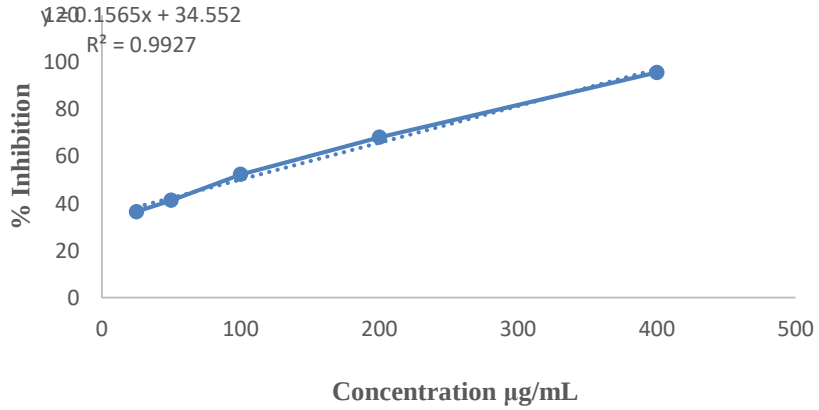

Figure 4. Percent inhibition of ethanol extract in various concentrations

Table 8. Antioxidant Activity of Ascorbic Acid *D. cultrata*

No	Sample concentration (µg/mL)	Absorbance	(%) Inhibition	IC_{50} (µg/mL)
1	1	0.228	32.34	
2	2	0.219	35.01	
3	4	0.178	47.18	5.23
4	8	0.129	61.72	
5	16	0.021	93.77	

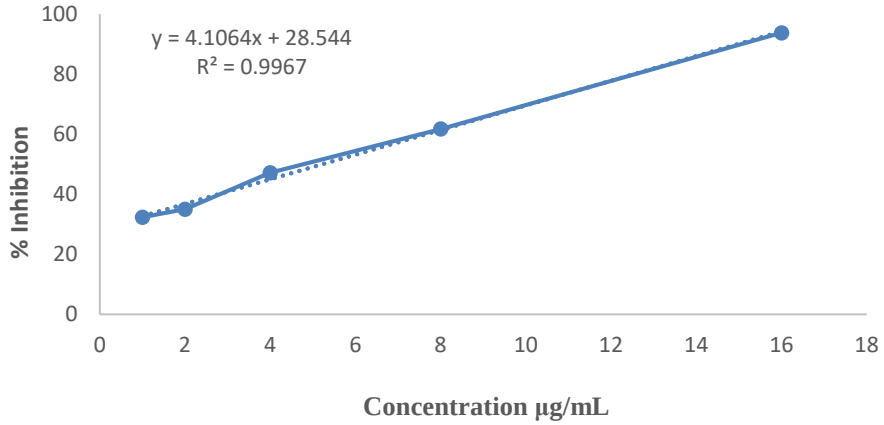

Figure 5. Percent inhibition vs various concentrations of ascorbic acid

From these results, the antioxidant activity of ethyl acetate extract was found to be higher than ethanol extract and it was also found to be lower than that of standard ascorbic acid (IC_{50} = 5.23 µg/mL). Therefore, this result indicates that the ethyl acetate extract of the stem bark of *D. cultrata* has significant antioxidant activity.

Conclusion

The stem bark of *D. cultrata* was chosen for chemical investigation and pharmacological activity screening. The stem bark of *D. cultrata* contains various chemical constituents such as α-amino acids, carbohydrates, flavonoids, glycosides, phenolic compounds, reducing sugars, saponins, tannins, steroids, and terpenes. Additionally, an acute oral toxicity test of 95 % ethanolic extract from the stem bark of *D. cultrata* was carried out following the OECD Guidelines of Limit Test (425), which are designed to determine the median lethal dose (LD_{50}) of a test sample. According to the results, it was found that none of the experimental mice showed signs of acute toxicity at 2000 mg/kg of *D. cultrata* extract. However, at 5000 mg/kg, one animal died, suggesting that this dosage is near or exceeds the LD_{50} threshold. In addition, a 2000 mg/kg dose of the extracted sample resulted in normal to significant weight gain in all animals. In contrast, at 5000 mg/kg, animal 3 experienced considerable weight loss, implying that this higher dose may have caused adverse effects in certain individuals. The antimicrobial activity of *n*-hexane extract, dichloromethane extract, ethyl acetate extract, watery extract, and ethanol extract of the stem bark of *D. cultrata* were investigated by agar well diffusion method. It was found that *n*-hexane extract did not show antimicrobial activity on all tested organisms. Furthermore, dichloromethane extract showed very high activity on *Pseudomonas fluorescens,* high activity on *Escherichia coli,* and low activity on *Bacillus substilis* but had no activity on other test organisms. Moreover, the ethanol and ethyl acetate extract showed very high activity on all tested

organisms except *Bacillus substilis* and *Escherichia coli.* Watery extract had very high activity on *Pseudomonas fluorescens* and *Salmonella typhi* but no activity on the remaining test organisms. The antioxidant activity of ethyl acetate and ethanol extracts of the stem bark of *D. cultrata* was evaluated by the DPPH assay method. It was found that the ethyl acetate extract was more potent than the ethanol extract of the sample in the antioxidant activity.

Acknowledgements

I wish to express my sincere thanks to Professor and Head, Dr. Thinn Myat Nwe, Department of Chemistry, University of Mandalay for their kind permission, invaluable advice and kind guidance on my research work. I wish to express my sincere thanks to Professor and Head, Dr Suu Suu Win, Department of Chemistry, Yadanabon University for their close supervision and kind guidance on my research work.

References

Aye, M. M., H.T. Aung, M.M. Sein, and C. Armijos. (2019). "A Review on the Phytochemistry, Medicinal Properties and Pharmacological Activities of 15 Selected Myanmar Medicinal Plants". *Journal of Molecules,* vol. 24(2), pp.293-297.

Bekker, M., E. Malan, J.A. Steenkamp, and E.V. Brandt. (2002). "An Isoflavanoid–neoflavonoid and O-methylated Isoflavone from the Heartwood of *Dalbergia nitidula"*. *Journal of Phytochemistry*, vol. 59(4), pp.415–418.

Chan, S.C., Y.S. Chang, and S.C. Kuo. (1997). "Neoflavonoids from *Dalbergia odorifera*". *Journal of Phytochemistry*, vol. 46(5), pp. 947–949.

Collins, C. H., P.M. Lyne, J.M. Grange, and J.O. Falkinham. (2004). *Microbiological Methods*. New York: 8th Ed., CRC Publisher, Oxford University Press Inc., pp. 82-90.

Harborne, J. B. (1998). *Phytochemical Methods, A Guide to Modern Techniques of Plant Analysis.* New York: 2nd Ed., Chapman and Hall, pp. 120-160.

Innocent, E. (2012). "A new isoflavone glycoside from *Dalbergia vacciniifolia* (Fabaceae)*". Journal of Scientia Pharmaceutica,* vol. 8, pp. 469-474

OECD, O. "425-Guidelines for the Testing of Chemicals Acute Oral Toxicity-Fixed Dose Procedure." *Animals* (2001).

Saha, S., M. Anisuzzman, M.K. Islam, H. Mondal, and C. Talukder. (2013). "Antibacterial and cytotoxic potential of *Dalbergia spinosa* Roxb. Leaves*". International Journal of Pharmaceutical Sciences and Research*, vol. 4(2), pp. 512-515.

ASSESSMENT OF THE WATER QUALITY NEAR SPECIAL ECONOMIC ZONE (THILAWA)

Soe Yan Naing Win[1], Jue Jue Khin[2], Ye Myint Aung[3], Hnin Hnin Than[4]

Abstract

This study highlights growing concerns about water pollution due to the development of the Thilawa Special Economic Zone (SEZ) and ongoing BOBLME activities, emphasizing the urgent need for action. Water samples were collected from 5 ft depth at 10 GPS-marked sites in June 2024. The analysis focuses on the physicochemical, elemental, and microbial properties of the water. The research aims to evaluate environmental impacts by analyzing various water quality parameters, such as pH, temperature, dissolved oxygen, and biological and chemical oxygen demand, to determine the aquatic environment's health. Electrical conductivity, total dissolved solids, alkalinity, hardness, chlorinity, and salinity were measured to understand ionic composition and salinity levels. Chlorophyll-*a* was analyzed to estimate the abundance of phytoplankton, and nutrient concentrations (nitrogen and phosphate) were evaluated for nutrient pollution. Total nitrogen (1.58 to 1.92 ppm) and orthophosphate (0.062 to 0.215 mg/L) contents indicated moderate nutrient levels of mesotrophic. Microbial analysis targeted coliforms and *E. coli* to assess contamination risks, while trace metals were examined to detect potential toxic elements. The results were compared to WHO, EPA, and ASEAN standards.

Keywords: Thilawa (SEZ), water quality parameters, trace metals, chlorinity, mesotrophic

Introduction

Water covers 70% of the Earth's surface and is the most abundant liquid, essential for all living things. Without water, there would be no plants, animals, or humans (Maung Kyaw, 2016). This highlights the need to study water quality and ensure access to clean water for both human health and the environment. The BOBLME is innovative with a strong focus on how fishery and management, habitats, and livelihoods interest. The project will also have a focus on marine pollution and reduction of plastics from fishing (Kyaw Naing, 2011). Thilawa Special Economic Zone (SEZ) serves as a major industrial hub and the largest port for international cargo and gas tankers, playing a key role in the transportation of gas, oil, and petroleum products. However, leaks of these substances into the river have caused environmental pollution, threatening aquatic life and human health. Such incidents raise concerns about the ecological health of the river system. As important as Myanmar's central industrial area, Thilawa SEZ requires a thorough evaluation of water quality to monitor pollution effectively. This research aims to systematically collect and analyze water samples from Thilawa SEZ, addressing issues of contamination from chemicals, waste, and bacteria. Ensuring water quality is critical for sustaining both the environment and public health (Kaly, 2004).

Materials and Methods

The research was conducted in the Thilawa Special Economic Zone (SEZ), located at 20°35'18" N latitude and 93°35'11" E longitude. Water samples were collected 5 feet from ten sampling sites (Table 1) below the surface water using a water pump in June 2024 to evaluate the physicochemical characteristics of the aquatic environment. On-site measurements for parameters like water temperature, pH, and dissolved oxygen (DO) were taken immediately after collection. The samples were stored in pre-cleaned polyethylene bottles, pre-treated by soaking in

[1] Department of Chemistry, Dagon University
[2] Department of Chemistry, University of Yangon
[3] Department of Chemistry, University of Yangon
[4] Department of Chemistry, Dagon University

5 M HCl for over three days and rinsed with distilled-deionized water. After five days of incubation, the biochemical oxygen demand (BOD) was measured using a dissolved oxygen meter (Model HI-9145, Portugal). Chemical oxygen demand values were analyzed by using a COD meter (Model MD-200, Germany). Electrical conductivity and total dissolved solids of the collected water samples were determined by using EC/TDS meter (Model HI-99301, Romania). Alkalinity of water samples was determined by the titration method, and total hardness values were examined by Total Hardness Photometer (Model HI-9773, Romania). Chlorinity and salinity were determined using Mohr's titration method, and chlorophyll *a* values were determined by the Spectrophotometric method, while some mineral contents (Cr, Mn, Cd, Zn, Fe, As, and Hg) were analyzed via atomic absorption spectrophotometry. The total nitrogen content of the ten water samples was determined using the Azo dye method, while the total phosphate content was analyzed using the colorimetric molybdenum blue method. Microbial properties (total coliform and *E.coli*) of water samples were investigated by multiple tube method. The ten sampling locations are displayed in Table 1, with satellite images of Thilawa SEZ in Figure 1.

Table 1. Sampling Locations of Water Samples in Thilawa (SEZ)

No.	Sampling sites	Positions	
		Longitude (E)	Latitude (N)
1	Site 1	96° 14′ 30.9″	16° 40′ 16.9″
2	Site 2	96° 14′ 52.9″	16° 39′ 56.3″
3	Site 3	96°15′ 16.9″	16° 39′ 08.4″
4	Site 4	96° 15′ 43.5″	16° 38′ 56.5″
5	Site 5	96° 15′ 46.9″	16° 38′ 47.2″
6	Site 6	96° 15′ 48.5″	16° 38′ 26.3″
7	Site 7	96° 15′ 47.1″	16° 37′ 50.1″
8	Site 8	96° 15′ 40.5″	16° 37′ 25.6″
9	Site 9	96° 15′ 33.6″	16° 37′ 08.1″
10	Site 10	96° 15′ 29.1″	16° 36′ 32.0″

Figure 1. Satellite image of Thilawa (SEZ) and sampling location sites

Sample Preparation of Water Samples from Thilawa (SEZ)

The study was carried out in the Thilawa Special Economic Zone (SEZ), located at 20°35’18” N and 93°35’11” E. In June 2024, water samples were collected from a depth of 5 feet below the surface using a water sampler (pump) at ten sampling sites (Figure 2). These sites were selected based on their potential impact from local industrial activities. The water samples were preserved in pre-cleaned polyethylene bottles that had been soaked in 5 M HCl for more than three days and subsequently rinsed with distilled-deionized water before sampling.

Figure 2. Photograph of water sample collection in Thilawa (SEZ)

Results and Discussion

pH and Temperature of the Collected Water Samples from Thilawa (SEZ)

The pH values of the water samples ranged from 7.3 to 7.6, indicating a slightly basic nature, well within the acceptable limits set by WHO (2022) , EPA (2017), and ASEAN (2010). These values are suitable for fisheries and aquatic life. The water temperature during sampling ranged from 31.2°C to 32.4°C. This variation is typical for the region and can influence other water quality parameters, such as dissolved oxygen (Table 2).

Dissolved Oxygen, Biological Oxygen Demand and Chemical Oxygen Demand of the Collected Water Samples from Thilawa (SEZ)

Dissolved oxygen (DO) levels, which are critical for aquatic organisms, were recorded between 5.01 and 6.29 ppm (Table 2). These values align with WHO, EPA, and ASEAN standards, indicating unpolluted water that is safe for aquatic life, as DO levels below 5 ppm can harm biological communities, and levels below 2 ppm can cause fish mortality. The biological oxygen demand (BOD), measured after 5 days of incubation at 20°C, was found to be below WHO, EPA, and ASEAN standards. Since BOD levels below 2 ppm suggest unpolluted water, these results indicate the water is likely unpolluted in terms of organic matter

The chemical oxygen demand (COD) of the river water, ranging from 9.30 to14.28ppm, needs regular monitoring and pollution source mitigation to protect the aquatic ecosystem.

Electrical Conductivity, Total Dissolved Solids, Total Alkalinity and Total Hardness of the Collected Water Samples from Thilawa (SEZ)

The electrical conductivity ranged from 0.16 to 1.25 mS/cm (Table 3), showing differences in the water's ionic content, suggesting the need to investigate natural and human-related causes. The total dissolved solids (TDS) of the collected samples from Thilawa Special Economic Zone (SEZ) ranged from 0.08 to 0.63 ppt. The resulting data suggest the water quality needs further investigation and monitoring. The total alkalinity of water samples, ranging from 83 to 283 ppm, shows it can neutralize acids effectively. Its total hardness of 192 to 202 ppm indicates the water is moderately hard, which can affect mineral buildup and water quality.

Table 2. Some Physicochemical Characteristics of Collected Water Samples from-Thilawa (SEZ)

Sampling Sites	pH	Temperature (°C)	DO (ppm)	BOD (ppm)	COD (ppm)
S-1	7.3	31.8	6.02	0.89	12.94
S-2	7.3	31.2	6.29	1.20	9.57
S-3	7.4	31.7	5.59	0.98	11.34
S-4	7.5	31.3	5.26	0.78	10.87
S-5	7.5	31.5	5.80	1.40	9.30
S-6	7.5	31.5	5.87	1.37	9.57
S-7	7.6	32.2	5.67	1.07	14.28
S-8	7.5	32.3	5.39	0.54	13.30
S-9	7.5	32.4	5.01	0.71	10.51
S-10	7.6	32.3	5.20	0.66	11.43
WHO (2022)	6.5 – 8.5	30 – 32	>5	<3	<20
EPA (2017)	6.5 – 8.5	30 – 32	>5-6	<3-5	<20
ASEAN Standard (2010)	6.5 – 8.5	30 – 32	>5	<5	<20

Table 3. Electrical Conductivity, Total Dissolved Solid, Total Alkalinity, and Total Hardness of Collected Water Samples from Thilawa (SEZ)

Sampling Sites	EC (mS/cm)	TDS (ppt)	Total alkalinity (ppm)	Total hardness (ppm)
S-1	0.16	0.08	83	192
S-2	0.17	0.07	100	202
S-3	0.16	0.08	116	192
S-4	0.17	0.08	116	192
S-5	0.16	0.08	133	202
S-6	0.15	0.07	133	201
S-7	0.37	0.18	166	201
S-8	0.50	0.24	183	201
S-9	0.88	0.45	266	201
S-10	1.25	0.63	283	202
WHO (2022)	<1.5	<0.3	100 – 250	50 – 250
EPA (2017)	<1.5	<0.5	100 – 250	50 – 250
ASEAN Standard (2010)	<1.5	<0.3	100 – 250	50 – 250

Chlorinity and Salinity of the Collected Water Samples from Thilawa (SEZ)

Chlorinity values ranged from 0.063 to 0.113 ppt, i.e., 63 to 113 ppm, below the WHO limit of 0.25 ppt (250 ppm,), indicating moderate salinity. Salinity levels ranged from 0.113 to 0.204 ppt, also below the WHO standard (1-2 ppt) for freshwater. These results suggest a low to moderate level of dissolved salts, classifying the water as slightly brackish with minimal saline influence, suitable for various uses (Table 4).

Table 4. Chlorinity and Salinity of Collected Water Samples from Thilawa (SEZ)

Sampling Sites	Chlorinity (ppt)	Salinity (ppt)
S-1	0.073	0.131
S-2	0.073	0.131
S-3	0.063	0.113
S-4	0.073	0.131
S-5	0.070	0.126
S-6	0.065	0.117
S-7	0.113	0.204
S-8	0.113	0.204
S-9	0.099	0.178
S-10	0.099	0.178
WHO (2022)	0.05 – 19	1 – 2
EPA (2017)	0.05 – 19	1 – 2
ASEAN Standard (2010)	0.05 – 19	1 – 2

Chlorophyll *a* and Total Nitrogen of the Collected Water Samples from Thilawa (SEZ)

The chlorophyll-a provides valuable insight into the level of phytoplankton activity and nutrient status of the aquatic ecosystem. In this study, the chlorophyll-a levels in the water samples range from 0.749 to 2.138 µg/10 mL (Table 5), which are well below the acceptable limits set by WHO (2022), EPA (2017), and ASEAN (2010) standards. This indicates minimal algal presence and suggests that the aquatic system is not experiencing significant algal blooms

The total nitrogen concentrations in the samples range from 1.58 to 1.92 ppm, exceeding the recommended limit of 1 ppm established by WHO (2022), EPA (2017), and ASEAN(2010) standards. These elevated levels suggest nutrient enrichment in the water, potentially posing a risk of eutrophication and impacting water quality.

Table 5. Chlorophyll *a*, and Total Nitrogen of the Collected Water Samples from Thilawa (SEZ)

Sampling sites	Chlorophyll *a* (µg/10 mL)	Total nitrogen (ppm)
S-1	2.138	1.58
S-2	0.938	1.76
S-3	1.324	1.64
S-4	1.082	1.64
S-5	1.102	1.74
S-6	1.820	1.68
S-7	1.384	1.92
S-8	1.089	1.81
S-9	0.749	1.82
S-10	0.820	1.83
WHO (2022)	<10	<1
EPA (2017)	<10	<1
ASEAN Standard (2010)	<10	<1

Orthophosphate and Organic Phosphate of the Collected Water Samples from Thilawa (SEZ)

Orthophosphate levels within the range of 0.062 to 0.215 ppm are typical of healthy aquatic environments, where nutrient levels support plant growth. Organic phosphate concentrations between 5.61 and 7.83 ppm suggest substantial organic matter presence, which may indicate decomposition or pollution sources like untreated sewage or industrial waste (Table 6).

Nutrient Levels of the Collected Water Samples from Thilawa (SEZ)

Based on the medium values of DO, orthophosphate, and total nitrogen, the water samples were conclusively classified as a mesotrophic level (Tables 7 and 8), indicating moderate nutrient availability and balanced aquatic productivity. This classification highlights the importance of monitoring nutrient inputs to prevent a shift toward eutrophic conditions, which could lead to ecological imbalance and degradation of water quality.

Table 6. Orthophosphate and Organic Phosphate of the Collected Water Samples from Thilawa (SEZ)

Sampling sites	Orthophosphate (ppm)	Organic phosphate (ppm)
S-1	0.062	5.61
S-2	0.108	6.36
S-3	0.123	7.83
S-4	0.113	6.17
S-5	0.106	6.16
S-6	0.131	7.83
S-7	0.212	6.87
S-8	0.169	6.24
S-9	0.213	6.21
S-10	0.215	6.38

Table 7. Nutrient Levels of Brackish Water Samples from Thilawa (SEZ)

Sampling sites	DO (pm)	Orthophosphate (ppm)	Total nitrogen (ppm)	Nutrient enrichment
S-1	6.02	0.062	1.58	Medium
S-2	6.29	0.108	1.76	Medium
S-3	5.59	0.123	1.64	Medium
S-4	5.26	0.113	1.64	Medium
S-5	5.80	0.106	1.74	Medium
S-6	5.87	0.131	1.68	Medium
S-7	5.67	0.212	1.92	Medium
S-8	5.39	0.169	1.81	Medium
S-9	5.01	0.213	1.82	Medium
S-10	5.20	0.215	1.83	Medium

Table 8. Criteria for Evaluating Degree of Nutrient Over-Enrichment

Parameter	Low	Medium	High
Nitrogen (ppm)	≤ 0.1	> 0.1 - < 1.0	≥ 1.0
PO_4^{3-} (ppm)	< 0.03	> 0.03 - < 0.3	≥ 0.3
DO (ppm)	≥ 5	> 2 - ≤ 5	0 - ≤ 2

Low nutrient enrichment = Oligotrophic level*
Medium nutrient enrichment = Mesotrophic level
High nutrient enrichment = Eutrophic level
* Tong and Deocadiz, 1999

Some Mineral Contents of the Collected Water Samples from Thilawa (SEZ)

At various sampling sites, the concentration of metals (in ppm) varied significantly, with notable detections including chromium (Cr) up to 4.59 ppm, manganese (Mn) reaching 6.84 ppm, cadmium (Cd) peaking at 4.21 ppm, and copper (Cu) at 3.81 ppm. Zinc (Zn) and iron (Fe) were present at moderate levels, while arsenic (As) and mercury (Hg) remained undetected across all sites (Table 9).

Table 9. Some Mineral Contents of the Collected Water Samples from Thilawa (SEZ) by AAS

Sampling sites	Some mineral contents (ppm)							
	Cr	**Mn**	**Cd**	**Cu**	**Zn**	**Fe**	**As**	**Hg**
S-1	ND	2.91	ND	ND	0.61	3.14	ND	ND
S-2	ND	ND	ND	ND	ND	ND	ND	ND
S-3	ND	2.44	ND	ND	0.91	ND	ND	ND
S-4	ND	2.59	0.19	ND	0.60	1.41	ND	ND
S-5	ND	0.43	4.11	3.81	ND	ND	ND	ND
S-6	4.59	3.96	2.56	ND	0.92	1.68	ND	ND
S-7	3.63	ND	1.72	ND	2.69	ND	ND	ND
S-8	ND	5.61	4.21	ND	3.57	0.89	ND	ND
S-9	ND	6.84	ND	ND	ND	0.02	ND	ND
S-10	1.16	2.48	0.22	ND	ND	ND	ND	ND

*ND = Not Detected

Microbial Properties of the Collected Water Samples from Thilawa (SEZ)

The absence of total coliforms in all water samples and the detection of *E. coli* only at site 2 indicate overall good microbial water quality. However, the presence of *E. coli* at site 2 suggests localized contamination, highlighting the need for targeted investigation and remediation efforts in that area (Table 10).

Table 10. Total Coliform and *E.coli* Values of Brackish Water Samples from Thilawa (SEZ)

Sampling Sites	Total coliform (cfu/mL)	*E.coli* (cfu/mL)
S-1	0	0
S-2	0	100
S-3	0	0
S-4	0	0
S-5	0	0
S-6	0	0
S-7	0	0
S-8	0	0
S-9	0	0
S-10	0	0
WHO (2022)	0	0
EPA (2017)	0	0
ASEAN Standard (2010)	0	0

Conclusion

The water quality analysis indicates that the aquatic environment is generally suitable for supporting life, with parameters like pH, temperature, dissolved oxygen, BOD, salinity, and chlorinity within acceptable limits. However, certain factors require attention, including elevated COD levels indicating moderate pollution, localized contamination from metals like chromium, manganese, and cadmium, and high organic phosphate concentrations suggesting pollution from organic matter. Nutrient levels suggest a mesotrophic state without immediate eutrophication risks. The absence of total coliforms in all water samples and the detection of *E. coli* only at site 2 indicate overall good microbial water quality across the study area. Continuous microbial monitoring is needed to prevent future risks and maintain water quality standards. While the absence of arsenic, mercury, and microbial contamination is reassuring, continuous monitoring and management of potential pollution sources are crucial to maintaining water quality and protecting public health.

Acknowledgement

The authors express gratitude to the Myanmar Academy of Arts and Science for permitting the submission of this paper and to Dr Ni Ni Than, Professor and Head, Department of Chemistry, University of Yangon for her valuable suggestions.

References

ASEAN Marine Environmental Management. (2010). *ASEAN Marine Water Quality Management Guidelines and Monitoring Manual*. Jakarta: 1st Ed., ASEAN Publication, pp. 27-52.

Kaly, U.L. (2004). *Review of Land-based Sources of Pollution to the Coastal and Marine Environments in the BOBLME Region.* Bay of Bengal Large Marine Ecosystem (BOBLME) Theme Report. FAO-BOBLME Program

Kyaw Naing. (2011). *National Report of Myanmar on the Coastal Pollution Loading and Water Quality Criteria (Land-based Sources of Marine Pollution).* Bay of Bengal Large Marine Ecosystem Project of the Food and Agriculture Organization of the United Nations, FAO, pp.1-53.

Kyaw Naing, Ye M. Aung, Win Aung, Myat K. Thu, San S. Myint, Thida Win, Soe S. Naing, Myat M. Thaw, Aye A. Myat, Swe Z. Win, Khin M. Cho, Kyi K. Lwin, Aye A. Lwin, and Khin Htay.(2012). "Some Physicochemical Properties of Sea Water in Tanintharyi Coastal Zone, Myanmar". *Thai Environmental Engineering Journal*, special vol., pp.145-149.

Maung Kyaw. (2016). *Conservation of Water.* Yangon: Myanmar Academy of Arts and Science.

Tong, S.L. and E.S. Deocadiz. (1999). *Principles for Developing ASEAN Marine Environmental Quality Criteria*. In: McPherson, C.A., P.M. Chapman, G.A. Vigers and K.S. Ong (Eds.). ASEAN Marine Water Quality Criteria. Kuala Lumpur: Department of Fisheries (Malaysia), pp. 1-12.

U.S. Environmental Protection Agency (EPA). (2017). *Water Quality Standards Handbook: Standards related to conservation of living environment*. Washington DC: U.S. EPA, pp. 6-34.

World Health Organization. (2022). *Guidelines for Drinking-water Quality*. Geneva: 4th Ed., WHO. pp. 167-215.

PREPARATION, CHARACTERIZATION AND APPLICATION OF SPINEL $MgFe_2O_4$ NANOPARTICLE

U Toe [1]

Abstract

The present research deals with a study on the preparation, characterization and application of spinel $MgFe_2O_4$ nanoparticles. The spinel $MgFe_2O_4$ nanoparticle was synthesized by sol-gel method using oxalic acid. Magnesium nitrate and ferric nitrate were used as starting materials. The elemental composition of the prepared nanoparticle was characterized by Energy Dispersive X-ray Fluorescence (EDXRF). The crystallite size, phase ID and lattice parameters of the prepared nanoparticle were characterized by X-ray powder diffraction (XRD) spectroscopy. The type of chemical bonding in the prepared nanoparticle was characterized by Fourier Transform Infrared (FT IR) spectroscopy, and porosity and morphology of the prepared nanoparticle were characterized by Scanning Electron Microscopy (SEM) spectroscopy. The energy band gap of the prepared nanoparticle was determined by the Tauc Plot method. The electrochemical property of the prepared nanoparticle was determined by the cyclic voltammetry method. The specific capacitance of the prepared nanoparticle was determined from the cyclic voltammetry graph.

Keywords: spinel nanoparticles, sol-gel method, XRD, EDXRF, cyclic voltammetry and specific capacitance

Introduction

The environment has become contaminated in, i.e. air, water, and land, due to excess use of pesticides, fertilizers, global industrialization, and dumping of chemicals and pollutants from industries. An attempt to solve diverse problem is now being sorted out by the use of nanotechnology (Paramita, 2018). Environmental engineering science is witnessing drastic changes. In a similar manner, nanotechnology is moving from one visionary paradigm toward another. Nanotechnology is the frontier of science and engineering today for solving such problems. (Sukanchan, 2018).

Nanotechnology has emerged as a rapidly growing field with multifaced application for new materials at the nanoscale level. Nanoparticles are of great interest due to their unique physicochemical, magnetic, and optoelectronic properties that are governed by their size, shape, and size distribution and they have a small size and large surface area to volume ratio that lead to the significant differences in properties in their bulk form. Due to unique physicochemical and optoelectronic properties, nanoparticles are interest for a number of applications like catalysts, chemical sensors, electronic components, medical diagnostic imaging, pharmaceutical products and medical treatment proposal (Babita, 2018).

Today, various methods such as the sol-gel method (solution method), vapor phase compression method, mechanical alloying method or collision with high-energy pellets, plasma method, and electrochemical methods are used for the production and synthesis of nanoparticles. Although all the mentioned methods have the ability to produce large volumes of nanomaterial, the sol-gel method has a higher popularity and industrial application than other existing methods [Feinle, Haruta, 2016]. Due to its unique properties and characteristics, this method is capable of producing high quality nanoparticles of the same size on an industrial scale [Tian, 2007].

The sol-gel process is a bottom-up synthesis method. In this process, the final products are formed by performing a number of irreversible chemical reactions [Sarkar, 2012]. The rate of reaction of salts depends on various factors such as pH, concentration, type of solvent, and temperature. The main advantages of the sol-gel process are the high purity of the product, the

[1] Department of Chemistry, Kyaukse University

narrow particle size distribution, and the achievement of uniform nanostructure at low temperatures. This method is commonly used to synthesize metal nanooxides.

In this research, $MgFe_2O_4$ nanoparticle was synthesized from magnesium nitrate, ferric nitrate, oxalic acid and ethylene glycol by so-gel method. $MgFe_2O_4$ is an important multifunctional material, which has been widely applied in catalysts and lithium-ion batteries because of their interesting catalytic and electrochemical properties [Hench, 1990]. Recently, $MgFe_2O_4$ nanoparticle has been successfully used as electrode material for pseudocapacitors due to the synergistic effects from iron and magnesium [Verma, et al 2015].

Materials and Methods

All chemicals were analytical grade. Magnesium nitrate ($Mg(NO_3)_2.6H_2O$), ferric nitrate ($Fe(NO_3)_3.\ 9H_2O$) and oxalic acid ($C_2H_2O_4$) were Merck product with a purity of 99.99 %. Ethylene glycol was product from Applichem, Germany. All solutions were prepared using distilled water during preparation procedures. Various conventional and modern instrumental techniques were used throughout the experimental procedure. These include Energy Dispersive X-ray Fluorescence (EDXRF), X-ray Diffraction (XRD), Fourier transform infrared (FT IR) spectroscopy, Scanning electron microscopy, cyclic voltammetry and UV-Visible spectroscopy.

Preparation of spinel $MgFe_2O_4$ nanoparticle using oxalic acid

In a typical experiment, 50 mL of 0.8 M $Mg(NO_3)_2.6H_2O$ was dissolved in 100 mL distilled water as well as 50 mL of 0.8 M $Fe(NO_3)_3.9H_2O$ was dissolved in 100 mL distilled water and they were mixed to obtain the first solution. The second solution was prepared by dissolving 50 mL of 0.8 M oxalic acid in 100 mL of distilled water and the first solution was mixed with the second solution. 10 mL ethylene glycol was added into the above mixture solution. The solution was heated and stirred at 80 ℃ for about 4 h on a magnetic stirrer to get gel material. The gel was dried at 100 ℃ in a hot air oven for about 2 h. The dried material was obtained. The dried material was crushed to fine powder with a mortar and pestle. The fine powder was transferred into a crucible and calcinated at 500 ℃ for about 4 h in a muffle furnace. Then the required $MgFe_2O_4$ nanoparticle was obtained.

Characterization of prepared spinel $MgFe_2O_4$ nanoparticle

Crystal structure and phase analysis were performed by X-ray diffraction (XRD) using Rigaku, D-Max 2200, Japan in the Department of Chemistry, Yangon University. The elemental composition of the prepared $MgFe_2O_4$ NP was confirmed by using the EDXRF 700 spectrometer in the Department of Chemistry, Monywa University. The chemical bonding in the prepared nanoparticle was characterized by (FT IR) in the Department of Chemistry, Monywa University. Porosity and morphology of prepared nanoparticles were determined by (SEM) in the Department of Chemistry Magway University.

Determination of crystallite size and interatomic spacing of prepared spinel $MgFe_2O_4$ nanoparticle

The crystallite sizes of spinel $MgFe_2O_4$ NP can be calculated by using Debye-Scherrer's formula,

$$D = \frac{0.9\lambda}{\beta \cos\theta}$$, and

interatomic spacing (d) was calculated by Bragg's equation

$$d = \frac{\lambda}{2 \sin\theta}$$

Where, λ = the wave length of X-rays (λ =1.540560Å)

θ = the diffraction angle

β = full width at half maximum in radian

D = average crystallite size

d = interatomic spacing

Determination of energy band gap of prepared spinel $MgFe_2O_4$ nanoparticle

The energy band gap of the prepared nanoparticle was measured by UV-Vis spectroscopy in the Department of Chemistry, University of Mandalay.

0.01g of $MgFe_2O_4$ NP was dissolved in 5 mL of distilled water and was settled for 12 h. 2 mL of the upper layer of the solution was taken and its absorbance was measured at 200 -750 nm range. To measure energy, the band gap of the prepared $MgFe_2O_4$ NP, the wavelength and related absorbance data were used in scientific 2018 origin software.

Cyclic voltammetry of prepared spinel $MgFe_2O_4$ nanoparticles

The electrochemical properties of the prepared $MgFe_2O_4$ nanoparticles were determined by cyclic voltammetry technique. 0.05 g of prepared $MgFe_2O_4$ NP was used. Electrochemical properties of the prepared nanoparticle were determined using three electrode systems (Ag/AgCl as a reference electrode, platinum as a counter electrode and FTO coated with $MgFe_2O_4$ NP as a working electrode) in 1 M KOH as a supporting electrolyte with scan rates of 50 mVs^{-1}.

Fabrication of prepared spinel $MgFe_2O_4$ nanoparticles

0.05 g of $MgFe_2O_4$ nanoparticles and 5 mL of ethylene glycol were mixed. The solution was heated in the water bath for 2 h. The $MgFe_2O_4$ nanoparticle gel solution was obtained. And then fluorine doped tin oxide (FTO) was coated with $MgFe_2O_4$ nanoparticle gel solution and dried at 80℃. $MgFe_2O_4$ coating film was obtained.

Determination of electrochemical behaviors of prepared spinel $MgFe_2O_4$ nanoparticle from cyclic voltammograms

To determine the electrochemical properties of prepared $MgFe_2O_4$ nanoparticles, the data of the CV graph were obtained by the cyclic voltammetry technique at a scan rate of 50 mVs^{-1} and 1M KOH electrolyte solution. The CV graph was plotted using origin 2018 software based on the obtained CV data. The electrochemical properties of the prepared nanoparticles were analyzed by interpreting the current and potential values.

Determination of specific capacitance of prepared spinel $MgFe_2O_4$ nanoparticle

The specific capacitance of prepared $MgFe_2O_4$ nanoparticles was determined using cyclic voltammetry in Department of Chemistry, at the University of Mandalay.

The cyclic area of the CV graph was measured from CV graph in origin software. The specific capacitance of the prepared nanoparticle was calculated using cyclic area and CV data according to the following equation.

$$C_p = \frac{A}{2mk\Delta V}$$

Where: C_p = specific capacitance

A = cyclic area

m = mass of active material

k = scan rate

ΔV = potential window

Results and Discussion

In this section, it contains characterization of the prepared spinel $MgFe_2O_4$ nanoparticles by EDXRF, XRD, FT IR, and SEM spectroscopic techniques. Furthermore, determination of energy band gap, and specific capacitance of the prepared spinel $MgFe_2O_4$ nanoparticle were discussed.

Yield percent of prepared spinel $MgFe_2O_4$ nanoparticle

The prepared powder was calcinated at 500˚C for 4h in a muffle furnace. The yield % of spinel $MgFe_2O_4$ NP was calculated from the mass of metals in initial nitrates. The value of this sample was shown in Table 1.

Table 1 Result of Yield Percent of Prepared Spinel $MgFe_2O_4$ Nanoparticle

Sample	Yield percent of sample (%)
$MgFe_2O_4$	88

According to the Table 1, it is found that yield percent of calcinated prepared spinel $MgFe_2O_4$ NP is 88%.

EDXRF analysis of prepared spinel $MgFe_2O_4$ nanoparticle

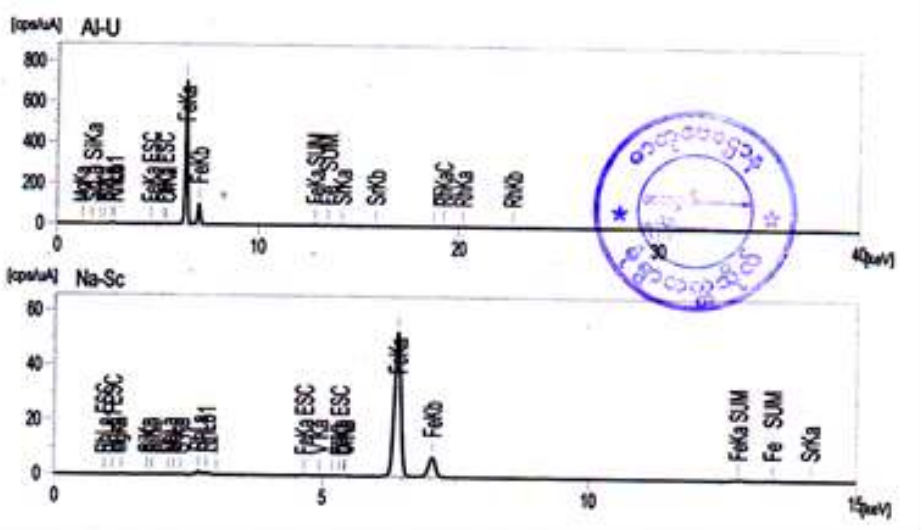

Figure 1 EDXRF spectrum of prepared spinel $MgFe_2O_4$ NP

Table 2 Elemental Composition of Prepared Spinel $MgFe_2O_4$ NP by EDXRF

No	Analytes	Results (%)
1	Fe	59.342
2	Mg	38.976
3	Si	1.174
4	S	0.327
5	Sr	0.106
6	Cr	0.075

From the EDXRF data, amount of Fe, Mg, Si, S, Sr and Cr in prepared spinel $MgFe_2O_4$ NP were found to be 59.342 %**,** 38.976 %, 1.174 % , 0.327%, 0.106 % and 0.075 % respectively.

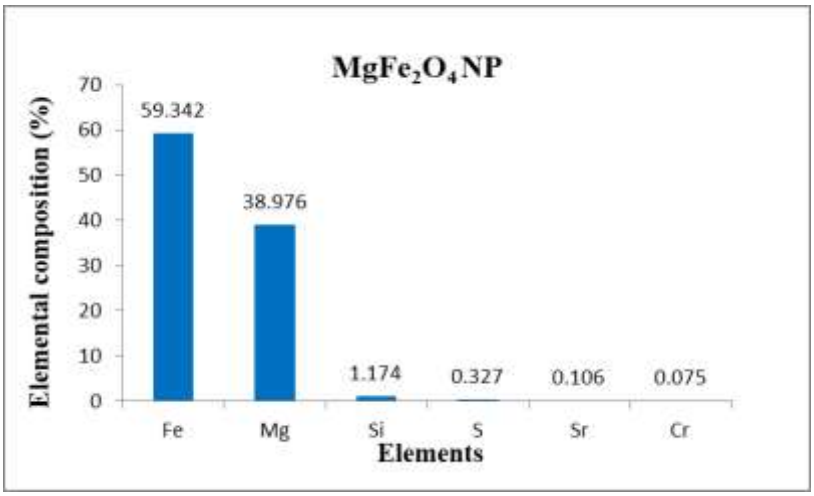

Figure 2 Bar graph showing elemental composition of prepared spinel $MgFe_2O_4$ NP

XRD analysis of prepared spinel $MgFe_2O_4$ nanoparticle

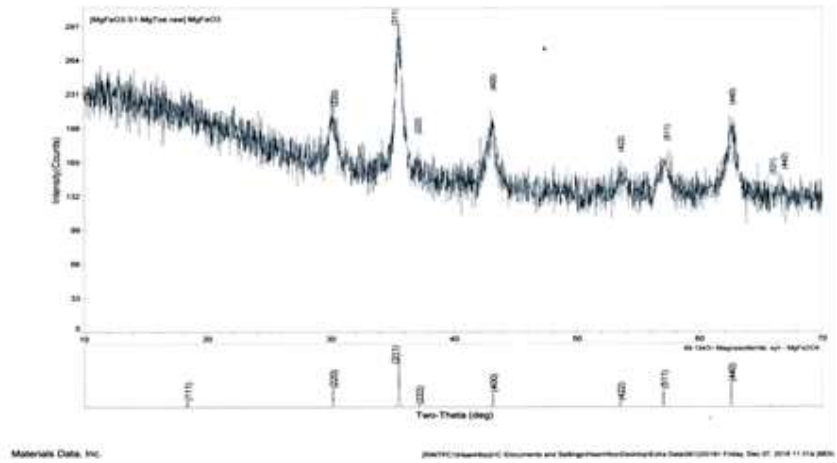

Figure 3 XRD Diffractogram of prepared spinel $MgFe_2O_4$ NP

Table 3 The Crystallite Size and Phase ID of Prepared Spinel $MgFe_2O_4$ NP

No	Bragg angle (2θ)	Miller indices (h k l)	β (radian)	Inter planar spacing d(nm)	Crystallite size D (nm)	Phase ID
1	30.261	2 2 0	0.01195	0.29511	13.85	$MgFe_2O_4$
2	35.483	3 1 1	0.01059	0.25278	29.42	$MgFe_2O_4$
3	37.028	2 2 2	0.00508	0.24258	28.89	$MgFe_2O_4$
4	43.113	4 0 0	0.00723	0.20965	20.69	$MgFe_2O_4$
5	53.490	4 2 2	0.01227	0.17116	12.72	$MgFe_2O_4$
6	57.251	5 1 1	0.01166	0.16078	13.59	$MgFe_2O_4$
7	62.614	4 4 0	0.01185	0.14824	13.73	$MgFe_2O_4$
8	65.910	5 3 1	0.00795	0.14160	20.69	$MgFe_2O_4$
9	66.859	4 4 2	0.00212	0.13982	81.56	$MgFe_2O_4$

The XRD spectrum of $MgFe_2O_4$ nanoparticles was indicated in Figure 3. The diffracted peaks are (220), (311), (222), (400), (422), (511), (440), (531) and (442). All peaks were well matched with those of the standard JCPDF (Joint Committee on Powder Diffraction standards) library file of magnesium ferrite ($MgFe_2O_4$). The most dominant peak at (222) plane was found at 37.028 deg. XRD patterns indicate that the crystal structures of $MgFe_2O_4$ were cubic structures. The crystallite sizes of $MgFe_2O_4$ were tabulated in Table 3. The average crystallize size was 26.13 nm.

Table 4 Lattice Parameters for Prepared Spinel $MgFe_2O_4$ Nanoparticle

Crystal Structure	a-Axis (nm)	b-Axis (nm)	c-Axis (nm)	α, °	β, °	γ, °
Cubic	0.83469	0.83469	0.83469	90.00	90.00	90.00
Cubic	0.83838	0.83838	0.83838	90.00	90.00	90.00
Cubic	0.84031	0.84031	0.84031	90.00	90.00	90.00
Cubic	0.83859	0.83859	0.83859	90.00	90.00	90.00
Cubic	0.83853	0.83853	0.83853	90.00	90.00	90.00
Cubic	0.83545	0.83545	0.83545	90.00	90.00	90.00

The average lattice constants calculated from the XRD pattern for spinel $MgFe_2O_4$ nanoparticles are a= b = c = 0.838 nm and $\alpha = \beta = \gamma = 90^{\circ}$. The crystal structures are cubic structures.

FT IR Analysis of Prepared Spinel $MgFe_2O_4$ Nanoparticle

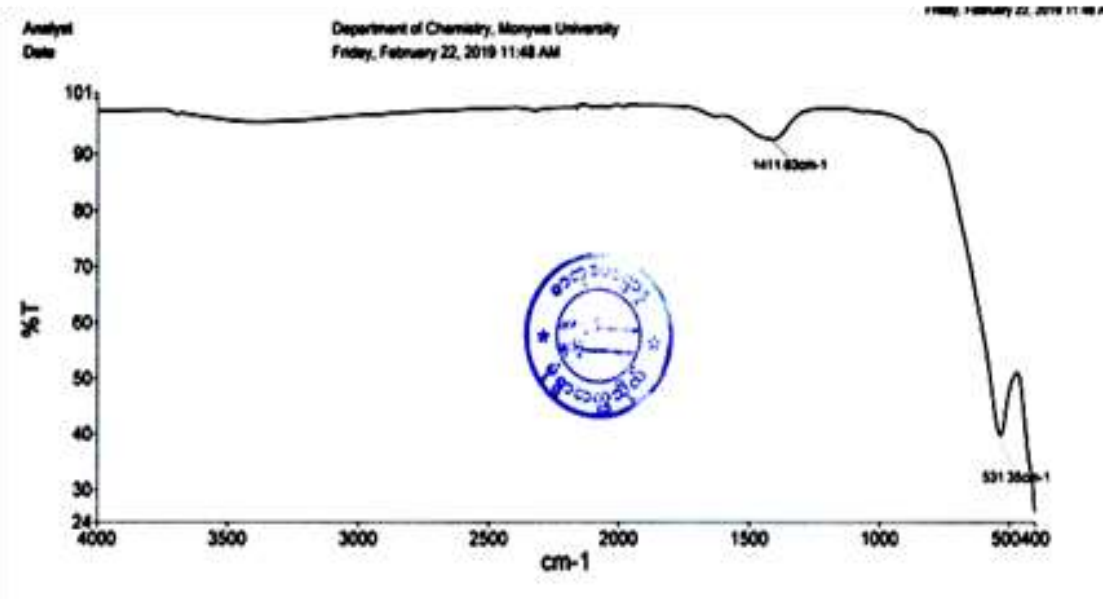

Figure 4. FT IR spectrum of prepared spinel $MgFe_2O_4$ NP

Table 5 FT IR Spectra Data for Prepared Spinel $MgFe_2O_4$ NP

Sample	Wave number (cm^{-1})	Remark	*Literature values
$MgFe_2O_4$	531.35	Stretching vibration of Mg-O and Fe-O bonds	650-430cm^{-1}

* Waldron R D (1955), Infrared Spectroscopy of Ferrites Phy Rev.

According to the Table 5, in FT IR spectrum of $MgFe_2O_4$ NP, stretching vibration of Mg-O and Fe-O bonds occurred at 531.35 cm^{-1} of wavenumber.

SEM analysis of prepared spinel $MgFe_2O_4$ nanoparticle

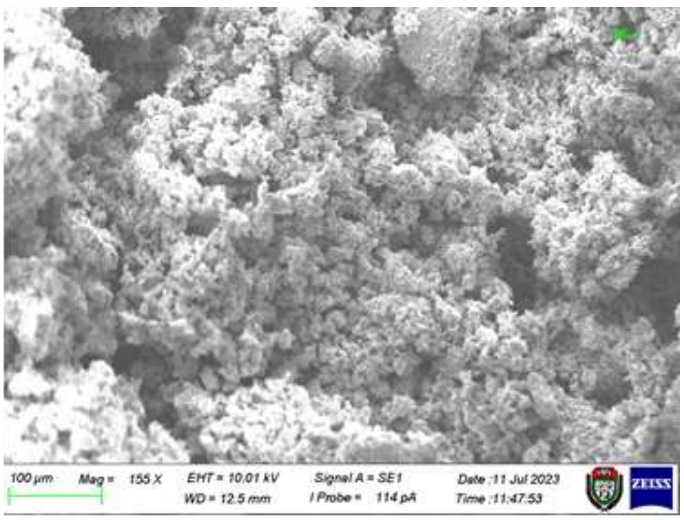

Figure 5 SEM spectrum of prepared spinel $MgFe_2O_4$ NP

The morphology of the spinel $MgFe_2O_4$ nanoparticles indicates irregular cubic shapes of various sizes that are agglomerated.

Determination of energy band gap of prepared spinel $MgFe_2O_4$ NP

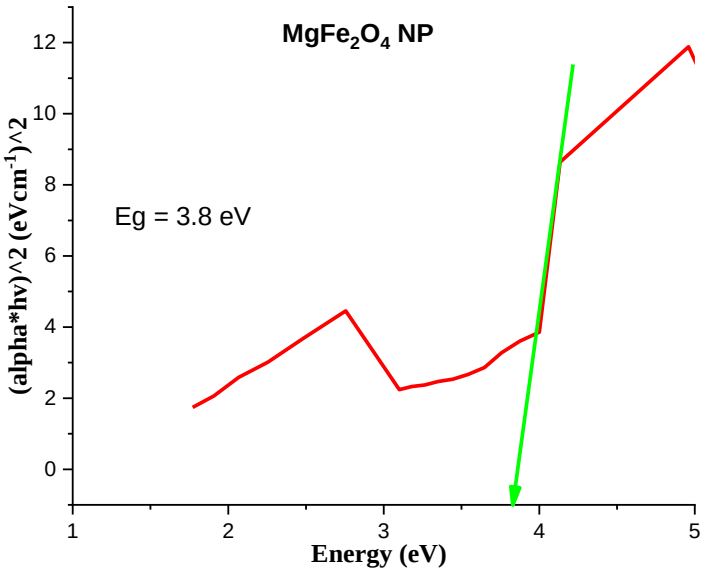

Figure 6 Tauc plot graph of prepared spinel $MgFe_2O_4$ NP

The energy band gap of prepared $MgFe_2O_4$ NP was found to be 3.8 eV. According to the Tauc plot method, $MgFe_2O_4$ NP is a type of little semi-conductor.

Determination of electrochemical property of prepared spinel $MgFe_2O_4$ NP

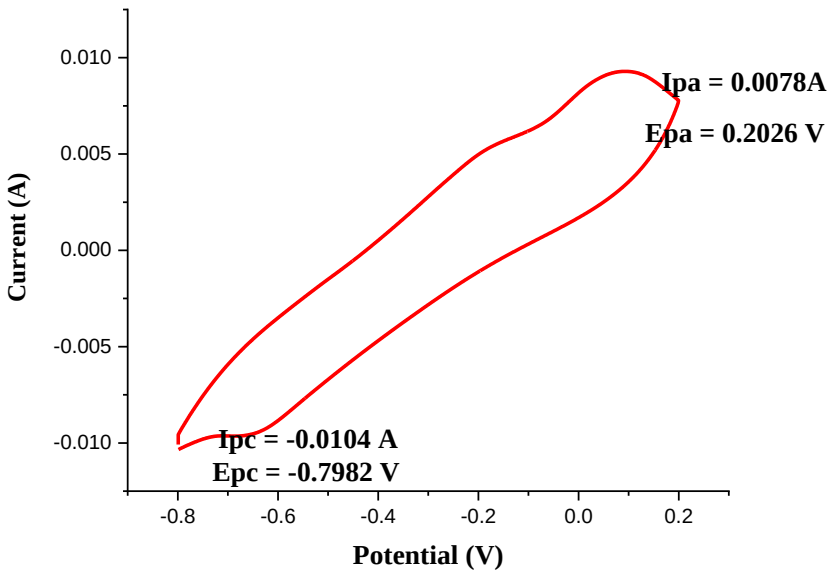

Figure 7. Cyclic voltammetry graph of $MgFe_2O_4$ NP with scan rate of 50 mVs^{-1} in 1M KOH solution

Table 6 The Value of Anode and Cathode Peak Current Densities of 0.05 g of $MgFe_2O_4$ NP in 1 M of KOH Electrolyte Solution

Scan rate (mV/s)	Electrolytes (1M)	Samples	Ipc(A)	Epc(V)	Ipa(A)	Epa(V)
50	KOH	$MgFe_2O_4$	-0.0104	-0.7982	0.0078	0.2026

According to this table, cathode and anode peaks potentials of $MgFe_2O_4$ were found at -0.7982V and 0.2026 V, respectively.

Determination of specific capacitance of prepared spinel $MgFe_2O_4$ NP

Parameters of $MgFe_2O_4$NP Data were as follows.

Scan rate (K) = 50 mV/s

Mass of $MgFe_2O_4$ nanoparticle (m) = 0.05g

Potential window (V_2-V_1) ΔV = 0.2- (-0.8) = 1.00 V

Area inside the CV curve (A) = 0.0051 AV

$$C_p = \frac{A}{2mK\Delta V} = \frac{0.00506}{2\times 0.05\times 50\times 1.00\times 10^{-3}}$$

$$= 1.012 \text{ F/g}$$

Calculated Specific Capacitance Cp of $MgFe_2O_4$ NP = 1.01 F/g

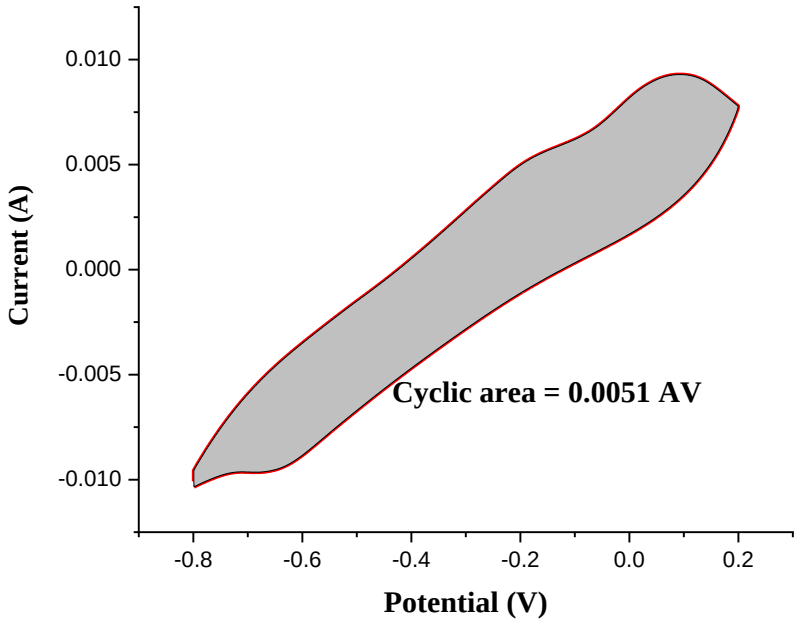

Figure 8 Cyclic area of prepared spinel $MgFe_2O_4$ NP

Conclusion

In this research, spinel $MgFe_2O_4$ nanoparticle was synthesized from magnesium nitrate and cobalt nitrate by sol gel method using oxalic acid. The prepared spinel nanoparticle was characterized by modern sophisticated methods such as EDXRF, XRD, FT IR and SEM spectroscopic techniques. From the characterization of modern techniques, the prepared $MgFe_2O_4$ particle is a nanoparticle since its crystallite size is in the range of nanoscale (1 – 100 nm). The crystal structure of the prepared spinel $MgFe_2O_4$ nanoparticle is cubic.

According to the determination of the energy band gap of prepared $MgFe_2O_4$ NP by the Tauc Plot method, it is a type of semiconductor because of the 3.8 eV energy band gap value. Therefore it can be used in electronic devices such as solar cells. According to the determination of electrochemical property by cyclic voltammetry, it is found that $MgFe_2O_4$ NP performs as an electrode in 1M KOH electrolyte solution. According to the determination of specific capacitance of prepared $MgFe_2O_4$ NP, its capacitance value is 1 F/g. So this nanoparticle can also be used in charging batteries since its capacitance value is a significant amount.

Acknowledgements

I am to grateful to Dr. Ye Ye Oo, Rector, Kyaukse University for her permission to this research paper. I am also grateful to ethical research committee of Kyaukse University for their examination on my paper and findly. I also express my profound gratitude to Dr. Kaythy Myint Thu, Professor and Head, Department of Chemistry, Kyaukse University for her suggestions to this work.

References

Babita, T. and M. Ahmaruzzaman. (2018). *GREEN METAL NANOPARTICLES; Green Synthesis of Silver, Copper, and Iron Nanoparticles and Their Application*. Department of Chemistry National Institute of Technology, Silchar, Assam, India, 1st Ed, pp. 441-466.

Ben, G.S. (2014). *Solid state Electronic Device.* Pearson, University of Texas at Austin, 7th Ed, pp.1-8.

Feinle, A., M. S. Elsaesser, and N. Husing, (2016). "Sol-gel synthesis of monolithic materials with hierarchical porosity," *Chemical Society Reviews*, vol. 45, (12), pp. 3377–3399.

Hench, L. L. and J. K. West, (1990). "The sol-gel process," *Chemical Reviews*, vol. 90(1) pp. 33–72.

James, A. and De Haseth (2007). *Fourier Transform Infrared Spectrometry*. Atlanta, University of Georgia, pp. 401-405.

Mohd Fahmi bin A.L. (2022). *Capacitor and Capacitance, Department of Engineering* Politeknik Kuala Terengganu, Malaysia. 1st Edition, pp.8-9.

Paramita, K. and R. Madhuri. (2018). *GREEN METAL NANOPARTICLES; Green Tiny Magnets: An Economic*

and Eco-friendly Remedy for Environmental Damage. Department of Applied Chemistry, Indian Institute of Technology, Dhanbad Jharkhand, India. 1st Ed, pp. 245-292.

Sarkar, D., C. K. Ghosh, and K. K. Chattopadhyay, (2012). "Morphology control of rutile TiO_2

hierarchical architectures and their excellent field emission properties," *CrystEngComm*, vol. 14,(8), pp. 2683–2690.

Sukanchan, P. and C. Hussian. (2018). *GREEN METAL NANOPARTICLES; Recent*

Advances in Green Nanotechnology and the Vision for the Future. Department of Chemical Engineering, University of Petroleum and Energy Studies, Energy Acres, Uttrakhand, India. 1st Ed, pp.3-21.

Tian, N., Z. Y. Zhou, S. G. Sun, Y. Ding, and Z. L. Wang, (2007). "Synthesis of

tetrahexahedral platinum nanocrystals with high-index facets and high electro-oxidation activity," *Science*, vol. 316, pp.732–735.

Waldron, R.D. (1995). "Infrared Spectroscopy of Ferrites". *Phys Rev*, vol. 99, pp. 1727-1734.

Here are some suggested questions based on the provided research summary:

1. Questions on Synthesis and Characterization:

- What is the role of oxalic acid in the sol-gel synthesis of $MgFe_2O_4$ nanoparticles?
- Why were magnesium nitrate and cobalt nitrate chosen as precursor materials?
- What evidence from XRD confirms that the prepared $MgFe_2O_4$ nanoparticle has a cubic spinel structure?
- How do EDXRF, XRD, FT-IR, and SEM contribute to the characterization of $MgFe_2O_4$ nanoparticles?
- What is the observed crystallite size of the synthesized $MgFe_2O_4$ nanoparticles, and how was it determined?

2. Questions on Optical and Semiconductor Properties:

- How was the energy band gap of $MgFe_2O_4$ determined using the Tauc Plot method?
- What is the significance of the 3.8 eV band gap in classifying $MgFe_2O_4$ as a semiconductor?
- How does the band gap value affect the potential application of $MgFe_2O_4$ in solar cells?

3. Questions on Electrochemical Properties and Applications:

- How was cyclic voltammetry used to determine the electrochemical performance of $MgFe_2O_4$ nanoparticles?
- What does the specific capacitance value of 1 F/g indicate about the potential use of $MgFe_2O_4$ in energy storage devices?
- Why was 1M KOH chosen as the electrolyte in electrochemical studies?
- How does the electrochemical behavior of $MgFe_2O_4$ compare to other common electrode materials used in supercapacitors or batteries?

4. Questions on Potential Applications:

- What are the advantages of using $MgFe_2O_4$ nanoparticles in electronic devices such as solar cells?
- How does the specific capacitance value of $MgFe_2O_4$ compare to conventional capacitor materials?
- What are the possible improvements or modifications to enhance the performance of $MgFe_2O_4$ in energy storage applications?

These questions can help guide further discussions and exploration of the research findings. Let me know if you need more specific questions!

PHYTOCHEMICAL SCREENING AND *IN VITRO* BIOACTIVITY INVESTIGATION OF *CISSUS DISCOLOR* BLUME (TABINDING MYA NAN) STEM

Myint Myint Khin[1], Nang Soe Htwe Khaing[2], Tin Myo Khaing[3], Aye Aye Tun[4]

Abstract

The stem of *Cissus discolor* Blume (Tabinding Mya Nan) was investigated for its phytochemical components and their bioactivities, including antioxidant, antimicrobial, and antiarthritic properties. A quantitative analysis was conducted to determine the phenolic and flavonoid content, which are known for their diverse bioactive potential. Antioxidant activity was evaluated using ethanol and aqueous extracts, demonstrating significant activity. Antimicrobial activity was assessed against six microorganism strains using the agar well diffusion method, revealing promising results. Antiarthritic activity was examined *in vitro* using the protein denaturation method, where the crude extracts exhibited activity comparable to standard drugs, with relatively high efficacy. The findings suggest that the antioxidant, antimicrobial, and antiarthritic properties of *C. discolor* extracts highlight their potential for developing enhanced traditional medicines.

Keywords: *Cissus discolor* Blume, elemental contents, phytochemical constituents, antioxidant, antimicrobial and antiarthritic activities

Introduction

Cissus discolor Blume (Tabinding Mya Nan), a member of the Vitaceae family, is native to tropical and subtropical regions of Asia. Figure 1 represents images of plant and dried powder of the stem of *C. discolor*. The plant is rich in bioactive components, including alkaloids, flavonoids, glycosides, cinnamic acids, gallic acid, quercetin, and sitosterol. *C. discolor* has been traditionally used in folk medicine to treat ailments such as cough, cholera, and stomach disorders. Its pharmacological activities include anti-inflammatory, antimicrobial, wound-healing, pain-relieving, analgesic, antibiotic, antidiabetic, antioxidant, anticancer, and antiviral properties. Notably, the combination of honey and the root of *C. discolor* has been reported to aid in treating gastric cancer (Khin *et al.*, 2017).

Recent studies have demonstrated that *C. discolor* possesses anti-inflammatory, antifungal, and antimycobacterial properties. Despite these findings, synthetic agents used for disease treatment are often associated with adverse effects and limited therapeutic efficacy. Although the biological activities of *C. discolor* have been studied extensively over the years, the total phenolic and flavonoid contents—key compounds known to reduce oxidative stress and relieve joint pain—have yet to be quantified. Therefore, this study aimed to quantitatively determine the total phenolic and flavonoid contents, and the antioxidant, antimicrobial, and antiarthritic activities of the stem solvent extracts of *C. discolor*, to provide further evidence supporting its potent antioxidant and antiarthritic properties.

[1] Department of Chemistry, Taunggyi University
[2] Department of Chemistry, Taunggyi University
[3] Department of Chemistry, Taunggyi University
[4] Department of Chemistry, Taunggyi University

(a) **(b)**

Figure 1. Images of (a) plant and (b) dried powder of *Cissus discolor* Blume (Tabinding Mya Nan) stem

materials and methods

Sample Collection and Preparation

The stem of *C. discolor* was collected from Myo Ma Market in Taunggyi in December 2023. Distilled water was used to clean the stems, removing dust and impurities thoroughly. The cleaned samples were then shade-dried to preserve bioactive components before being ground into a fine powder using a grinding machine. To prevent moisture absorption and contamination, the powdered samples were stored in air-tight containers. These dried and powdered samples were subsequently used for chemical and biological analyses.

Determination of Moisture and Ash Contents

The 2 g sample was used for the determination of moisture and ash contents.

Moisture content determination: The sample was placed in a pre-weighed porcelain crucible and kept in an oven at 105 °C for 2 h. After removal from the oven, it was cooled in a desiccator and then weighed. The process of heating, cooling, and weighing was repeated until a constant weight was achieved. The loss in weight corresponds to the moisture content, and the percentage of moisture was then calculated.

Ash content determination: The sample was placed in a pre-dried, cooled, and weighed porcelain crucible. It was gently heated over a burner until thoroughly charred, then transferred to a muffle furnace at 550 °C until the residue was free of carbon. The crucible and residue were cooled in a desiccator and weighed. This process was repeated until a constant weight was achieved. The ash content was then calculated.

Elemental Analysis of *C. discolor* by Energy Dispersive X-ray Fluorescence (EDXRF) Spectrometer

The relative abundance of elements in the stem of *C. discolor* was determined using an Energy Dispersive X-ray Fluorescence (EDXRF) spectrometer (Shimadzu EDX-700) at the Department of Chemistry, Monywa University.

Preliminary Phytochemical Constituents Tests

Preliminary phytochemical tests were conducted on the sample following standard methods to classify the types of organic constituents present. These included alkaloids, α-amino acids, cyanogenic glycosides, flavonoids, phenolic compounds, saponins, steroids, tannins, and terpenoids. The tests were performed using established protocols as described by M-Tin Wa (1972) and Harborne (1984).

Quantitative Determination of Total Phenolic and Flavonoid Contents

The antioxidative factors, total phenolic content, and total flavonoid content, of watery and ethanol extracts were measured spectrophotometrically according to the Folin-Ciocalteu method (Saxena *et al.,* 2013) and the aluminium chloride colorimetric assay (Zhishen *et al.*, 1999). The absorbance of the reaction mixture was read at λ_{max} 765 nm to determine phenolic content and 415 nm for flavonoid content using a spectrophotometer (Jenway, 6300 Spectrophotometer). The concentrations in terms of gallic acid equivalent of each of the extracts were calculated by using the linear regression equation from the standard curve of gallic acid. Total phenolic contents in the watery and ethanol extracts were expressed as mg of gallic acid equivalent per 1 g extracts. Similarly, the concentration of quercetin equivalent in the extracts was calculated using the linear regression equation from the standard calibration curve of quercetin. The total flavonoid contents of the watery and ethanol extracts were expressed as mg quercetin equivalent per 1 g sample extract.

Investigation of Antioxidant Activity

DPPH radical scavenging activity of ethanol and watery extracts was spectroscopically determined using a UV-visible spectrophotometer (Marinova and Batchvarov, 2011). The control solution was prepared by mixing 1.5 mL of 0.002 % DPPH solution and 1.5 mL of ethanol. The sample solution was also prepared by mixing 1.5 mL of 0.002 % DPPH solution and 1.5 mL of test sample solution. These prepared solutions were kept in brown bottles. Then the solutions were incubated at room temperature and shaken on the shaker for 30 min. After 30 min, the absorbance of different concentrations of tested samples was measured at 517 nm using Jenway, 6300 Spectrophotometer. Absorbance measurements were done three times for each solution and the mean value so obtained was used to calculate the percentage of radical scavenging activity. The butylated hydroxytoluene (BHT) was used as a standard for this activity.

Screening of Antimicrobial Activity

The antimicrobial activity of petroleum ether, ethyl acetate, ethanol, and watery extracts of the sample was determined against six strains of microorganisms such as *B. pumilus, B. subtilis, C. albicans, E. coli, P. aeruginosa,* and *S. typhi* by employing agar well diffusion method (Finegold and Martin, 1982). The tests were conducted at the Department of Chemistry, Madalar University.

In Vitro Determination of Antiarthritic Activity

The *in vitro* antiarthritic activity was studied using the Bovine Serum protein denaturation method and the Egg Albumin denaturation method at a concentration of 125 to 500 μg mL^{-1}. In the Bovine Serum protein denaturation method, the reaction mixture (5 mL) consisted of 0.2 mL of BSA, 2.8 mL of phosphate-buffered saline (pH 6.4), and test solutions of different concentrations (500, 250, and 125 μg/mL) were mixed to form a reaction mixture of 5 mL. Double distilled water of the same volume served as control. The samples were incubated at 37±2 ºC in an incubator for 15 min followed by heating at 70 ºC for 5 min. UV-vis spectrophotometer (Jenway, 6300 Spectrophotometer) was used to measure the absorbance at 660 nm. Similarly, in the egg albumin denaturation method, egg albumin was used instead of BSA.

Results and Discussion

Moisture and Ash Contents of *C. discolor* (Tabinding Mya Nan) Stem

The analysis revealed that the dried stem powder contained **2 % moisture** and **8 % ash.** The low moisture content suggests that the stem can serve as a stable and suitable ingredient for use in conventional medicine, supporting its potential application in treating

various diseases. Moreover, the ash content indicates a high mineral presence, highlighting the stem as a valuable source of essential minerals.

Semiquantitative Elemental Analysis of *C. discolor* (Tabinding Mya Nan) Stem

The semi-quantitative elemental analysis of *C. discolor* stem was conducted using the **EDXRF (Energy Dispersive X-Ray Fluorescence) technique**, which identified the presence of **K, Ca, S, Fe, Cu, Zn, Mn, Rb, and Sr** in the sample. The EDXRF spectra data, illustrating the relative abundance of these elements in the dry powdered stem sample, are presented in **Figure 2** and summarized in **Table 1.** The results are further depicted as bar graphs in **Figure 3.**

The analysis revealed that **calcium (1.247 %)** was the most abundant element in the sample, followed by significant amounts of **potassium (0.519 %)** and **sulphur (0.109 %)**. Calcium and potassium are essential for several physiological functions, including **valence regulation, electrolyte balance, muscle contraction, and blood pressure regulation**. Potassium also plays a critical role in promoting the health of **teeth and bones**. Sulphur contributes to **food metabolism** and supports various bodily functions, including maintaining healthy **skin**. Furthermore, trace elements such as **manganese (Mn)**, **iron (Fe)**, **copper (Cu)**, and **zinc (Zn)** were also detected, highlighting the nutritional value of the sample. Based on these findings, *C. discolor* stem may be considered a beneficial resource for promoting health.

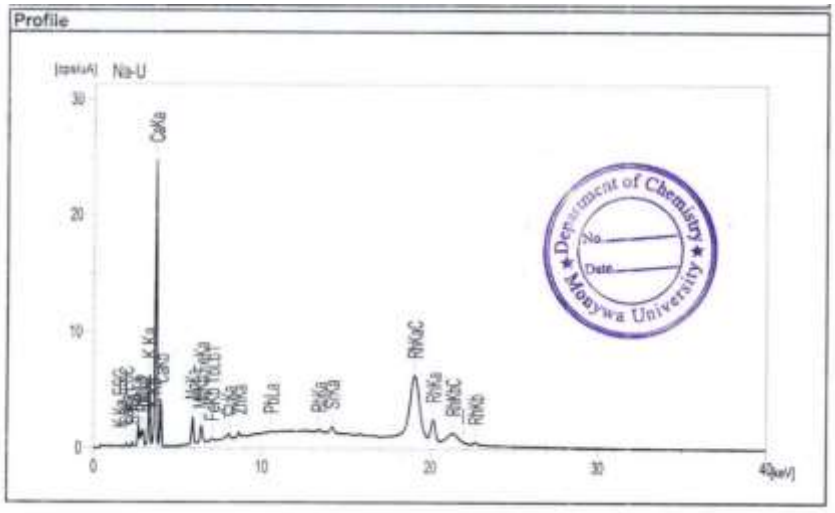

Figure 2. EDXRF spectrum of *C. discolor* (Tabinding Mya Nan) stem

Table 1. Relative Abundance of Some Elements in *C. discolor* (Tabinding Mya Nan) Stem

Elements	Relative abundance (% w/w)
Ca	1.249
K	0.519
S	0.109
Mn	0.022
Fe	0.009
Cu	0.002
Zn	0.001
Sr	0.001
Rb	0.001
C, H	98.086

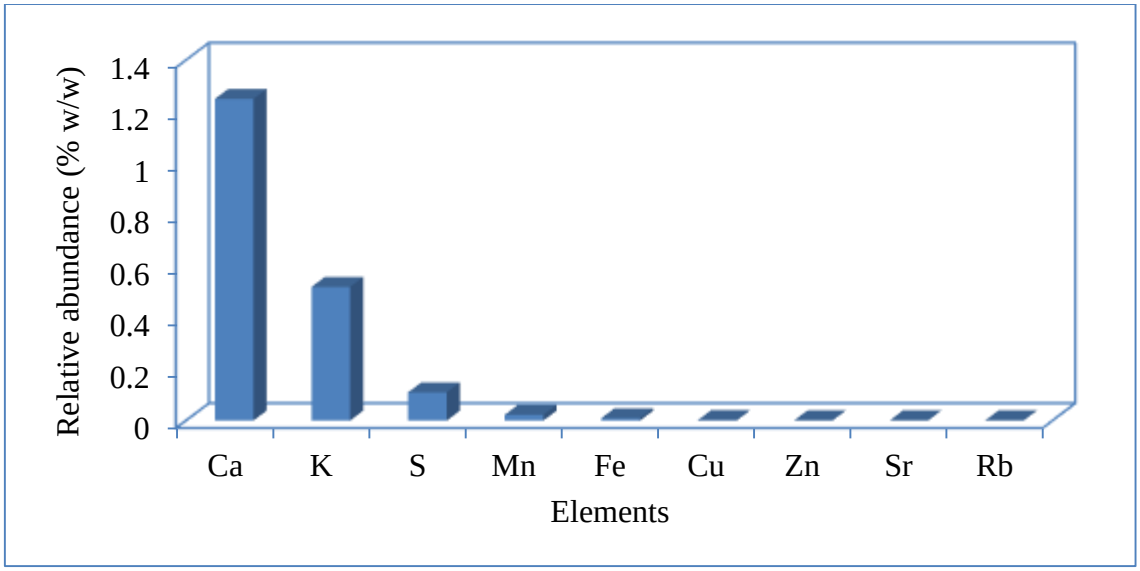

Figure 3. A bar graph of the relative abundance of elements in *C. discolor* (TabindingMya Nan) stem

Phytochemical Constituents of *C. discolor* (Tabinding Mya Nan) Stem

When humans consume phytochemicals, these compounds can exhibit significant biological activity. Phytochemicals are primarily obtained from various plant-based foods, including fruits, vegetables, whole grains, and seeds. This literature survey suggests a more systematic approach is needed to conduct preliminary phytochemical studies on the *C. discolor* stem.

Various phytochemical tests were conducted to determine the presence or absence of alkaloids, α-amino acids, cyanogenic glycosides, flavonoids, and phenolic compounds. The results indicate that all bioactive compounds, except cyanogenic glycosides, are present.

This study provides valuable insights into the presence of diverse phytochemicals, which may contribute to the tested sample's potential antioxidant, antimicrobial, and antiarthritic properties.

Total Phenolic Content of Watery and Ethanol Extracts of *C. discolor* (Tabinding Mya Nan) Stem

The Folin-Ciocalteu (F-C) assay is one of the most widely used methods for phenolic analysis. The principle of the F-C assay is based on the reduction of the Folin-Ciocalteu reagent in the presence of phenolic compounds, resulting in the formation of molybdenum-tungsten blue. This blue complex is measured spectrophotometrically at 765 nm, with the intensity of the colour increasing linearly with the concentration of phenolic compounds in the reaction medium. A higher concentration of phenolic compounds in the extracts leads to a darker colour and higher absorbance.

Gallic acid (3,4,5-trihydroxybenzoic acid) was used to construct a standard calibration curve. The total phenolic content, expressed as micrograms of gallic acid equivalent per milligram (µg GAE/mg) of crude extract, was calculated from this standard curve (Saxena *et al.*, 2013). The total phenolic content of ethanol extract (84.5 ± 0.04 µg GAE/mg extract ± SD) was observed to be nearly twice as high as that of the watery extract (43.5 ± 0.01 µg GAE/mg extract ± SD). The data supporting these findings is presented in Table 2.

Total Flavonoid Content of Crude Extracts of *C. discolor* (Tabinding Mya Nan) Stem

To confirm the presence of active compounds in *C. discolor* (particularly flavonoids), a content analysis was conducted using a colourimetric assay specifically designed to target flavonoids conveniently and appropriately (Cook, 1996). The aluminum chloride colourimetric assay, as reported by Woisky and Salatino (Rice-Evans, 1995), is effective in detecting flavonoids in the flavone and flavanol groups, such as quercetin. In this assay, aluminum chloride reacts with quercetin to form a stable, colour-signature complex.

The reaction involves the C-4 keto group and either the C-3 or C-5 hydroxyl group of the flavonoid compounds to produce an acid-stable complex. Additionally, reactions within the ortho-dihydroxyl groups in flavonoids' A- and B-ring can also form several acid-labile complexes (Agati, 2012). These complexes, formed by flavonols (including kaempferol, rutin, quercetin, and quercitrin), exhibit maximum absorbance at 415 nm (Cook, 1996). By employing the aluminum chloride colourimetric assay, the total flavonoid content can be accurately measured.

A standard calibration curve of quercetin was constructed using varying concentrations of quercetin. From this experimental study, the total flavonoid content of the watery and ethanol extracts of the *C. discolor* stem is presented in Table 2. The results indicate that the ethanol extract (104.03 mg QE/g) contained a higher flavonoid content compared to the watery extract (55.64 mg QE/g).

Table 2. Total Phenolic Content and Total Flavonoid Content in Watery and Ethanol Extracts of *C. discolor* (Tabinding Mya Nan) Stem

Extracts	TPC (µg GAE/mg extract ± SD)	TFC (mg of QE/ g of extract ± SD)
Watery	43.5 ± 0.01	55.64 ± 0.002
Ethanol	84.5 ± 0.04	104.03 ± 0.001

Radical Scavenging Activity of Crude Extracts of *C. discolor* (Tabinding Mya Nan) Stem by DPPH Radical Scavenging Assay

According to the description by Marinova and Batchvarov (2011), the antioxidant activity of watery and ethanol extracts of the *C. discolor* stem was evaluated using a DPPH radical scavenging assay. The assay is based on the violet-coloured ethanolic DPPH solution, which has a maximum absorption wavelength of 517 nm. Neutralisation of the DPPH free radical results in a colour change from violet to pale yellow under daylight. Test substances with anti-radical properties cause decolourisation of the original colour. As the concentration of the test substance increases, absorption values decrease, indicating stronger antioxidant activity.

In this study, butylated hydroxytoluene (BHT) was used as a standard. Experimental data revealed that the *C. discolor* stem exhibits high antioxidant activity. The IC_{50} values of the stem extracts and the standard BHT, along with their percent radical scavenging activity, are presented in Figure 4. Additional details are provided in Table 3.

The antioxidant potency of the ethanol extract (IC_{50} = 13.60 µg/mL) was found to be higher than that of the watery extract (20.49 µg/mL); however, both are lower than the standard BHT (IC_{50} = 3.43 µg/mL).

Evidence suggests a positive association between the scavenging ability against DPPH radicals and the presence of phenolic and flavonoid compounds. This finding indicates that these

compounds contribute significantly to the antioxidant capacity of both ethanol and watery extracts of the *C. discolor* stem.

Table 3. Radical Scavenging Activity of Watery and Ethanol Extracts of *C. discolor* Stem and Standard BHT

Extracts	% RSA ± SD of different concentrations (µg/mL)				IC_{50} (µg/mL)
	3.125	6.25	12.5	25	
Watery	44.44 ± 0.175	46.67 ± 0.175	48.37 ± 0.175	50.92 ± 0.175	20.49
Ethanol	46.75 ± 0.232	48.37 ± 0.355	49.53 ± 0.235	54.85 ± 0.23	13.60
BHT (Std.)	49.11 ± 0.009	58.31 ± 0.008	68.69 ± 0.001	82.05 ± 0.001	3.43

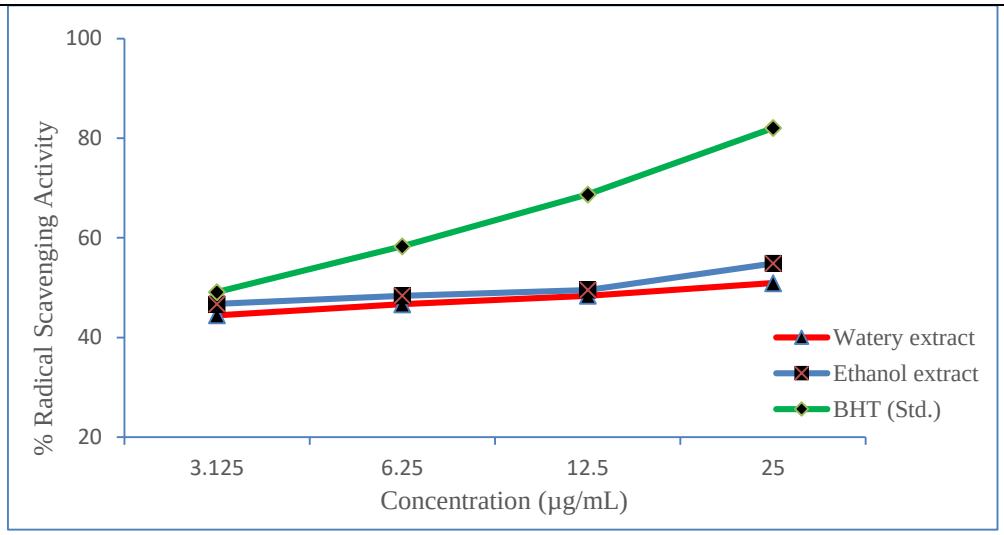

Figure 4. Percent radical scavenging activity vs concentration (µg/mL) of watery and ethanol extracts of stem of *C. discolor* and standard BHT

Screening of Antimicrobial Activity of Crude Extracts of *C. discolor* Stem by Agar Well Diffusion Method

In this study, the antimicrobial activity of four crude extracts (H_2O, EtOH, EtOAc, and PE) obtained from the stem of *C. discolor* was evaluated against six different microbial strains: *B. subtilis*, *B. pumilus*, *C. albicans*, *E. coli*, *P. aeruginosa*, and *S. typhi*. The agar well diffusion method was used to assess antimicrobial activity, with the measurable zone of inhibition (including the 8 mm well diameter) indicating the degree of effectiveness. A larger zone diameter corresponds to greater antimicrobial activity.

Photographic records of the results are presented in Figure 5, while the inhibition zone diameters are summarized in Table 4. The results revealed that the ethyl acetate (EtOAc) and ethanol (EtOH) extracts exhibited mild antimicrobial activity against all tested microorganisms, whereas the petroleum ether (PE) and watery (H_2O) extracts showed no activity.

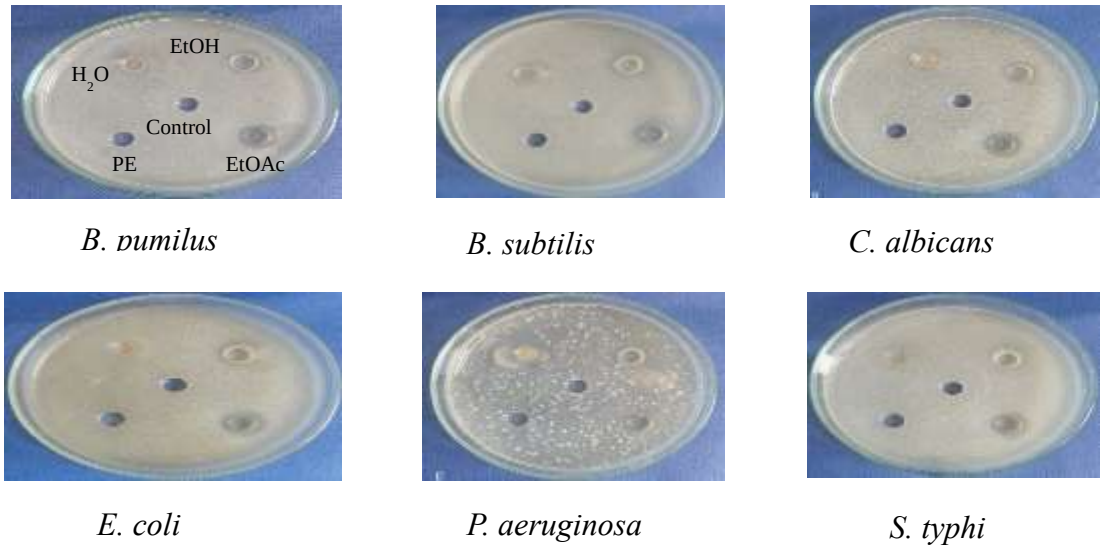

Figure 5. Photo records showing inhibition zone due to the effect of different crude extracts *C. discolor* stem on six different microorganisms

Table 4. Inhibition Zone Diameters of Various Crude Extracts of *C. discolor* Stem on Six different Microorganisms

Microorganisms	Inhibition zone diameter of different extracts (mm)			
	PE	**EtOAc**	**EtOH**	**H_2O**
B. pumilus	-	12.03	12.89	-
B. subtilis	-	13.10	12.00	-
C. albicans	-	11.75	11.00	-
E. coli	-	12.50	11.30	-
P. aeruginosa	-	10.33	11.21	-
S. typhi	-	12.00	12.50	-

Agar well (8 mm); 9 mm ~ 14 mm = mild activity; 15 mm ~ 20 mm = medium activity;
21 mm and above = high activity; (-) = no activity

Antiarthritic Activity of Crude Extracts of *C. discolor*

In the anti-arthritis assay using the protein denaturation method, both extracts demonstrated significant results, as detailed in Table 5. A decrease in the absorbance of test samples compared to the control indicates protein stabilization. The ethanol extract exhibited a higher inhibition percentage than the aqueous extract. The IC_{50} value for the inhibition of bovine serum albumin (BSA) protein denaturation was 744.05 µg/mL for the ethanol extract and 856.16 µg/mL for the watery extract. Similarly, in the egg albumin protein denaturation method, the IC_{50} value for the ethanol extract was 415.28 µg/mL, compared to 775.90 µg/mL for the watery extract. These results are illustrated in Figure 6. As a result, the ethanol extract was found to exhibit a higher inhibition of protein denaturation compared to the watery extract. However, both extracts were less potent than the standard drug Allopurinol (IC_{50} = 204.75 µg/mL in BSA assay and 335.57 µg/mL in egg albumin assay)

Protein denaturation is a primary cause of arthritic diseases (Hossain *et al.*, 2015). Based on this study, it can be concluded that both extracts possess anti-arthritic properties and can prevent the efflux of intracellular components. These properties are likely due to the production of various phytoconstituents within the plant. Phenolics and flavonoids are well-documented for their biological activities, including antioxidant, anticarcinogenic, anti-inflammatory, cardiovascular protection, and cell proliferation effects (Rice-Evans et al., 1996). According to Singh and Sharma (2016), anti-arthritic activity can be attributed to phenols, tannins, and flavonoids. Additionally, many flavonoids and related polyphenols contribute to the antioxidant and anti-inflammatory activities of numerous plants (Govindappa *et al.*, 2011). Therefore, the presence of these bioactive compounds in the extracts suggests that the samples possess membrane-stabilizing properties.

Table 5. Antiarthritic Activity of Crude Extracts of *C. discolor* Stem on Protein Denaturation Method by Using Bovine Serum Albumin and Egg Albumin

Extracts	Conc. (µg/mL)	% Inhibition		IC_{50} (µg/mL)	
		BSA	EA	BSA	EA
Watery	125	15.78	19.31	856.16	775.90
	250	21.05	30.68		
	500	36.84	43.18		
	1000	52.63	55.36		
Ethanol	125	14.85	19.64	744.05	415.28
	250	25.74	41.07		
	500	47.77	53.57		
		57.89			
Allopurinol	125	47.36	30.36	204.75	335.57
	250	52.63	51.79		
	500	54.89	64.29		

Conc.= Concentration; BSA = Bovine Serum Albumin; EA = Egg Albumin

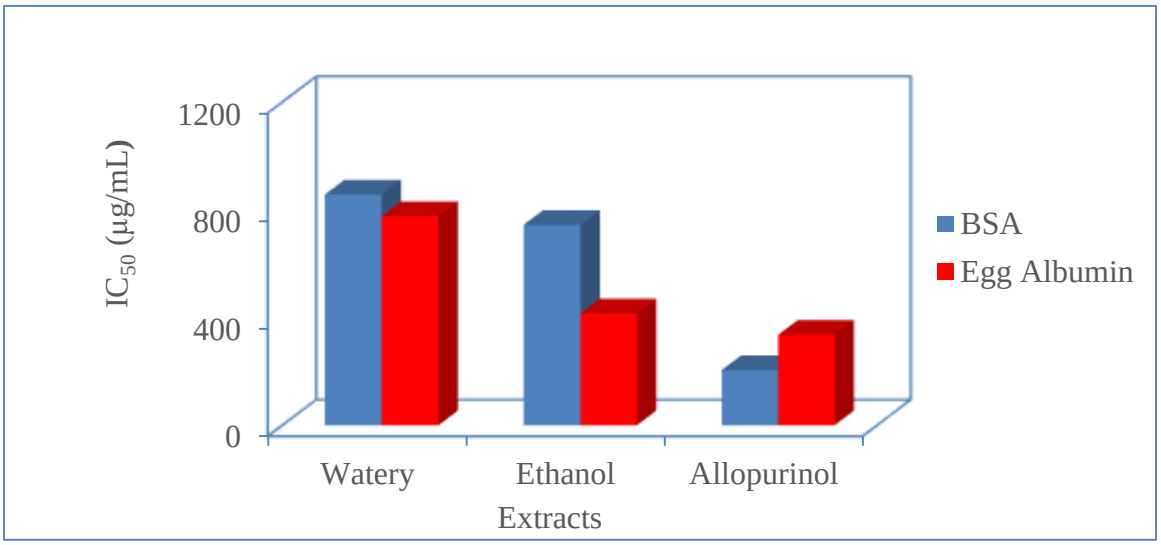

Figure 6. A bar graph of IC_{50} values of watery, ethanol, and Allopurinol in bovine serum albumin and egg albumin protein denaturation

Conclusion

The study analyzed the composition and bioactivities of the *C. discolor* (Tabinding Mya Nan) stem, including its moisture, ash, elemental, and phytochemical contents, as well as antioxidant, antimicrobial, and antiarthritic properties. High ash and low moisture contents highlight its suitability for medicinal use, with significant levels of calcium, potassium, and sulfur supporting micronutrient-related treatments.

Phytochemical screening revealed all tested constituents except cyanogenic glycosides. The ethanol extract, rich in phenolic and flavonoid compounds, exhibited strong antioxidant activity but limited antimicrobial efficacy. Both ethanol and aqueous extracts demonstrated antiarthritic activity, suggesting their potential as natural therapeutic agents.

Overall, the stem of *C. discolor* demonstrates potential as a natural alternative medicine, exhibiting antioxidant, antimicrobial, and antiarthritic properties.

Acknowledgements

The authors are grateful to the Myanmar Academy of Arts and Science for allowing them to submit this paper. We also thank Professor and Head, Dr. Thin Thin Nwe, Department of Chemistry, Taunggyi University for her kind interest and encouragement of this paper.

References

Agati, G., A. Elisa, P. Susanna and T. Massimiliano. (2012). "Flavonoids as Antioxidant in Plants: Location and Functional Significance, A Review", vol. 196, pp. 67-76.

Cook, N. C. and S. Samman. (1996). "Flavonoids—Chemistry, Metabolism, Cardioprotective Effects, and Dietary Sources, a Review". *J. of Nutritional Biochemistry*, vol. 7 (2), pp. 66-76.

Finegold, S. M., W. J. Martin and E. G. Scott. (1982). *Diagnostic Microbiology*. London, 6th Ed., Mos by Co. Ltd., pp. 586-588.

Govindappa M., R. Channabasava, D. V. Sowmya, J. Meenakshi, M. R. Shreevidya, A. Lavanya, G. Santoyo and T. S. Sadananda. (2011). "Phytochemical Screening, Antimicrobial and *in vitro* Anti-inflammatory Activity of Endophytic Extracts from *Loranthus* sp". *Pharmacogn. J.*, vol. 3 (25), pp. 82–90.

Harborne, J. B. (1984). *Phytochemical Methods, A Guide to Modern Techniques of Plant Analysis.* New York: 2nd Ed., Chapman and Hall, pp. 120-126.

Hossain M. M., K. M. S. Hafez, M. A. Hasanat, K. Imtiazul, C. T. Ahmad, A. M. Sayeed, and K. Golam. (2015). "Investigation of *in vitro* Anti-arthritic and Membrane Stabilizing Activity of Ethanol Extracts of Three Bangladeshi Plants". *Pharm. Innov. J.*, vol. 4 (1), pp. 76–80.

Khin Phyu Phyu, Khaing Khaing Mar, Kyi San, Khin Lay Sein, Thandar Myat Thaw, Mya Mar Lar, Lei Lei Win, Kyae Mhon Htwe and Aung Thura. (2017). "Accumulative Study of Heavy Metals in Soils Water Uptake by Rhizome of Two Species of Various Sites", *Myanmar Health Sciences Research J.*, vol. 29 (1), pp. 65-69.

Marinova, G. and V. Batchvarov. (2011). ″Evaluation of the Methods for Determination of the Free Radical Scavenging Activity by DPPH″. Bulgarian *Journal of Agricultural Science*, vol. 17 (1), pp. 11-24.

M-Tin Wa. (1972). "Phytochemical Screening Methods and Procedures", *Phytochemical Bulletin of Botanical Society of America*, vol. 5 (3), pp. 4-10.

Rice-Evans C. A., N. J. Muller and G. Paganga. (1996). "Structure-antioxidant Activity Relationships of Flavonoids and Phenolic Acids". *Free Radic. Biol. Med.* vol. 20 (7), pp. 933–956.

Saxena, M., S. Jyoti, R. Nema, S. Dharmendra and G. Abhishek. (2013). "Phytochemistry of Medicinal Plants." *J. of Pharmacognosy and Phytochemistry*, vol. 1 (6), pp. 168-182.

Zhishen, J., T. Mengcheng and W. Jianming. (1999). ″The Determination of Flavonoid Contents in Mulberry and Their Scavenging Effects on Superoxide Radicals″. *Food Chem*., vol. 64, pp. 555-559.

PREPARATION AND PHYSICOCHEMICAL ANALYSIS OF ECO-ENZYME FROM *CITRUS LIMON* L. BURM. F. (SHAUK) FRUIT PEELS WASTE

Nwe Mar Lin[1], Myatt Hla Wai [2], Sandar Aung [3]

Abstract

Eco-enzyme, an organic solution derived from the fermentation of fruit waste, brown sugar, and water in a 3:1:10 ratio, offers a sustainable alternative to chemical-based solutions. In this study, *Citrus limon* L. Burm. f. (Shauk) peels were collected and fermented for three months. The resulting eco-enzyme exhibited a dark brown colour, a fermented aroma, and physicochemical properties including pH 3.9, total acidity 1.74 g/L, density 0.953 g/mL, and alcohol content 2.50%. Alkaloids, organic acids, glycosides, flavonoids, saponins, and phenolic compounds were present in the prepared eco-enzyme, contributing to its antibacterial and cleaning properties. The prepared eco-enzyme was successfully applied as a cleaning agent for ceramics and whiteboards. Wastewater samples from Nantawgone Quarter, Meiktila Township, were treated with the eco-enzyme at concentrations of 5%, 10%, and 20% (v/v). The treatment effectively improved water quality parameters, including pH, total alkalinity, hardness, total dissolved solids, and chloride and sulphate contents. This study highlights the potential of eco-enzymes as an eco-friendly, cost-effective solution for environmental hygiene and wastewater treatment while also promoting the recycling of organic waste.

Keywords: *Citrus limon* L. Burm. f., eco-enzyme, fermentation, physicochemical properties, cleaning agent, wastewater treatment

Introduction

Eco-enzyme is a type of vinegar made by fermenting fruit waste with sugar to form organic acid and alcohol. Eco-enzymes are also called bio-enzymes, garbage enzymes, fruit enzymes, flower enzymes, etc. It is a type of homemade vinegar, reduced from alcohol by fermentation of kitchen waste as substrate with sugar. The liquid eco-enzyme contains protease, lipase, and amylase, all of which could be employed as cleaning agents (Indraloka *et al.,* 2023). It is a universal, natural cleaner produced from vegetable/fruit peels or waste. These organic substances are capable of breaking down chemical and other organic waste, thus helping us in removing stains, odours, getting rid of other harmful microbes, etc. Organic waste is frequently disposed of directly into the environment without treatment, causing negative environmental effects such as pollution, disruption of environmental aesthetics, and disruption of public health (Rusdianasari *et al.,* 2021). They also greatly neutralize toxins and pollutants. Eco-enzyme acts as an antifungal, antibacterial, and insecticidal agent (Pawar *et al.,* 2022).

Almost a fifth of the total citrus cultivars are subjected to industrial processes, mainly for the production of their juices, which represent the most consumed fruit juices worldwide, thus generating a large amount of processing waste (about 120 million tons per year) (Zema *et al.,* 2018). The high rate of pollution given by citrus waste depends on its easy fermentability, since it is abundant, and chemically complex, biodegradable, thus requesting high oxygen demand (Russo *et al.,* 2021). One method for reducing organic waste is to use fruit peel and vegetable waste to make eco-enzyme. An eco-enzyme is a complex organic liquid that contains a number of organic enzymes and acids that developed from waste lemon, lime, cabbage, pineapple, orange, and mango peels (Arun and Sivashanmugam, 2015).

[1] Department of Chemistry, Meiktila University
[2] Department of Chemistry, Meiktila University
[3] Department of Chemistry, Meiktila University

The main aim of this research is to prepare and analyze some physicochemical properties of eco-enzyme from peels of citrus fruits and to apply it as a cleaning reagent for ceramic products and wastewater treatment.

Materials and Methods

Sample Collection and Preparation

Citrus limon L. Burm. f. (Shauk) fruit peels samples were collected from the local market, Meiktila Township, Mandalay Region. *Citrus limon* L. Burm. f. (Shauk) fruit peels were cut with a knife into small pieces. Then 600 g of sample were mixed with 200 g of brown sugar as a carbon source and 2 L of water inside an airtight plastic bottle with a 5 L capacity and left standing overnight. After overnight, 0.3% yeast culture solution was added to the above bottle and stirred thoroughly. This was kept in a dark place at room temperature. Fermentation was conducted for 90 days in sun-protected conditions at room temperature (Figure 1). After 90 days, the content in the plastic bottle was filtered (Suliestyah *et al.*, 2022).

Figure 1. Fermentation vessel of eco-enzyme from *Citrus limon* L. Burm. f. (Shauk) fruit peels

Determination of Physicochemical Properties of Prepared Eco-enzyme Sample

During the fermentation period (15, 30, 45, 60, 75 and 90 days), the pH, total acidity, density, total dissolved solids and alcohol contents were determined by the AOAC method (AOAC, 2000). For the determination of the properties of the prepared eco-enzyme, pH values were determined by a pH meter, the total acidity contents by titrimetric method, density by a density bottle, total dissolved solids by an oven drying method, and alcohol contents by a hydrometer.

Qualitative Tests for Metabolite

Qualitative tests were carried out on eco-enzyme with a view to determine the presence of active constituents namely, alkaloids, flavonoids, phenolic compounds, saponins and glycosides (Trease and Evans, 1980; Harborne, 1993; Marini-Bettolo *et al.*, 1981).

Application of Prepared Eco-enzyme

Application of eco-enzyme as a cleaning agent

In this study, 50% eco-enzyme has been used as a cleaning agent for whiteboard marker residue and ceramic items (dishes and basins).

Application of eco-enzyme in wastewater treatment

Wastewater sample was collected from the Nantawgone quarter, Meiktila Township, Mandalay Region. In this study, 5%, 10%, and 20% (v/v) of eco-enzyme dosage with the wastewater samples were selected. Four beakers were filled with 100 mL of wastewater sample and the respective dosage of eco enzyme solution. These beakers were covered and were left for a 1-day digestion period. Some physicochemical properties of wastewater samples before and after treatment with eco-enzyme were determined by AOAC method. In this study, pH values were measured by a pH meter, the total alkalinity, total hardness, and chloride contents were determined by titrimetric method, total dissolved solids were determined by an oven drying method, and sulphate contents were determined by UV-Visible spectrophotometer.

Results and Discussion

Fermentation Process in Preparation of Eco-Enzyme

In this study, eco-enzyme is a fermentation product of *Citrus limon* L. Burm. f. (Shauk) fruit peels, brown sugar, and water in a proportion of 3:1:10. During the fermentation process of making eco-enzyme, naturally occurring microorganisms on fruit scraps break down the organic material, producing enzymes, organic acids like acetic acid, and carbon dioxide, resulting in a liquid with cleaning and potentially fertilizing properties due to the breakdown of complex organic compounds into smaller, readily usable components; essentially, the microbes "digest" the waste, lowering the pH level and creating a beneficial enzyme-rich solution. After fermentation of 90 days, the final product of eco-enzyme is in the form of suspended residue and fermented liquid. The residue can be used as organic fertilizer residue. The total volume of eco-enzyme was found to be 2000 mL.

Physicochemical Properties of Eco-enzyme

pH and total acidity

Microorganisms, such as yeast and bacteria, play a crucial role in fermentation. The growth and multiplication of these organisms are also influenced by pH levels. In this research work, the pH of the eco-enzyme was within the acidic range throughout the period of fermentation. After 90 days of fermentation, the pH of the eco-enzyme was decreased from 6.3 to 3.9. The low pH of the eco-enzyme is caused by the high content of organic acids. The longer the fermentation time, the lower the pH of the eco-enzyme (Table 1 and Figure 2).

Eco-enzyme contains organic acids in the form of acetic acid and lactic acid. The organic acids contained in eco-enzymes are the result of the fermentation process (Natasya *et al.*, 2023). In this study, the total acidity of eco-enzyme was found to increase from 0.58 g/L to 1.74 g/L (Table 2 and Figure 3). This is due to one of the organic acids, acetic acid, which is produced through the fermentation process, is obtained when the sucrose contained in the fermentation solution turns into alcohol and continues to become acetic acid (Kamaliya and Lusiani, 2023).

Table 1. pH Values of Eco-enzyme Sample at Different Fermentation Periods

Fermentation period (day)	pH
0	6.3
15	5.9
30	5.3
45	4.8
60	4.5
75	4.1
90	3.9

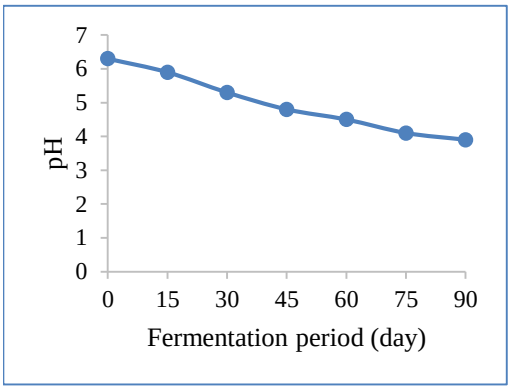

Figure 2. Changing in pH of eco-enzyme during fermentation

Table 2. Total Acidity of Eco-enzyme Sample at Different Fermentation Periods

Fermentation period (day)	Total acidity (g/L)
0	0.58
15	1.35
30	1.49
45	1.58
60	1.65
75	1.70
90	1.74

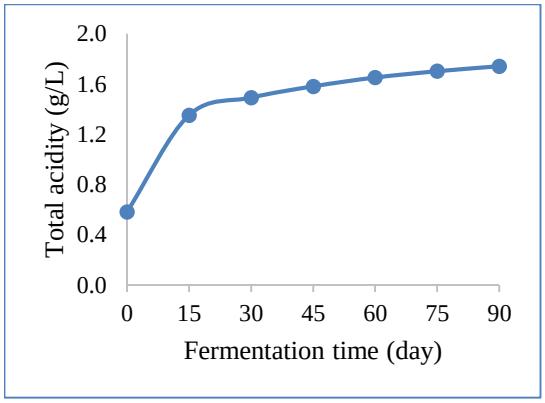

Figure 3. Changing in total acidity of eco-enzyme during fermentation

Density and total dissolved solids

The changes in density of the eco-enzyme sample during fermentation at different periods are shown in (Table 3 and Figure 4). Throughout the fermentation, the density values of the prepared eco-enzyme sample were found to decrease slightly. The density of eco-enzyme was found to be 0.953 g/mL after 90 days of fermentation.

The decrease in total dissolved solids of eco-enzyme was observed throughout the period of fermentation. In this study, the total dissolved solid of eco-enzyme was found to be 1357 mg/L after 90 days of fermentation (Table 4 and Figure 5). The total dissolved solid will vary depending on the type and amount of fruit waste used in the eco-enzyme through fruit waste. Generally, the total dissolved solid level of the eco -enzyme through fruit waste will be relatively low, as most of the components in the waste will break down during the fermentation process,

typically ranging between 200 and 400 ppm. However, certain types of fruit waste, such as citrus fruits, may contain higher levels of minerals, resulting in a higher TDS level (Benny *et al.*, 2023). Total Dissolved Solids (TDS) decrease as microorganisms break down complex organic compounds in fruit waste into smaller, soluble molecules like citric and acetic acids. These are absorbed by the water, reducing TDS levels.

Table 3. Density of Eco-enzyme Sample at Different Fermentation Periods

Fermentation period (day)	Density (g/mL)
0	1.023
15	1.010
30	1.003
45	1.000
60	0.990
75	0.959
90	0.953

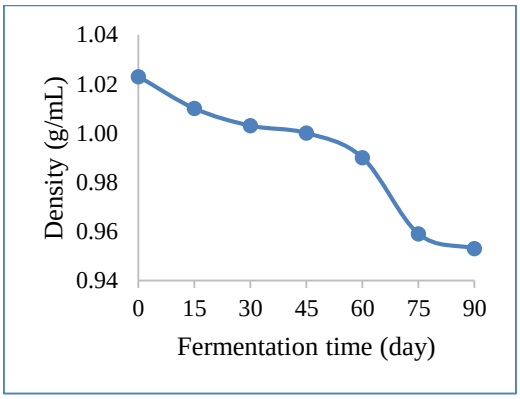

Figure 4. Changing in density of eco-enzyme during fermentation

Table 4. Total dissolved solids of Eco-enzyme Sample at Different Fermentation Period

Fermentation period (day)	Total dissolved solids (mg/L)
0	2200
15	1988
30	1710
45	1655
60	1490
75	1362
90	1357

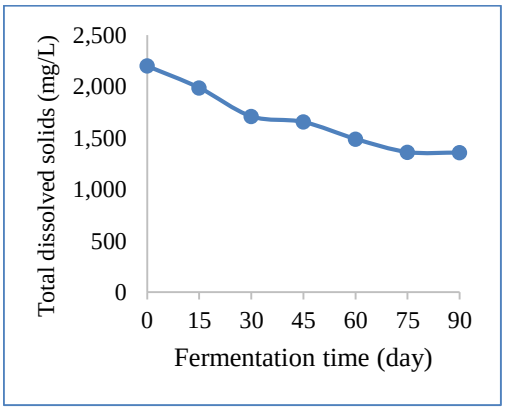

Figure 5. Changing in total dissolved solids of eco-enzyme during fermentation

Alcohol contents

Fermentation is a metabolic process in which organisms convert carbohydrates, like starch or sugars, into either alcohol or acids. Alcoholic fermentation is mainly carried out by yeast. In this study, the alcohol content of eco-enzyme was found to increase from 0.0% to 2.50%. This is because naturally occurring yeasts on the fruit peel break down sugars present in the fruit, converting them into ethanol (alcohol) as a byproduct of their metabolic process during anaerobic fermentation. It was found that, the longer the fermentation time, the higher the alcohol content (Table 5 and Figure 6).

Table 5. Alcohol Contents of Eco-enzyme Sample at Different Fermentation Periods

Fermentation period (day)	Alcohol content (%)
0	0.00
15	0.96
30	1.83
45	1.95
60	2.25
75	2.45
90	2.50

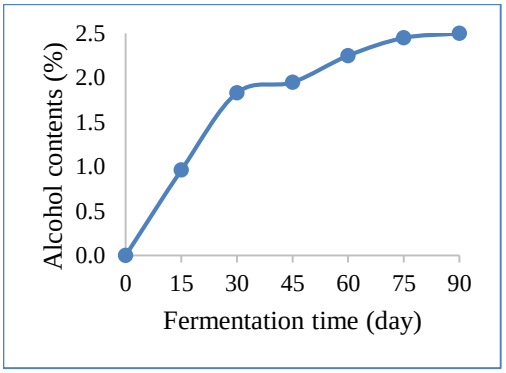

Figure 6. Changing in alcohol contents of eco-enzyme during fermentation

Physicochemical Properties of Eco-enzyme After 90 Days of Fermentation

After 90 days of fermentation, the eco-enzyme developed a dark brown colour and a distinct fermented aroma, influenced by the composition of the ingredients used. At the end of the fermentation process, the eco-enzyme exhibited a pH of 3.9, total acidity of 1.74 g/L, density of 0.953 g/mL, total dissolved solids of 1,357 mg/L, and an alcohol content of 2.50%. These physicochemical parameters agree with the ranges reported in the literature, indicating the preparation process yielded expected and consistent results.

Table 6. Some Physicochemical Properties of Eco-enzyme after 90 Days of Fermentation

No.	Properties	Prepared eco-enzyme	Literature values of eco-enzyme*
1.	colour	dark brown	-
2.	odour	fermented	-
3.	pH	3.9	2.9 - 6.5
4.	total acidity (g/L)	1.74	1.63-5.30
5.	density (g/mL)	0.953	0.999-1.035
6.	total dissolved solids (mg/L)	1357	1000-2000
7.	alcohol contents (%)	2.50	-

*(Abdullah *et al.*, 2023; Ismali, 2024; Lakra *et al.*, 2022; Kamaliya and Lusiani, 2023)

Metabolites in Prepared Eco-enzyme

The prepared eco-enzyme contained alkaloids, organic acids, glycosides, flavonoids, saponins and phenolic compounds (Table 7). Alkaloids have potent antibacterial activity. Organic acids such as acetic acid, lactic acid, and their mixtures possess strong antimicrobial activity and have been used as cleaning reagents and hand sanitizers. Phenolic compounds and flavonoids may affect growth and metabolism of bacteria. They could have an activating or inhibiting effect on microbial growth according to their constitution and concentration**.** Saponins and glycosides could be used for several biological effects, such as antimicrobial, antibacterial etc. Saponin is also an effective cleaning agent. It is a natural detergent and foaming substance that is effective at lifting grease, dirt and grime from ceramic products.

Table 7. Test of Eco-enzyme after 90 days of Fermentation

No.	Tests compounds	Test reagents	Observation	Remark
1	alkaloids	Mayer's reagent	white ppt	+
		Dragendorff's reagent	brown ppt	+
		Wagner's reagent	brown ppt	+
2	organic acids	bromocresol green indicator	green colour solution	+
3	glycosides	10% lead acetate	white ppt	+
4	flavonoids	conc. HCl solution and Mg turnings	pale yellow colour solution	+
5	saponins	distilled water	frothing	+
6.	phenolic compounds	1 % $FeCl_3$ and $K_3[Fe(CN)_6]$	blue-black colour solution	+

(+) = presence, (-) = absence, ppt = precipitate

Application of Eco-Enzyme

Cleaning agent

In households, eco-enzyme cleaners are an eco-friendly alternative to traditional chemical cleaning products. They are equally effective at removing stains, disinfecting surfaces, and cleaning drains.

In this study, 50% eco-enzyme has been used as a cleaning agent for ceramic products (basins and dishes) and whiteboard marker residues. Figures 8, 9 and 10 show the before and after cleaning of the ceramic basin, oily dishes, and whiteboard marker residues. When the prepared eco-enzyme was applied to ceramic basins, it effectively removed calcium deposits and organic residues. Proteases break down protein-based stains, including food residues, eggs, blood, urine, feces, wine, and other beverages. Amylases break down starch-based residues, such as those from sauces, ice cream, and gravy. On greasy, oil-coated dishes, the lipase enzymes efficiently dissolve fats, making it easier to rinse away residues (Aartheeswari and Kirthiga, 2021). The prepared eco-enzyme was capable of removing whiteboard marker residues by breaking down the organic compounds in the ink, leaving the surface clean and residue-free.

Figure 7. Before and after cleaning of ceramics basin with 50% eco-enzyme

(a) dirty dish with grease (b) dirty dish with oil (c) clean dish

Figure 8. Before and after cleaning of ceramic dishes with 50% eco-enzyme

Figure 9. Before and after cleaning of whiteboard with 50% eco-enzyme

Wastewater treatment with eco-enzyme

Water quality parameters were evaluated to study the efficiency of the eco-enzyme solution in wastewater treatment. In this study, the collected wastewater sample was treated with different concentrations of eco-enzyme (5%, 10%, and 20%) (v/v), and some physicochemical parameters (pH, total alkalinity, hardness, total dissolved solids, chloride, and sulphate) were determined before and after treatment (Table 8). The results were compared with the standard values recommended by the World Health Organization (WHO, 1984).

The pH values of water treated with 10% and 20% eco-enzyme (7.2 and 6.6, respectively) fall within WHO standards, while that treated with 5% eco-enzyme (8.5) is at the upper limit but still acceptable. In terms of total alkalinity, the 10% eco-enzyme treatment is closest to the desirable limit (240 mg/L vs. 200 mg/L) (Singh and Simgh, 2008). Both 10% and 20% eco-enzyme treatments meet the acceptable range for total hardness, but only the 10% treatment meets the WHO standard for total dissolved solids (TDS) at 1000 mg/L. Chloride contents in all

treated samples are within acceptable limits. Although sulphate contents exceed WHO standards in all cases, the 10% eco-enzyme treatment shows the lowest level, making it the closest to the standard. It was found that different concentrations of eco-enzyme treatment reduced the values of pH, total alkalinity, total hardness, total dissolved solids, chloride contents, and sulphate contents of the wastewater. However, the 10% eco-enzyme treatment demonstrates the optimum condition, meeting pH, total alkalinity, total hardness, TDS, and chloride standards, with sulphate slightly above the recommended limit but lower than other treatments.

Table 8. Some Physicochemical Properties of Wastewater Samples before and after Treatment with Prepared Eco-enzyme Sample

No.	Wastewater Sample	pH	Total alkalinity (mg/L)	Total hardness (mg/L)	Total dissolved solids (mg/L)	Chloride contents (mg/L)	Sulphate contents (mg/L)
1.	before treatment	9.4	390	339	1500	256	497
2.	5 % eco-enzyme	8.5	290	290	1350	230	431
3.	10 % eco-enzyme	7.2	240	235	1000	213	423
4.	20 % eco-enzyme	6.6	110	202	1300	210	460
5.	WHO Standards	6.5-8.5	200	300	1000	250	400

Conclusion

This study focused on producing eco-enzyme from *Citrus limon* peels through fermentation with brown sugar and water. Over 90 days, the fermentation process altered its properties, increasing acidity and alcohol content while reducing pH, density, and total dissolved solids. The prepared eco-enzyme contained alkaloids, flavonoids, and organic acids, contributing to its antibacterial properties. It proved effective as a natural cleaning solution for ceramics and whiteboards. It is also effective in wastewater treatment, offering a sustainable, low-cost alternative to synthetic chemicals. The prepared eco-enzyme not only reduces organic waste but also supports environmental hygiene and agricultural applications.

Acknowledgments

The authors would like to thank the Myanmar Academy of Arts and Science for allowing them to present this paper and Dr Ba Han (Rector, Meiktila University), Dr Kyaw Linn, and Dr Min Thaung, Pro Rectors, Meiktila University) for their kind encouragement.

References

Aartheeswari, S. and B. Kirthiga. (2021). "Production of an Ecofriendly Enzyme Biocleaner from Fruit Wastage". *International Journal for Research in Engineering Application & Management*, vol. 06 (12), pp. 285-290.

Abdullah, N. O., A. Zubair, N. A. P. Mangarengi, R. M. Rachman, M. Tumpu, and D. Djamaluddin. (2023). "Identification of Eco Enzyme Characteristics from Organic Waste". *IOP Conf. Series: Earth and Environmental Science*, vol. 1268 (1), pp. 1-6.

AOAC, (2000). *Official Methods of Analysis.* USA: 17th Ed, The Association of Official Analytical Chemists, pp. 178-189.

Arun, C. and P. Sivashanmugam (2015). "Identification and Optimization of Parameters for The Semi-Continuous Production of Garbage Enzyme from Pre-Consumer Organic Waste by Green RP-HPLC Method". *Waste Management,* vol. 44, pp. 28-33.

Benny, N., R. Shams, K. K. Dash, V. K. Pandey, and O. Bashir. (2023). "Recent Trends in Utilization of Citrus Fruits in Production of Eco-enzyme". *Journal of Agriculture and Food Research,* vol. 13, p. 100657.

Harborne, J. B. (1973). *Phytochemical Methods: A Guide to Modern Technique of Plant Analysis*. London: Chapman and Hall Ltd.

Indraloka, A. B., A. Istanti, and S. W. Utami1. (2023). "The Physical and Chemical Characteristics of

Eco-enzyme Fermentation Liquids from Several Compositions of Local Fruits and Vegetables in Banyuwangi". *IOP Conference Series: Earth and Environmental Science,* vol. 1168, pp. 1-6.

Ismail, A. Y., M. F. Nainggolan, and A. P. Nauli. (2024). "Characterizing The Chemical Composition of Eco-Enzymes Derived from Vegetable and Fruit Sources". *International Journal of Design & Nature and Ecodynamics,* vol. 19 (3), pp. 1051-1060.

Kamaliya, N. and C. E. Lusiani. (2023). "Effect of Baker's Yeast Concentrations on Eco Enzyme Products by the Fermentation Process". *Distilat Jurnal Teknologi Separasi.,* vol. 9 (4), pp. 412-424.

Lakra, P., S. K. Saini, and A. Saini. (2022). "Synthesis, Physio-Chemical Analysis and Applications of Bio-Enzymes Based on Fruit and Vegetable Peels". *Journal of Emerging Technologies and Innovative Research,* vol. 9 (9), pp. 670-681.

Marini-Bettolo, G. B., M. Nicoletti, and M. Patamia. (1981). "Plant Screening by Chemical and Chromatographic Procedure under Field Conditions". *J. Chromato.,* vol. 213, pp. 113-129.

Natasya, N., M. Fadilah, R. Fitri, S. A. Farma, and M. Simwela. (2023). "Analyzing the Quality of Eco-Enzymes Based on Differences in Plant Tissue on the Organic Matter". *Jurnal Biota,* vol. 9 (1), pp. 45-53.

Pawar, V. V., V. G. Kulkarni, P. N. Chavan, G. E. Kanse, and M.B. Bhadange. (2022). "Citrus Bio-Enzyme Production and Application for Waste Water Treatment". *International Journal of Advance Research and Innovative Ideas in Education*, vol. 8 (3), pp. 2395-4396.

Rusdianasari, A. Syakdani, M. Zaman, F. F. Sari, N. P. Nasyta., and R. Amalia. (2021). "Production of Disinfectant by Utilizing Eco-enzyme from Fruit Peels Waste". *International Journal of Research in Vocational Studies,* vol. 1 (3), pp. 01-07.

Russo, C, A. Maugeri, G. E. Lombardo, L. Musumeci, D. Barreca, a. Rapisarda, S. Cirmi, and M. Navarra. (2021). "The Second Life of Citrus Fruit Waste: A Valuable Source of Bioactive Compounds". *Molecules.*, vol. 26 (19), p. 5991.

Singh, V. and U. C. Singh. (2008). "Assessment of Groundwater Quality of Parts of Gwahor (India) for Agricultural Purposes". *Indian Journal of Science and Technology,* vol. 1(4), pp. 1-5.

Suliestyah, S., R. Aryanto, C. Palit, R. Yulianti, B.C. Suudi, and A. Meitdwitri. (2022). "Eco Enzyme Production from Fruit Peel Waste and its Application as an Anti-Bacterial and TSS Reducing Agent". *International Research Journal of Engineering, IT & Scientific Research.,* vol. 8 (6), pp. 270-275.

Trease, G. E. and W. C. Evans. (1980). *Pharmacognosy.* London: 1st Ed., Spottiswoode Ballantyne Ltd., pp. 108-529.

WHO. (1984). *Guidelines for Drinking Water Quality.* Geneva: World Health Organisation. vol 7, p. 130.

Zema, D. A., P. S. Calabro, A. Folino, V. Tamburino, G. Zappia, and S. M. Zimbone. (2018). "Valorisation of Citrus Processing Waste: A Review". *Waste Management,* vol. 80, pp. 252-273.

INVESTIGATION OF RADON CONCENTRATION AND TOXIC ELEMENTS IN WELL WATER AND SURFACE WATER IN MONYWA, MYANMAR

Win Ko[1], Mar Mar Win[2]

Abstract

This study evaluates radon concentration and toxic element levels in water samples collected from various locations in Monywa, Myanmar. Samples were obtained from wells, rivers, and lakes, with radon concentrations measured using an LR-115 Type II detector and toxic elements quantified using an atomic absorption spectrophotometer (AA-7000, Shimadzu). The highest average radon concentration was recorded in well water used for drinking (30.02 Bq/m³), while surface water exhibited a maximum radon concentration of 13.94 Bq/m³. All measured radon concentrations were below the lower limit of the recommended action level. Additionally, the presence of toxic elements such as Cu, Zn, Pb, Cd, and As was detected in surface and well water. Radon levels in well water exceeded the EPA's recommended limit but remained below the WHO action level. Overall, the radon concentrations and toxic element levels observed in this study were within acceptable safety thresholds, providing valuable insights into water quality in the region.

Keywords: LR-115, radon, alpha track, well water, surface water and heavy metals

Introduction

Radon is a radioactive noble gas that does not chemically react with other elements. Radon emanation is a well understood phenomenon. It is a colorless, odorless and tasteless gas, which is 7.5 times heavier than air. Hence its presence in drinking water is not felt during consumption. The decay product of radon, i.e., its progeny is highly radioactive and gets absorbed to aerosol particles suspended in water. The range of recoil radon atom in water is about 0.1 μm but it emits alpha particle which has energy 5.5 MeV and can travel up to a few centimeters in air.

It has three isotopes, namely, ^{222}Rn (Radon), ^{220}Rn (Thoron) and ^{219}Rn (Actinon). All three are decay products (daughters) of ^{238}U, ^{232}Th and ^{235}U series, respectively. Thoron and Actinon have very short half-lives (in seconds) and Radon (222) represent the most essential isotope, with a half-life of 3.825 days which allows it to migrate over long distances and get accumulated into the indoor environment. Radon (^{222}Rn) and its short-lived decay products (^{218}Po, ^{214}Pb, ^{214}Bi and ^{214}Po) have been recognized globally as the main sources of exposure to the public in dwellings from the natural radioactivity, contributing to nearly 50% of the global mean effective dose to the public. In the United States of America, exposure to radon is the second cause of lung cancer after smoking. Scientists estimate that about 20,000 lung cancer deaths per year are related to radon (Seltenrich, N., 2019).

Radon is the most important source of naturally occurring radiation exposure for humans. For the world population, radon exposure represents 50% of the total exposure to natural background radiation, followed by earth gamma radiation at 20%, cosmic radiation at 18% and natural radiation from food and water at 12%. 95% of exposure to radon is from indoor air, with about 1% coming from drinking water (WHO, 2009).

Radon in domestic water supplies can cause human exposure to a radiation dose both through inhalation and ingestion. Radon is easily released from water into the atmosphere by agitation or heating. Many domestic uses of water result in such a release and can contribute to

[1] Department of Chemistry, Monywa University
[2] Department of Chemistry, Monywa University

the total indoor air radon concentration. It has been estimated that 1000 Bq/L of radon in water will, on average, increase the radon concentration in indoor air by 100 Bq/m^3. It has been observed that the risk of lung cancer increases if the public is exposed to high concentrations of radon in indoor air. The organ at greatest risk from the ingestion of water containing radon and radon decay products is considered to be the stomach (Khursheed A., 2000).

Unfortunately, radon can lead to major health risks via two methods. The first method in which radon can be exposed to the human body is the inhalation of radon that escapes from groundwater to the air of homes. A second method is the ingestion of radon in drinking water. Long-term exposure to radon gas can result in lung cancer. In fact, approximately 16% of lung cancer deaths in Canada are due to long-term exposure to radon gas indoors. Furthermore, the studies reveal that radon gas is the primary cause of lung cancer in non-smokers and the second leading cause in smokers (Virk, J., & Virk, H. S. 2021).

The associated health risks due to inhalation and ingestion of radon and its progeny when present in enhanced levels in an indoor environment, water and soils surrounding a human dwelling have been well documented. There are many factors which influence the radon concentration in dwellings and environment, namely, radium content in the soil, meteorological parameters and the radon emanating from soils and rocks in the surroundings (Singh, M., *et al*, 1988).

Materials and Methods

The sources of water in the area under study are wells, river and lakes and water used for irrigation is wells, river and lakes water. Samples of water were collected from wells, river and lakes. Before the collection of water samples, bottles were rinsed with 15% HNO_3 and with distilled water in triplet. In order to insure sample quality, samples from wells were collected directly from well after purging for 10 min. Surface water was collected directly from river and lakes within 5 cm of the water surface. All samples were labeled with date, time and sample code.

Radon concentration in these samples was measured using LR-115 Type II detector.

Toxic elements (As, Pb, Cd, Cu and Zn) in water samples were measured by using atomic absorption spectrophotometer (AA-7000, Shimadzu).

Treatment of LR-115 Detector with Standard Source

LR-115 detectors were cut into small pieces of 1 cm × 1 cm. These detectors were irradiated with alpha from Am-241 source. The LR-115 was removed from the source and etched chemically in 10% NaOH solution at 60 °C for 90 minutes in an oven. The etched tracks on the detectors were scanned, using a microscope with magnification of 40X manually. It was also concerned with examining the composition of SSNTDs before and after irradiation by using FTIR method.

Detection of Radon via Alpha Particles in Water Samples

In this work, LR-115 detectors were used for measuring radon via alpha particles in the surface water and well water samples. 1000 mL of water was collected in an airtight plastic bottle with dimensions approximately 12 cm height ×6.5 cm length ×6.5 cm width. The LR 115 detector was putted on the inner side of the lid of the container with the active side facing the water. The active side will be the side that is curved in a concave manner. This container was sealed for 90 days to collect radon by emanation in water. During this time the alpha particles

from radon and its daughter would leave tracks on the detector. The LR-115 was removed from the plastic bottle and etched chemically in the above procedure.

The track density of surface water and well water samples was calculated by dividing the number of tracks by the microscope view area (19.635 10^{-4} cm^2). The radon concentration in water was calculated using the track density (tracks/cm^2), a calibration factor (0.034 tracks.cm^{-2}.d^{-1}/Bq.m^{-3}) and exposure time (days). The track count was converted into a radon concentration level in Bq/m^3 using the formula: (Virk, J., & Virk, H. S., 2021).

$$C_{Rn} = \rho/k.t$$

Where, k is the calibration constant (0.034 track.cm^{-2}.d^{-1}/Bq.m^{-3}), ρ is track density (tracks/cm^2), t is exposure period (days).

Results and Discussion

Effect of Etching Parameters on LR-115 Detectors

Six LR-115 detectors were irradiated with Am-241 alpha radiation for 20 min. These detectors were etched in 10 % NaOH solution with different etching times (50, 60, 70, 80, 90, and 100 min) at 60 °C. The etching time (90 min) was chosen optimum condition for this research.

Observation of Tracks with Standard Sources

The detection of LR-115 with alpha radiations was studied. LR-115 can detect especially for alpha. From the study on different alpha irradiation times (15, 30, 60, 90 min), the greater the irradiation times, the higher the track density on LR-115. But it will be damaged at irradiation time over 60 min. It was used for radon level measurement from the different water samples.

Examination of Effect of Radiation on LR-115 by Using FT IR Method

From the FT IR spectra of the alpha irradiated LR-115 detectors, it was found that the wavenumbers of functional groups in all irradiated detectors of different irradiation times do not differ before and after irradiation. The observations suggested that the potentiality of LR-115 can be used as dosimeters.

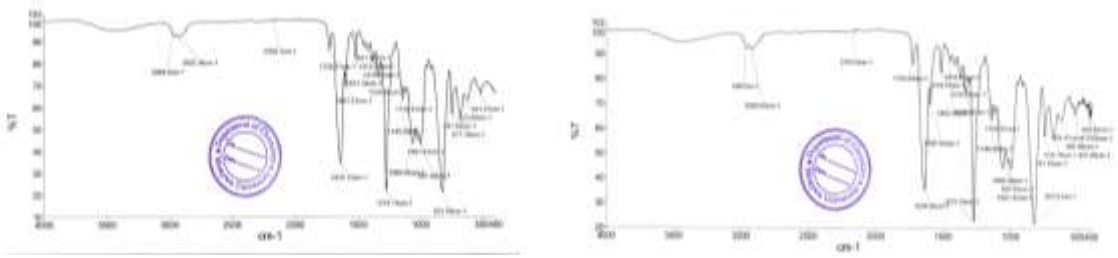

(a) (b)

Figure 1 FT IR spectra of (a) before irradiation and (b) after irradiation of LR-115 detectors with standard alpha source

Observation of Radon via Alpha Particles from the Water Samples

According to the experimental results, the LR-115 detector is more effective in alpha detection. Hence, it was used for observation of radon via alpha particles emitting from the surface water and well water.

Each LR-115 detector was fixed at the top of inside each plastic bottle according to facing the detector and α-emitted via radon in water samples. Radon gas, thoron gas and their progeny

formed by decays inside the container irradiate the LR-115 detectors and form damaged trails. After the exposure period of three months, they were etched in 10 % NaOH at 60 °C for 90 min.

The experimental results revealed that the whole tracks were found in all the LR-115 detectors placed in water samples. The shape of the track observed agrees with the literature and it indicates that this is due to an interaction between detectors and alpha particles via radon present in it.

From Table 1, the track density was found to be between 45.27 and 84.88 track/cm^{2}d in all detectors in the well water (WW1) sample. The average value was found to be 63.38 track/cm^{2}d. According to the observed track density, the radon level was found to be between 21.45 and 40.21 Bq/m^3. Therefore, the radon concentration in well water sample was found to be 30.02 Bq/m^3.

From Table 2, the track density was found to be between 39.61 and 67.91 track/cm^{2}d in all detectors in well water (WW2) sample. The average value was found to be 54.32 track/cm^{2}d. According to the observed track density, the radon concentration level was found to be between 18.76 and 29.49 Bq/m^3. The average was 25.73 Bq/m^3.

From Table 3, the track density was found to be between 39.61 and 96.20 track/cm^{2}d in all detectors in well water (WW3) sample. The average value was found to be 59.98 track/cm^{2}d. According to the observed track density, the radon level was found to be between 18.76 and 45.57 Bq/m^3. The average was 28.42 Bq/m^3.

From Table 4, the track density was found to be between 11.32 and 39.61 track/cm^{2}d in all detectors in surface water (SW1) sample. The average value was found to be 21.50 track/cm^{2}d. According to the observed track density, the radon level was found to be between 5.36 and 18.76 Bq/m^3. The average was 10.19 Bq/m^3.

From Table 5, the track density was found to be between 22.64 and 39.61 track/cm^{2}d in all detectors in surface water (SW2) sample. The average value was found to be 29.43 track/cm^{2}d. According to the observed track density, the radon level was found to be between 10.72 and 18.76 Bq/m^3. The average was 13.94 Bq/m^3.

From Table 6, the track density was found to be between 11.32 and 45.27 track/cm^{2}d in all detectors in surface water (SW3) sample. The average value was found to be 23.77 track/cm^{2}d. According to the observed track density, the radon concentration was found to be between 5.36 and 21.45 Bq/m^3. Therefore, the average radon concentration in the water was found to be 11.26 Bq/m^3.

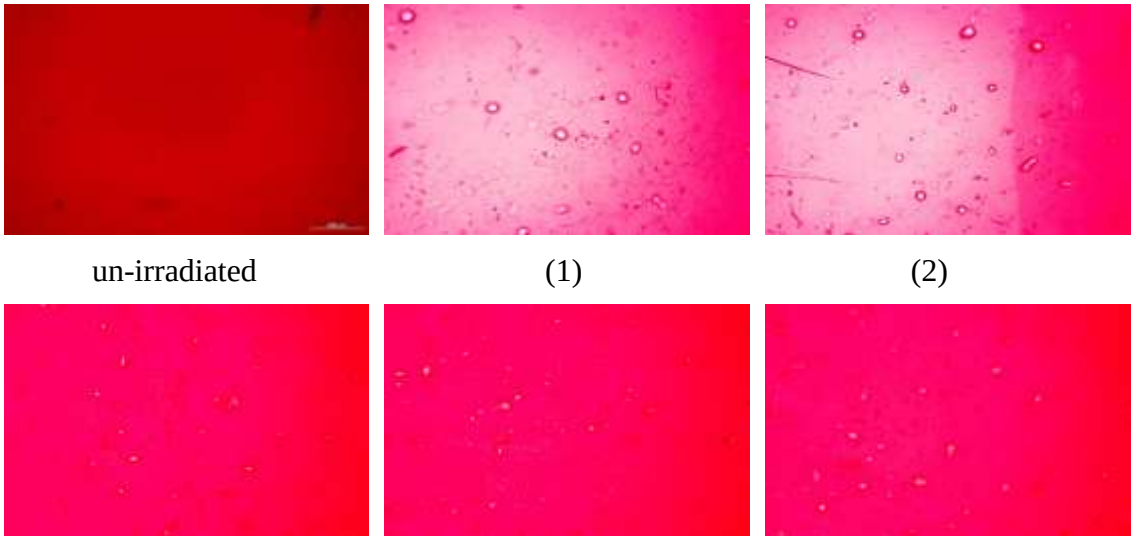

un-irradiated (1) (2)

(3) (4) (5)

Figure 1. Photomicrographs of alpha tracks in LR-115 type II detectors for WW1

Table 1. Measurement of Track Density and Radon Concentration of WW1

LR-115	Track density (tracks/cm^{2}d)	Radon concentration (Bq/m^3)
1	56.59	26.81
2	84.88	40.21
3	67.91	32.17
4	45.27	21.45
5	62.25	29.49
Mean Value	63.38	30.02

* International reference level of radon concentration = 100 Bq/m^3

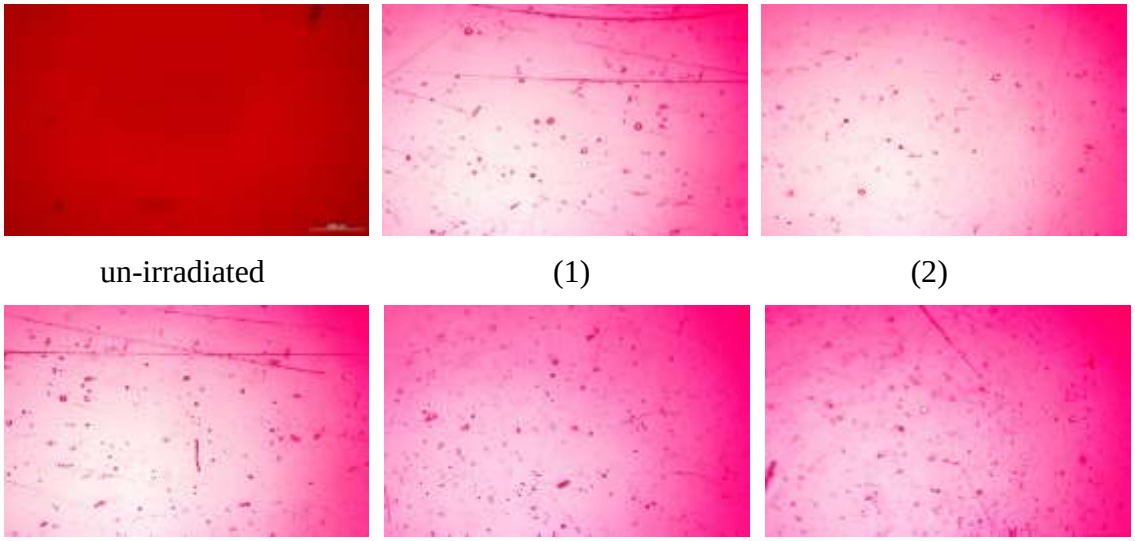

un-irradiated (1) (2)

(3) (4) (5)

Figure 2. Photomicrographs of alpha tracks in LR-115 type II detectors for WW2

Table 2. Measurement of Track Density and Radon Concentration of WW2

LR-115	Track density (tracks/cm^{2}d)	Radon concentration (Bq/m^3)
1	45.27	21.45
2	56.59	26.81
3	67.91	32.17
4	39.61	18.76
5	62.25	29.49
Mean Value	54.32	25.73

* International reference level of radon concentration = 100 Bq/m^3

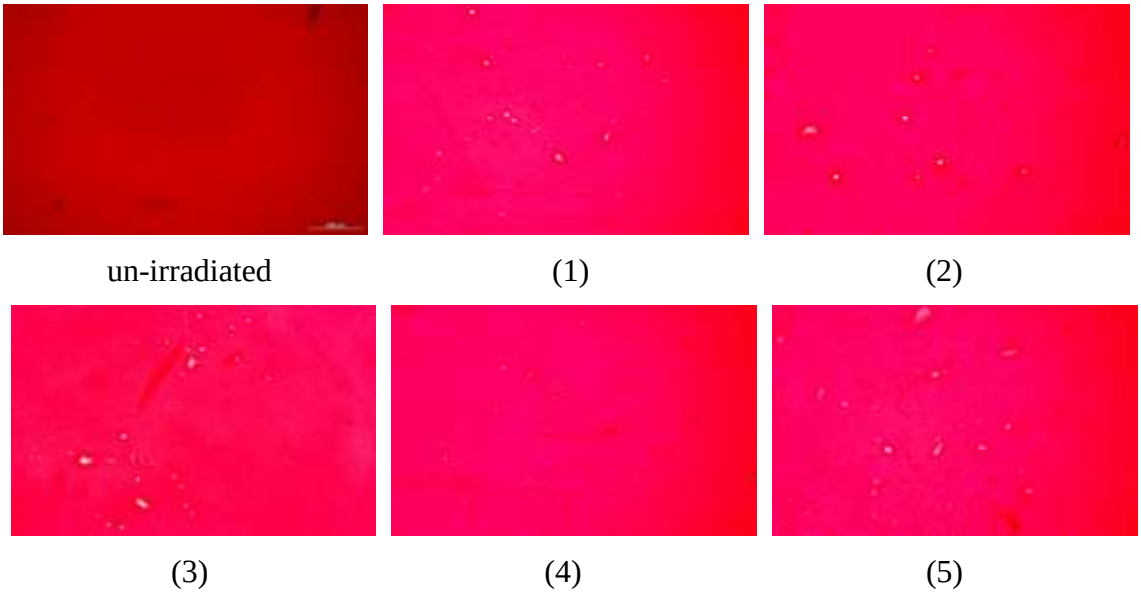

un-irradiated (1) (2)

(3) (4) (5)

Figure 3. Photomicrographs of alpha tracks in LR-115 type II detectors for WW3

Table 3. Measurement of Track Density and Radon Concentration of WW3

LR-115	Track density (tracks/cm^{2}d)	Radon concentration (Bq/m^3)
1	62.25	29.49
2	39.61	18.76
3	96.20	45.57
4	56.59	26.81
5	45.27	21.45
Mean Value	59.98	28.42

* International reference level of radon concentration = 100 Bq/m^3

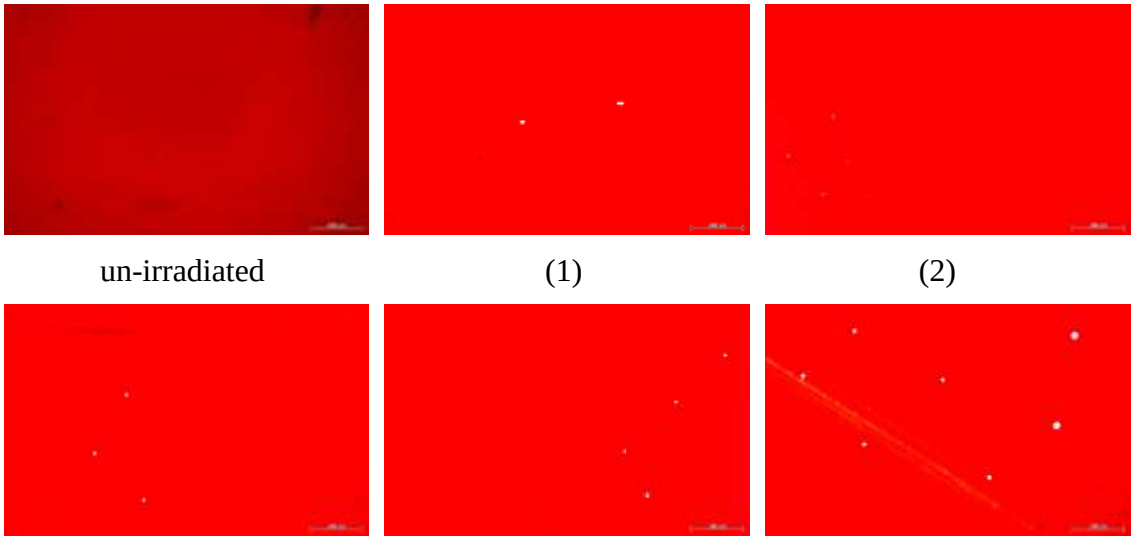

un-irradiated (1) (2)

(3) (4) (5)

Figure 4. Photomicrographs of alpha tracks in LR-115 type II detectors for SW1

Table 4. Measurement of Track Density and Radon Concentration SW1

LR-115	Track density (tracks/cm^{2}d)	Radon concentration (Bq/m^3)
1	11.32	5.36
2	16.98	8.04
3	16.98	8.04
4	22.64	10.72
5	39.61	18.76
Mean Value	21.50	10.19

* International reference level of radon concentration = 100 Bq/m^3

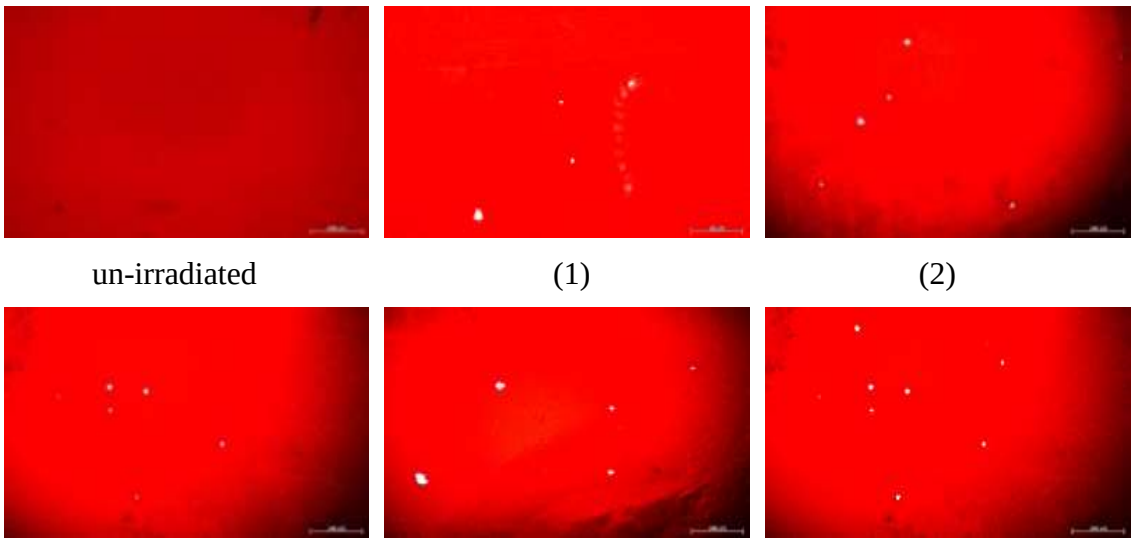

un-irradiated (1) (2)

(3) (4) (5)

Figure 5. Photomicrographs of alpha tracks in LR-115 type II detectors for SW2

Table 5. Measurement of Track Density and Radon Concentration of SW2

LR-115	Track density (tracks/cm^{2}d)	Radon concentration (Bq/m^3)
1	22.64	10.72
2	28.29	13.40
3	28.29	13.40
4	28.29	13.40
5	39.61	18.76
Mean Value	29.43	13.94

* International reference level of radon concentration = 100 Bq/m^3

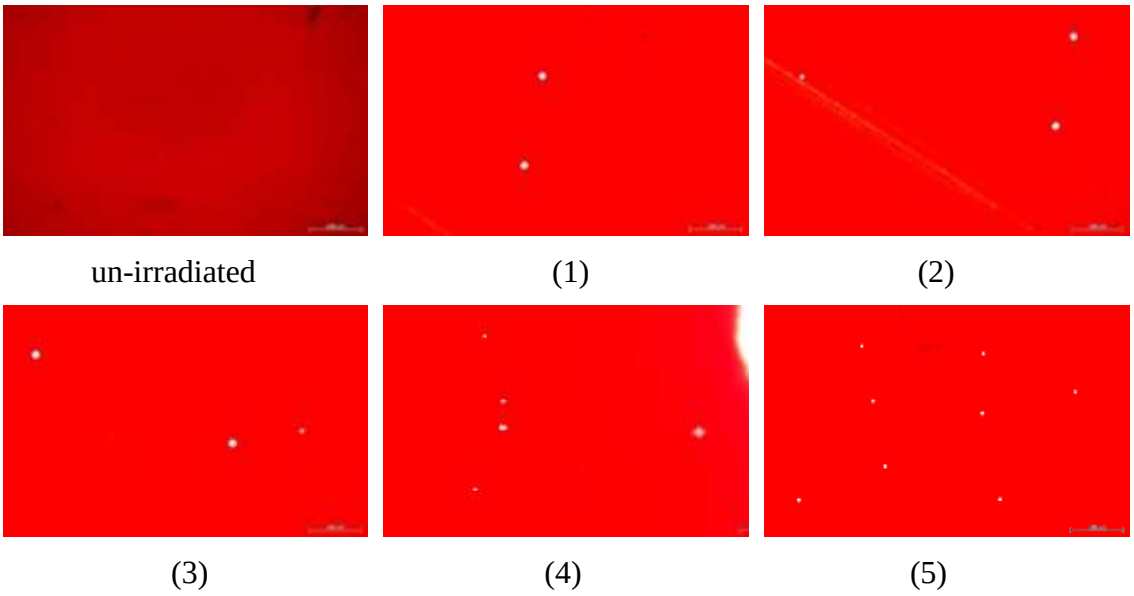

un-irradiated (1) (2)

(3) (4) (5)

Figure 6. Photomicrographs of alpha tracks in LR-115 type II detectors for SW3

Table 6. Measurement of Track Density and Radon Concentration of SW3

LR-115	Track density (tracks/cm^{2}d)	Radon concentration (Bq/m^3)
1	11.32	5.36
2	16.98	8.04
3	16.98	8.04
4	28.29	13.40
5	45.27	21.45
Mean Value	23.77	11.26

* International reference level of radon concentration = 100 Bq/m^3

Table 7. Comparison of Track Density and Radon Level of Each Water Source

Sr No.	Source of water	Sample Code	Track density (tracks/cm^{2}d)	Radon concentration (Bq/m^3)
1	Well	WW1	63.38	30.02
2	Well	WW2	54.32	25.73
3	Well	WW3	59.98	28.42
4	Chindwin River	SW1	21.50	10.19
5	Sarkyin Lake	SW2	29.43	13.94
6	Nyaungkine Lake	SW3	23.77	11.26

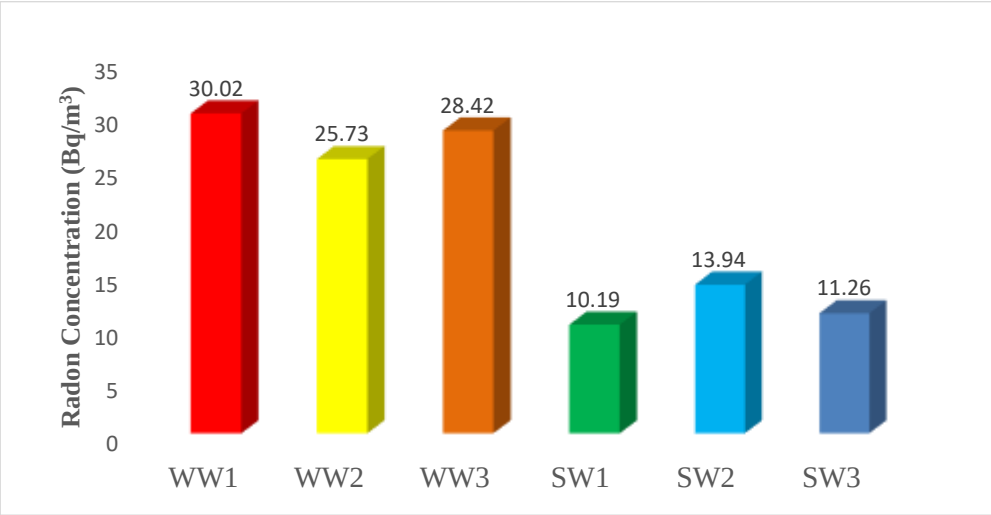

Figure 7. Track density recorded in different water samples using LR-115 Type II detectors

From this figure, radon was found to be present in all samples. Whether its concentration is low or high, it should be aware of the risk for people.

Table 8. Toxic Elements in Water and International Standard Limits

Sr No.	Sample Code	Source of water	As (mg/L)	Pb (mg/L)	Cd (mg/L)	Cu (mg/L)	Zn (mg/L)
1	WW1	Well	0.0010	0.0130	0.001	0.012	0.03
2	WW2	Well	0.0016	0.0170	0.001	0.014	0.02
3	WW3	Well	0.0018	0.0180	0.001	0.017	0.03
4	SW1	River	0.0228	0.2102	0.0153	0.0266	0.0050
5	SW2	Lake	0.0339	0.2570	0.0180	0.0266	0.0039
6	SW3	Lake	0.0359	0.3154	0.0187	0.0301	0.0044
WHO	mg/L		0.01	0.01	0.005	2	3
USEPA	mg/L		0.01	0.01	0.005	1.3	3

Conclusion

This study assessed the human health risks associated with radon concentrations and toxic elements in water collected from various locations in Monywa, Myanmar. Elevated radon levels were detected in well water, with the highest concentration recorded at 30.02 Bq/m³, while surface water showed lower radon levels, with a maximum of 13.94 Bq/m³. Radon concentrations in well water exceeded the EPA's recommended limit of 11 Bq/m³ but remained below the WHO's action level of 100 Bq/m³. In contrast, all surface water samples fell within acceptable limits set by both the USEPA and WHO. It is advised to boil well water before drinking to reduce radon levels. Results of heavy and hazardous metal concentrations in both well and surface water, As, Pb, Cd, Cu and Zn, were found to be less than the lower limit of the recommended action level of WHO/USEPA. But the concentrations of As, Pb, and Cd metals in surface water have a little exceeded the recommended limit.

It is recommended that drinking water is monitored by regular heavy metals to prevent excessive accumulation of heavy metals in the body.

Acknowledgments

We would like to thank Dr Than Than Win, Rector of Monywa University, for her permission to conduct this research as well as her invaluable suggestions. We are also grateful to Professor Dr Ei Ei Lwin, Head of the Chemistry Department at Monywa University, for her kind assistance and suggestions.

References

Ahmad, N., Jaafar, M. S., & Alsaffar, M. S. (2015). Study of radon concentration and toxic elements in drinking and irrigated water and its implications in Sungai Petani, Kedah, Malaysia. *Journal of Radiation Research and Applied Sciences*, 8(3), 294-299.

Al-Nafiey, M. S., Jaafar, M. S., & Bauk, S. A. B. A. R. (2014). Measuring radon concentration and toxic elements in the irrigation water of the agricultural areas in Cameron Highlands, Malaysia. *Sains Malaysiana*, 43(2), 227-231.

Ha, N. T. T., Van Giap, T., & Cuong, L. D. (2016). Technical Procedure Determination of Thoron Indoor Concentration by LR-115 Type II. *Journal of Environmental Science and Engineering B*, *5*, 109-114.

Jidele, P. A., Dosunmu, O. G., Kolapo, A., Ajayi, K. F., & Ademola, K. A. (2021). Measurement of radon and potentially toxic elements concentrations in groundwater around Ota, Ogun State, Nigeria. *International Journal of Environmental Quality*, 42-49.

Khursheed, A. (2000). Doses to systemic tissues from radon gas. *Radiation Protection Dosimetry*, 88(2), 171-171.

Seltenrich, N. (2019). Radon risk: A global estimate of radon's contribution to lung cancer. *Environmental health perspectives*, 127(2), 024001.

Singh, M. A. N. W. I. N. D. E. R., Ramola, R. C., Singh, S. U. R. I. N. D. E. R., & Virk, H. S. (1988). Influence of meteorological parameters on soil gas radon. *J. Assoc. Explor. Geophys. (India)*, 9(2).

Virk, J., & Virk, H. S. (2021). Radon estimation in water of surrey region of British Columbia, Canada using LR-115 type II nuclear track detector. *Earth*, 12, 50.

World Health Organization. (2009). *WHO handbook on indoor radon: a public health perspective*. World Health Organization.

SYNTHESIS, CHARACTERIZATION AND APPLICATION OF CALCIUM ALUMINATE NANOPARTICLES

Naw Yoon Eimzi Tun[1], Hlaing Hlaing Oo[2], Hnin Yu Wai[3]

Abstract

In recent years, scientists have recently turned to the green synthesis of nanoparticles from solid wastes and used these in many applications. The calcium aluminate phase has been made by fusing or sintering together an appropriate mixture of CaO and Al_2O_3. These two metal oxides were investigated by using waste powder as raw materials. The key distinction in this research lies in the synthesis of calcium aluminate nanoparticles from waste quail eggshells and discarded aluminum cans (specifically, Coca-Cola cans) using the sonochemical method. The synthesis of calcium aluminate with two different weight ratios of CaO: Al_2O_3 (1:1 and 1:2), as well as different calcination periods and temperatures. The calcium aluminate ($Ca_{12}Al_{14}O_{33}$) was synthesized at a calcination temperature of 1200°C, a calcination period of 1 h, and a 1:2 weight ratio of CaO to Al_2O_3. The average crystallized size of synthesized calcium aluminate nanoparticles was 43.82 nm. The antimicrobial investigation of synthesized calcium aluminate nanoparticles revealed significant antimicrobial activity against eight tested microorganisms. The inhibition zone diameters ranged from 20 to 29 mm. These results demonstrated that synthesized calcium aluminate nanoparticles hold potential as antimicrobial substances for other application fields.

Keywords: green synthesis, nanoparticles, calcium aluminate, quail eggshell, Coca-Cola cans, sonochemical method, antimicrobial activity

Introduction

The binary oxide system CaO-Al_2O_3 has been extensively researched due to the unique properties developed by the calcium aluminate phases. Calcium aluminates compounds consist of a wide range of combinations of calcium oxide and aluminum oxide, and many of these powders are found in cement technology as hydraulic powder. The calcium aluminates are described in the CaO-Al_2O_3 binary phase diagram. Within this system, five binary compounds can be distinguished that generically go by the name of calcium aluminate: $CaAl_2O_4$, $CaAl_4O_7$, $Ca_{12}Al_{l4}O_3$, Ca_3AlO_6, and $CaAl_{12}O_{19}$**.** This system is also attractive as ceramic powder for high-temperature refractory applications. These compounds play important roles in the steel industry as metallurgical slag. Calcium aluminates have a wide range of potential technological applications due to their unusual optical, electrical, thermal, and mechanical properties. The calcium aluminate phase diagram shows a low melting point, the eutectic point, located at 1400 and 1395ºC, where $C1_2A_7$ (mayenite), and C_3A (celite) are the main coexisting phases. That eutectic point composition of 50% calcium oxide and 50% aluminium oxide shows the existence of two main phases that emerge simultaneously: celite and mayenite; these two phases coexist, and thus different heat treatments and synthesis procedures can modify the proportion of each phase in the final material (Gaki, 2007).

The name mayenite was originally given to an isostructural mineral with a composition close to $Ca_{12}Al_{14}O_{33}$ (dodacacalcium hepta aluminate) discovered at the Bellerberg volcano near Mayen, Eifel, Germany (Galuskin *et al*., 2015). Mayenite compounds can be applied as an ion or electron conductor, catalyst in fuel processing, or hydraulic active phase in cement due to their chemical and physical properties such as conductivity, or the potential for water accumulation (Amer *et al*., 2022).

[1] Department of Chemistry, East Yangon University
[2] Department of Chemistry, West Yangon University
[3] Department of Chemistry, Yangon University of Distance Education

In the present research, calcium aluminate nanoparticles were synthesized by sonochemical method. The obtained calcium aluminate nanoparticles were characterized by X-ray Diffraction (XRD), Fourier Transformed Infrared (FT IR) Spectrometers, Raman and Scanning Electron Microscope (SEM). And then, the synthesized calcium aluminate was tested in antimicrobial activity.

Materials and Methods

Synthesis of Calcium Aluminate Nanoparticles

The synthesized calcium oxide and aluminum oxide powders were mixed stoichiometrically according to the calcium aluminate powder desired predominantly, *i.e*., in weight-by-weight proportions of 1:1 and 1:2. An aqueous suspension was synthesized by hand mixing powders with distilled water. This suspension was subjected to an ultrasonic bath for 1 h at room temperature. The suspension was shaken periodically during the process to enhance the sonochemical effect. Finally, the suspension was filtered and oven-dried at 110 °C for 24 h on each composition. The resulting solid material was calcined at 1100 and 1200 °C for 1 and 2 h. And then, the synthesized samples were ground with a motor and pastel. Finally, calcium aluminate powder was obtained.

Characterization of Synthesized Calcium Aluminate Nanoparticles

The synthesized calcium aluminate was identified and characterized by X-Ray Diffraction Spectrometer (XRD-2000 Diffractometer, Enraf Nonius Co., Bohemin NY) in accordance with the recommended standard as reported in the catalogue. The functional groups of synthesized calcium aluminate were evaluated by FT IR spectrometer (Perkin Elmer Spectrum GX, USA). The synthesized calcium aluminate was identified by Raman Spectrometer ((LABRAM HR Evolution, HORIBA France SAS) in accordance with the recommended standard procedure reported in the Raman spectrometer catalogue. The surface morphology of the synthesized sample was studied with a Scanning Electron Microscope (JSM-5610, JEOL Ltd., Japan). And then, calcium aluminate nanoparticles were tested with *Agrobacterium tumefaciens, Bacillus pumilus, Bacillus subtilis, Candida albicans, Escherichia coli, Micrococcus luteus, Pseudomonas fluorescens, and Staphylococcus aureus* to investigate the nature of antimicrobial activity.

After preparing the bacterial media, the sample calcium aluminate was placed on the agar well with flamed forceps and gently pressed down to ensure proper contact. The plates were incubated immediately or within 30 min after incubation. After overnight incubation at 37 ºC.

Results and Discussions

Characterization of Calcium Aluminate Nanoparticles

XRD Analysis

The synthesized calcium aluminate was characterized by an XRD spectrometer, and the recorded diffractograms are shown in Figures 1(a)(b) - 4(a)(b), and the results data are described in Table 1. Figures 1(a)(b) to 2(a)(b) showed X-ray diffraction patterns of synthesized calcium aluminate by a 1: 1 weight ratio of synthesized CaO and Al_2O_3 at different temperatures of 1100 °C and 1200 °C for 1 h and 2 h. It appeared that calcium carbonate and one of the calcium aluminate phases as hydrocalumite [di-calcium aluminum hexa-hydroxide chloride di-hydrate: $Ca_2AlCl(OH)_6(H_2O)_2$]. The peaks of $CaCO_3$ were shown at 2θ values around 23°, 29°, 36°, 39°, 43°, and 47° (Chengli *et al*., 2013). Obviously, the peaks of Hydrocalumite: $Ca_2AlCl(OH)_6(H_2O)_2$ at 2θ values of 11°, 22°, 23° and 31° **(**Xinhong *et al*., 2015). The Hydrocalumite calcium aluminates phase pattern showed no significant effect of calcination temperature and calcination period. The increasing amount of Al_2O_3 using 1: 2 (w/w) of synthesized CaO: Al_2O_3 at calcination temperatures of 1100 °C and 1200 °C for 1 h and 2 h was also performed. Figures

3(a)(b)-4(a)(b). Figure 3 (a) showed the XRD pattern of calcite at calcination temperature 1100 °C and a calcination time for 1 h. Figures 3 (b) to 4 (a) (b) clearly showed that the sharp peaks and pure calcium aluminate (calcium aluminium oxide): $Ca_{12}Al_{14}O_{33}$, peaks at 2θ values of 10.0°-80.0° corresponded to (211), (220), (310), (321), (420), (332), (422), (521), (611), (532), (631), (640) and (642) planes as indexing the $Ca_{12}Al_{14}O_{33}$ phase of cubic structure with space group of *I*-43*d* in the standard data (Guoqing et al., 2018). Therefore, XRD data proved that the molecular formula of synthesized calcium alulminate was $Ca_{12}Al_{14}O_{33}$ ($12CaO•7Al_2O_3$), it is also called dodecacalcium hepta aluminate. The smallest crystallite size was found at 1200 °C for 1 h, and its value is 43.82 nm. According to the XRD results, the synthesized calcium aluminate was affected by the composition of metal oxides, calcination temperatures, and calcination times. The transformation process at 1200 °C, a calcination period of 1 h, and a composition of a 1:2 ratio of CaO and Al_2O_3 was better than that of others. The lattice parameters for the synthesized dodecacalcium hepta aluminate was 11.99856 Å, which proved to be slightly larger than the value reported in the literature for pure synthetic mayenite (11.989 Å), implying the presence of the dodecacalcium hepta aluminate phase.

The reported literatures revealed that Mayenite ($12CaO·7Al_2O_3$) have drawn intensive attention because of a variety of promising applications, including display devices, catalysis, and transistors. This material possesses a porous cubic structure (*I*43*d*) made up of twelve Ca-Al-O nanocages, two of which are randomly occupied by the free oxygen ions inside. Such unique geometry leads to appealing characteristics including exceptional ionic conductivity, electronic conductivity, and optical transparency (Parinya Tangpakonsab *et al*., 2021).

Thus, XRD data demonstrated that utilizing synthesized CaO and Al_2O_3 nanoparticles as starting materials resulted in the formation of calcium aluminate phases at 1100 °C / 1 h**,** 1200 °C/ 1 h, and 1200 °C / 2 h**,** respectively.

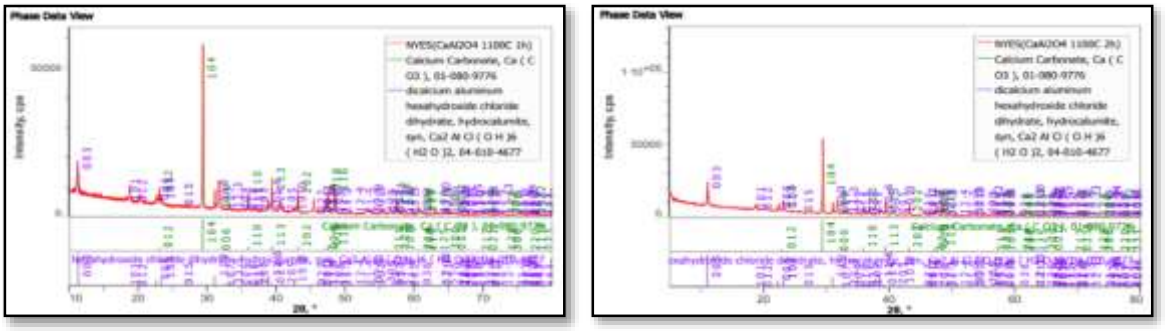

(a) **(b)**

Figure 1 X-ray diffraction pattern of synthesized calcium aluminate calcined at 1100 °C for (a) 1 h and (b) 2 h using 1:1 w/w ratio of $CaO:Al_2O_3$

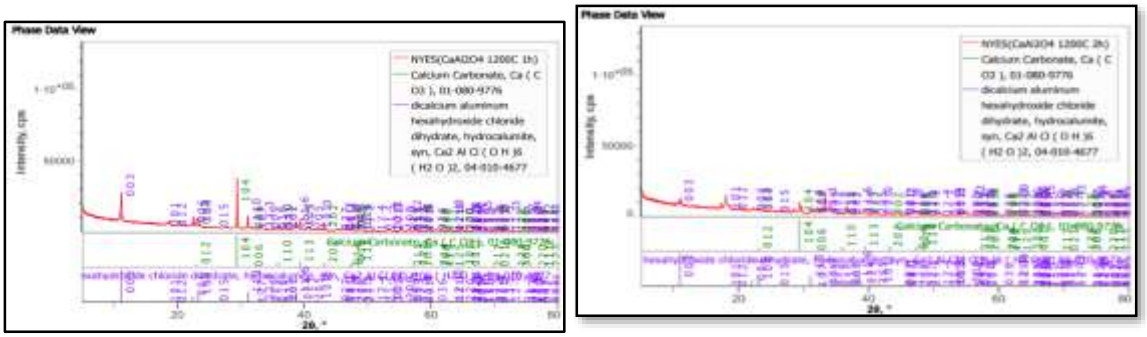

(a) **(b)**

Figure 2 X-ray diffraction pattern of synthesized calcium aluminate calcined at 1200 °C for (a) 1 h and (a) 2 h using 1:1 w/w ratio of $CaO:Al_2O_3$

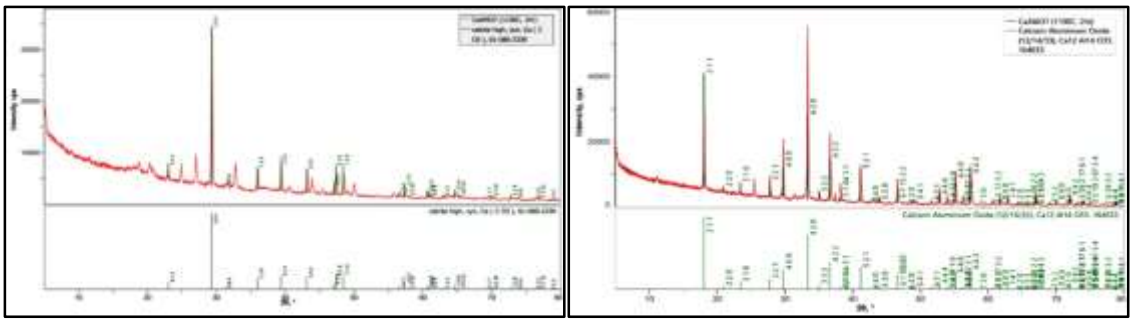

(a) **(b)**

Figure 3 X-ray diffraction pattern of synthesized calcium aluminate calcined at 1100 °C for (a) 1 h and (b) 2 h using 1: 2 w/w ratio of CaO : Al_2O_3

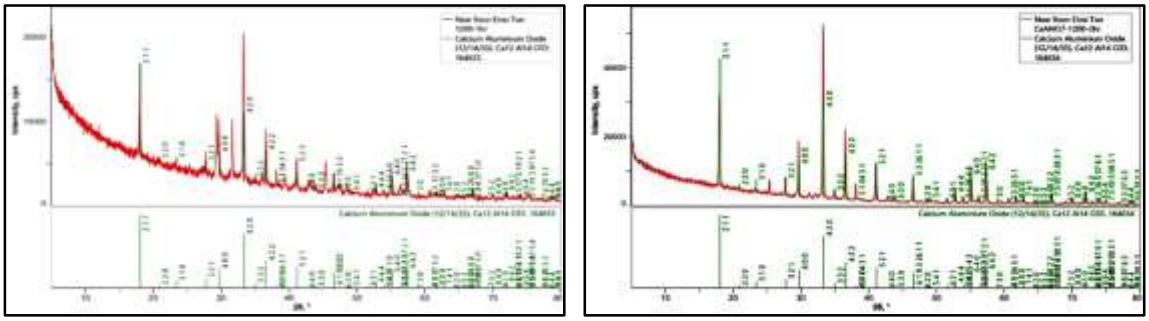

(a) **(b)**

Figure 4 X-ray diffraction pattern of synthesized calcium aluminate calcined at 1200 °C for (a) 1 h and (b) 2 h using 1: 2 w/w ratio of CaO : Al_2O_3

Table 1 XRD Analysis of Synthesized Calcium Aluminate

Sample	$CaO:Al_2O_3$	Calcined temperature (°C)	Calcined period (h)	Compound	Average crystallite size (nm)
CAP-1	1:1	1100	1	$CaCO_3$ $Ca_2AlCl(OH)_6(H_2O)_2$	59.21
CAP-2	1:1	1100	2	$CaCO_3$ $Ca_2AlCl(OH)_6(H_2O)_2$	62.36
CAP-3	1:1	1200	1	$CaCO_3$ $Ca_2AlCl(OH)_6(H_2O)_2$	38.72
CAP-4	1:1	1200	2	$CaCO_3$ $Ca_2AlCl(OH)_6(H_2O)_2$	25.05
CAP-5	1:2	1100	1	$CaCO_3$	50.61
CAP-6	1:2	1100	2	$Ca_{12}Al_{14}O_{33}$	80.35
CAP-7	1:2	1200	1	$Ca_{12}Al_{14}O_{33}$	43.82
CAP-8	1:2	1200	2	$Ca_{12}Al_{14}O_{33}$	76.65

FT IR analysis

The FT IR spectra of synthesized calcium aluminate (CAP-6, CAP-7 and CAP-8) are shown in Figure 5 (a) to (c) and Table 2. It was found that the formation peaks of water at 4000-

3000 cm^{-1}, corresponding to the presence of O-H stretching of hydroxyl. The peak at 1650-1400 cm^{-1}, due to -C=O stretching of carbonyl/carboxyl. The band at ~1030 cm^{-1} was assigned to C-O-C- stretching of epoxy groups. The peaks at about 900 cm^{-1} were assigned to stretching vibrations of a lattice of interlinked AlO_4 tetrahedral lattice. The band at about 890-750 cm^{-1} can be associated with the stretching mode of the free oxygen ions (O^{2-}) in the extra framework of the CaO structure. The vibration peaks at approximately 500 and 410 cm^{-1} are attributed to the stretching mode of Ca, Al and O atoms, which are characteristic of insulating $Ca_{12}Al_{14}O_{33}$ (David Torrens-Martin *et al.*, 2013).

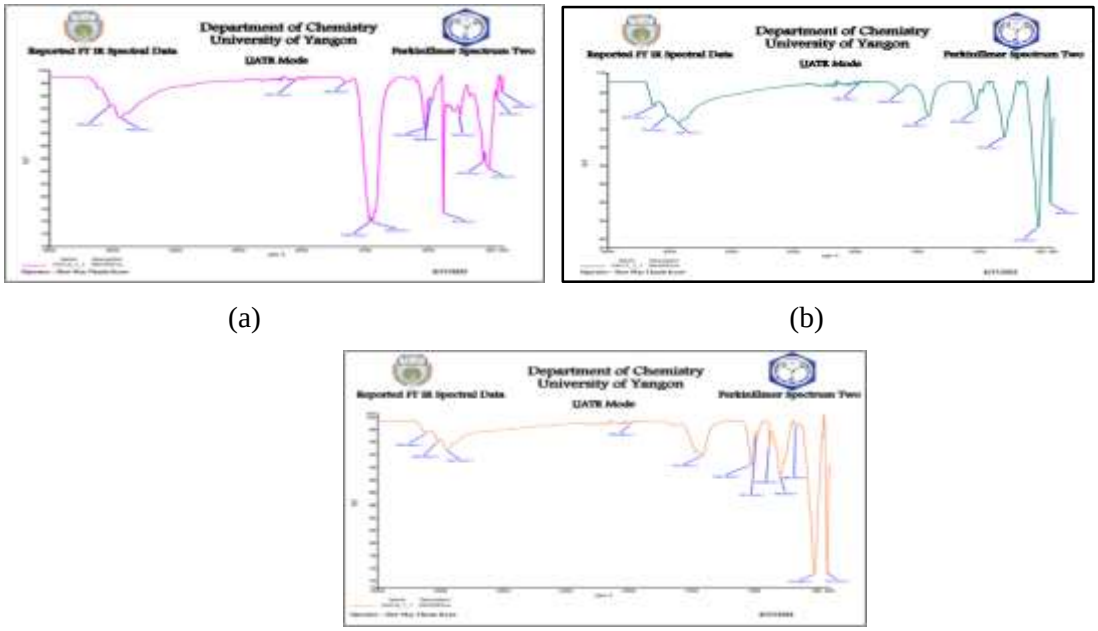

(a) (b)

(c)

Figure 5 FT IR spectrum of calcium aluminate nanoparticles (a) CAP-6, (b) CAP-7 (c)CAP-8

Table 2 FT IR Spectral Data of Calcium Aluminate Nanoparticles (CAP-6, CAP-7 and CAP-8)

Wavenumber (cm^{-1})				Band assignment
CAP-6	**CAP-7**	**CAP-8**	***Literature**	
3436	3427	3447	4000-3000	O-H stretching of hydroxyl
1640	1628	-	1650-1400	C=O stretching of carbonyl/carboxyl
1459	1406	1413		
-	1023	1022	~1030	C-O-C stretching of epoxy groups
969	-	971	900	stretching vibrations of a lattice of interlinked AlO_4 tetrahedral
874	-	875	890-750	stretching mode of the free oxygen ions (O^{2-}) in extra framework of the CAO structure
744	786	789		
558	519	518	500-410	stretching mode of Ca, Al and O atoms as the characterization of insulating $Ca_{12}Al_{14}O_{33}$
520	420	419		

***Literature** - (David Torrens-Martin *et al.*, 2013)

Raman analysis

The Raman spectra of synthesized calcium aluminate nanoparticles (CAP-6, CAP-7 and CAP-8) are presented in Figures 6 (a) to (c). In CAP-6 and CAP-7, the strong Raman band was observed at 1084 cm^{-1} corresponding to the calcite bond. The band at 521 cm^{-1} may be associated with symmetric stretching vibration of Al-O groups and Al-O-Al linkage bonds. The remaining signals at 270 and 153 cm^{-1}, can be assigned to Ca-O bonds. In CAP-8, the Raman peak at 1088 cm^{-1} is also associated with the calcite band. The band at below 300 cm^{-1} is assigned to the Ca-O vibrations. It is shown in Table 3 (David Torrens-Martin *et al.,* 2013).

SEM analysis

The surface morphology of synthesized calcium aluminate (CAP-6, CAP-7 and CAP-8) was observed by scanning electron microscope. From Figures 7 (a) to (c), this can be seen in the presence of rigid agglomerates of flake-shaped nanoparticles. The SEM images clearly showed that synthesized calcium aluminate exhibited leaves-platelet like structure.

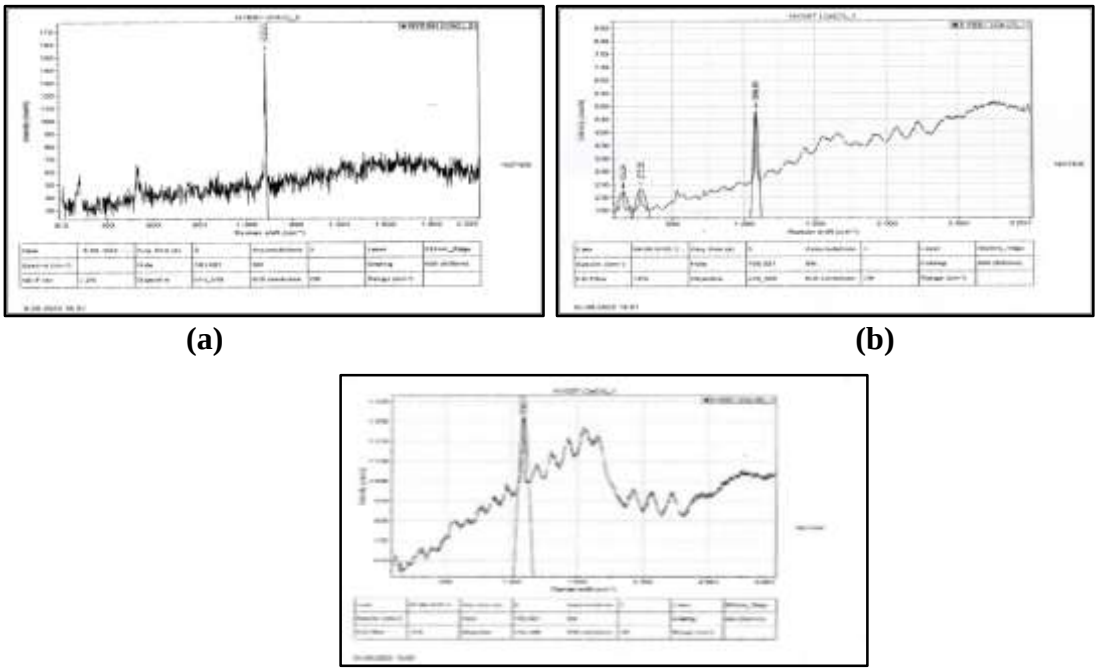

(a) **(b)**

(c)

Figure 6 Raman spectrum of calcium aluminate nanoparticles (a) CAP-6, (b) CAP-7 and (c) CAP-8

***CAP= Calcium Aluminate Nanoparticles**

Table 3 Raman Spectral Data of Calcium Aluminate Nanoparticles (a) CAP-6, (b) CAP-7 and (c) CAP-8)

Wavenumber (cm^{-1})				Band assignment
CAP-6	**CAP-7**	**CAP-8**	***Literature**	
1085	1084	1088	1000	calcite band
520	521		518	symmetric stretching vibration of Al-O groups and Al-O-Al linkage bonds (υ_1 Al_4^{5-}).
280	270 153	145	<300	vibration of oxygen (O^{2-}) framework in Ca (AlO_4) crystalline and Ca-O bonding

***Literature-** David Torrens-Martin *et al.*, 2013

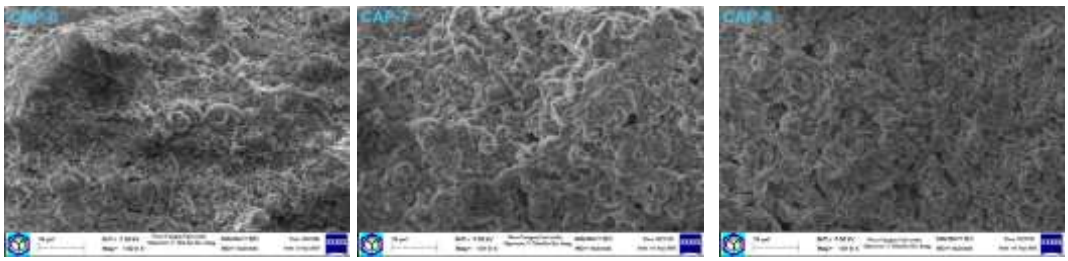

(a) (b) (c)

Figure 7 SEM image of calcium aluminate nanoparticles (a) CAP-6, (b) CAP-7 and (c)CAP-8

Antimicrobial Activity of Synthesized Calcium Aluminate Nanoparticles

In the environment, organisms can be exposed to nanoparticles *via* ingestion, inhalation, and penetration through the skin surface. Several investigations have reported the use of metal nanoparticles as an antimicrobial agent. Antimicrobial applications of nanoparticles cover not only bactericidal and bacteriostatic activities but also the possibility to detect potentially pathogenic microorganisms in medicine and food. They can be applied as components of coatings for medical devices, modification agents and impregnates for textiles, and "construction" elements for implants, cements, and resins.

Consequently, the antimicrobial activity of synthesized calcium oxide, aluminium oxide, and calcium aluminate nanoparticles against eight microbial strains (*Escherichia coli*, *Candida albicans*, *Bacillus subtilis*, *Staphylococcus aureus*, *Pseudomonas fluorescens*, *Agrobacterium tumefaciens*, *Bacillus pumilis*, and *Micrococcus luteus*) was assessed using the agar well diffusion method. The results of the antimicrobial investigation are presented in Table 4 and Figure 8. According to the results, a larger inhibition zone diameter indicates that the bacteria and fungus were more susceptible to the antibiotic and that the antibiotic has a higher antibacterial and antifungal activity. The agar diffusion antimicrobial assay proved that the synthesized calcium oxide, aluminium oxide, and calcium aluminate had good inhibitory responses against eight tested microorganisms. Thus, in the search for new applications for nanocomposites, it will be essential to evaluate their antimicrobial response in the coating of food containers, medical devices, packaging, and other fields of applications.

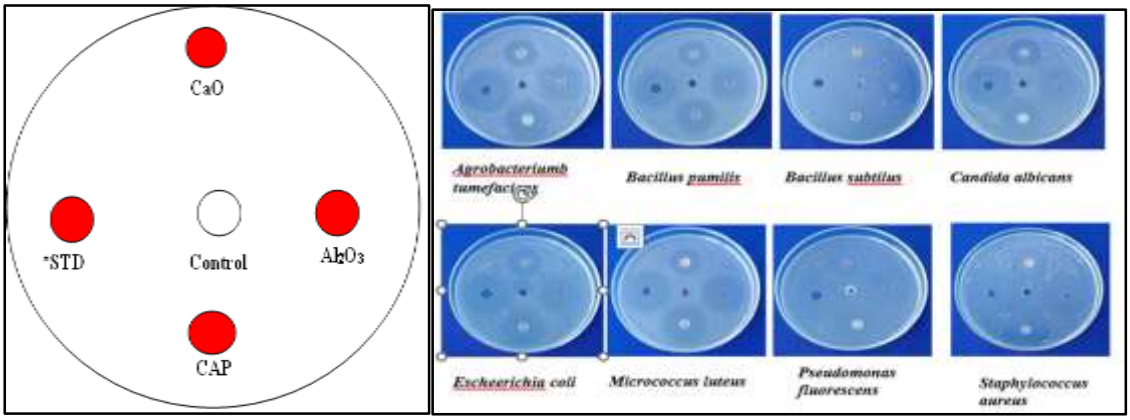

*Std = Standard, *CAP = Calcium aluminate nanoparticles

Figure 8 Antimicrobial activity of synthesized calcium oxide, aluminium oxide, and calcium aluminate nanoparticles

Table 4 Antimicrobial Activity of Synthesized Calcium Oxide, Aluminium Oxide, and Calcium Aluminate Nanoparticles Using Agar Well Diffusion Method

No.	Sample	Inhibition zone diameter (mm)							
		E.coli	***C.albicans***	***B.subtilis***	***S.aureus***	***P.fluorescens***	***A.tumefaciens***	***B.pumilus***	***M.luteus***
1.	**CaO**	20.8	22.2	20.0	21.4	23.4	22.0	23.0	22.9
2.	**Al_2O_3**	28.1	26.1	25.1	27.0	28.0	28.1	27.2	27.7
3.	**CAP**	27.0	24.5	25.0	26.4	27.7	29.0	27.0	27.6
4.	**STD**	33.4	30.2	28.8	31.6	33.1	33.4	33.1	32.9

Agar well diameter = 8 mm
10 mm – 14 mm = + (low activity)
15 mm – 19 mm = ++ (medium activity)
20 mm and above = +++ (very high activity)

Conclusion

In this study, calcium aluminate nanoparticles were successfully synthesized using different weight ratios of CaO and Al_2O_3 powders through a controlled calcination process. The optimal synthesis conditions, including a calcination temperature of 1200 °C, a duration of 1 hour, and a CaO-to-Al_2O_3 ratio of 1:2, led to the formation of pure dodecacalcium heptaaluminate ($Ca_{12}Al_{14}O_{33}$) with a well-defined cubic structure. XRD analysis confirmed the crystallographic planes characteristic of the $Ca_{12}Al_{14}O_{33}$ phase, with an average crystallite size of 43.82 nm. Structural characterization through Raman and FT-IR spectroscopy validated the presence of key functional groups, while SEM imaging revealed a leaf-platelet-like morphology.

Furthermore, the antimicrobial properties of the synthesized nanoparticles, assessed using the agar diffusion assay, demonstrated their potential for biomedical and environmental applications. Notably, the synthesis process employed waste quail eggshells and aluminum cans from Coca-Cola, offering an eco-friendly and sustainable approach to material development. This green synthesis method not only contributes to waste reduction and environmental sustainability but also highlights the potential of calcium aluminate nanoparticles for use in diverse technological and medical applications.

Acknowledgements

The author would like to express my deepest gratitude to the Department of higher Education (Lower Myanmar), Ministry of Education, Yangon, Myanmar, for provision of opportunity to do this research and Myanmar Academy of Arts and Science for allowing to present this paper. Thanks for providing essential research facilities.

References

Amer, A. A., H. E. Didamony, M. Tarek, E. Sokkary and I. Mohamed. (2022). "Synthesis and Characterization of Some Calcium Aluminate Phases from Nano-size Starting Powder". *Boletin de la Sociedad Espanola de Ceramicay Vidrio*. vol. 61, pp. 98–106

Chengli, Y., X. Anjian, S. Yuhua, Z. Jinmiao and L. Tengjiao. (2013). "Green Synthesis of Calcium Carbonate with Unusual Morphologies in the Presence of Fruit Extracts". *Journal of the Chilean Chemical Society*, vol.58, pp 1-9

David, T. M., F. C. Lucia and M. R. Sagrario. (2013). "Hydration of Calcium Aluminates and Calcium Sulfoaluminate Studied by Raman Spectroscopy". *Journal of Cement and Concrete Research.* vol. 47, pp. 43-50

Gaki, A., R. Chrysafi and G. Kakali. (2007). **"**Chemical Synthesis of Hydraulic Calcium Aluminate Compounds Using the Pechini Technique". *Journal of European Ceramic Society*. vol. 27, pp. 1781–1784

Galuskin, E. V., I. O. Galuskina, J. Kusz, F. Gfeller, T. Armbruster, R. Bailau, M. Dulski, V. M. Gazeev, N. N. Pertsev, A. E. Zadov and P. R. Dzierżanowski**.** (2015). "Mayenite Supergroup, Part II: Chlorkyuygenite from Upper Chegem, Northern Caucasus, Kabardino-Balkaria, Russia, A New Microporous Mineral with 'Zeolitic' H_2O". *European Journal of Mineralogy*. vol. 27, pp.113-122

Guoqing, G., L. Jiaqi, Z. Yang, L. Lin, Y. Jinyuan, K. Martin and J.M. M. Paulo. (2018). "A high-pressure X-ray diffraction study of the crystalline phases in calcium aluminate cement paste". *Cement and Concrete Research*, Vol. 108, pp 38-45

Parinya, T., K. Banlusan., MPairot, N. Supawadee, A. Vittaya and K. Thanayut. (2021). "Electronic structures and optical properties of nanoporous complex oxide $12CaO{\cdot}7Al_2O_3$ (C12A7) under high pressure". *Computational Materials Science*. vol.194, pp. 41-44

Xinhong, Q., S. Keiko, T. Yu, H. Tsuyoshi, I. Keiko, M. Jin. (2015). "Mechanism of boron uptake by hydrocalumite calcined at different temperatures". *Journal of Hazardous Materials*, Vol. 287, pp 268-277

Here are some suggested questions based on the study:

Synthesis and Characterization

1. What was the rationale behind selecting CaO and Al_2O_3 powders in different weight ratios for the synthesis of calcium aluminate nanoparticles?
2. How does the calcination temperature and duration influence the phase formation and crystallinity of the synthesized nanoparticles?
3. What structural or morphological advantages does the dodecacalcium heptaaluminate ($Ca_{12}Al_{14}O_{33}$) phase offer compared to other calcium aluminate phases?
4. How did the XRD analysis confirm the formation of pure $Ca_{12}Al_{14}O_{33}$, and what were the key crystallographic planes identified?
5. How do Raman and FT-IR spectroscopy validate the structural integrity and functional groups of the synthesized nanoparticles?
6. What does the SEM imaging reveal about the morphology of the nanoparticles, and how does it impact their functionality?

Antimicrobial and Practical Applications

7. What were the results of the antimicrobial activity tests, and how do they compare with existing antimicrobial materials?
8. What specific microbial strains were tested in the agar diffusion assay, and how effective were the nanoparticles against them?
9. What potential biomedical and environmental applications can benefit from these calcium aluminate nanoparticles?
10. How does the morphology of the synthesized nanoparticles influence their antimicrobial properties?

Sustainability and Green Synthesis

11. What are the advantages of using waste quail eggshells and aluminum cans from Coca-Cola as raw materials for nanoparticle synthesis?
12. How does this green synthesis approach contribute to environmental sustainability and waste reduction?
13. Are there any limitations or challenges associated with using waste-derived precursors in the synthesis of calcium aluminate nanoparticles?
14. How does this method compare with conventional calcium aluminate synthesis techniques in terms of cost, efficiency, and environmental impact?

Future Perspectives

15. What further modifications or improvements can be made to enhance the synthesis process and properties of the nanoparticles?
16. Are there any potential industrial applications where these nanoparticles can be commercially utilized?
17. How could the synthesis parameters (e.g., temperature, time, precursor ratios) be optimized further for better performance?
18. What are the next steps in exploring the full potential of calcium aluminate nanoparticles in medical or technological applications?

Would you like me to refine or add more questions based on a specific focus area?

ASTAXANTHIN DIESTER AND MONOESTER FROM FRESHWATER PRAWN WASTE AND THEIR ANTIOXIDANT ACTIVITY

Yin Yin Myint[1], Pa Pa Lin[2], Myint Myint Khine[3]

Abstract

The major carotenoids present in prawn waste include astaxanthin complexes. Astaxanthin is a lipid-soluble, and orange-reddish carotenoid pigment. Two astaxanthin compounds, AS-I (astaxanthin diester, an orange oil, 1.84%) and AS-III (astaxanthin monoester, a yellow oil, 1.13%), were isolated from the ethanol crude astaxanthin extract of freshwater prawn waste using silica gel column chromatography with *n*-hexane-acetone eluents. The chemical structures of these isolated compounds were confirmed by UV-Vis spectroscopy, FT-IR spectroscopy, GC-MS spectrometry, and visualization reagents, as well as solubility and R_f values. The antioxidant activity of the isolated astaxanthin compounds was evaluated using IC_{50} values. AS-III (astaxanthin monoester, IC_{50}: 36.84 µg/mL) exhibited greater antioxidant activity than standard ascorbic acid (IC_{50}: 47.48 µg/mL) and AS-I (astaxanthin diester, IC_{50}: 263.53 µg/mL) as determined by the DPPH free radical assay using a UV-Vis spectrophotometer at a wavelength of 517 nm.

Keywords: astaxanthin diester, astaxanthin monoester, prawn wastes, antioxidant activity

Introduction

Astaxanthin (3,3'-dihydroxy-β,β-carotene-4,4'-dione), a prominent carotenoid, is also found in microorganisms, insects, crustaceans, and micro-green algae (*Haematococcus pluvialis*). Astaxanthin, a red pigment, exhibits a shift in light absorbance when complexed with different proteins, resulting in a colour spectrum ranging from green, yellow, blue, to brown in crustaceans. The red colour is due to the conjugated double bonds at the center of the compound. Astaxanthin protects the neurons of the retina, is a cancer-protective agent that inhibits cancer metastasis, and can prevent various types of cancer. No toxic effects were found, although excessive astaxanthin consumption leads to yellow to reddish pigmentation of the skin in animals. Astaxanthin is a natural antioxidant with some advantageous properties are prevention of cardiovascular and immune system, anti-cancer, anti-aging, Alzheimer disease, athletic performance, muscle soreness, cosmetics, protecting eyesight, and fodder (Hu, *et. al*., 2019). The potency of astaxanthin's antioxidant activities has been reported the efficacy of astaxanthin to be 65 times more than vitamin C (Bayan, *et. al*., 2020). Myanmar name of freshwater prawn is Pujawn and common name is giant river prawn. The scientific name of *Macrobrachium rosenbergii*, belongs to Palaemonidae**.** The colour of *Macrobrachium rosenbergii* can vary according to where the prawns are found but the body can be greenish-grey (Brown, 2019). They are found in most inland freshwater areas including lakes, rivers, swamps, irrigation ditches, canals and ponds, as well as in estuarine areas. It is indigenous in the whole of the South and Southeast Asian including Myanmar as well as in northern Oceania and in the western Pacific islands (FAO, 2009). This research focuses on isolating astaxanthin compounds from freshwater prawn waste and determining their antioxidant activity.

[1] Department of Chemistry, Hinthada University
[2] Department of Chemistry, Hinthada University
[3] Department of Chemistry, Myingyan University

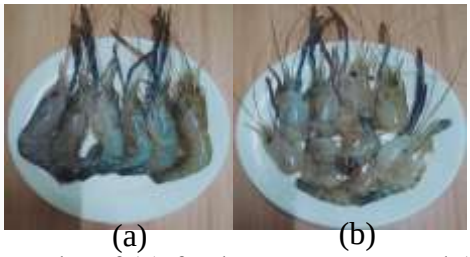

(a) (b)

Figure 1. Photographs of (a) freshwater prawn and (b) prawn wastes

Materials and Methods

Collection, Identification and Preparation of Freshwater Prawn

The freshwater prawn (exoskeletons including shell, claw duo and pincers) were collected from markets nearby, Hinthada Township, Ayeyawady Region. The scientific name was identified at the Zoology Department, Hinthada University. The freshwater prawn waste was cleaned with water. The waste was boiled with 2.0 % aqueous acetic acid for about 15 minutes and dried at room temperature and ground into fine powder. The crude astaxanthin extract was prepared by macerating 200 g of dried powder in 600 mL of ethanol, stirring for one hour on a magnetic stirrer. This procedure was repeated three times, followed by filtering and drying.

Chemicals

All chemicals and organic solvents were used laboratory grade.

Apparatus

UV-Vis (UV 1800, Shimadzu), FT IR spectrophotometer (Perkin Elmer, Spectrum II) and GC-MS_QP2010_Ultra spectrometer (Shimadzu) were used for structural identification of isolated compounds. The spectra were measured at the Department of Chemistry at Pathein University and Mandalay University.

Separation of Astaxanthin Compounds from Ethanol Crude Astaxanthin Extract

To separate the astaxanthin compounds, pet ether and ethyl acetate soluble materials were firstly extracted by liquid-liquid extraction from ethanol extract (7.53 g). Pet ether (4.25 g) and ethyl acetate (1.19 g) soluble organic constituents were primarily TLC checking carried out to isolated specific compounds. Both soluble extracts were applied to separate astaxanthin compounds by column chromatography.

Separation from pet ether soluble extract

Gradient elution was performed successively with *n*-hexane only (F-1); *n*-hexane: acetone,10:1 (F-2); *n*-hexane: acetone, 5:1 (F-3) and *n*-hexane: acetone, 3:1 (F-4), *n*-hexane: acetone, 1:1 (F-5) v/v and totally of five fractions were collected. All separated fractions were checked on TLC chromatograms under UV Lamp (254 and 365 nm) as well as using silver nitrate in methanol and 5 % sulphuric acid reagents. Fractions F-1 and F-5 were obtained as oil mixtures, F-2 was directly isolated as orange oil, F-3 as colourless needle crystal, and F-4 as yellow oil. The isolated compound from fraction F-2, named AS-I, was obtained as an orange oil (0.14 g), R_f value 0.80. The colorless needle crystal from fraction F-3 washed with *n*-hexane,

correspond to compound AS-II, a fatty acid (0.28 g), with an R_f value 0.55. From fraction F-4, a yellow oil (0.08 g), named AS-III, was obtained with an R_f value 0.53. All R_f values were determined using *n*-hexane: acetone 3:1 v/v as the eluent.

AS-I (0.0034 g), AS-II (0.0860 g), and AS-III (0.0231 g) were isolated from ethyl acetate soluble extract. In this isolation, the eluents were similarly carried out as described in the isolation of pet ether soluble extract.

Determination of Physicochemical Characteristic and Structural Identification

The isolated compounds AS-I and AS-III were characterized by structural identification as UV chromophores and functional groups using UV-Vis and FT IR spectroscopy, as well as fatty acid esters using GC-MS spectrometry. In this study, solubility comparisons, reported R_f values, and spectral data were used to determine the chemical structure.

Screening of Antioxidant Activity of Isolated Compounds: AS-I and AS-III

The antioxidant activity of the isolated compounds (astaxanthin compounds) from prawn waste was screened by 2,2-diphenyl-1-picrylhydrazyl **(**DPPH) free radical scavenging assay using the UV- Vis spectrophotometer according to Baliyan, *et. al*., 2022 with slight modification. DPPH powder (2 mg) and methanol (100 mL) were thoroughly mixed by a vortex to obtain the 20 µg/mL DPPH solution which was freshly prepared in a brown colored bottle. The standard ascorbic acid (100 µg/mL) solution was two-fold serially diluted with methanol to get the concentrations of 100, 50, 25, 12.5, 6.25 and 3.125 µg/mL, respectively. The solution of isolated compounds (400 µg/mL) were two-fold serially diluted with methanol to get the concentrations of 400, 200, 100, 50, 25, and 12.5 µg/mL, respectively. The blank solution of tests with desired concentrations were prepared by mixing 2 mL of each concentrations of test solutions with 2 mL of methanol. The control solution was prepared by mixing 2 mL of 20 µg/mL DPPH solution with 2 mL of methanol in the bottle.

DPPH free radical scavenging assay

The standard ascorbic acid and each of the test solutions were separately prepared by mixing 2 mL of 20 µg/mL DPPH solution with 2 mL of each test solution in a brown bottle. The solutions were mixed using a vortex and incubated at room temperature for 30 minutes. The absorbance of each concentration of solution was measured at λ_{max} 517 nm using a UV-Visible spectrophotometer (BK-V1000, Biobase). The experiment was carried out in triplicate for each concentration. The percentage of radical scavenging activity (% RSA) was calculated by plotting the absorbance against the concentration of the test solutions shown in Tables 2 and 3 and Figures 7.

$$\%RSA = \frac{\text{Absorbance of DPPH- (Absorbance of Sample-Absorbance of blank)} \times 100}{\text{Absorbance of DPPH}}$$

The IC_{50} (half-maximal inhibitory concentration) value was calculated using a linear regressive excel program. The standard deviation was also calculated.

Results and Discussion

Isolation of Astaxanthin Compounds and Structural Identification

The solubilities, R_f values, and chemical characteristics of the isolated compounds AS-I and AS-III were determined and compared with reported data for astaxanthin diester, astaxanthin monoester, and free astaxanthin. The isolated compounds were soluble in petroleum ether, *n*-hexane, ethyl acetate, and acetone, but showed poor solubility in ethanol, methanol, and water. Their solubility in moderately polar solvents (ethyl acetate and acetone) suggests the presence of some polar functional groups; however, their overall low polarity indicates a predominantly lipophilic character. Based on these observations, AS-I and AS-III are likely lipid-like compounds, possibly carotenoid esters rather than free fatty acids.

Based on the R_f values provided, it may deduce some preliminary inferences about the polarity and potential identities of the compounds: AS-I appears to be the least polar, AS-III is the most polar compound. The reported R_f values of astaxanthin diesters (0.75–0.85) and astaxanthin monoesters (0.6) were compared with the observed R_f values of AS-I and AS-III by same solvent system (Minyuk and Solovchenko, 2018) described in Table 1. The R_f values of astaxanthin diester and monoester are consistent with the observed R_f values of AS-I and AS-III. However, additional analysis is required to definitively identify these compounds.

Determination of chemical characteristic of isolated compounds

When examined under a UV lamp at 254 nm, AS-I and AS-III appeared as dark spots against a green background, suggesting the presence of conjugated systems typical of carotenoids. Both compounds were charred upon spraying with 5% sulfuric acid followed by heating, indicating the presence of carbon-based organic matter (Jork et al., 1990).

Table 1. Comparing the R_f values: AS-I, AS-III and Literature Astaxanthin diester, Astaxanthin Monoester and Astaxanthin Free Ester

Isolated compound	R_f value in *n*-hexane: acetone (3:1 v/v)		Remark
	Observed	*Literature	
AS-I	0.80	0.75-0.85	Astaxanthin diester
AS-III	0.53	0.60	Astaxanthin monoester
-	-	0.33	Astaxanthin free ester

* Minyuk and Solovchenko, 2018

On TLC developed with n-hexane–acetone (3:1 v/v) and visualized with silver nitrate in methanol, AS-I appeared orange, while AS-III exhibited a yellow coloration. Such differences in colouration are consistent with the behaviour of keto-carotenoids, which typically display orange to red shades depending on the number and position of keto groups. Moreover, free keto-carotenoids bearing hydroxyl groups at the 3, 3′-positions and keto groups at the 4, 4′-positions are known to display low R_f values in hexane-based solvent systems due to their stronger interaction with silica gel (Minyuk and Solovchenko, 2018).

The observed TLC characteristics suggest that AS-I and AS-III may contain two keto groups in their structures, possibly resembling astaxanthin derivatives.

Further spectroscopic analyses, including UV-Vis and FT-IR spectroscopy as well as GC-MS, were conducted to characterize the functional groups of AS-I and AS-III.

Isolated compound AS-I

The UV-Vis spectrum of AS-I in methanol (see in Figure 2) displayed absorption in the range of 265–600 nm when measured using a UV-Vis spectrophotometer (UV-1800, Shimadzu). Two distinct absorption maxima (λ_{max}) were observed at 275 nm and 449 nm. The major band at 449 nm is characteristic of $\pi \rightarrow \pi$ electronic transitions in conjugated polyene systems typical of carotenoids, while the additional band at 275 nm may correspond to higher-energy electronic transitions associated with the extended conjugated structure (Field et al., 2008). On TLC, AS-I appeared as an orange spot, which is consistent with carotenoid-type compounds possessing extended conjugated systems (Minyuk and Solovchenko, 2018).

The FT-IR spectrum of AS-I was compared with reported spectra of free astaxanthin (Nemani et al., 2024) and astaxanthin diesters (Subramanian et al., 2013) see in Figure 4 (a),(b) and (c). The FT-IR spectral profile of AS-I provides strong evidence for its structural similarity to astaxanthin derivatives. The presence of two distinct absorption bands at 1737 cm^{-1} and 1715 cm^{-1} indicates both esterified carbonyl groups and the characteristic carbonyl vibration at the 4, 4′-positions of the β-ionone rings. The additional ν_{C-O} stretching absorptions at 1185 and 1082 cm^{-1} further support the presence of aliphatic ester functionalities. Importantly, the absence of a broad ν_{O-H} stretching band in the 3550–3200 cm^{-1} region suggests that the hydroxyl groups at the 3, 3′-positions have undergone esterification, consistent with fatty acid ester derivatives of astaxanthin (Subramanian et al). The absorption band at 1222 cm^{-1} indicates υ_{C-C-C} and $\delta_{C-C(=O)-C}$ for the C-C-C of the ketone (Silverstein, *et. al*., 2005). Moreover, the absorption at 3007 cm^{-1}, assigned to ν_{C-H} of alkenes, together with the CH_2 and CH_3 stretching and bending vibrations at 2924, 2854, 1438, and 964 cm^{-1}, indicates the presence of long hydrocarbon chains, characteristic of esterified carotenoids (Pretsch et al., 1989 and Silverstein et al., 2005). These observations, taken together, suggest that AS-I is not a free astaxanthin but rather an esterified form, most likely a diester, in agreement with previously reported spectral features of astaxanthin diesters (Nemani et al., 2024).

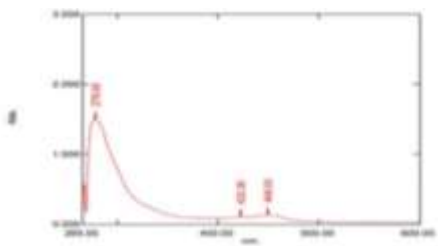

Figure 2. UV-Vis spectrum of isolated compound AS- I

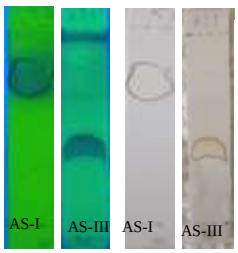

(a) (b)

Figure 3 TLC chromatograms of AS-I and AS-III
(a) under 254 nm of UV lamp
(b) after spraying with $AgNO_3$

Identification of fatty acids of astaxanthin diester by GC-MS

The fatty acid esters of AS-I were identified by GC-MS spectrometry. The analysis revealed a total of nine fatty acid esters, comprising both saturated and unsaturated derivatives. Among these, five unsaturated fatty acid esters were detected: ethyl 9-hexadecenoate (RT 15.825 min), 9,12-octadecadienoic acid (*Z, Z*)-, methyl ester (RT 19.046 min), 9-octadecen oic acid (*Z*)-, methyl ester (RT 19.226 min), *trans, trans*-9,12-octadecadienoic acid, propyl (RT 21.334 min) and (*E*)- 9- octadecenoic acid ethyl ester (RT 21.552 min). Typically, the hydroxyl groups at the 3- and 3'-positions of the β-ionone rings in astaxanthin can form ester bonds with various fatty acids, such as oleic or linoleic acid, resulting in diester derivatives (Brotosudarmo et al., 2020). The relatively high R_f value of AS-I compared to another isolated compound, AS-III, in the same solvent system further supports the presence of ester groups at these positions. Based on the combined spectral and physicochemical data suggest that AS-I is an astaxanthin unsaturated fatty acid diester.

Isolated compound AS-III

AS-III exhibits a more polar nature than AS-I, as indicated by their respective R_f values. The R_f value of AS-III aligns with the reported value for R_f astaxanthin monoester in an *n*-hexane: acetone (3:1 v/v) solvent system (Minyuk and Solovchenko, 2018). The FT IR spectrum of AS-III clearly differentiates between mono- and diester of astaxanthin through distinct spectral shifts. A board absorption band of observed at 3505 cm^{-1} corresponds to υ_{O-H} stretching vibration, suggesting the presence of a free hydroxyl group at either the ~~in~~ 3- or 3′-position of β-ionone rings. A very strong absorption band at 1707 cm^{-1} is attributed to the $\upsilon_{C=O}$ stretching of the 4,4'-β-ionone rings carbonyl groups. This band exhibits greater intensity and higher energy compared to the stretching C=O vibration at 1657 cm^{-1} reported for free astaxanthin esters (Subramanian, *et. al*., 2013), indicating potential overlap of carbonyl signals from both ester and keto functionalities. A strong absorption band at 1092 cm^{-1} confirms the presence of aliphatic esters through C-O stretching (Pretsch, *et. al*., 1989). The absorption at 1222 cm^{-1} is consistent with stretching υ_{C-C-C} and bending ($\delta_{C-C(=O)-C}$) vibrations characteristic of ketone group (Silverstein, *et. al*., 2005). The band at 3006 cm^{-1} arises from the C–H stretching of alkene groups (–C=C–H), influenced by the fatty acid environment on one end of the astaxanthin molecule.Additional absorption bands at 2924 cm^{-1} and 2855 cm^{-1} corresponds to aliphatic C-H stretching, while those at 1438 cm^{-1}, 1362 cm^{-1} and 904 cm^{-1} are associated with C-H bending vibrations of -CH_2 and -CH_3 groups. In monoester, esterification typically occurs at only one end of the astaxanthin molecule, leaving the –OH group at the other end unmodified. The presence of stretching O-H band at 3505 cm^{-1} supports this structural arrangement. Comparison of the observed FT IR spectrum of AS-III with reported spectra reveals consistency, particularly in the absorption bands associated with O-H, C=O, C=C, C-C(=O)-C, and the fingerprint region as illustrated in Figure 5 (a), (b) and (c) (Subramanian, *et al*., 2013). The lower R_f value of AS-III (0.53) compared to AS-I (0.80) in the same solvent system further supports its higher polarity, suggesting the presence of a free hydroxyl group at the 3- or 3′-position of the β-ionone ring. Based on the collective spectral and physicochemical data, the isolated compound AS-III can be considered an astaxanthin monoester. However, the specific fatty acid moiety attached to the esterified end of AS-III cannot be identified using the FT IR data alone. Further structural elucidation using techniques such as NMR or mass spectrometry, is required for complete characterization.

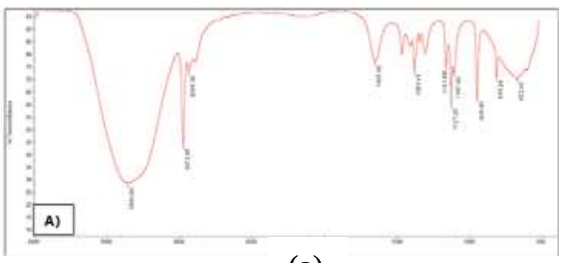

(a) (Nemani, *et. al*., 2024)

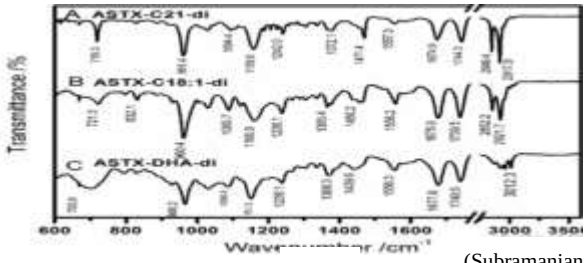

(b) (Subramanian, *et. al*., 2013)

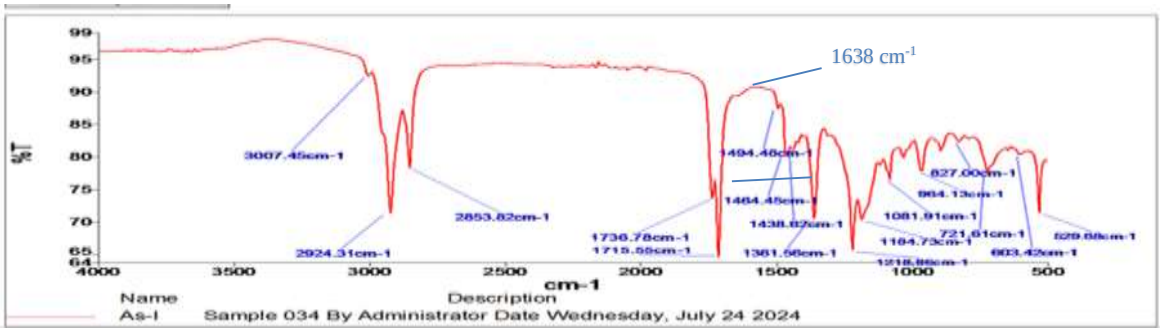

(c)

Figure 4 Comparing FT IR spectra of (a) pure astaxanthin (b) astaxanthin diester and (c) isolated compound AS-I

Antioxidant activity of Isolated Astaxanthin Compounds

DPPH (2,2-diphenyl-1-picrylhydrazyl) is a relatively stable, hydrophobic free radical. A greater decrease in absorbance indicates more effective DPPH radical scavenging activity. The antioxidant activity of standard ascorbic acid, isolated astaxanthin compounds, AS-I and AS-III, were evaluated by determining their IC_{50} values (half-maximal inhibitory concentration). This was achieved by plotting the % RSA (radical scavenging activity) against compound concentration using linear regression in Excel. The IC_{50} values obtained were 263.53 µg/mL for AS-I (astaxanthin diester) and 36.84 µg/mL for AS-III (astaxanthin monoester) and 7.48 µg/mL for ascorbic acid. These results indicate that AS-III exhibits stronger antioxidant activity than the standard ascorbic acid, while AS-I shows lower activity in comparison. Given that DPPH is a hydrophobic, the lipid solubility of astaxanthin monoester (AS-III) likely enhances its ability to interact with and scavenge DPPH more effectively than the hydrophilic ascorbic acid and the bulkier astaxanthin diester (AS-I). This greater interaction may facilitate a more efficient electron transfer process, resulting in superior antioxidant performance. The percent of radical scavenging activity (%RSA) and IC_{50} values are presented in Tables 2 and 3 and Figure 7. According to the findings, astaxanthin compounds are natural carotenoid pigment with a long polyconjugated chain, which confer unique properties, including strong antioxidant activity due to their ability to delocalize electrons.

Furthermore, astaxanthin monoester also possesses hydroxyl group that can donate hydrogen atoms to neutralize free radicals. This enables it to neutralize more DPPH radicals per molecule than astaxanthin diester. From this study suggest that AS-III (astaxanthin monoester) is important constituents of prawn waste for the antioxidant potential and the natural carotenoid

pigment with a long polyconjugate chain prevent oxidative damage that can be therapeutically useful.

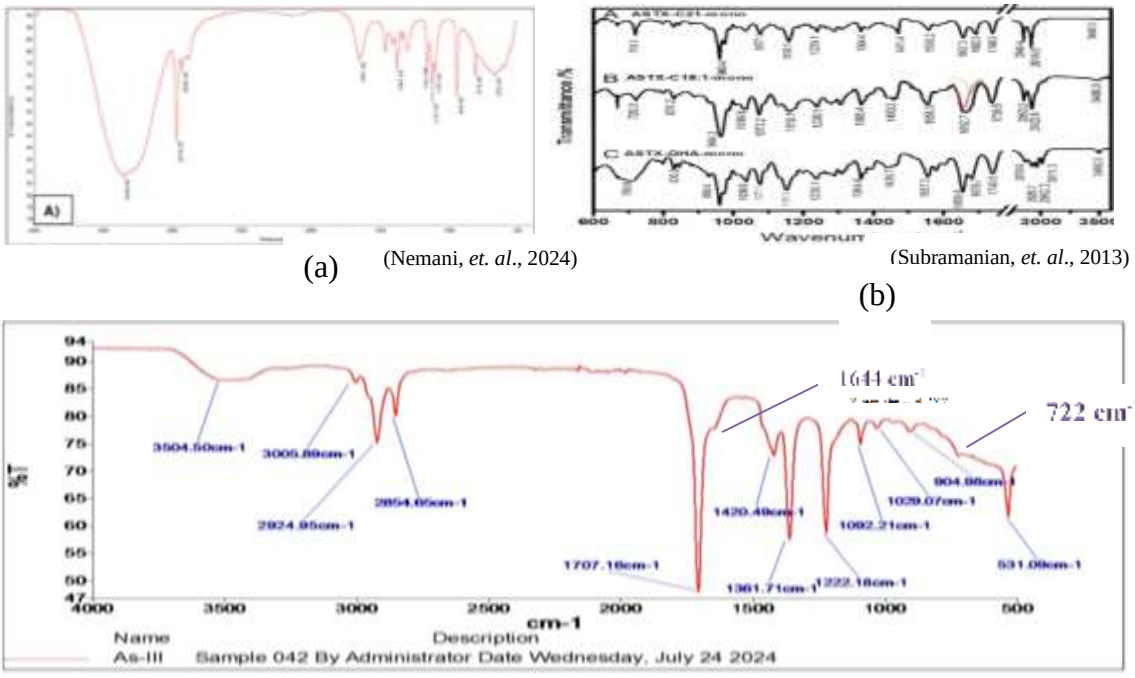

(a) (Nemani, *et. al*., 2024) (Subramanian, *et. al*., 2013) (b)

(c)

Figure 5 FT IR spectra of (a) pure astaxanthin (b) astaxanthin monoesters and (c) isolated compound AS-III

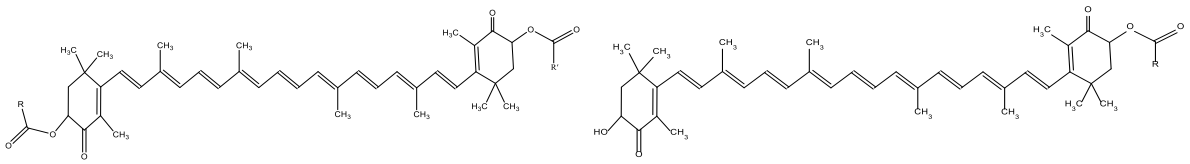

(a) (b)

Figure 6 Possible chemical structures of isolated compounds (a) AS-I, astaxanthin diester and (b) AS-III, astaxanthin monoester

Table 2. Absorbance Values, Percent Radical Scavenging (% RSA) and IC_{50} Values of Standard Ascorbic Acid

Conc.(µg/mL)	Absorbance at λ_{max} 517 nm	% RSA± SD	IC_{50} (µg/mL)
6.25	0.299	26.53± 0.05	
12.50	0.283	30.46±0.01	47.48
25.00	0.274	32.67±0.04	
50.00	0.194	52.33±0.05	
100.00	0.074	81.81±0.01	

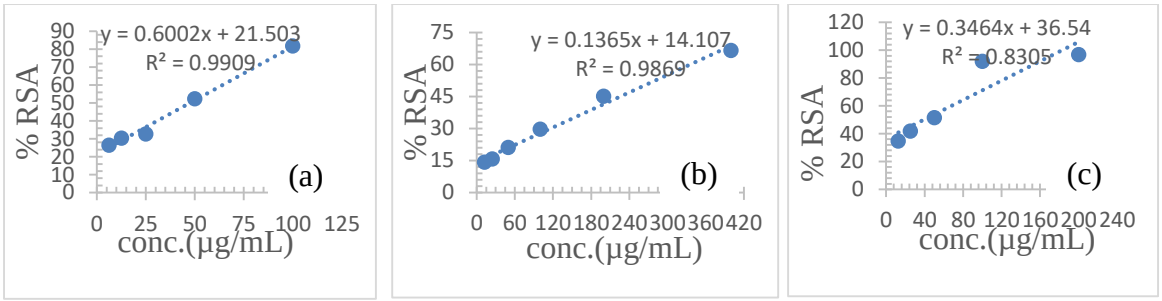

Figure 7 Plot of % Radical Scavenging Activity *versus* concentrations of (a)standard ascorbic acid (b) AS-I and (c) AS-III

Table 3. Absorbance Values, Percent Radical Scavenging (% RSA) and IC_{50} Values of Isolated Compound AS-I and AS-III

Conc. (µg/mL)	Absorbance at λ_{max} 517 nm		% RSA with SD		IC_{50} (µg/mL)	
	AS-I	AS-III	AS-I	AS-III	AS-I	AS-III
12.50	0.471	0.327	14.16 ±0.00	34.74±0.03		
25.00	0.464	0.303	15.64±0.03	41.94±0.08	263.53	36.84
50.00	0.438	0.262	21.14±0.03	51.44±0.17		
100.00	0.401	0.104	29.59±0.02	92.01±0.06		
200.00	0.333	0.077	45.03±0.02	96.80±0.00		
400.00	0.243	0.075	66.59±0.04	97.78±0.01		

Conclusion

The possible chemical structures of isolated compounds AS-I (1.84 %, orange oil) and AS-III (1.13 %, yellow oil) were identified as astaxanthin diester and astaxanthin monoester, respectively, from the ethanol crude extract of prawn waste. Their identification was based on comparisons of R_f values, visual observation tests, and FT-IR and UV-Vis spectral data with those of known astaxanthin esters. Additionally, the presence of fatty acid esters in AS-I (astaxanthin diester) was confirmed through GC-MS analysis. The antioxidant activity of the isolated astaxanthin compounds was determined by their IC_{50} values, which were found to be 36.84 µg/mL for AS-III and 263.53 µg/mL for AS-I. These results indicate that the monoester form (AS-III) exhibits significantly stronger antioxidant activity than the diester form (AS-I). Overall, the extraction and isolation of astaxanthin derivatives from prawn waste represent a sustainable and eco-friendly alternative to conventional sources and methods, offering both environmental and economic benefits.

Acknowledgements

I would like to thank Rector Dr Theingi Shwe, Pro-rectors Dr Ye Ye Than and Dr Aye Lwin and Professor and Head Dr Tin Htwe Mu for their permission to submit the paper.

References

Baliyan, S., R. Mukherjee, A. Priyadarshini, A. Vibhuti, A. Gupta, R. P. Pandey and C-M. Chang. (2022). "Determination of Antioxidants by DPPH Radical Scavenging Activity and Quantitative Phytochemical Analysis of Ficus religiosa, Molecule*"*, **27**(1326), 1-19

Bayan, Y. A-T., A. Mahmood, S. Assaw and H. I. Sheikh. (2020). "Application of Astaxanthin and its Lipid Stability in Bakery Product".8(3), 962 – 974

Brotosudarmo, T.H.P., L. Limantara, E. Setiyono, and Heriyanto. (2020). "Review Article, Structures of Astaxanthin and Their Consequences for Therapeutic Application", *International Journal of Food Science*, 1-16

Brown, J. (2019). *Macrobrachium rosenbergii* (Giant Freshwater Prawn), Host Animal, Cultured Species, Invasive Species, CABI Compendium, 96269

FAO. (2009). *"Macrobrachium rosenbergii"*. In Cultured aquatic species fact sheets

Field, L. D., S. Sternhell, and J. R. Kalman. (2008). *Organic Structures from Spectra*, New York, 4th edition, Jon Wiley and Sons, Ltd, 7-14

Guerin, M., E. H. Mark, M. Olaizola. (2003). "*Haematococcus* Aastaxanthin: Applications for Human Health and Nutrition". *Trends in Biochem*, **21**(5), 210 - 216.

Hu, J., W. Lu, M. Lv, Y. Wang, R. Ding and L. Wang. (2019). "Extraction and Purification of Astaxanthin from Shrimp Shells and the Effects of Different Treatments on its Content". **29**(1), 24 - 29

Jork, H., W. Funk, W. Fischer, and H. Wimmer. (1990). *Thin Layer Chromatography Reagents and Detection Methods, Physical and Chemical Detection Methods: Fundamentals, Reagents I*, Weinheim (Federal Republic of Germany), VCH Verlagsgesellschaft mbH, D-6940, **la**

Minyuk, G. S. and A. E. Solovchenko. (2018). "Chapter 4, Express Analysis of Microalgal Secondary Carotenoids by TLC and UV-Vis Spectroscopy, New York, Humana Press, **1852**, 73-95

Nemani, N., S. M. Dehnavi and G. Pazuki. (2024). "Extraction and Separation of Astaxanthin with the Help of Pre-treatment of *Haematococcus pluvialis* Microalgae Biomass Using Aqueous Two-phase Systems Based on Deep Eutectic Solvents", *Nature Portfolio,* **14** (5240), 1-13

Pretsch, E., W. Simon, J. Seibl and T. Clerc. (1989). *Tables of Spectral Data for Structure Determination of Organic Compounds*, Berlin, 2nd edition, Springer-Verlag, I5-I142

Silverstein, R. M., F. X. Webster and D. J. Kiemel. (2005). *Spectrophotometric Identification of Organic Compounds*, New York, 7th edition., John Wiley and Sons, Inc., 82-98

Subramanian, B., M. H. Thibault, Y. Djaoued, C. Pelletier, M. Touabia, and N. Tchoukanova. (2013). "Chromatographic, NMR and Vibrational Spectroscopic Investigations of Astaxanthin Esters: Application to "Astaxanthin Rich Shrimp Oil" Obtained from Processing of Nordic Shrimps", The *Royal Society of Chemistry's Journals*, *Analyst,* 1-10

PREPARATION, CHARACTERIZATION AND APPLICATION OF PVA-RICE STARCH-CHITOSAN BLENDED FILMS

Khin Sandar Kyi[1], Tun Zaw Moe[2], Aung Chan Thar[3]

Abstract

Chitosan was prepared from shrimp shells and rice starch were extracted from rice grain. The polymeric films of PVA-rice starch-chitosan and PVA-rice starch-chitosan-glycerol-citric acid with various ratios were prepared by casting methods. The physicomechanical properties such as thickness, tensile strength, elongation at break**,** and tear strength of the prepared films were determined by mechanical testing. PVA-rice starch-chitosan-glycerol-citric acid films showed the potent antimicrobial activity on seven tested microorganisms such as *Agrobacterium tumefaciens, Bacillus pumilus, Bacillus subtilis, Candida albicans, Escherichia coli, Pseudomonas fluorescens and Staphylococcus aureus* by the agar disc diffusion method. Medicinal application of PVA-rice starch-chitosan-glycerol-citric acid films with various ratio was studied by using Wistar rats. After 15 days, the wound healing activity of the PVA- starch-chitosan-glycerol-citric acid film with the ratio of 2: 1: 2:0.5:1 was found to be effective on treated lesions of Wistar rats.

Keywords: chitosan blended films, physicomechanical properties, antimicrobial activity, wound healing activity

Introduction

The development of environmental friendly polymer materials can be classified into two categories based on the raw material used: degradable synthetic polymers and renewable natural polymers. Renewable natural polymer resources include starch, cellulose and chitosan. Starch is the most attractive candidate because of its low cost, ready availability, its inherent biodegradability and potential for mass production from renewable resources. However, the poor mechanical properties and relatively hydrophilic nature of starch compared to most petroleum-based polymers prevent its use in widespread applications. Recently, several attempts have been made to blend starch with biodegradable synthetic polymers. Starch itself is very brittle and has poor mechanical properties for plastic applications. This condition necessitates the addition of plasticizers. Plasticizers include polyols such as glycerol and polyethylene glycol. In this study glycerol is used as plasticizer because of its ready availability. In addition, citric acid was used as the additive in this study. Citric acid is rated as nutritionally harmless since it is a nontoxic metabolic product of the body.

PVA is a synthetic water-soluble and biodegradable polymer (Chiellini *et al*., 2003). PVA has excellent mechanical properties and compatibility with starch, PVA/starch blend is assumed to be biodegradable since both components are biodegradable in various microbial environments. The biodegradability of blends consisting of starch, PVA, Glycerol and urea is performed by bacteria and fungi isolated from the activated sludge of a municipal sewage plant and landfill, which indicate that microorganisms consumed starch and the amorphous region of PVA as well as the plasticizers (Tudorachi *et al*., 2000). Because both starch and PVA are polyols, starch, will form continuous phase with PVA during blending.

Starch and chitosan are abundant naturally occurring polysaccharide. Both of them are cheap, renewable, non-toxic, and biodegradable. Starch is totally biodegradable in a wide variety

[1] Department of Chemistry, MeiklitaUniversity
[2] Department of Chemistry, Sagaing University
[3] Department of Chemistry, Mandalar University

environment. It can be hydrolyzed into glucose by microorganisms or enzymes, and then metabolized into carbon dioxide and water. Carbon dioxide will recycle into starch again by plants and sunshine. Starch itself is poor in processability, also poor in the dimensional stability and mechanical properties for its end products (Choi *et al*., 1999). Therefore, native starch is not used directly.

Materials and Methods

Extraction of Rice Starch

Rice starch was extracted from rice grain. Rice grains were ground in a grinding machine and the rice powder was passed through 250 mesh screens. Rice powder sample (100 g) was placed in a 2 L steel pot. Distilled water (1500 mL) was added to the rice powder, stirred manually for 1 h and the liquid detained was centrifuged for 30 min. The supernatant was decanted off and the residue was extracted with 1liter distilled water for 24 h. The rice sample residues were put into a Petri dish and air dried in the laboratory (Valgadde *et al*., 2015). The yield of extracted rice starch was calculated. (Appendix-I)

Preparation of Chitosan

The shrimp shells (100 g) were deproteinised by using 5% NaOH with a 1: 8 (w/v) ratio and refluxed at 60°C for 2 h. Then the product was collected with 300 µm sieve, washed and dried under the fume hood to constant weight. The deprotonised product was then decolourised with acetone for 24 h, and was demineralised with 1 % HCl with 1:10 (w/v) for 24 h at room temperature. The light brown powder was obtained as chitin (Hossain and Iqbal 2014). Then, the chitin was deacetylated with a 1: 5 (w/v) ratio of 5 % NaOH at 100 °C for 10 h (Kandile *et al*., 2018). Finally, the prepared chitosan was washed with distilled water and dried under a fume hood to yield a constant weight. The yield of chitosan was 69.03 %.

Preparation of PVA-Starch-Chitosan Blended Films

PVA, starch, and chitosan films with various ratios of 2:1: 2 (PVA: starch: chitosan), 2:1:3, 2:1:4, and 2:1:5 were also prepared. Starch (1.0 g) was added into 250 mL beakers. Next, 100 mL of distilled water were added to the beakers. The solution mixtures were stirred for 10 min. The chitosan (2.0 g) was added to the starch solution, and the solution mixtures were stirred for 10 min. After that, 2.0 g of PVA was added. The solution mixture was stirred by using a magnetic stirrer at 150 ˚C for 30 min at a rate of 1000 rpm and then autoclaved at 0.1 MPa, 121 ˚C for 20 min. The polymeric solution was cast on the melamine plate and oven-dried for 2 h 30 min, and air dried for 2.5 days to obtain the PVA, starch, and chitosan films with a PVA, starch, and chitosan films ratio of 2:1:2. Similarly, the films with different ratios of PVA, starch, and chitosan; 2:1:3, 2:1:4, and 2:1:5 were prepared using the procedure as mentioned above (Brandelero *et al*., 2019).

Preparation of PVA-Rice Starch-Chitosan-Glycerol-Citric Acid Films

The films with PVA, rice starch, chitosan, glycerol, and citric acid ratios of 2:1:2:0.5:0.5 2:1:3:0.5:1, 2:1:4:0.5:1.5, and 2:1:5:0.5:2 were also prepared. Rice starch (1.0 g) was added into 250 mL beakers. Next, 100 mL of distilled water was added to the beakers. The solution mixtures were stirred for 10 min. The chitosan (2.0 g) was added to the rice starch solution and the solution mixtures were stirred for 10 min. After that, 2.0 g of PVA, 0.5 g of glycerol, and 0.5 g of citric acid were added. The solution mixture was stirred by using a magnetic stirrer at a temperature of 150 ˚C for

30 min at a rate of 1000 rpm and then autoclaved at 0.1 MPa, 121 ˚C for 20 min. The polymeric solution was cast on the melamine plate and oven-dried for 2 h 30 min and air-dried for 2.5 days to obtain the PVA-rice starch-chitosan-glycerol-citric acid film with a ratio of 2:1:2:0.5:0.5. Similarly, films with varying ratios of 2:1:3:0.5:1, 2:1:4:0.5:1.5, and 2:1:5:0.5:2 were prepared as the procedure mentioned above (Brandelero *et al*., 2019).

Determination of Physicomechanical Properties of PVA-Rice Starch-Chitosan Films and PVA-Rice Starch-Chitosan-Glycerol-Citric Acid films

Physicomechanical parameters of PVA-rice starch-chitosan films and PVA-rice starch-chitosan-glycerol-citric acid films, such as tensile strength, elongation at break, and tear strength were tested at the Development Centre for Rubber Technology, Yangon. Dog bone-shaped test specimens were cut from the PVA-rice starch-chitosan films and PVA-rice starch-chitosan-glycerol-citric acid films. Mechanical testing for tensile strength properties was performed by a testing machine. The tensile strength, elongation at break, and tear strength of PVA- rice starch-chitosan films, and PVA-rice starch-chitosan-glycerol-citric acid films were calculated**.** (Appendix– II)

(a) Determination of thickness

The thickness of the prepared PVA-rice starch-chitosan films was measured by using NSK micrometers. The thickness of the films were measured at five locations (1 centre and 4 corners) using a micrometer.

(b) Determination of tensile strength and elongation at break

Dog-bone shaped test specimens were cut from the films. Both ends of the test pieces were firmly clamped in the jaw of the test machine. One jaw was fixed, and the other was moveable. The rate of the moveable jaw was bold 100 mm/min. This procedure for tensile strength was repeated three times.

(c) Determination of tear strength

Test specimen was cut off by a die from the above films. The specimen was cut with a single nick (0.04 mm) at the entire inner concave edge by a special cutting device using a razor blade. The clamping of the specimen in the jaw of the test machine was aligned with the travel direction of the grip at 100 mm/min. The recorder of the machine was shown the highest force to tear from a specimen nicked. The procedure was done in triplicate.

Investigation of Antimicrobial Activity

Antimicrobial activities in PVA-rice starch-chitosan-glycerol-citric acid (PSCGC II) film was determined by applying agar well diffusion method against seven microorganisms such as *Agrobacterium tumefaciens, Bacillus pumilus, Bacillus subtilis, Candida albicans, Escherichia coli, Pseudomonas fluorescens and Staphylococcus aureus* at Chemistry Depatrment, Meiktila University.

A 18 g of nutrient agar powder was suspended in 100 mL of distilled water. The mixture was heated while stirring to well dissolve all components. The dissolve mixture was placed in the autoclave at 121 ˚C for 45 min. Then the flasks were cooled down at room temperature and 0.2 mL of spore suspension were added into it and poured into the sterilized Petri dish. The agar was allowed to set for 2 h and then 8 mm plate agar disc was made with the help of sterilized cork

borer. After that about 5 mm of the sample was introduced into the agar-disc and incubated at 37 ˚C for 24 h. The inhibition zone (clear zone) which appeared around the agar disc, indicated the presence of antimicrobial activity.

Wound-Healing Activity of Prepared Films tested by Animal Experiment

The adult male Wistar rats from Laboratory animal services division, Department of Medical Research (Lower Myanmar) DMR-LM were included in this study to determine the proper healing agent in the treatment of incision wound. All Wistar rats were admitted to the study approximately 4 months of age and between 250-300 g of body weight. Free access was allowed to use standard diet (pellet food), water, temperature, humidity and light period. The Wistar rats received only clean water wash and the treatment groups received PVA-rice starch-chitosan-glycerol-citric acid (2: 1: 2: 2: 0.5: 1) film one time /day for 14 days.

Results and Discussion

Sample Preparation

Rice starch 32.48 g was extracted from 100 g of rice grain and yield percent was found to be 32.48 %. Chitosan 69.03 g was prepared from 100 g of shrimp shells and yield percent was found to be 69.03 %.

Physicomechanical Properties of PVA-Rice Starch-Chitosan Films

PVA, rice starch and chitosan films were prepared with four different ratios of 2: 1: 2, 2: 1: 3, 2: 1: 4, and 2: 1: 5 respectively. PVA-rice starch-chitosan film PSC (I) with the ratio of (2:1:2) was found to have good physicomechanical properties, such as tensile strength (7.1 MPa), elongation at break (10 %), and tear strength (37.8 kN/m), as shown in Table 1 and Figure 1.

Table 1. Physicomechanical Properties of PVA-Rice Starch-Chitosan Blended Films

No	Sample	Weight ratio of PVA, rice starch and chitosan	Tensile strength (MPa)	Elongation at break (%)	Tear strength (kN/m)
1.	PSC(I)	2: 1: 2	7.1	10	37.8
2.	PSC(II)	2: 1: 3	7.3	9	29.1
3.	PSC(III)	2:1: 4	8.1	7	35.3
4.	PSC(IV)	2: 1: 5	9.6	10	7.7

Thickness = 0.29 mm
PSC(I) = 2% PVA + 1% rice starch + 2% chitosan
PSC(II) = 2% PVA + 1% rice starch + 3% chitosan
PSC (III) = 2% PVA + 1% rice starch + 4% chitosan
PSC(IV) = 2 % PVA + 1% rice starch + 5% chitosan

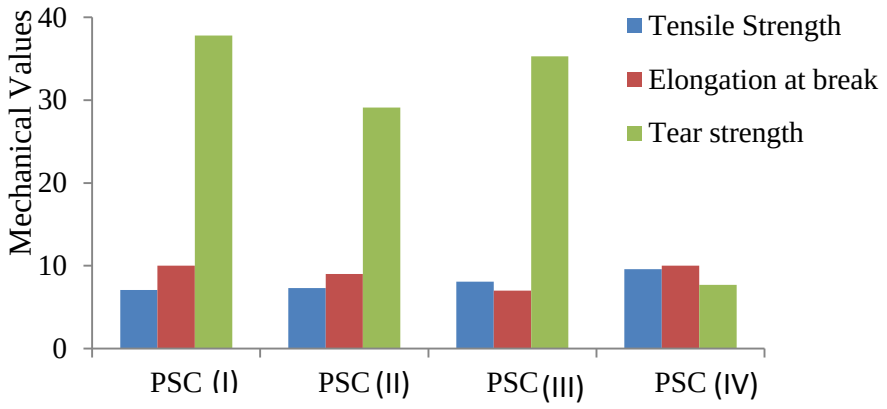

PSC = PVA-rice starch-chitosan

Figure 1. Histogram of some mechanical values of prepared PVA- rice starch-chitosan blended films

Physicomechanical Properties of PVA-Rice Starch-Chitosan-Glycerol-Citric Acid Films

Effect of citric acid on the PVA-rice starch-chitosan films was studied by the addition of 0.5, 1, 1.5, 2 g of citric acid into the mixture of PVA, rice starch, chitosan, glycerol with the ratios 2: 1: 2: 0.5.

Citric acid was added as an additive. It has two functions i.e., as a cross linker and as a plasticizer. The mechanical properties are not only related with the plasticizer. Generally, the tensile strength increased and the elongation at break increased as the percentage of cross linker increased. The citric acid acted both as the cross linker and the plasticizer in the PVA-rice starch-chitosan composites. So, the different functions of citric acid exhibited different amount of citric acid added. The tensile strength and elongation at break as the function of citric acid concentration are shown in Table 2 and Figure 2. The tensile strength of PSCGC (II) was 6.6 MPa which was found to be higher than 4.8 MPa of PSCGC (IV). But adding more citric acid to the blends as a plasticizer made the macromolecules interact less, which led to decrease in tensile strength (4.8 MPa). And thus, elongation at break increased to 392. From the experimental data, the film with the PVA: rice starch: chitosan: glycerol: citric acid ratio of 2: 1: 2: 0.5: 1 (PSCGC II) was found to have the best physicomechanical properties.

Table 2. Physicomechanical Properties of PVA-Rice Starch-Chitosan-Glycerol-Citric Acid (PSCGC) Films

No	Sample	Weight ratio of PVA, rice starch, chitosan, glycerol and citric acid	Tensile strength (MPa)	Elongation at break (%)	Tear Strength (kN/m)
1.	PSCGC(I)	2: 1: 2: 0.5: 0.5	3.7	71	16.5
2.	PSCGC (II)	2: 1: 2: 0.5: 1.0	6.6	123	35.0
3.	PSCGC(III)	2: 1: 2: 0.5: 1.5	4.0	78	31.0
4.	PSCGC (IV)	2:1 :2: 0.5: 2.0	4.8	392	32.9

Thickness = 0.38 mm
PSCGC (I) = 2 % PVA+ 1 % rice starch+ 2 % chitosan+ 0.5 % glycerol+ 0.5 % citric acid
PSCGC (II) = 2 % PVA+ 1 % rice starch+ 2 % chitosan+ 0.5 % glycerol+ 1 % citric acid
PSCGC (III) = 2 % PVA+1 % rice starch+ 2 % chitosan+ 0.5 % glycerol+ 1.5 % citric acid
PSCGC (IV) = 2 % PVA+ 1 % rice starch+ 2 % chitosan+0.5 % glycerol+ 2 % citric acid

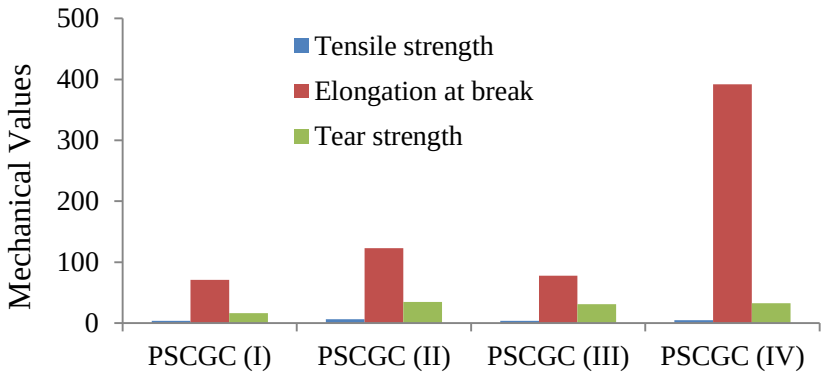

PSCGC = PVA-rice starch-chitosan-glycerol-citric acid

Figure 2. Histogram of some mechanical values of prepared of PVA- rice starch-chitosan-glycerol-citric acid films

Antimicrobial Activity of the PVA-Rice Starch-Chitosan-Glycerol-Citric acid Films

Antimicrobial activity of the selected PVA-rice starch-chitosan-glycerol-citric acid films (PSCGC II) was tested by agar-well diffusion method on seven microorganisms such as *Agrobacterium tumefaciens, Bacillus pumilus, Bacillus subtilis, Candida albicans, Escherichia coli, Pseudomonas fluorescens and Staphylococcus aureus.* The results are shown in Table 3 and Figure 3. PVA-rice starch-chitosan-glycerol-citric acid films (PSCGC II) were found to show active on all tested microorganisms.

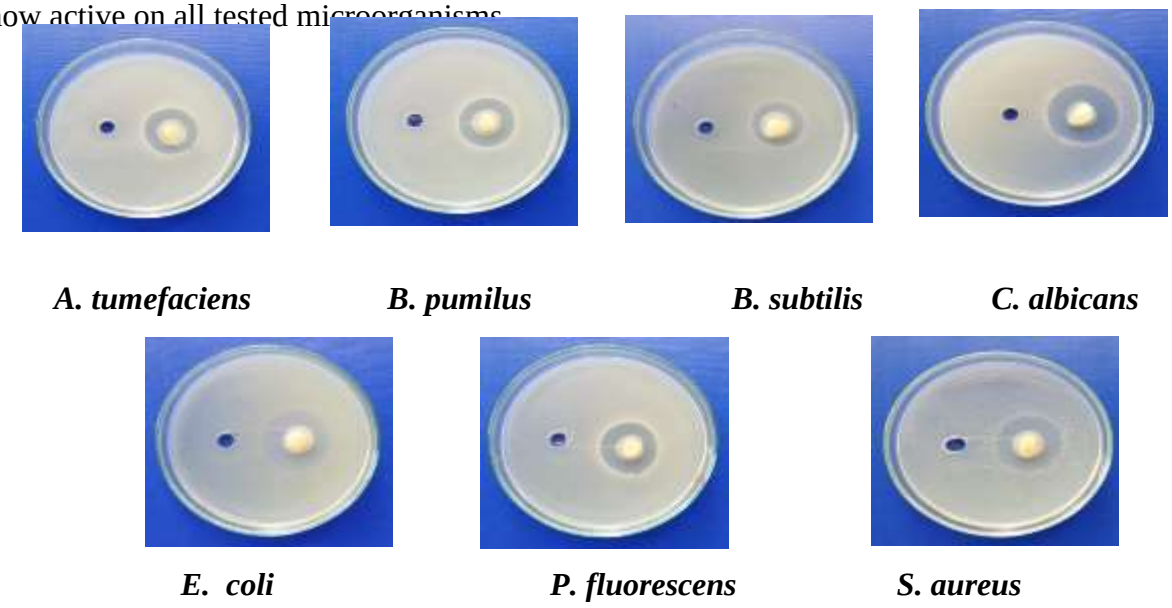

Figure 3. Antimicrobial activity of PVA-rice starch-chitosan-glycerol-citric acid (PCSGS II)Films

Table 3. Results of Antimicrobial Activity of PVA-Rice Starch-Chitosan-Glycerol-Citric Acid (PSCGC II) Films

No.	Microorganisms	Inhibition Zone Diameters (mm)
1.	*A. tumefaciens*	+++
2.	*B. pumilus*	+++
3.	*B. subtilis*	+++
4.	*C. albicans*	+++
5.	*E.coli*	+++
6.	*P.fluorescens*	+++
7.	*S.aureus*	+++

Agar-well – 8 mm
8 mm-12 mm (+) (mild activity)
13 mm-17 mm (++) (moderate activity)
18 mm above (+++) (potent activity)

Wound-Healing Activity of Prepared Film

The skin incision of Wistar rats was treated with PVA-rice starch-chitosan-glycerol-citric acid film (PSCGC (II)) (Kornblum *et al.*, 1973). After 15 days of treatment, the wound healing places of the rat closed, and their hair regrew. The photographs recorded during the study process are shown in Figure 4. The appearance of the skin treated with the cross-linker PVA-rice starch film (15 days) was observed to be nearly the same as the normal skin (Sharif and Yamaura, 2002).

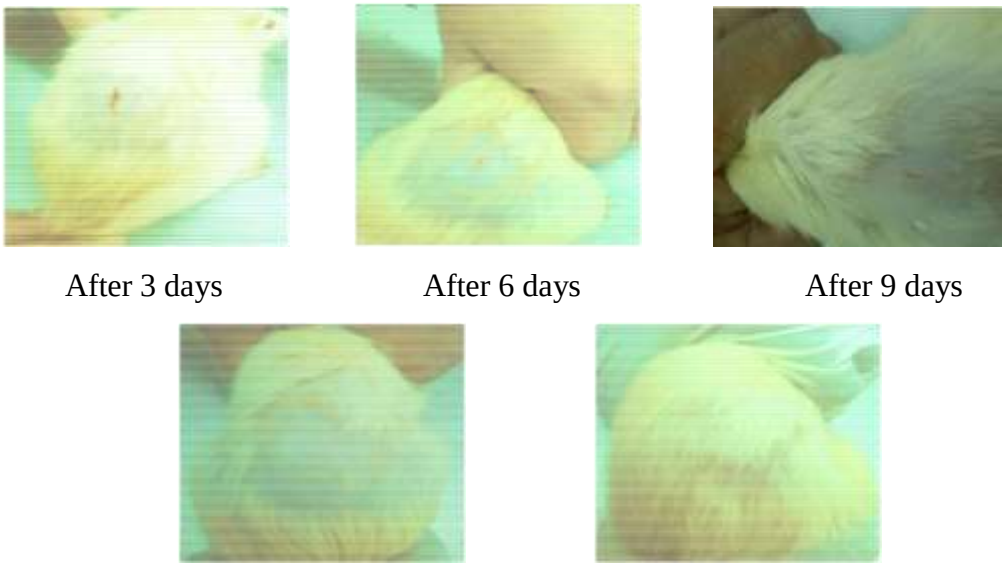

After 3 days After 6 days After 9 days

After 12 days After 15 days

Figure 4. Wound-healing progress after one time per day treated with skin incision wounded on Wistar rats

Conclusion

This research deals with the preparation and some physicomechanical properties of rice starch-chitosan blend films. Chitosan was prepared from shrimp-shells and yield percent was 69.03 %. Rice starch was extracted from rice grain was investigated. Yield percent of rice starch was 32.48 %. PVA-rice starch-chitosan films were prepared by varying the amount of chitosan, rice starch and PVA concentration were kept at 1 % and 2 % film made up of PVA-rice starch-chitosan with a ratio of 2: 1: 2 showed high tensile strength (7.1 MPa), high elongation at break (10 %) and the highest tear strength (37.8 kN/m). The addition of citric acid to PVA-rice starch-chitosan-glycerol-citric acid films decreased their tensile and tear strength, revealing the film (PSCGC II) with a 2:1:2:0.5:1 ratio with the highest tensile strength (6.6 MPa) and elongation at break (123 %). The PVA-rice starch-chitosan-glycerol-citric acid blend film showed potent antimicrobial activity on all tested microorganisms *vis., A. tumefaciens, B. pumilus, B. subtilis, C. albicans, E. coli, P. fluorescens, and S. aureus*. Furthermore, the biomedical application of the prepared film has better and faster wound healing activity on incision Wistar rats. From these results the PVA-rice starch-chitosan-glycerol-citric acid film ratio of 2: 1: 2: 0.5: 1 can be used as a wound healing agent.

Appendix-I

Yield of Extracted Rice Starch

$$\text{Yield \%} = \frac{\text{Weight of Rice Starch}}{\text{Weight of Rice Powder}} \times 100$$

Appendix-Ii

Determination of Physicomechanical Properties of Rice Starch-Chitosan-PVA Films

(a) Elongation (%) $= \frac{\Delta L}{\mathrm{L}} \times 100$

Where, ΔL = Difference in length

L = Original length

(b) Tensile strength$= \frac{(\text{load of break})}{\text{Original width} \times \text{original thickness}}$

(c) Tear strength $= \frac{F}{t}$

Where, F = Force (kN)

t = Specimen thickness (m)

Acknowledgements

The authors would like to express our profound gratitude to Myanmar Academy of Arts and Sciences. Our deepest gratitude is expressed to Rector and Pro-Reactor at University of Mandalay, and Dr Thinn Myat Nwe, Professor and Head, Department of Chemistry, University of Mandalay for their permission and suggestions for this research.

References

Brandelero, R. P. H., A. T. Alfaro, P. T. Marques, and E. M. Brandelero. (2019). "New Approach of Starch and Chitosan Films as Biodegradable Mulching" *Rev. Virtual Quim*,vol. 11(3), pp. 1-13.

Chiellini, E., A. Corti, D. Corti, S. Antone, and R. Solaro. (2003). "Biodegradation of Poly (vinyl alcohol) Based Material", *Progress in Polymer Science*, vol. 28, pp. 963-1014.

Choi, E-J., C-H. Kim, and J-K. Park. (1999). "Synthesis and Characterization of Starch-g-Polycaprolactone Copolymer", *Macromolecules*, vol. 32, pp. 7402-7408.

Hossain, M. S., and A. Iqbal. (2014). "Production and Characterization of Chitosan from Shrimp Waste", J. Bangladesh Agril. Univ, vol.12(1), pp. 153–160.

Kandile, N. G., H. T. Zaky, M. I. Mohamed, A. S. Nasr, and Y. G. Ali. (2018). "Extraction and Characterization of Chitosan from Shrimp Shells" *Open Journal of Organic Polymer Materials*, vol.8, pp. 33-42

Kornblum, S. S. and S.B. (1973). "A New Tablet Disintegrant Agent: Cross Linked Polyvinylpyrollidone.*J. Pharm. Sci*., vol. 62(1), pp.43-49.

Sharif, S.M, and K. Yamaura. (2002). "Preparation of Theophylline Hydrogels of Atactic Polyvinyl Alcohol /Alcohol /NaCl/H_2O System for Drug Delivery System" *Journal of Controlled Release* vol. 81(3), pp.367-377.

Tudorachi, N., C.N. Cascaval, M. Rusu, and M. Pruteanu. (2000)**.** "Testing of Polyvinyl Alcohol and Starch Mixtures as Biodegradable Polymeric Materials as Biodegradable Polymeric Materials", *Polymer Testing*, vol. 19, pp. 785-799.

Valgadde, P. S., V. Wankhade, and A. K. Sahoo. (2015). "Isolation of Starch from the Brokens of Sona Masuri Rice (Oryza Sativa L.)", *International Journal of Engineering Research & Technology* (IJERT), vol. 4(9), pp. 467-469.

PREPARATION AND CHARACTERIZATION OF CELLULOSE DIACETATE DERIVED MODIFIED MAGNETIC BIOCHAR FOR REMOVAL OF CHROMIUM(VI) IONS FROM AQUEOUS SOLUTION

May Thazin Kyaw[1], Aung Than Htwe[2]

Abstract

Biochar (BC) derived from peanut hulls is a potential low-cost adsorbent for metal ions and organic pollutants, but its practical application is still limited by the adsorption capacity. In this study, cellulose diacetate (CDA) was prepared from waste cigarette filters by solution casting method. A cellulose diacetate magnetic biochar (CDMBC) and cellulose diacetate biochar (CDBC) were synthesized through chemical co-precipitation, with cellulose diacetate from prepared magnetic biochar (MBC) and biochar (BC). The morphologies, surface chemical structures, and crystallinity of the prepared BC, MBC, CDBC and CDMBC were characterized by SEM, XRD, TG-DTA, and FT IR. The adsorption of Cr(VI) ions by using different biochars as adsorbents was investigated under different adsorption conditions. Batch experiments were conducted to investigate the effect of metal concentrations, adsorbent dosage, time and pH values on the adsorption of Cr(VI). The Freundlich and Langmuir isotherm models were utilized in the analysis of experimental results to determine the optimal fit for the adsorption process of Cr(VI). CDMBC biochar showed the highest removal efficiency of Cr(VI) ions, attributed to enhanced surface area, active sites, and improved magnetic properties. In this research, the cellulose diacetate derived magnetic biochar could be used to remove the Cr(VI) ions in the environmental pollution of Cr(VI) contaminated waste water.

Keywords: biochar, cellulose diacetate, magnetic biochar, isotherm models, adsorption

Introduction

The rapid development of modern industry, has caused most industrial wastewater to contain toxic metals or other ions that affect environmental pollution and endanger human health. Heavy metal ions such as copper, cadmium, chromium, lead and mercury ions are highly dangerous to human beings as well as the environment, even at low concentration levels in water. These heavy metal ions tend to accumulate in the tissues of living organisms, whether in plants or animals, and cause many problems such as inhibiting natural growth and changes in the structure and function of cells resulting in disease and even cell death. For this reason, the treatment of toxic heavy metal ion pollution in water has received and extensive concern (Cao *et al*., 2010).

Chromium is used in electroplating, leather, textile, and tanning industries, and these industries discharge chromium-rich effluents into the nearby waterbodies, thus contaminating the environment (Saravanan *et al*. 2017). In aqueous media, chromium exists in two forms: Cr (III) and Cr (VI). The oxidation number of chromium depends on the pH value of the aqueous medium, and changing the pH can change chromium from one form to another (Sharma *et al*. 2008).

[1] Department of Chemistry, University of Yangon
[2] Department of Chemistry, University of Yangon

The toxicity of chromium for humans is dependent on the exposure duration and dose, and it has been found that hexavalent chromium is more toxic than trivalent. Long-term exposure to chromium can damage the skin, eyes, blood, immune system, and respiratory system (Zhang *et al.* 2014). Chromium also damages DNA, creates oxidative stress, and can cause the development of tumors in the human body (Mishra *et al.* 2016). Various methods have been reported for the removal of chromium and various adsorbents have been employed for the elimination of heavy metals from wastewater (Wu *et al*, 2013).

The aim of this study is to prepare cellulose diacetate derived waste cigarette filters modified magnetic biochar for removal of Cr(VI) ions from aqueous solution. The prepared cellulose diacetate modified magnetic biochar were characterized using SEM, XRD, FTIR, TG-DTA and UV-Vis. The effect of loading samples, contact time, solution pH, adsorbent dosage, temperature and initial Cr(VI) concentration as well as the adsorption isotherm of Cr(VI) on prepared cellulose acetate modified magnetic biochar were investigated in batch experiments.

Materials and Methods

Waste cigarettes and peanut hulls were collected from domestic waste. Glycerol, and potassium dichromate were purchased from the British Drug House (BDH) Chemical Ltd, England. Chemicals such as glacial acetic acid, and ferric chloride were purchased from Merck, Indonesia. All of the chemicals used in this study were of analytical grade. In all investigations, the recommended standard methods and techniques involving both conventional and modern methods were used.

Preparation of Cellulose Diacetate (CDA)

The CDA were prepared via a solution casting method. Firstly, collected waste cigarette filters were washed with ethanol and hot water several times and then were dried at 60 °C. Secondly, the above waste cigarette filters were dissolved in glacial acetic acid at the ratio of 1:15 (w/w), and then were treated using an overhead stirrer for 4 h to form a homogeneous emulsion.

Synthesis of Biochar (BC) and Magnetic Biochar (MBC)

Peanut hulls were washed with water and dried in an oven at 70°C for 9 h. The purified peanut hull powder was placed in a crucible and heated at 250°C in the muffle furnace for 1h, followed by washing with 0.1 M sulphuric acid (H_2SO_4) to remove the ash powder and washing with distilled water. Finally, the neutralized char powder was dried in oven at 70°C for 24 h. The biochar sample obtained was coded as BC. For magnetic biochar (MBC), the grounded peanut hull was soaked in 2M ferric chloride ($FeCl_3$) solution 1:8 (w/v), and then treated using an overhead stirrer for 1 h with heat at 60°C for 30 min. The hot solution was filtered, and the residue was dried in an oven at 70°C for 24 h. The residue was washed with water several times, and then the residue was placed into the muffle furnace at 600°C for 2 h (Zhang and Mao, 2013). Figure 1 shows the diagram for preparation of biochar and magnetic biochar from peanut hull.

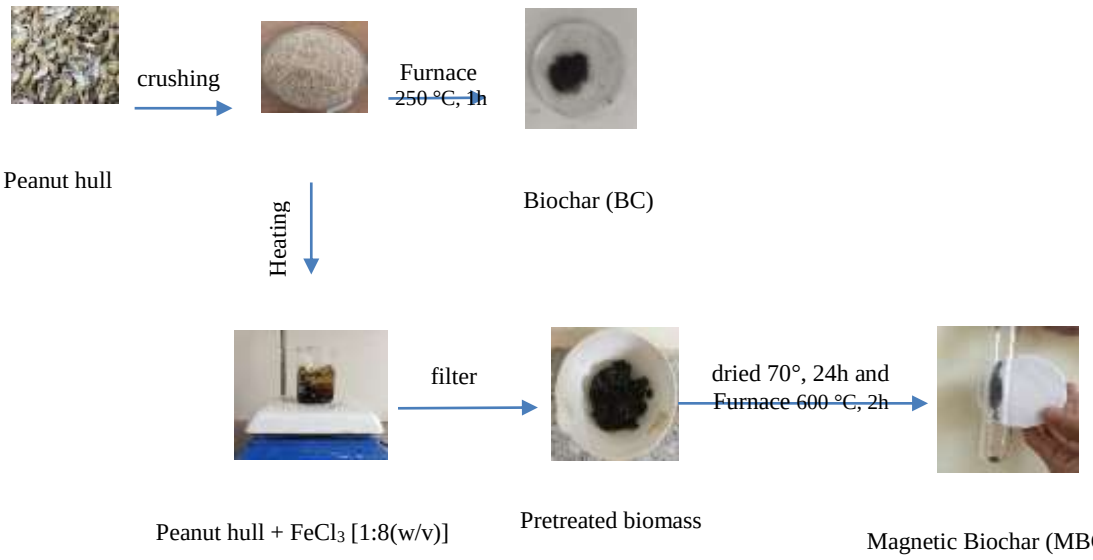

Figure 1. A diagram for preparation of biochar (BC) and magnetic biochar (MBC) from peanut hull

Synthesis of Cellulose Diacetate Coated Biochar (CDBC) and Magnetic Biochar (CDMBC)

Firstly, 1 g each of BC and MBC was mixed with the 3% cellulose diacetate (CDA) solution and stirred for 30 min to form a homogenous solution. Secondly, that solution was made into a bead by dropping it into 450 mL of 1M NaOH solution. And then the beads were placed in NaOH solution for overnight, filtered, and washed with ethanol followed by water. In the next step, the beads were dried in oven at 70°C for 2 h and ground with a motor and pestle. Figure 2 shows the preparation diagram of cellulose diacetate biochar (CDBC) and cellulose diacetate magnetic biochar (CDMBC) from peanut hull.

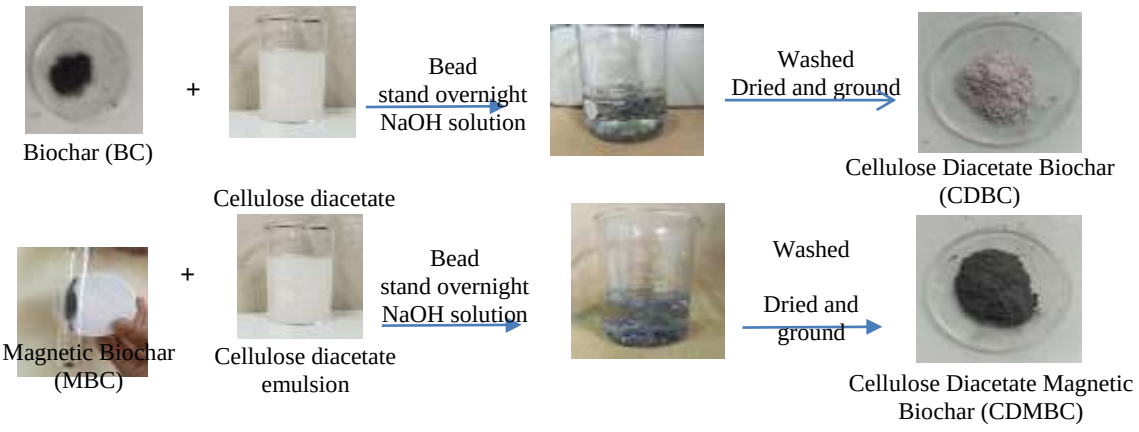

Figure 2. A diagram for preparation of cellulose diacetate biochar (CDBC) and cellulose diacetate magnetic biochar (CDMBC) from peanut hull

Characterization

The surface morphology of different biochars was studied using SEM (JOE-JSM-5610 LV model, Japan). SEM images of samples were collected under an accelerating voltage of 5 kV. Fourier transform infrared spectrophotometer (Shimadzu, Japan) was used. The resolution was 4 cm^{-1} with 64-time scanning, in the range of 4000–400 cm^{-1}. The X-ray diffraction (XRD) measurements of the different biochars were recorded using the Shimadzu 8000 X-ray diffractometer (Shimadzu, Japan) with a detector operating under a voltage of 40.0 kV and a current of 30.0 mA using Cu Kα radiation (λ = 0.15418 nm). The recorded range of 2θ was 5–40°, and the scanning speed was 6°/min. The thermal properties of different biochars were characterized by thermogravimetric analysis (TGA) on a thermogravimetric analyzer (Rigaku Thermoplus TG 8120) in the range of 30-600°C at a heating rate of 10°C min^{-1} under N_2 flow.

Batch Adsorption Experiment

Batch equilibrium tests were carried out for the adsorption of Cr^{6+} on different sample adsorbents. The samples (BC, CDBC, MBC, CDMBC) of certain doses were introduced into the 250 mL conical flasks containing 20 mL of Cr^{6+} solution of decided concentration and pH value, respectively (Ma *et al*. 2016). The flasks were then placed on a shaker and shaken with a stirring speed of 200 rpm for 2 h~~ours~~ until adsorption equilibrium was obtained. During the experiment, the initial pH 1 to 8 value of the solutions was adjusted by adding either 0.1 M HCl or 0.1 M NaOH solution before the adsorption experiment (Liu *et al*. 2010). The adsorption capacity q_e (mg/g) was calculated by Eq 1. (Chen *et al*. 2012), and the removal rate W (%) of heavy metals calculated from the following Eq. 2,

$$q_e = \frac{(C_i - C_e)V}{M} \quad (1)$$

$$\% \text{ removal (W)} = \frac{C_i - C_e}{C_i} \times 100\ \% \quad (2)$$

Where, C_i is the initial concentration of chromium ions and C_e is the equilibrium or final concentration of chromium ions, V is the volume of aqueous solution (mL), and M is the weight (g) of sample produced.

Results and Discussion

Scanning electron microscopy (SEM) Analysis

The surface morphology of the prepared BC, MBC, CDBC and CDMBC is shown in Figure 3. The SEM images in Figures 3(a) and (b) indicate that the structure of biochar (BC), possessed a more porous and rougher than that of MBC. In addition, a distinct change was found in the image of MBC which has small iron oxide particles loaded on the biochar surface. As seen in Figures 3(c) and (d), CDBC shows a flat-like structure, whereas CDMBC possesses more aggregate with small iron particles in the surface.

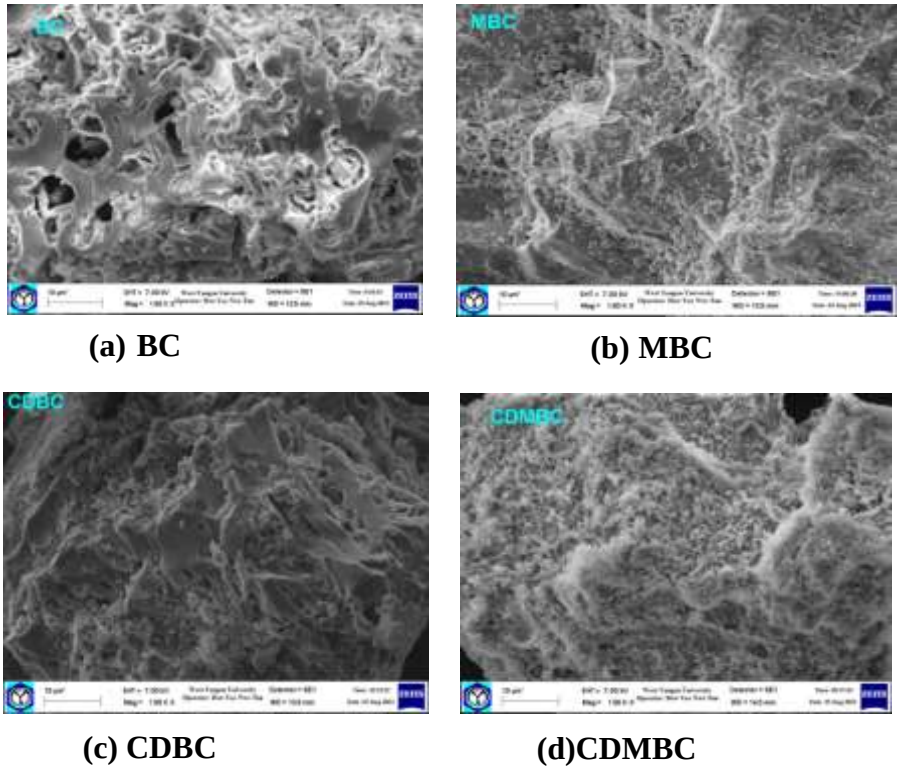

(a) BC **(b) MBC**

(c) CDBC **(d)CDMBC**

Figure 3. SEM images of (a)BC, (b) MBC, (c) CDBC, and (d) CDMBC

X-ray diffraction analysis

The XRD analysis of BC, MBC, CDBC, and CDMBC are shown in Figure 4. The diffractogram indicates the more or less amorphous by the blend with graphitization. If it is totally amorphous wood charcoal or biochar, the 2θ value will be about 20° and only a big hump will be observed. The diffractograms of all samples are observed to show the same pattern as each other. The graph indicates that BC and CDBC had a graphite crystal structure with the diffraction peaks at 21.85° and 23.45° In the XRD patterns of MBC and CDMBC, the new peaks appeared at 21.61° and 35.51° were assigned as γ-Fe_2O_3 and Fe_3O_4, respectively. These results further confirmed that iron oxide particles were successfully loaded onto cellulose diacetate and γ-Fe_2O_3 particle-containing biochar formed (Hong *et al.*, 2019). From the diffractograms, it was found that all samples show amorphous nature, which is supported to better sorption behavior for BC, MBC, CDBC, and CDMBC samples.

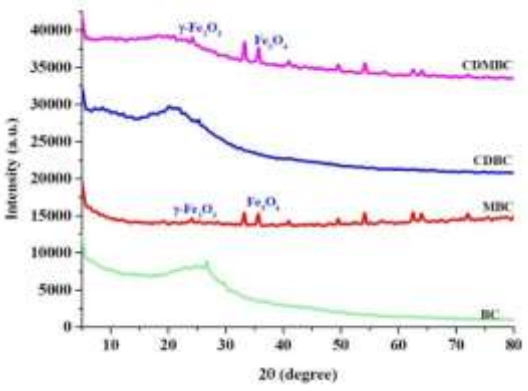

Figure 4. XRD diffratograms of (a)BC, (b) MBC, (c) CDBC, and (d) CDMBC

FT IR Spectroscopy

The FT IR spectra and spectroscopic assignment of BC, MBC, CDBC, and CDMBC are shown in Figure 5. The most characteristic peaks for CD are 3460 cm^{-1} corresponding to OH group, 2930 cm^{-1} attributed to asymmetric and symmetric C-H stretching, 1758 cm^{-1} due to carbonyl -C=O of COOR group, 1377 cm^{-1} resulted from methyl group and 1060 $cm^{-1}$for cyclic ether bonds (Gulec *et al.,* 2010). In addition, BC and MBC, a broad peak at approximately 3464 cm^{-1} were assigned the stretching of the O–H group. The peak around 1629 cm^{-1} was attributed to C=C stretching vibration of an aromatic ring. The characteristic bands at 1062 cm^{-1} involve the stretching vibration of C–O esters and ethers. The FT IR spectrum of MBC exhibited three new peaks at 2345 cm^{-1}, 2356 cm^{-1} and 2369 cm^{-1} in comparison with BC and CDBC. Moreover, the peaks at 1629 cm^{-1} became stronger, while the peak at 1062 cm^{-1} was weaker than that in BC. This is due to the effect of the iron presence in the surfaces of MBC and CDMBC. In MBC and CDMBC, there were new peaks at 495 cm^{-1}, 563 cm^{-1}, and 612 cm^{-1}, due to Fe–O, testifying to the formation of iron oxides (Fe_3O_4) (Hoang *et al*., 2019). These results further ascertained that iron was successfully loaded onto biochar and led to an increase in the amount of surface functional groups of MBC and CDMBC. These functional groups enhance adsorption through hydrogen bonding and complexation with metal ions (Tan *et al*., 2017). This can be an important factor to enhance the Cr(VI) adsorption onto MBC and CDMBC from aqueous solution.

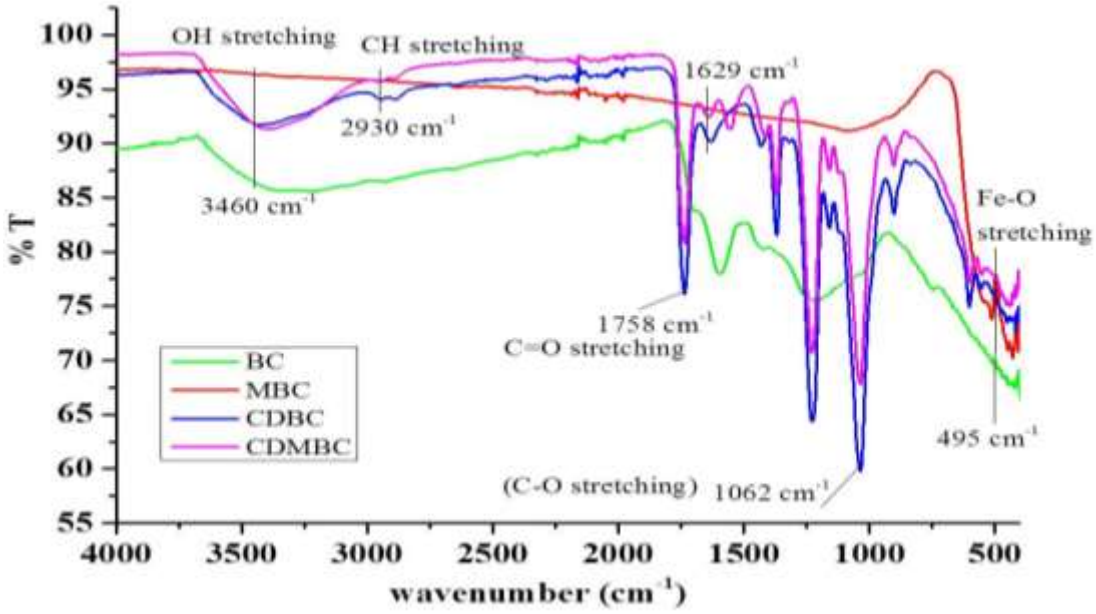

Figure 5. FT IR spectra of BC, CDBC, MBC, CDMBC

TG-DTA analysis

Thermogravimetric analysis was performed to evaluate the thermal stability of materials as well as to confirm the amount of BC, CDBC, MBC and CDMBC. The thermograms of BC, MBC, CDBC and CDMBC show the (a)thermogravimetry (TG) curves and (b) differential thermal analysis (DTA) curves (Figure 6). According to the TG thermogram profiles, BC showed three decomposition stages with weight loss of 10.83% at a temperature range of 38.86 °C to 280.97 °C, 29.68% at a temperature range of 280.97 °C to 433.02 °C, and 55.36% at a

temperature range of 433.02 °C to 600 °C, respectively. The process involves firstly the removal of water (endothermic peak at 78.4 °C) and light volatile components; secondly, the degradation of hemicellulose (exothermic peak at 338.7 °C); and lastly, the decomposition of lignin and cellulose (exothermic peak at 478.73 °C) in three stages. CDBC also showed three decomposition stages with weight losses of 7.22 %, 60.82 % and 29.39%, respectively. These stages were attributed to the loss of surface water followed by the combustion of polymer materials. CDMBC showed three decomposition stages with weight losses of 6.62%, 50.67% and 7.07%, respectively.

It can be seen that the mass losses at around 750 °C could be the reduction of magnetite Fe^{3+} to Fe^{2+} by the following reactions (1) and (2). Thus, it agrees with the observation of the Fe–O bond in the FTIR spectra.

$C_nH_nO \rightarrow$ C + volatiles (CO_x, H_2O, organics) (1)

$2Fe_3O_4 + C \rightarrow 6FeO + CO_2$ (2)

TGA results also demonstrated that the MBC exhibited more thermally stable than the original biochar. This is due to the activation effect during pyrolysis observed by adding the $FeCl_3$ to the biomass (Htwe *et al*., 2022).

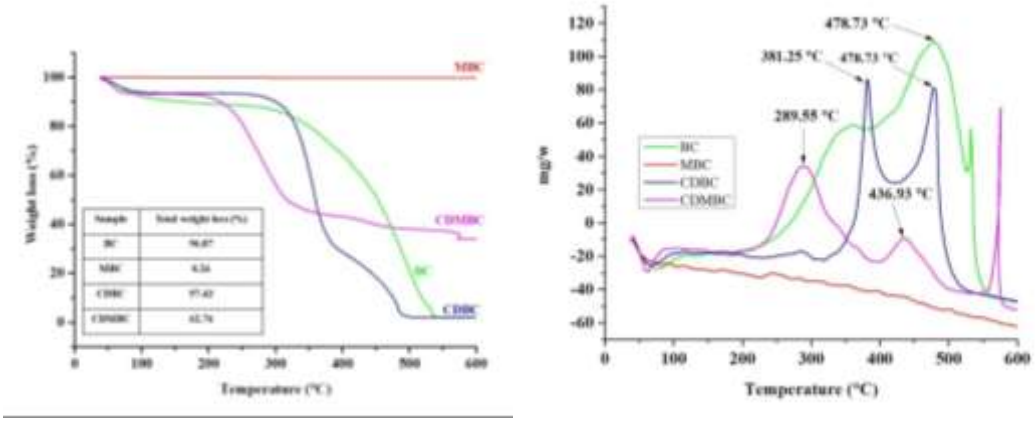

Figure 6. (a) TG curves and (b) DTA curves for BC, MBC, CDBC and CDMBC

UV-Vis absorption spectra

The UV-vis spectrum (Figure 7) of BC and MBC showed a single peak at around 216 nm. The CDBC and CDMBC peaks show at 227 nm. It was found that the intensity of BC and MBC is lower than that of CDBC and CDMBC. According to this figure, cellulose diacetate coated magnetic biochar change in the UV–vis spectra, and this confirms the binding of cellulose diacetate binding magnetic biochar.

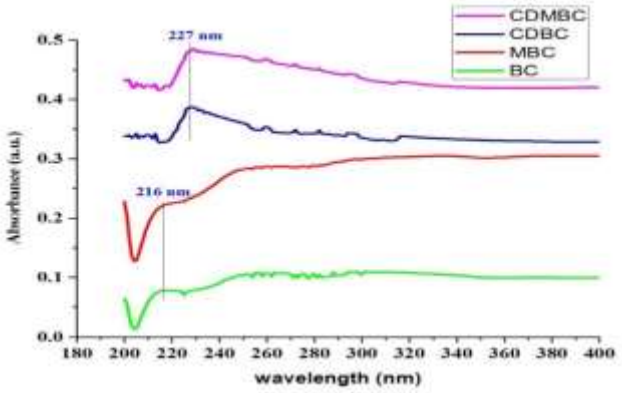

Figure 7. UV-vis spectra for BC, MBC, CDBC and CDMBC

Adsorption performances of Cr(VI) ion with BC, MBC, CDBC and CDMBC

Effect of solution pH

The pH plays a crucial role in the determination of the ionization degree and the surface properties of the adsorbents. The solution pH ranged from 3-8 for an initial metal ion concentration of 100 ppm, was determined by a UV-Visible spectrophotometer at 540 nm (Figure 8). At pH 5, the maximum removal efficiencies were observed, with CDMBC achieving the highest removal rate of 76.50%. Below pH 6, Cr(VI) exists as $HCrO^{4-}$ and $Cr_2O_7^{2-}$, which interact strongly with the positively charged adsorbent surface. As pH increases from 6 to 8, the OH–ions dominate, reducing adsorption due to competition for active sites and decreased surface protonation. Magnetic biochar (MBC) and cellulose diacetate magnetic biochar (CDMBC) consistently outperformed other samples, showcasing enhanced removal rates at acidic pH levels (Hoang *et al.*, 2019).

The higher efficiency of MBC and CDMBC is attributed to their increased surface functionality and charge density. These biochar demonstrated better performance across varying dosages (0.1–0.5 g), with adsorption efficiency slightly decreasing due to site saturation at higher dosages. The Cr(VI) adsorption mechanism involves the electrostatic attraction at lower pH and ion exchange at higher pH. These findings suggest that modified biochars are particularly effective for Cr(VI) removal, especially at lower pH levels where adsorption is more favorable. This highlights their potential for practical applications in treating Cr(VI)-contaminated water (Inyang *et al.*, 2012)..

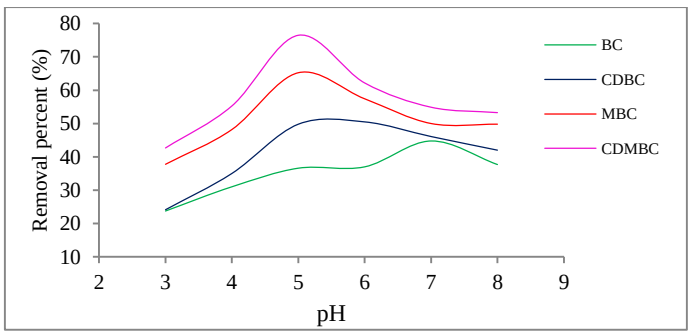

Figure 8. Effect of pH of BC, CDBC, MBC CDMBC on adsorption of Cr^{6+} ions (condition: dosage of 0.1 g; initial concentration of 100 ppm; volume of 25 mL, contact time of 3 h, temperature of 25 °C)

Effect of Initial Concentration of Cr^{6+} ion

The effect of initial concentration on the Cr(VI) removal by BC, MBC, CDBC and CDMBC is shown in Figure 9. The removal efficiency of 35.0 % found to be decreased with the initial concentration of Cr(VI) increasing from 100 to 500 mg/L. Apparently, an adsorbent with a certain mass had a limited number of active sites and these sites progressively approached saturation as the Cr(VI) concentration increased. Thus, the saturated adsorbent cannot adsorb more Cr(VI) ions, which resulted in a decrease in removal efficiency in high concentration of Cr(VI).

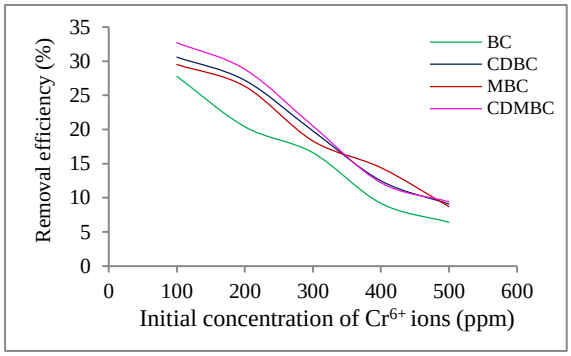

Figure 9. Effect of initial concentration of BC, CDBC, MBC CDMBC on adsorption of Cr^{6+} ions (condition: dosage of 0.1g; pH 5; volume of 25 mL, contact time of 3 h, temperature of 25 °C)

Effect of Dosage

This study, investigate the effect of adsorbent amount on 100 ppm Cr(VI) solution in varying adsorbent dosages (0.1-0.5 g) as shown in Figure 10. As the dosage increased, the removal efficiency improved particularly for BC and CDMBC, indicating that the availability of more adsorption sites facilitates enhanced the ions capture. However, beyond a certain dosage (0.3 g), the removal rate plateaued, due to the aggregation of biochar particles at higher dosages, reducing the effective surface area and active sites accessible for Cr(VI). CDMBC maintained a consistently higher removal efficiency, making it a cost-effective option for large-scale applications (Bandaru *et al*., 2013).

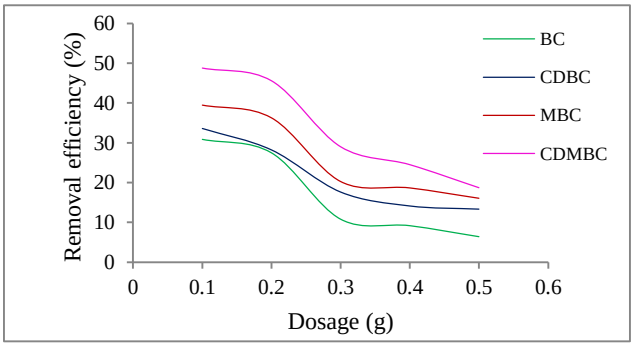

Figure 10. Effect of dosage of BC, CDBC, MBC CDMBC on adsorption of Cr^{6+} ions (condition: initial concentration 100 ppm; pH 5; volume of 25 mL, contact time of 3 h, temperature of 25 °C)

Effect of Time

This study investigated the effect of contact time on 100 ppm Cr (VI) solution at pH 5 with 0.1 g adsorbent for varying time intervals at temperature 25 °C (Figure 11). Rapid adsorption round about 33.2 % removal efficiency occurred in the first three hours and peaked for the majority of adsorbents, such as MBC and CDBC, as the contact period increased from one to five hours.

After 3 h, the adsorption process reaches equilibrium, with the removal rates either leveling off or decreasing, was observed in BC. This initial rapid adsorption can be attributed to the availability of abundant active sites on the adsorbents surface, facilitating quick Cr(VI) ion binding. The drop in removal efficiency for BC beyond 3 h may be due to desorption or competition between Cr (VI) ions and other ions present in the solution (Jain *et al*., 2010) Therefore, an optimal contact time of around 3 h is optimized for maximum Cr (VI) removal.

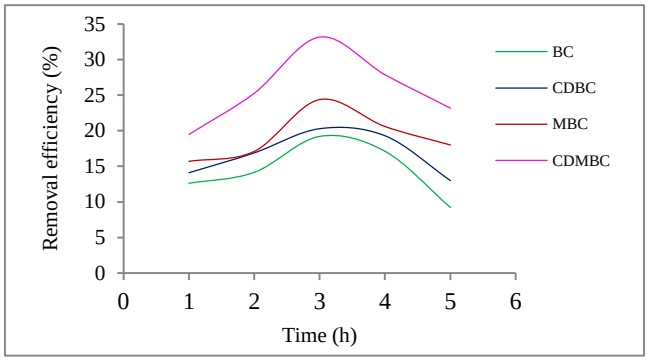

Figure 11. Effect of contact time of BC, CDBC, MBC CDMBC on adsorption of Cr^{6+} ions (condition: initial concentration 100 ppm; pH 5; volume of 25 mL, dosage of 0.1 g, temperature of 25 °C)

Effect of Temperature

The results indicate that the removal efficiency of Cr (VI) varies with temperature for all samples (Figure 12). For BC, the removal percentage peaks at 30 °C with approximately 99.3 % efficiency, then decreases slightly before increasing again at 40 °C. This suggests that higher temperatures enhance the kinetic energy of the ions, promoting interaction with the active adsorption sites on the biochar surfaces. In contrast, MBC and CDMBC exhibit more stable removal efficiencies across all temperature, suggesting that their adsorption processes are less temperature sensitive. The decreased removal rates at higher temperatures for CDBC, could be due to the weakening of physical adsorption forces and possible desorption of Cr (VI) ions (Foo and Hameed, 2010). Thus, 30 °C is optimal for the maximum removal efficiency of BC, while other adsorbents show more stability across the tested temperature range.

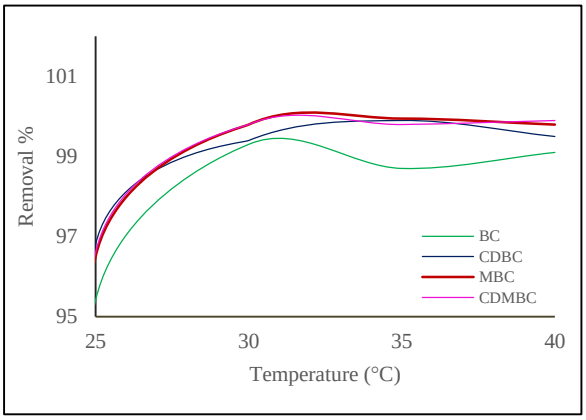

Figure 12. Effect of temperature of BC, CDBC, MBC CDMBC on adsorption of Cr^{6+} ions (condition: initial concentration 100 ppm; pH 5; volume of 25 mL, dosage of 0.1 g, contact time of 3 h)

Isotherm Modeling

The sorption isotherms were generated by varying the ratio of sorbate. Langmuir and Freundlich models were used to simulate the adsorption isotherms of Cr (VI) to the BC, CDBC, MBC and CDMBC.

Langmuir: $\frac{1}{q_e} = \frac{1}{q_m K_L C_e} + \frac{1}{q_m}$ (Langmuir, 1918)

Freundlish: $\log q_e = \log K_F + \frac{1}{n} \text{Log } C_e$ (Freundlish, 1906)

Where q_e is the amount of adsorbate adsorbed per unit mass of adsorbent at equilibrium (mg/g), C_e is the equilibrium concentration of the adsorbate in the solution (mg/L), q_m is the maximum adsorption capacity (mg/g), K_L is the Langmuir constant related to the affinity of the binding of the binding sites (L/g), K_F is the Freundlish constant, and n is the Freundlish constant indicative of the adsorption intensity or surface heterogeneity.

Table 1. Langmuir and Freundlish Isotherm Constants for Cr(VI) Adsorption onto BC, CDBC, MBC, CDMBC

Isotherm Model	Parameters	BC	CDBC	MBC	CDMBC
	q_m (mg/g)	83	23.26	8.93	2.13
Langmuir	K_L (L/g)	0.045	2.18	0.5	1.74
	R^2	0.98	0.89	0.81	0.88
	K_F	5.6	4.9	7.67	1.51
Freundlish	n	-5.32	-6.7	-5.46	-11.1
	R^2	0.88	0.85	0.86	0.94

Table 1 shows the Langmuir and Freundlish isotherm constants for Cr (VI) adsorption onto different biochar samples: BC, CDBC, MBC, and CDMBC. In the Langmuir model, the maximum adsorption capacity q_m is the highest for BC at 83 mg/g, indicating that it has the most adsorption sites available for Cr (VI). The q_m values for CDBC, MBC, and CDMBC are 23.6,

8,93, and 2.13 mg/g respectively. The Langmuir constant K_L is the highest for CDBC at 2.18 L/g, suggesting a strong affinity between Cr(VI) and the adsorption sites (Wang and Peng, 2010). The K_L values for BC, MBC and CDMBC are 0.045, 0.5 and 1.74 L/g respectively. The R^2 values close to 1 for all samples indicate that the Langmuir model fits the adsorption data well (Foo and Hameed, 2010). In the Freundlish isotherm model. the K_F value, indicative of adsorption capacity, is the highest for MBC (7.67) followed by BC (5.6), CDBC (4.9) and CDMBC (1.51). The negative (n) values suggest a non-ideal adsorption process, possibly due to heterogeneous surface conditions. The R^2 values for the Freundlish model also suggest a good fit to the experimental data (Yang, 2003). Overall, BC exhibits the highest adsorption capacity for Cr (VI), making it the most effective adsorbent among the samples tested. This suggests that the unmodified biochar sites is suitable for Cr(VI) adsorption compared to the modified versions.

Conclusion

This study demonstrated the synthesis and application of various biochars, including biochar (BC), magnetic biochar (MBC), cellulose diacetate biochar (CDBC), and cellulose diacetate magnetic biochar (CDMBC), for the adsorption of Cr (VI) ions from aqueous solutions. The characterization techniques such as SEM, XRD, FT IR, and TG DTA provided insights into the structural and chemical properties of the synthesized biochars. The adsorption experiments revealed that the removal efficiency of Cr (VI) ions was significantly influenced by parameters such as initial metal ion concentration, pH, and adsorbent dosage. Among the biochars studied, CDMBC exhibited the highest removal efficiency for Cr (VI) ions, particularly at lower pH levels and higher dosages. This performance can be attributed to the enhanced surface area, increased active sites, and improved magnetic properties provided by the cellulose diacetate coating and the magnetic modification. The maximum adsorption capacities (q_m) derived from the Langmuir isotherm model were the highest for BC, followed by CDBC, MBC, and CDMBC. The Langmuir constant (K_L) values suggested a strong affinity between Cr (VI) ions and the adsorption sites, particularly for CDBC. The Freundlich isotherm model also supported the high adsorption capacity and intensity, especially for MBC. The Langmuir and Freundlich isotherm models are in good agreement with the adsorption results of Cr (VI) ions onto the biochars.

Overall, this study highlights the potential of using waste-derived biochars, particularly CDMBC, as cost-effective and efficient adsorbents for the removal of toxic Cr(VI) ions from wastewater. These findings suggest that CDMBC could be a promising material for managing industrial effluents and protecting water resources from heavy metal contamination.

Acknowledgements

The authors owe their gratitude to Professor Dr. Ni Ni Than, Head of Department, Department of Chemistry, University of Yangon, Yangon, Myanmar, for her stimulating suggestion for MAAS.

References

Ahmad, M., S.S. Lee, X. Dou, D. Mohan, J.K. Sung, J.E. Yang, and Y.S. Ok. (2012). "Effects of Pyrolysis Temperature on Soy bean Stover-and Peanut Shell-derived Biochar Properties and TCE Adsorption in Water". *Bioresource Technology*, vol.118, pp.536-554.

Bandaru, N.M., N. Reta, H. Dalal, A.V. Ellis, J. Shapter and N.H. Voelcker. (2013). "Enhanced Adsorption of Mercury Ions on Thiol Derivatized Single Wall Carbon Nanotubes". *Journal of Hazardous Materials*, vol. 261, pp. 534-541.

Cao, J., Y. Tan, Y. Che, and H. Xin. (2010). "Novel Complex Gel Beads Composed of Hydrolyzed Polyacrylamide and Chitosan: An Effective Adsorbent for The Removal of Heavy Metal from Aqueous Solution". *Bioresource. Technol*, vol. 101, pp.2558-2561.

Chen, J. H., J.C. Ni, L.Q. Liu, and S.X. Li. (2012). "Adsorption Behavior of Cd (II) Ions on Humic Acid-Immobilized Sodium Alginate and Hydroxyethyl Cellulose Blending Porous Composite Membrane Adsorbent". *Desalination* vol.285(3), pp. 54-61.

Foo, K.Y. and B.H. Hameed. (2010). "Insights into the Modeling of Adsorption Isotherm Systems". *Chemical Engineering Journal*, vol.156 (1), pp.2-10.

Freundlish, H. (1906). "Over the Adsorption in Solution". *International Journal of Research in Physical Chemistry and Chemical Physics*,vol. 57, pp. 387-470.

Gulec H., A. Topacli, C.F. Topacli, N. Albayrak, and M. Mutlu. (2010). "Modification of Cellulose Acetate Membrane via Low-pressure Plasma Polymerization for Sugar Separation Applications: part I. Membrane Development and Characterization", *J. Membrane Sci.*, vol.350, pp. 310–321.

Hoang L. P., H. T. Van, L. H. Nguyen, D. Mac, T. T. Vu, L. T. Ha and X. C. Nguyen. (2019). "Removal of Cr(VI) from Aqueous Solution using Magnetic Modified Biochar Derived from Raw Corncob", *New J. Chem.*, vol.43, pp.18663-18672

Htwe, A.T., M.T.M. Maung, and Z. Naing. (2022). "Synthesis of Chitosan-coated Magnetite Nanoparticles using Co-precipitation Method for Copper (II) ions Removal in Aqueous Solution". *World Journal of Engineering*, vol. 19 (5), pp.726-734

Inyang, M., B. Gao, Y. Yao. Y. Xue, A. R. Zimmerman, P. Pullammanappallil and X, Cao. (2012). "Removal of Heavy Metals from Aqueous Solution by Biochars Derived from Anaerobically Digested Biomass". *Bioresource Technology*, vol.110, pp. 50-56.

Jain, M., V.K. Garg, and K. Kadirvelu. (2010). "Chromium Removal from Aqueous System using Helianthus Annuus (Sunflower) Stem Waste". *Journal of Hazardous Materials*. vol. 173 (1-3). pp. 448-454.

Langmuir, I. (1918). "The Adsorption of Gases on Plane Surfaces of Glass, Mica and Platinum". *J. Am. Chem. Soc*, vol.40, pp. 1361-1403.

Lin, S.H., R.S. Jaung. (2009). "Adsorption of Phenol and Its Derivatives from Water using Synthetic Resins and Low-Cost Natural Adsorbents". *J. Environ. Manag*. vol.90, pp. 1336-1349.

Liu, J., Y. Ma, T. Xu, and G. Shao. (2010). "Preparation of Zwitterionic Hybrid Polymer and Its Application for the Removal of Heavy Metal Ions from Water". *J. Hazard. Mater*. vol.**178** (1-3), pp. 1021-1029.

Mishra, S., T.N. Toxic. (2016). "Genotoxic Effects of Hexavalent Chromium in Environment and its Bioremediation Strategies". *J. Environ. Sci. Health Part C,*vol. 34, pp.1-32.

Mohan, D., C.U. Pittman, and P.H. Steele. (2006). "Pyrolysis of Wood/Biomass for Bio-oil: a Critical Review". *Energy and Fuels*, vol.20 (3), pp. 848-889.

Wu, Y., H. H. Wang, C. Zhang, J. Zhang and Z. L. Zhang. (2013). "Adsorption of Hexavalent Chromium from Aqueous Solutions by Graphene Modified with Cetytrimethylammonium Bromide". *J. Colloid Interface Sci.*, vol. 394, pp. 183-191.

Saravanan, R., P.S. Kumar, and M. Yashwanthraj. (2017). "Sequestration of Cr (VI) ions from Industrial Wastewater using Waste Biomass: A review". *Desalination Water Treat.* vol.68, pp. 245-266.

Sari, A., and M. Tuzen. (2009). "Biosorption of Pb (II) and Ni (II) from Aqueous Solution by Lichen (Cladonia frucata) Biomass." *Biochemical Engineering Journal*. vol.**42** (3) pp. 194-201.

Sharma, S. K., B. Petrusevski, and G. Amy. (2008). "Chromium Removal from Water: A Review". *J. Water Supply Res. Technol. AQUA* vol. 57, pp. 541-553.

Tan, X. F., S. B. Liu, Y. G. Liu, Y. L. Gu, G. M. Zeng, X. J. Hu, X. Wang, S. H. Liu and L. H. Jiang. (2017) "Biochar as Potential Sustainable Precursors for Activated Carbon Production: Multiple Applications in Environmental Protection and Energy Storage". *Bioresource Technology*, vol. 227, pp. 359-372

Wang, S. and Y. Peng. (2010). "Natural Zeolites as Effective Adsorbents in Water and Wastewater Treatment". *Chemical Engineering Journal*, vol.156 (1), pp. 11-24.

Yang, R. T. (2003) *Adsorbents: Fundamentals and Applications*. Hoboken, John Wiley and Sons.

Zhang, R., Y. Xiang, Q. Ran, X. Deng, Y. Xiao, L. Xiang, and Z. Li. (2014). "Involvement of Calcium, Reactive Oxygen Species, and ATP in Hexavalent Chromium-Induced Damage in Red Blood Cells". *Cells. Phsysial, Biochem*, vol.**34**, pp. 1780-1791.

Zhang, W., and S. Mao. (2013). "Pb (II) and Cr (VI) Sorption by Biochar Pyrolyzed from The Municipal Wastewater Sludge Under Different Beating Conditions". *Bioresource. Technol*. vol 147, pp.545-552.

INFLUENCE OF PLANT LEAF EXTRACTS ON THE STRUCTURAL AND BIOLOGICAL PROPERTIES OF SYNTHESIZED MAGNESIUM OXIDE NANOPARTICLES

Thu Zin Tun[1], Ye Myint Aung[2],Yee Mun Than[3]

Abstract

This research investigates the impact of different leaf extracts on the characteristics (such as morphology, size, and crystallinity) and biological activities (including antidiabetic, antioxidant, anti-inflammatory, and antacid effects) of magnesium oxide nanoparticles. The green synthesis of MgO NPs was performed using aqueous leaf extracts from *Oroxylum indicum* and *Moringa oleifera* as eco-friendly stabilizing agents. The synthesized MgO NPs underwent characterization through various techniques, including X-ray diffraction (XRD), Fourier transform infrared spectroscopy (FTIR), UV-visible spectroscopy (UV-Vis), scanning electron microscopy with energy-dispersive X-ray analysis (SEM-EDX), and thermogravimetric analysis (TG-DTA) to assess their structural, morphological, and thermal properties. Biological studies assessed antioxidant activity using the DPPH radical scavenging method, while anti-inflammatory, anti-diabetic, and acid-neutralizing activities were evaluated through egg albumin denaturation, α-amylase inhibition, and back titration methods, respectively. Results showed that both *Oroxylum indicum* and *Moringa oleifera* extracts produced MgO NPs with excellent structural and biological properties, but significant differences were noted between the two. This study highlights the critical role that the choice of plant extracts plays in green synthesis, significantly impacting the structural and biological properties of the nanoparticles.

Keywords: MgO NPs, *Oroxylum indicum* and *Moringa oleifera*, green synthesis, structural and biological properties

Introduction

Nanotechnology has emerged as a transformative field in modern science, leveraging materials at the nanoscale to develop innovative solutions across various domains, including medicine, electronics, and environmental science. Among the various nanomaterials, magnesium oxide nanoparticles (MgO NPs) have garnered significant attention due to their unique structural, optical, and biological properties. These nanoparticles are known for their antibacterial, antifungal, and antioxidant activities, making them promising candidates for biomedical applications (Karthikeyan *et al.*, 2020). The traditional methods of synthesizing MgO NPs often involve chemical reagents that may pose environmental and health risks. In contrast, green synthesis offers a more sustainable approach, utilizing plant extracts as reducing and stabilizing agents. This method not only minimizes toxic by-products but also harnesses the natural properties of phytochemicals present in plant materials (Parveen *et al.*, 2019). Two plants that have shown potential for this purpose are *Oroxylum indicum* and *Moringa oleifera*, both renowned for their medicinal properties and rich phytochemical compositions. *Oroxylum indicum*, commonly known as the trumpet tree, is noted for its diverse therapeutic applications, including anti-inflammatory and antimicrobial effects (Singh *et al.*, 2017). Meanwhile, *Moringa oleifera*, often referred to as the "drumstick tree," is celebrated for its nutritional and medicinal benefits, with various studies highlighting its antioxidant and antibacterial activities. This research aims to compare the structural and biological properties of MgO NPs synthesized via

[1] Department of Chemistry, University of Yangon
[2] Department of Chemistry, University of Yangon
[3] Department of Chemistry, University of Yangon

green methods using leaf extracts of *Oroxylum indicum* and *Moringa oleifera*. By analyzing the differences in nanoparticle characteristics, including size, morphology, and biological efficacy, this study seeks to elucidate the potential of these plant extracts in enhancing the green synthesis of MgO NPs. These insights could lead to the creation of eco-friendly nanomaterials with improved structural and functional properties.

Materials and Methods

Materials

The leaves of *Oroxylum indicum* and *Moringa oleifera* used in this study were sourced from naturally growing plants. Commercial magnesium sulphate heptahydrate (Epsom salt) served as the precursor for the synthesis. The freshly collected leaves were cleaned, air-dried for 2–3 weeks, ground into a fine powder, and stored in air-tight container. For the synthesis process, 5 g of the dried powder from each plant were weighed and mixed separately with 100 mL of distilled water. These mixtures were heated to 60 °C for 30 minutes while stirring to ensure uniformity. Once heated, the solutions were cooled and filtered through Whatman No. 1 filter paper, with the resulting filtrates collected separately. These filtrates were subsequently utilized for the synthesis of magnesium oxide nanoparticles.

(i) (ii)

Figure 1. Photographs of (i) Moringa oleifera and (ii) Oroxylum indicum leaves

Preparation of magnesium oxide nanoparticles via different leaf extracts

Magnesium oxide nanoparticles were synthesized using aqueous extracts from *Oroxylum indicum* and *Moringa oleifera* leaf powders. During the process, 100 mL of the leaf extract solutions were gradually added dropwise to a 0.2 M solution of $MgSO_4 \cdot 7H_2O$ (200 mL) while stirring at 600 rpm. After thorough mixing, 2 M NaOH was introduced dropwise to bring the pH to around 10, and the mixtures were maintained at 90°C for 3 hours. These precipitates were separated via centrifugation at 7500 rpm for 20 minutes at room temperature, then washed three times with distilled water and once with ethanol. The precipitates were dried to remove any remaining moisture and ethanol, ground into powder using a mortar and pestle, and then calcined at temperatures of 600 °C for *both plant leaf* extracts, each for 5 hours.

Characterization

The formation of green-synthesized MgO nanoparticles was confirmed using a UV-visible spectrophotometer (UV-1800, Shimadzu). Their diffraction patterns, crystalline structure, and purity were analyzed with an X-ray diffractometer (MultiFlex 2kW, Rigaku, D/max 2200, Japan; D8 Advance X-ray Diffractometer, Bruker, Jermany). The morphology and elemental composition of the MgO nanoparticles were examined through scanning electron microscopy

(SEM) coupled with energy-dispersive X-ray analysis (SEM-EDX) (JSM-6701F/JED 2300, JEOL, Japan). A Fourier transform infrared (FT IR) spectrometer (PerkinElmer, Spectrum Two) was used to identify the functional groups present in the MgO nanoparticles. Raman spectroscopy (PerkinElmer) was employed for crystallinity and phase identification, complementing the XRD findings. Finally, the thermal stability of the MgO nanoparticles was assessed using a TG-DTA thermal analyzer (DTG-60H, SHIMADZU, Japan).

Determination of antioxidant activity

The antioxidant activity of the synthesized MgO nanoparticles has been evaluated using the DPPH (2,2-diphenyl-1-picrylhydrazyl) radical scavenging assay, a widely used method to assess antioxidant properties by measuring a substance's ability to neutralize free radicals with a UV-visible spectrophotometer. A sample solution was prepared by mixing 1.5 mL of 20 µM DPPH solution with 1.5 mL of MgO nanoparticle solution (ranging from 125 to 1.95 µg/mL) in a methanol and DMSO mixture. The solution was vigorously mixed and kept in the dark for 30 minutes before measuring its absorbance at 517 nm against a blank. Control absorbance was measured without the test samples, and the radical scavenging activity was calculated using the expressed formula:

$$\% \text{ RSA} = \frac{A_{\text{Control}} - (A_{\text{Sample}} - A_{\text{Blank}})}{A_{\text{Control}}} \times 100$$

Determination of anti-inflammatory activity

The inhibitory activity of the test samples on egg albumin denaturation was utilized to investigate the potential mechanisms behind the anti-inflammatory effects of MgO nanoparticles using UV-visible spectrophotometry (Naveed ***et al.,*** **2022**). This method measures the ability of a compound to inhibit protein denaturation, an indicator of anti-inflammatory potential, as protein denaturation is a process linked to inflammatory conditions. To prepare the sample solution, 400 µL of the test sample was mixed with 300 µL of egg albumin solution in separate test tubes. The reaction mixture's pH was adjusted to 6.4 with sodium phosphate buffer (2.9 mL). To induce denaturation of the egg albumin, the mixture was incubated at room temperature for 20 minutes and then heated in a water bath at 65–70 °C for 15 minutes. After cooling, the absorbance was measured at 660 nm, using a solution without test samples as the control and the radical scavenging activity was calculated using the expressed formula:

$$\% \text{ inhibition} = \frac{A_{\text{Control}} - A_{\text{Sample}}}{A_{\text{Control}}} \times 100$$

Determination of antidiabetic activity

The anti-diabetic activity of MgO nanoparticles was evaluated through an α-amylase inhibition assay, a standard assay for assessing the potential of compounds to reduce carbohydrate breakdown, which can help manage blood glucose levels, using a UV-visible spectrophotometer with slightly modified to previous studies. In separate test tubes, 1 mL of the sample solution and 1 mL of α-amylase solution were mixed to prepare different concentrations (ranging from 125 to 1.95 µg/mL). The reaction mixture was adjusted to pH 6.9 with 1 mL of sodium phosphate buffer and incubated at room temperature for 10 minutes to enhance α-amylase inhibitory activity. Afterward, 400 µL of 1% starch solution was added, followed by

another 10-minute incubation at room temperature. Next, 500 µL of DNSA reagent was added, and the mixture was heated in a water bath at 85–90°C for 10 minutes. Once cooled, the absorbance was measured at 540 nm. A control reading without test samples was also taken for comparison and the radical scavenging activity was calculated using the expressed formula:

$$\% \text{ inhibition} = \frac{A_{Control} - A_{Sample}}{A_{Control}} \times 100$$

Determination of acid neutralizing activity

The acid-neutralizing activity of magnesium oxide nanoparticles synthesized from *Moringa oleifera* and *Oroxylum indicum* leaf extracts was assessed using a back titration method. In the procedure, 20 mL of standardized hydrochloric acid (HCl) was added to a 250 mL Erlenmeyer flask, followed by 1 mL of the MgO NP sample solution. After mixing, three drops of phenolphthalein indicator were added, and the mixture was titrated with standardized sodium hydroxide (NaOH) until a pink color appeared. This titration was repeated three times, and the average titre volume of NaOH needed to neutralize the excess HCl was recorded. The experiment was conducted for various concentrations of MgO NPs and compared with a standard antacid drug, Siloxogene. The moles of excess HCl neutralized by each sample were calculated and expressed in milliequivalents (mEq). The acid-neutralizing capacity (ANC) was then computed using a specific formula, along with the ANC per dose of the test substances (Ramadan and Turk, 2023).

$$\text{ANC (mEq)} = (V_{HCl} \times N_{HCl}) - (V_{NaOH} \times N_{NaOH}) \quad \ldots\ldots. (1)$$

$$\text{ANC (mEq/g)} = \frac{\text{ANC (mEq)}}{\text{dose of test sample}} \quad \ldots\ldots. (2)$$

Where, mEq represents the milliequivalents of acid consumed; N_{HCl} is the normality of HCl; N_{NaOH} is the normality of NaOH;V_{HCl} is the volume of HCl used; V_{NaOH} is the volume of NaOH used.

Results and Discussion

Green synthesis of magnesium oxide nanoparticles

Magnesium oxide nanoparticles (MgO NPs) were synthesized from commercial Epsom salt ($MgSO_4 \cdot 7H_2O$) using phytochemicals present in *Oroxylum indicum* and *Moringa oleifera* leaf extracts as reducing and stabilizing agents. The resulting MgO NPs appeared white, powdery, crystalline, and insoluble in water, as confirmed by characterization techniques (Figure 2).

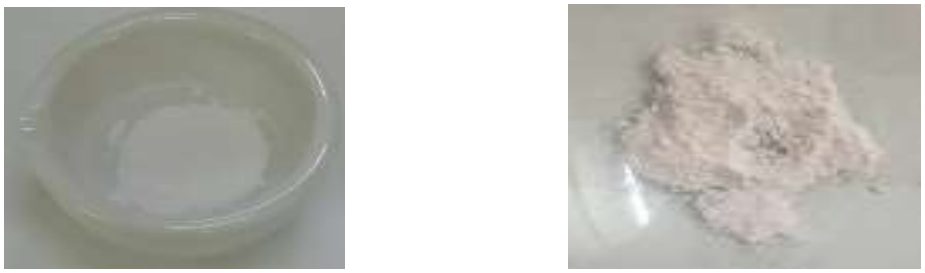

(i) (ii)

Figure 2. Magnesium oxide nanoparticles synthesized from aqueous leaf extracts of (i) Moringa oleifera and (ii) Oroxylum indicum

Characteristic analysis of synthesized MgO NPs

X-ray diffraction analysis

X-ray diffraction (XRD) analysis was employed to assess the crystalline structure and phase purity of magnesium oxide nanoparticles synthesized from *Moringa oleifera* and *Oroxylum indicum* leaf extracts (Figure 3). Both *Moringa oleifera* and *Oroxylum indicum* derived MgO NPs exhibited XRD peaks corresponding to the typical crystal planes 111, 200, 222, 311, and 222 of the MgO cubic rock-salt structure (JCPDS = 071-1176 and 01-075-0447). Lattice parameters for MgO NPs synthesized using *Moringa oleifera* extract are (a = b = c = 4.217 Å), while for MgO NPs synthesized using *Oroxylum indicum* extract, they are slightly shorter at (a = b = c = 4.213 Å). This minor variation in lattice parameters may be due to differences in organic stabilization layers imparted by each plant extract. Both lattice systems have axial angles of $\alpha = \beta = \gamma = 90°$, confirming a cubic crystal structure. MgO NPs synthesized using *Moringa oleifera* extract have a smaller crystallite size, averaging 10.39 nm, while MgO NPs synthesized using *Oroxylum indicum* extract have a larger average crystallite size of 14.03 nm. A smaller crystallite size increases surface energy, which leads to a higher surface area. This difference in crystallite sizes may influence properties like reactivity and stability, particularly beneficial in applications requiring high surface interaction, such as catalysis, coatings and sensors. While both extracts successfully produce MgO with a cubic structure, differences in crystallite sizes and lattice parameters demonstrated the different effects of each plant source on the nano structure.

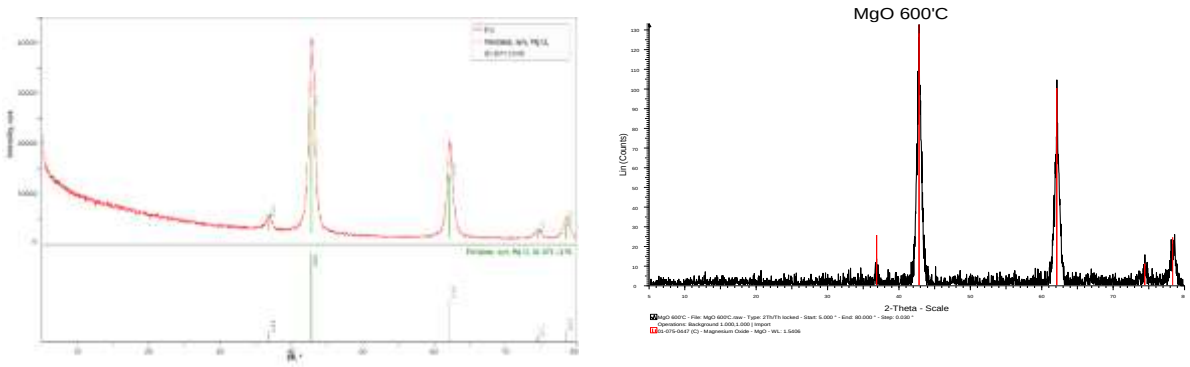

(i) **(ii)**

Figure 3. XRD patterns of MgO NPs using aqueous leaf extracts of (i) *Moringa oleifera* and (ii) *Oroxylum indicum* at 600 °C

SEM-EDX analysis

Scanning electron microscopy (SEM) and energy dispersive X-ray spectroscopy (EDX) were used to analyze magnesium oxide nanoparticles synthesized from *Moringa oleifera* and *Oroxylum indicum* leaf extracts, focusing on their morphology and elemental composition. SEM analysis revealed that MgO NPs synthesized using both plant leaf extracts–were primarily spherical and uniform (Figures 4 and 5). The nanoparticles exhibited some degree of agglomeration due to magnetic and van der Waals interactions, which may slightly reduce their surface area. However, this aggregation is unlikely to significantly affect their activity in certain applications.

The elemental mass ratio for *Moringa oleifera* based MgO NPs was found to be Mg = 47.65% and O = 50.43%, yielding an approximate Mg: O = 1:1, which closely matches the

stoichiometric composition expected for MgO. In its ideal stoichiometric condition, MgO NPs have a perfect face-centered cubic (FCC) structure with each magnesium ion being surrounded by six oxygen ions. This configuration results in a highly symmetric, well-ordered crystal lattice with an optimal lattice constant. In this configuration, the lattice parameter remains stable due to the highly symmetric and well-ordered crystal structure, with no significant lattice distortions. This ratio suggests a high purity level of MgO formation with minimal interference from impurities. The carbon content was measured at 1.92%, likely from the organic compounds present in the *Moringa oleifera* leaf extract, which may remain on the nanoparticle surface as a thin layer, potentially stabilizing the particles and contributing to their uniform morphology.

For MgO NPs synthesized using *Oroxylum indicum* extract, the elemental mass ratio was found to be Mg = 63.01% and O = 30.07%, resulting in an approximate Mg:O ratio of 2:1. This deviation from the standard 1:1 Mg:O ratio could be due to variations in synthesis conditions or differences in the binding and reduction capabilities of the Oroxylum indicum extract. The presence of non-stoichiometric conditions may influence Mg-O-Mg bonding, leading to deviations in the crystal structure. This indicates an excess of magnesium in the crystal lattice, as some magnesium ions may occupy interstitial sites or create clusters rather than participating in the ideal cubic lattice structure. This can result in a deviation from a purely cubic structure, as excess magnesium atoms may occupy interstitial sites or form clusters, leading to local structural variations. Despite the non-stoichiometric conditions, the overall structure can still be categorized as cubic. The higher carbon content of 6.92% may be attributed to residual organic compounds in *Oroxylum indicum* leaf extract that were not fully decomposed, potentially forming a carbonaceous layer on the nanoparticle surface (Sharma and Kumar 2020; Gupta and Sharmar, 2022).

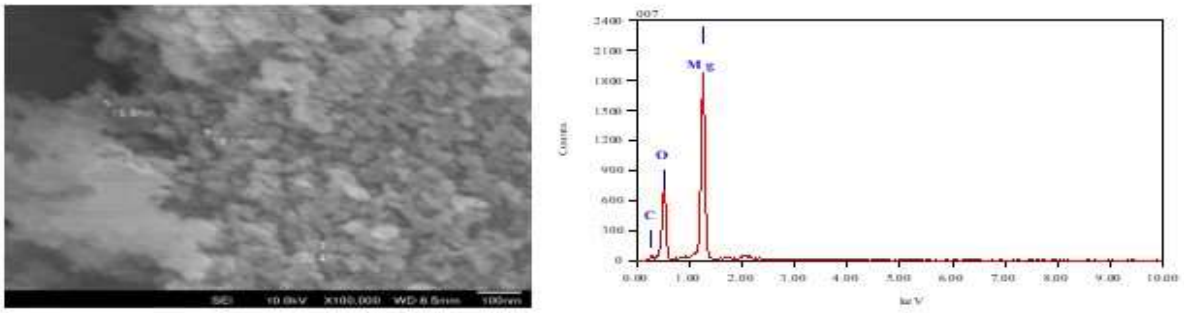

Figure 4. SEM-EDX image of MgO NPs using aqueous leaf extract of *Moringa oleifera*

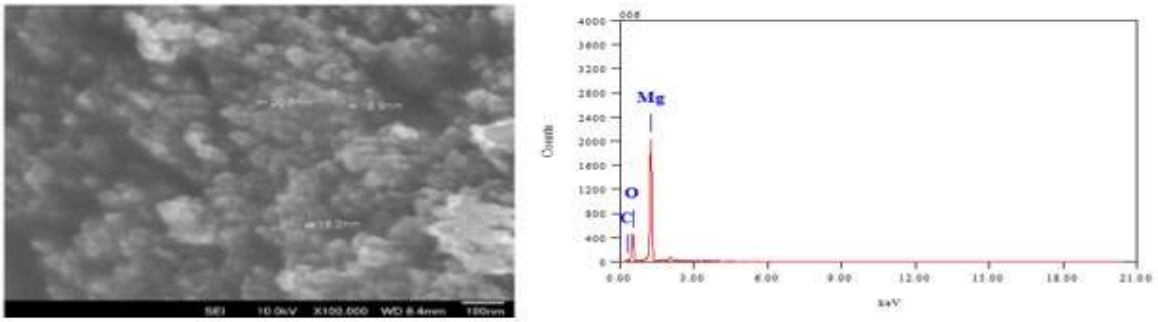

Figure 5. SEM-EDX image of MgO NPs using aqueous leaf extract of *Oroxylum indicum*

FT IR spectroscopic analysis

Fourier Transform Infrared (FT-IR) spectroscopy analysis of magnesium oxide nanoparticles synthesized from *Moringa oleifera* and *Oroxylum indicum* leaf extracts revealed the presence of various functional groups and chemical bonds on their surfaces, indicating successful capping and stabilization by phytochemicals from the extracts. For MgO NPs synthesized using *Moringa oleifera* extract, peaks at 1437, 1090, 861, and 683 cm^{-1} indicated the presence of organic compounds, which may act as stabilizing agents, influencing size and morphology (Figure 6a). The peaks at 861 and 683 cm^{-1} correspond to Mg-O vibrations, confirming the formation of MgO nanoparticles. The peak at 1437 cm^{-1} is associated with C–H bending vibrations, indicating the presence of organic compounds from the *Moringa oleifera* leaf extract which may contribute to nanoparticle stabilization. The peak at 1090 cm^{-1} correspond to C-O stretching, indicating the presence of phytochemicals from the plant extract on the MgO surface which may enhance stability and surface reactivity. In contrast, the FTIR spectrum for MgO NPs synthesized using *Oroxylum indicum* extract showed the peaks at 1439, 1107 and 860 cm^{-1} (Figure 6b). The peak at 1439 and 1107 cm^{-1}, similar to those observed in *Moringa oleifera*, correspond to C–H bending and C-O stretching vibrations. This indicates the presence of organic compounds from the *Oroxylum indicum* extract, which may contribute to the stabilization of MgO NPs. The peak at 846 cm^{-1} correspond to Mg-O bond vibrations, confirming the formation of MgO nanoparticles. The more complex FT IR pattern observed in *Moringa oleifera* based MgO NPs suggests a thicker organic layer, which may influence surface interactions and enhance nanoparticle reactivity (Verma and Soni, 2021; Patel and Mehta, 2022).

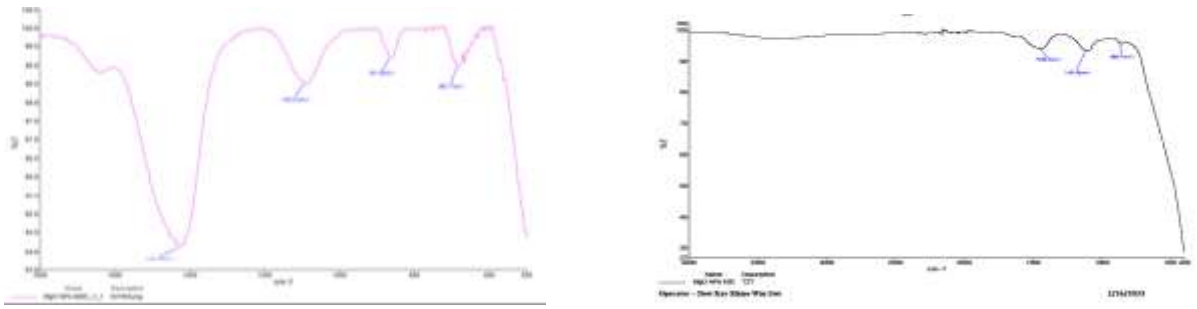

(a) (b)

Figure 6. FT IR spectra of MgO NPs using aqueous leaf extracts of (a) *Moringa oleifera* and (b) *Oroxylum indicum*

Raman spectroscopic analysis

Raman spectroscopy is a powerful analytical technique used to study molecular vibrations, crystal structures, and material properties. The Raman analysis of MgO nanoparticles synthesized using *Moringa oleifera* and *Oroxylum indicum* leaf extracts revealed the distinct vibrational modes that reflect the surface chemistry and stability of the NPs. MgO nanoparticles exhibit a Raman active vibrational mode with major Raman bands of 447 $cm^{-1,}$ 850 cm^{-1}, 1084 cm^{-1},1495 cm^{-1}, 1923 cm^{-1}, and 2322 cm^{-1} (Meenakshi *et al.*, 2012). For MgO NPs synthesized using *Moringa oleifera* extract, Raman peaks at 1497 and 1930 cm^{-1} correspond to C=C stretching of aromatic compounds or unsaturated bonds and C-H bending vibrations, suggesting interactions between the MgO matrix and organic residues from the *Moringa oleifera* extract,

which could stabilize the particles. MgO NPs synthesized using *Oroxylum indicum* extract show modes at 866 and 1495 cm^{-1}. The 866 cm^{-1} peak is typically associated with ~~of~~ vibrational mode of metal oxides. This peak may reflect lattice vibrations specific to MgO. The 1495 cm^{-1} peak closely matches that observed in *Moringa oleifera* based NPs, suggesting the presence of aromatic compounds in both plant extracts, which likely contribute to the stabilization of the MgO NPs. Variations in peak frequencies between the two extracts indicate that each plant's phytochemicals create different surface environments on the MgO NPs, possibly indicating the presence of varied stabilization mechanisms or interactions between ~~the~~ MgO and the bioactive compounds in these plant extracts (Bhatnagar *et al.,* 2021; Kumar *et al.,* 2018).

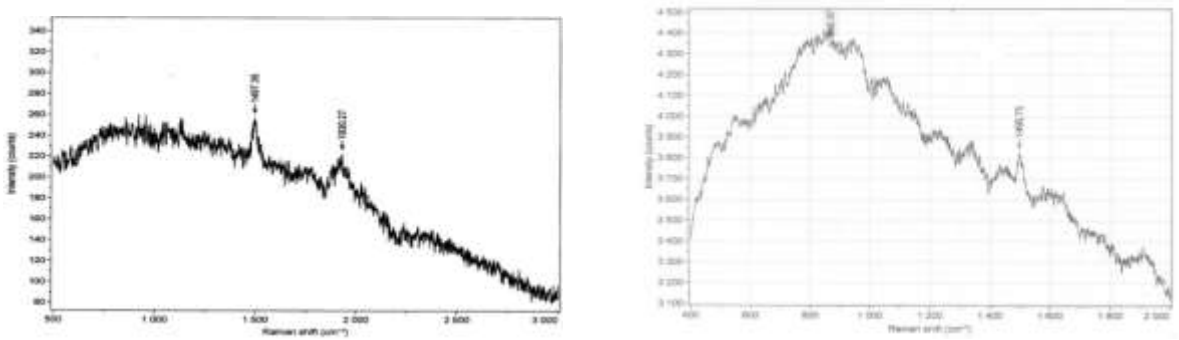

(a) (b)

Figure 7. Raman spectr*a* of MgO NPs using aqueous leaf extracts of (a) *Moringa oleifera* and (b) *Oroxylum indicum*

UV-visible spectroscopic analysis

Generally, green-synthesized MgO-NPs exhibit UV-visible absorption peaks typically ranging from 217 nm to 328 nm **(**Proniewicz *et al.,* 2024; Saidi *et al.,* 2023). Variations within this range are primarily due to differences in synthesis methods, particle sizes, and the nature of the biological reducing agents used. The UV-visible spectra of magnesium oxide nanoparticles synthesized using *Moringa oleifera* and *Oroxylum indicum* leaf extracts display a maximum absorption peak at 261 nm (Figure 8a and 8b). This characteristic peak is consistent with the typical UV absorption of MgO nanoparticles, indicating the successful synthesis and stability of these particles. The fact that both MgO NPs using *M. oleifera* and *O. indicum* leaf extracts show the same absorption peak suggests that the plant extracts did not significantly alter the electronic properties of the MgO core. This consistency implies that while the extracts act as capping agents, they do not alter the intrinsic optical characteristics of the MgO, making these NPs potentially suitable for various applications in catalysis and biomedicine. The plant-derived organic compounds likely surround the NPs but do not interfere with the MgO crystal structure, maintaining the characteristic UV absorption (Rao and Gupta, 2022).

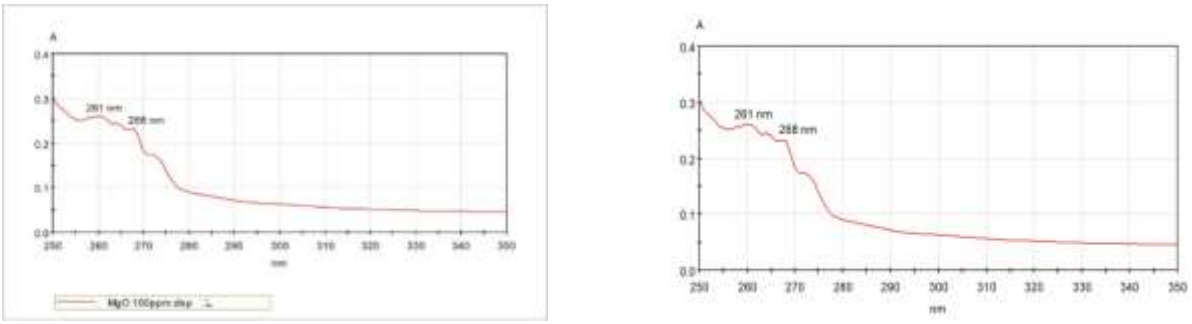

(a) (b)

Figure 8. UV-visible spectra of MgO NPs using aqueous leaf extracts of (a) *Moringa oleifera* and (b) *Oroxylum indicum*

TG-DTA thermographic analysis

Thermogravimetric analysis (TG) and differential thermal analysis (DTA) was employed to assess the thermal stability, decomposition behavior, and phase changes of MgO NPs synthesized from *Moringa oleifera* and *Oroxylum indicum* leaf extracts. In both thermographs of MgO NPs of two extracts, the TG curve indicates a 22.853% and 24.119% weight loss from 38.90°C to 600.97°C, attributed to moisture evaporation, volatile organic compounds, precursor decomposition. For MgO NPs synthesized using *Moringa oleifera* extract, DTA showed exothermic peaks at 174 °C and 280 °C, indicating energy release during the oxidation or decomposition of organic materials associated with the NPs. This dual peak pattern reflects the multi-step decomposition of lighter and heavier organic compounds in *Moringa oleifera.* The endothermic peak at 379.19 °C and 386.67°C for MgO NPs of both extracts confirmed the breakdown of organic stabilizers, leading to thermally stable crystalline MgO formation after 400 °C**.** Studies have shown that biosynthesized MgO nanoparticles exhibit high thermal stability, and their decomposition behavior depends on the nature of the stabilizing agents used during synthesis (Shanmugavel *et al.*, 2020; Yadav *et al.*, 2019, Kaviya *et al.*, 2011; Singh *et al.*, 2013).

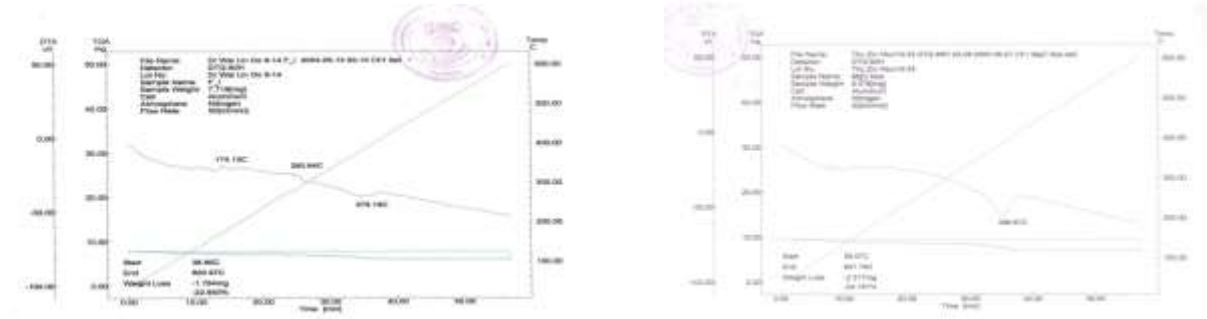

(a) (b)

Figure 9. TG-DTA thermograph*s* of MgO NPs using aqueous leaf extracts of (a) *Moringa oleifera* and (b) *Oroxylum indicum*

In vitro assessment of the biological properties of synthesized MgO NPs via *Moringa oleifera* and *Oroxylum indicum* leaf extracts

The unique phytochemicals in various plant extracts, including phenolics, flavonoids, alkaloids, terpenoids, and proteins, play a crucial role in the reduction, growth, and stabilization of green-synthesized nanoparticles. These bioactive compounds act as natural reducing, stabilizing, and capping agents, affecting the NPs' size, shape, surface charge, and stability, which in turn determine their biological activities. This study investigated the antioxidant, antidiabetic, anti-inflammatory, and acid-neutralizing properties of MgO NPs synthesized with *Moringa oleifera* and *Oroxylum indicum* leaf extracts. Antioxidant, antidiabetic, and anti-inflammatory activities are measured by IC_{50} values (lower IC_{50} indicates higher activity), while acid neutralizing activity is measured in mEq/g.

Antioxidant activity

The IC_{50} of ascorbic acid in this assay was 1.90 μg/mL, which is notably higher than the MgO NPs synthesized with either *Moringa oleifera* (1.21 μg/mL) or *Oroxylum indicum* (1.16 μg/mL), representing in Table 1. This finding indicates that both green-synthesized MgO NPs exhibit superior antioxidant activity compared to standard ascorbic acid. This superior effectiveness is probably due to the combined action of MgO NPs with plant-derived antioxidant compounds, enhancing ROS-scavenging activity more than pure ascorbic acid. MgO NPs synthesized with *Oroxylum indicum* leaf extract exhibited the strongest antioxidant activity, with an IC_{50} of 1.16 μg/mL, likely due to the high phenolic and flavonoid content known for their ROS-scavenging properties. The MgO NPs synthesized with *Moringa oleifera* leaf extract show slightly lower antioxidant activity, which may be due to lower concentrations or less potent radical-scavenging bioactive compounds in the extract.

Antidiabetic activity

The IC_{50} of the standard antidiabetic drug metformin was 3.79 μg/mL, indicating that it is a more potent α-amylase inhibitor than MgO NPs synthesized with *Moringa oleifera* (5.54 μg/mL) and *Oroxylum indicum* (4.78 μg/mL), representing in Table 2. The slightly lower inhibition of the MgO NPs from *Moringa oleifera* compared to those synthesized with ~~from~~ *Oroxylum indicum* may be attributed to differences in phytochemical ~~content~~ composition and the potency of specific compounds. Despite this, both types of MgO NPs exhibit notable antidiabetic activity, with inhibition levels approaching that of metformin. This suggests that these green-synthesized MgO NPs may serve as natural alternatives for antidiabetic therapy, particularly when used in conjunction with other treatments.

Anti-inflammatory activity

The IC_{50} value for diclofenac sodium, a standard anti-inflammatory drug, was 6.77 μg/mL, which is higher than the values for MgO NPs synthesized from *Moringa oleifera* (4.47 μg/mL) and *Oroxylum indicum* (4.48 μg/mL) leaf extracts, indicating stronger anti-inflammatory effects of the plant-based NPs, in Table 3. The enhanced anti-inflammatory activity may be attributed to the presence of bioactive compounds in the plant extracts, including flavonoids, isothiocyanates, eugenol, ursolic acid, and phenolic acids, which are known for their potent anti-inflammatory properties. The synergistic action between these phytochemicals and MgO NPs likely contributes to the observed improvement in activity. This enhanced effect is likely due to

the combined anti-inflammatory action of the MgO NPs and the phytochemicals present in both plant extracts.

Acid neutralizing activity

The acid-neutralizing capacity of the standard antacid drug Siloxogene is 20.2 mEq/g, which is lower than that of green-synthesized MgO NPs from *Moringa oleifera* (22.54 mEq/g) and *Oroxylum indicum* (22.06 mEq/g) leaf extracts. This approach evaluates acid-neutralizing capacity in milliequivalents per gram (mEq/g), with higher values indicating stronger neutralization capabilities. The superior acid-neutralizing ability of these MgO NPs may be attributed to their nanoscale structure and the stabilizing properties provided by plant-derived compounds, which enhance surface reactivity and dispersion in acidic environments. While MgO NPs synthesized from *Oroxylum indicum* have slightly lower capacity than those from *Moringa oleifera*, they still demonstrate significant potential as effective antacid agents (Varghese and Das, 2022).

Table 1. Antioxidant Activity (% Inhibition) and IC_{50} Values of Synthesized MgO NPs with Standard Ascorbic Acid

Samples	**% Radical Scavenging Activity (±SD)**							**IC_{50} µg/mL**
	62.5 µg/mL	**31.25 µg/mL**	**15.63 µg/mL**	**7.81 µg/mL**	**3.91 µg/mL**	**1.95 µg/mL**	**0.98 µg/mL**	
Ascorbic acid	75.74 ± 0.001	75.51 ± 0.000	75.28 ± 0.001	75.06 ± 0.002	72.79 ± 0.001	50.11 ± 0.002	47.85 ± 0.002	1.90
MgO NPs (*M.oleifera*)	69.37 ± 0.002	54.83 ± 0.001	53.11 ± 0.001	52.78 ± 0.002	51.85 ± 0.001	51.05 ± 0.003	49.67 ± 0.002	1.21
MgO NPs (*O.indicum*)	68.78 ± 0.003	59.66 ± 0.002	54.23 ± 0.001	52.64 ± 0.002	51.65 ± 0.001	51.19 ± 0.003	49.73 ± 0.003	1.16

Table 2. Antidiabetic Activity (% Inhibition) and IC_{50} Values of Synthesized MgO NPs with Standard Metformin Drug

Samples	**% α-amylase Inhibition Activity (±SD)**							**IC_{50} µg/mL**
	125 µg/mL	**62.5 µg/mL**	**31.25 µg/mL**	**15.625 µg/mL**	**7.8125 µg/mL**	**3.91 µg/mL**	**1.95 µg/mL**	
Metformin drug	59.94 ± 0.000	59.09 ± 0.000	58.81 ± 0.000	57.39 ± 0.000	52.27 ± 0.001	50.28 ± 0.001	45.74 ± 0.001	3.79
MgO NPs (*M.oleifera*)	61.36 ± 0.001	61.08 ± 0.001	59.94 ± 0.000	57.67 ± 0.001	51.99 ± 0.002	48.58 ± 0.001	40.34 ± 0.003	5.54
MgO NPs (*O.indicum*)	59.09 ± 0.001	55.97 ± 0.000	55.40 ± 0.001	52.84 ± 0.000	51.99 ± 0.001	49.43 ± 0.001	42.80 ± 0.000	4.78

Table 3. Anti-inflammatory Activity (% Inhibition) and IC_{50} Values of Synthesized MgO NPs with Standard Diclofenac Sodium Drug

Samples	% Inhibition of Albumin Denaturation Activity (±SD)							IC_{50} µg/mL
	125 µg/mL	62.5 µg/mL	31.25 µg/mL	15.625 µg/mL	7.8125 µg/mL	3.91 µg/mL	1.95 µg/mL	
Diclofenac sodium drug	84.39 ± 0.001	83.84 ± 0.002	81.91 ± 0.001	76.68 ± 0.002	56.20 ± 0.001	33.06 ± 0.001	10.56 ± 0.003	6.77
MgO NPs (*M.oleifera*)	88.43 ± 0.001	87.60 ± 0.001	83.38 ± 0.001	77.59 ± 0.003	71.72 ± 0.004	46.37 ± 0.002	35.28 ± 0.006	4.47
MgO NPs (*O.indicum*)	88.07 ± 0.002	86.24 ± 0.001	84.39 ± 0.001	81.65 ± 0.001	68.81 ± 0.003	46.19 ± 0.002	34.25 ± 0.002	4.48

Table 4. Acid Neutralizing Capacity of Synthesized MgO NPs with Standard Siloxogene Antacid Drug

Sample	Milliequivalent per gram of antacid activity (mEq/g) (±SD)
Siloxogene	20.20 ± 0.173
MgO NPs (*M. oleifera*)	22.54 ± 0.153
MgO NPs (*O. indicum*)	22.06 ± 0.200

Conclusion

Green-synthesized MgO nanoparticles using *Moringa oleifera* and *Oroxylum indicum* extracts exhibit promising antioxidant, antidiabetic, anti-inflammatory, and acid-neutralizing activities, with *Oroxylum indicum* based NPs showing slightly higher efficacy, likely due to its richer phytochemical profile. SEM-EDX and FTIR analyses revealed that the choice of plant extracts influence nanoparticle's morphology, elemental composition, and surface chemistry, with *Moringa oleifera* showing more complex interactions. TG-DTA results show that MgO NPs synthesized from *Moringa oleifera* decompose in multiple stages, while MgO NPs synthesized from *Oroxylum indicum* undergo a more direct decomposition, indicating fewer organic residues. XRD analysis confirmed that both MgO NPs retained a cubic crystal structure, with slight differences in crystallite size (10.39 nm for *Moringa oleifera* and 14.03 nm for *Oroxylum indicum*), affecting their surface area, reactivity, and stability. Notably, *Moringa oleifera*-based MgO NPs exhibited a more ideal face-centered cubic structure, potentially enhancing their capping efficiency and surface interactions. This study highlighted the role of plant extracts in enhancing NP properties without altering MgO's intrinsic optical characteristics, making them viable for biomedical and catalytic applications. While the study suggests that *Moringa oleifera*-based MgO NPs interact more effectively as capping agents, further research is needed to

confirm this conclusively. These differences concluded how plant extracts influence the crystallinity, morphology, composition, and potential applications of MgO NPs.

Acknowledgements

The authors would like to express their profound gratitude to the Myanmar Academy of Arts and Science for giving permission to submit this paper and to Professor and Head, Dr Ni Ni Than, Department of Chemistry, University of Yangon, for her kind encouragement. Special thanks to the Department of Chemistry, University of Yangon for providing the research and analytical instrument.

References

Bhatnagar, S., Raghav, S., & Saxena, A. (2021). "Synthesis and characterization of magnesium oxide nanoparticles using *Moringa oleifera* leaf extract: An eco-friendly approach". *Materials Today: Proceedings*, vol. 45, pp. 6882-6886.

Gupta, A., & Sharma, L. (2022). "Morphological and elemental analysis of green-synthesized MgO nanoparticles using SEM-EDX". *Materials Science Advances*, vol. 7 (1), pp. 34–41.

Karthikeyan, S., Kumar, S. P., & Kumar, R. S. (2020). Green synthesis of magnesium oxide nanoparticles using plant extracts: A review. *Journal of Environmental Chemical Engineering*, vol. 8 (5), pp. 104-143.

Kaviya, S., *et al*. (2011). "Green synthesis of silver nanoparticles using *Moringa oleifera* leaf extract and its antimicrobial activity". *Spectrochimica Acta Part A: Molecular and Biomolecular Spectroscopy*, vol. 79 (5), pp. 1251-1255.

Meenakshi, S. D., M. Rajarajan, S. Rajendran, Z. R. Kennedy, and G. Brindha (2012), "Synthesis and characterization of magnesium oxide nanoparticles", *Elixir Nanotechnology, vol.* **50, pp.** 10618-10620

Naveed, M., H. Batool, S. U. Rheman, A. Javed, S. I. Makhdoom, T. Aziz, A. A. Mohamed, M. Y. Sameeh, M. W. Alruways, A. S. Dablool, A. A. Almalki, A. S. Almari, and M. Alhomrani. (2022). "Characterization and evaluation of the antioxidant, antidiabetic, anti-inflammatory, and cytotoxic activities of silver nanoparticles synthesized using *Brachychiton populneus* leaf extract". *Processes*, vol. 10 (1521), pp. 1-18.

Parveen, F., Arooj, M., & Shahid, M. (2019). Green synthesis of magnesium oxide nanoparticles using plant extracts: A review. *Journal of Nanobiotechnology*, vol. 17 (1), pp. 47.

Patel, D., & Mehta, S. (2022). "Comparison of surface functional groups on MgO nanoparticles synthesized using different plant extracts". *International Journal of Nanoscience and Nanotechnology*, vol. 15 (1), pp. 40–52.

Proniewicz, E., A. M. Vijayan, O. Surma, A. Szkudlarek, M. Molenda. (2024). "Plant-Assisted Green Synthesis of MgO Nanoparticles as a Sustainable Material for Bone Regeneration: Spectroscopic Properties". International Journal of Molecular Science, vol. 25 (4242), pp. 1-20.

Ramadan, M., and S. Turk. (2023). "Assessment of the acid neutralizing capacity and other properties of antacid formulations marketed in the Gaza Strip". *Israa University Journal of Applied Science*, vol. 6 (2), pp. 97-110.

Rao, A., & Gupta, L. (2022). "*Analysis of UV-visible spectra in bio-synthesized metal oxide nanoparticles: Case study of MgO"*. *International Journal of Advanced Nanoscience*, vol.20 (2), pp. 23–30.

Saidi, N., S. M., K. J. Ying, H. M. Yusoff, and N. Badar. (2023). "Synthesis and Characterization of Magnesium Oxide Nanoparticles by Using Banana Peel (*Musa acuminata* Cavendish) Extract". *Malaysian Journal of Analytical Sciences*, vol. 27 (5), pp. 1017–1034.

Singh, G., Singh, R., & Bansal, M. (2017). Medicinal potential of *Oroxylum indicum*: A review. *Journal of Herbal Medicine*, vol. 9, pp. 7-12.

Singh, M., *et al*. (2013). "Nanoparticle characterization and application: An overview". *International Research Journal of Pharmacy*, vol. 4 (4), pp. 11-15.

Varghese, T., & Das, S. (2022). "Antacid efficacy of green-synthesized MgO nanoparticles compared with conventional antacids". *Journal of Biomedical Nanotechnology*, vol. 8 (1), pp. 45–53.

Verma, P., & Soni, R. (2021). "Functional group analysis of MgO nanoparticles synthesized using *Moringa oleifera* and *Ocimum indicum* extracts by FTIR spectroscopy". *Journal of Green Chemistry*, vol. 13 (2), pp. 113–119.

Suggested Questions Based on the Study

1. Questions on Green Synthesis and Phytochemical Influence

- How do the phytochemical compositions of *Moringa oleifera* and *Oroxylum indicum* influence the synthesis of MgO nanoparticles?
- Why do MgO NPs synthesized using *Oroxylum indicum* extracts show slightly higher efficacy in bioactivities?
- What role do plant extracts play in determining the morphology and elemental composition of MgO NPs?
- How does the choice of plant extract affect the surface chemistry of the synthesized MgO NPs?

2. Questions on Structural and Thermal Properties

- What are the key differences in the decomposition patterns of MgO NPs synthesized from *Moringa oleifera* and *Oroxylum indicum* based on TG-DTA analysis?
- How does the crystallite size variation (10.39 nm for *Moringa oleifera* and 14.03 nm for *Oroxylum indicum*) impact the surface area, reactivity, and stability of the nanoparticles?
- Why do MgO NPs synthesized from *Moringa oleifera* exhibit a more ideal face-centered cubic (FCC) structure?
- What are the implications of organic residue differences between the two synthesized MgO NPs?

3. Questions on Functional and Biomedical Applications

- How do the antioxidant, antidiabetic, anti-inflammatory, and acid-neutralizing activities of MgO NPs compare between the two plant-based synthesis methods?
- Why are MgO NPs considered promising for biomedical and catalytic applications?
- How does the capping efficiency of *Moringa oleifera*-based MgO NPs affect their stability and interactions?

4. Questions on Future Research and Optimization

- What further studies are needed to confirm the capping efficiency of *Moringa oleifera*-based MgO NPs?
- How can the synthesis process be optimized to maximize the beneficial properties of MgO NPs?
- What potential improvements could be made to enhance the stability and bioactivity of the synthesized MgO nanoparticles?

These questions can guide discussions and future research directions. Let me know if you need more specific ones!

ISOLATION, PARTIAL PURIFICATION, AND CHARACTERIZATION OF ALKALINE PROTEASE ENZYME FROM SOYBEAN AND ITS APPLICATION

Ei Pa Pa Zaw[1], Jue Jue Khin[2], Ye Myint Aung[3]

Abstract

This study focuses on the isolation, purification, and characterization of alkaline protease enzyme (EC 3.4.21.63) from soybean. The enzyme was extracted using a Tris base buffer solution and purified through 30–60% ammonium sulfate precipitation followed by gel filtration chromatography on a Sephadex G-100 column. The purification process achieved a 3-fold increase in purity with a protein recovery rate of 5.8%. Qualitative confirmation of the enzyme was demonstrated using a ninhydrin test, while the enzyme activity was quantified at 2734.96 EU/g. Characterization of the enzyme revealed an optimum pH of 9.0 and an optimum temperature of 55 °C. Enzyme kinetics were studied, yielding an activation energy (E_a) of 4.553 kcal/mol, a Michaelis constant (K_m) of 0.67×10^{-2} g/mL, and a maximum velocity (V_{max}) of 60.97×10^{-3} mM/min using Lineweaver-Burk plot. The reaction order was determined to be first-order. The enzyme exhibited pH stability and thermostability under tested conditions. Finally, the potential application of the crude alkaline protease enzyme in the detergent industry was evaluated, showing its effectiveness as a laundry detergent additive. These findings highlight its practical utility in industrial applications, particularly in environmentally friendly cleaning formulations.

Keywords: Soybean, alkaline protease enzyme, *gel filtration chromatography,* K_m, V_{max}, laundry detergent additive

Introduction

Enzymes are proteins that help speed up metabolism, or the chemical reactions in our bodies. They build some substances and break others down. All living things have enzymes. They can also be extracted from cells and then used to catalyze a wide range of commercially important processes. Proteases, also known as proteinases or proteolytic enzymes, are a large group of enzymes that catalyze the hydrolysis of peptide bonds in proteins and polypeptides (Rao *et al*., 1998). Proteases may be classified into acidic, neutral, and alkaline (basic) proteases according to the optimal pH. The proteases with pH optima in the range of 2.0-5.0 are called acid proteases; proteases having pH optima around 7.0 are neutral proteases, and alkaline proteases have pH optima in the range of 8.0-11.0. Neutral and alkaline proteases have a great application potential in the enzyme detergent and leather industry because of the increasing trend of development of ecofriendly technologies (Sawant and Nagendran, 2014). Proteases are usually produced in small amounts with high purity: they thus require large-scale purification processes. The reactants in an enzymatic chemical reaction are called substrates. Casein has a variety of uses, from those used as the main ingredient in cheese to those used as food additives (Lucey, 2002). A milk protein called casein can cause unnecessary distress in people with dairy allergies. Casein can used in paints, inks, coatings, emulsion stability, cement-based applications (Dyson and Wright, 2002).

Soybean, a rich source of protein, similar to beef in its amino acid composition, has been used as an inexpensive source of high-quality protein for humans and animals (Whitehurst and Oort, 2010). It is well reported that the consumption of soy protein in place of animal protein

[1] Department of Chemistry, University of Yangon
[2] Department of Chemistry, University of Yangon
[3] Department of Chemistry, University of Yangon

lowers blood cholesterol levels and may provide other cardiovascular benefits. The present study aimed to study the kinetic behaviour of the alkaline protease enzyme extracted from *soybeans.*

Materials and Methods

Sample Collection

Soybean (*Glycine max* (L.) Merr.) samples–were collected from local market, Yangon Region. Then, identification of the sample was done at the Department of Botany, University of Yangon. Sample extraction and purification were performed at the Analytical Chemistry Research Laboratory, Department of Chemistry, University of Yangon.

Materials

Casein and all other chemicals used in this work were of analytical grade and were products of BDH Chemical Limited (England).

Sample Isolation

Soybean (20 g) were washed and placed in distilled water, allowed to stand overnight and then homogenized for 3 min (as appropriate) using a blender (Philips, China) with 100 mL of 0.5 M tris base buffer pH 9.0 and stirring for 1 h. The homogenate was filtered through cheesecloth. The filtrate was centrifuged for about 30 min at 3000 rpm to obtain 75 mL of extract. Solid ammonium sulphate (13.18 g mL^{-1}) was added to this extract to obtain 30% saturation and stirred and allowed to stand for 2 h at 4°C. After standing for 2 h, the suspension was centrifuged (3000 rpm, 30 min), the precipitates were discarded, and supernatant liquid 66 mL was brought to 60% saturation with (12.87 g mL^{-1}) of solid ammonium sulphate and stored at 4°C (Adulyatham and Owusu-Apenten, 2005). After standing overnight, the precipitated protein containing alkaline protease enzyme was collected by centrifugation for 30 min at 3000 rpm (Ahmad *et al*., 2014).

Qualitative Test for Alkaline Protease Enzyme by Ninhydrin Test

Test tube A containing 1 mL of enzyme solution and 3 mL of ninhydrin solution was swirled for 30 min. Test tube B containing 1 mL of enzyme solution and 1 mL of 1% casein solution was incubated at 37°C for 15 min. After that, 1 mL of 5% TCA was added to stop the reaction and was centrifuged for 10 min at 3000 rpm. After centrifugation, 1 mL of supernatant was mixed with 3 mL of ninhydrin solution and incubated for 5 min. The colour of test tubes A and B after the reaction with ninhydrin was compared.

Enzyme Purification

The crude alkaline protease enzyme was dissolved in tris base buffer (0.5 M, pH 9.0) and then put into the column filled with Sephadex G-100 equilibrated with tris base buffer. The flow rate was adjusted to 1.5 mL per 3 min. A 1.5 mL fraction was collected per tube using a fraction collector. After collection, each fraction was checked for protein content by measuring the absorbance at 280 nm and enzyme activity by measuring the amount of tyrosine released from casein at 275 nm. The fraction with the highest enzyme activity was pooled to obtain a partially purified enzyme and stored at 4°C.

Assay of Partially Purified Enzyme

The enzyme activity was determined by measuring the release of sugar groups. In brief, 0.1 mL of enzyme solution and 0.4 mL of pH 9.0 Tris base buffer solution were mixed and kept

at room temperature for 30 min. Then 1 mL of 1% casein solution was added to the mixture and incubated at 37°C for 30 min. After that, 2 mL of 5% TCA solution was added to stop the reaction. The absorbance of the mixture was measured at 275 nm by using a UV-visible spectrophotometer. The enzyme unit (EU) of the alkaline protease enzyme from soybean was determined at 2734.96 EU/g.

Effects of pH, Temperature, and Enzyme Concentration of Alkaline Protease

To find out the optimum pH of the alkaline protease produced by soybean, the activity of the partially purified enzyme was measured at different pH values. The Tris base buffer solution (pH 7.0, 7.5, 8.0, 8.5, 9.0, 9.5, 10.0, 10.5, and 11.0) was used to determine the activity of alkaline protease as described above. Effect of temperature on protease activity was studied by incubating the reaction mixture at different temperatures ranging from 30°C to 70°C with a 5°C interval. The reactions were carried out at the optimum pH of 9, and the activity of the enzyme was measured. Different enzyme concentrations (1.0, 1.5, 2.0, 2.5, and 3.0%) were used to study the effect of enzyme concentration. The reactions were carried out at pH 9 and 37°C.

Kinetic Studies of Alkaline Protease Enzyme

The Michaelis-Menten constant (K_m) and maximum velocity (V_{max}) of partially purified enzymes were determined using casein as a substrate in the range of 2 mg $mL^{-1}$to 14 mg mL^{-1}. The reaction order and activation energy of the alkaline protease-catalyzed reaction were also evaluated.

Application of the Alkaline Protease Enzyme by Wash Performance Test

The three pieces of white cotton (5 × 5 cm) were stained by soaking in a tea-mix solution and left overnight to ensure uniform absorption of the stain. Then, they were washed with an alkaline protease enzyme solution (0.1 mL and 0.3 mL) and a 1% detergent solution. The stain removal of the enzyme was studied along with the same amount of detergent solution. The washing process was performed for 0, 30, 60, and 90 min, after which the residual absorbance was measured by the UV-visible spectrophotometric method at 280 nm for protein detection. The effectiveness of stain removal was quantified by measuring the change in absorbance.

Results and Discussion

Purification of Alkaline Protease Enzyme from Soybean

Enzyme purification is essential for various industrial applications of enzymes. The impurities present in the enzyme solution can affect the enzyme's stability, activity, and specificity, which can, in turn, affect the final product's quality and yield. Purified enzymes are more stable and active, and their specificity is higher, making them more efficient and effective in industrial processes (Liu *et al*., 2012). Figure 1 shows the chromatogram of alkaline protease on Sephadex G-100 gel. The protein content of the eluate was checked spectrophotometrically at 280 nm, and the enzyme activity was determined at 275 nm. The fractions with the highest activity (13-26 fraction number) were pooled. The partially purified alkaline protease enzyme was purified up to 3 folds with a specific activity of 0.00110 unit/mg over crude extract. The enzyme activity, specific activities of the enzyme solutions, and purity of the enzyme were described in Figure 1 and Table 1.

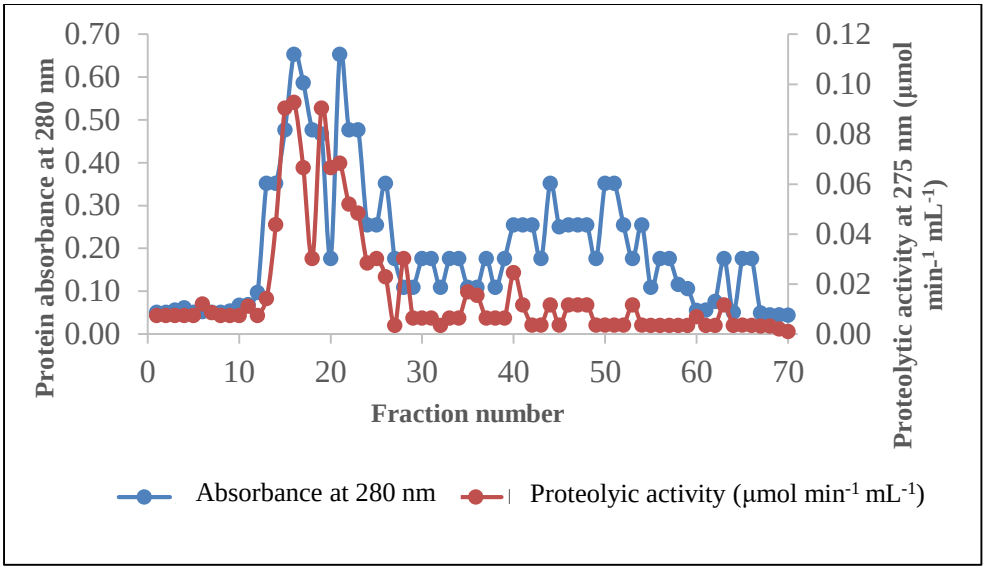

Figure 1. Purification of crude alkaline protease enzyme by Sephadex G-100 gel filtration chromatograph

Table 1. Alkaline Protease Enzyme Activities, Protein Contents and Specific Activities of the Enzyme Solution at Different Purification Steps

Fraction	Total volume (mL)	Total enzyme activity (unit)*	Total protein content (mg)	Specific activity (unit/mg)**	Protein recovery (%)	Degree of Purity (fold)
crude	85	13916.2	5.185	0.00037	100.00	1.00
30 % $(NH_4)_2SO_4$ filtrate	75	7708.5	4.050	0.00050	55.4	1.35
60 % $(NH_4)_2SO_4$ precipitate	66	4047.1	2.574	0.00063	29.1	1.70
after passing the Sephadex G-100	34	804.4	0.850	0.00110	5.80	3.00

* µmol min^{-1} mL^{-1} ** µmol min^{-1} mg^{-1}

Proteolytic Activity of Alkaline Protease Enzyme by Ninhydrin Test

The ninhydrin test assesses proteolytic activity by detecting free amino acids and amines, products of protease enzyme action on proteins. A positive result is indicated by deep blue or purple colour, reflecting successful hydrolysis. Conversely, a lack of colour change signals that no significant protein breakdown occurred, suggesting either insufficient enzyme activity or low enzyme concentration (Figure 2).

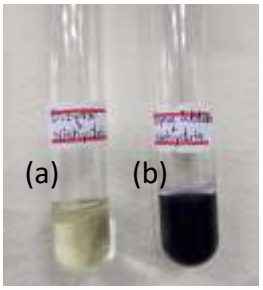

Figure 2. Ninhydrin test to detect presence of alkaline protease enzyme

(a) enzyme + ninhydrin: no colour change

(b) supernatant from enzyme substrate reaction mixture + ninhydrin: colour change to purple

Optimum pH for Alkaline Protease Enzyme Activity

In the present research, the tris base buffer solution (pH 7.0, 7.5, 8.0, 8.5, 9.0, 9.5, 10.0, 10.5, and 11.0) was used to determine the activity of alkaline protease. The nature of the activity vs pH curve of the enzyme (Table 2 and Figure 3) was found to be symmetrical, and it was found that the optimum pH for maximum alkaline protease enzyme activity was pH 9. This value is in agreement with the literature (Sawhney, 2000) which ranges between pH 7 and 11 for the alkaline protease enzyme. From lower to optimum pH, the activities increased with pH gradually, and beyond optimum pH, the activities decreased rapidly due to the denaturing of enzyme proteins (Bhaskar *et al*., 2006).

Table 2. Relationship between Alkaline Protease Activity and pH of the Tris Base Buffer Solution

No.	pH	Absorbance at 275 nm	Protease activity (μmol $min^{-1}mL^{-1}$)
1	7.00	0.053	0.009
2	7.50	0.087	0.016
3	8.00	0.124	0.022
4	8.50	0.172	0.031
5	9.00	0.202	0.037
6	9.50	0.165	0.030
7	10.0	0.105	0.019
8	10.5	0.055	0.010
9	11.0	0.018	0.003

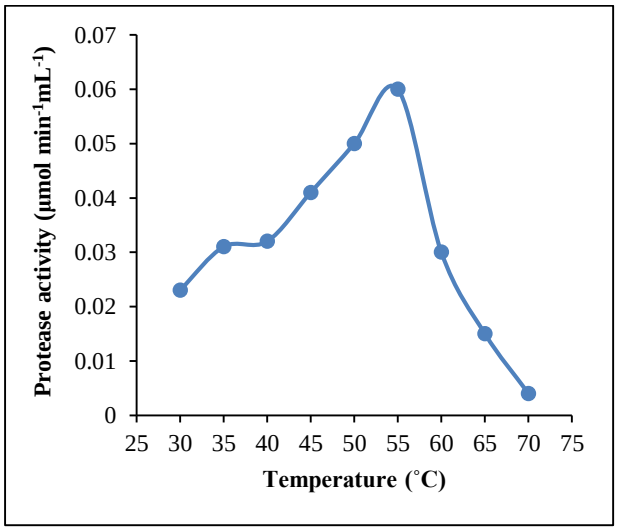

Figure 3. Plot of alkaline protease activity as a function of pH of the solution

Optimum Temperature for Alkaline Protease Enzyme Activity

In this study, the effect of temperature on the alkaline protease activity was investigated in the temperature range of 30 to 70°C. The optimum temperature for alkaline protease was found to be 55 °C in Tris base buffer pH 9.0 (Table 3 and Figure 4). It was found that the activity of alkaline protease increased from 30 to 55°C and then decreased from 55 to 70°C.

Table 3. Relationship between Protease Activity and Temperature of the Solution at pH 9.0

No.	Temperature (°C)	Absorbance at 275 nm	Protease activity (µmol $min^{-1}mL^{-1}$)
1	30	0.125	0.023
2	35	0.168	0.031
3	40	0.177	0.032
4	45	0.220	0.041
5	50	0.263	0.050
6	55	0.306	0.060
7	60	0.143	0.030
8	65	0.080	0.015
9	70	0.020	0.004

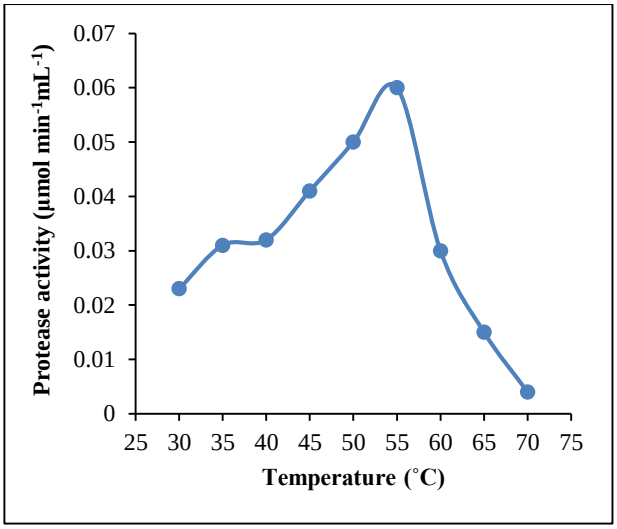

Figure 4. Plot of alkaline protease activity as a function of temperature of the solution at pH 9.0

Activation Energy for Alkaline Protease-Catalyzed Reaction

Enzymes are regarded as lowering the activation energy of a system by making it energetically easier for the transition state to form. In the presence of an enzyme catalyst, the formation of the transition state is energetically more favorable, thereby accelerating the rate at which the reaction will proceed but not fundamentally changing the energy levels of either the reactant or the product (Atkins, 1994). Table 4 shows the relationship between velocity of the protease-catalyzed reaction and temperature. Figure 5 shows a plot of Log V as a function of 1/T for the determination of activation energy and Arrhenius constants. Arrhenius constants of alkaline protease-catalyzed reactions were found to be 3.211×10^6. The activation energy (E_a) values of partially purified alkaline protease-catalyzed reaction were determined to be 4.553 kcal mol^{-1} from linear regression method.

Effect of Enzyme Concentration on Alkaline Protease-Catalyzed Reaction

In this present work, the validity of the enzyme assay method was tested using different concentrations of enzyme: 1.0, 1.5, 2.0, 2.5, and 3.0%. The enzyme activity was found to have a linear relationship with different enzyme volumes (Table 5 and Figure 6). It was found that the higher the enzyme concentration, the higher the alkaline protease enzyme activity in accordance with the literature (Walsh, 1968).

Table 4. Relationship between Alkaline Protease Enzyme Velocity and Temperature of the Solution at pH 9

No.	Temperature (°C)	Temperature (K)	1/T × 10^3 (K^{-1})	V (mM min^{-1})	Log V
1	30	303	3.300	0.0085	-2.0705
2	35	308	3.246	0.0094	-2.0268
3	40	313	3.194	0.0106	-1.9746
4	45	318	3.144	0.0119	-1.9244
5	50	323	3.095	0.0137	-1.8632
6	55	328	3.048	0.0147	-1.8326

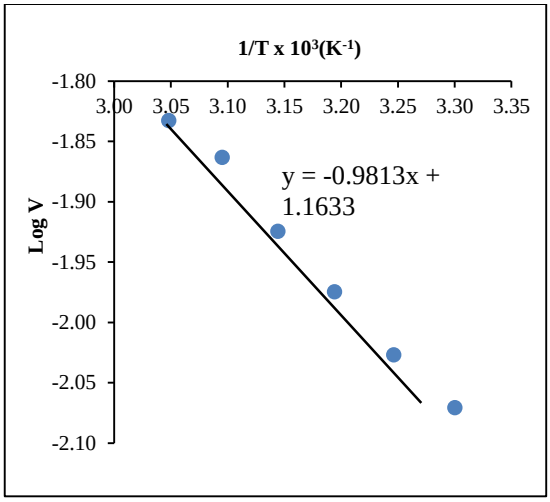

Figure 5. Plot of Log V as a function of 1/T for the determination of E_a

Table 5. Relationship between Enzyme Concentration and Activity of Alkaline Protease-Catalyzed Reaction

No.	Enzyme concentration (%)	Protease activity (µmol min^{-1} mL^{-1})
1	1.0	0.014
2	1.5	0.019
3	2.0	0.028
4	2.5	0.034
5	3.0	0.041

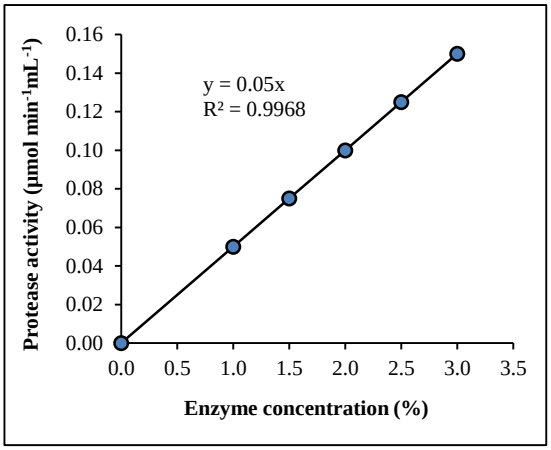

Figure 6. Plot of alkaline protease activity as a function of enzyme concentration of the solution

Effect of Substrate Concentration on Alkaline Protease-Catalyzed Reaction

In the present study, the velocities of enzyme reactions measured at varying levels of casein concentration and their reciprocal values are shown in Table 6. The Michaelis-Menten plot of V vs. [S] is shown in Figure 7. The alkaline protease enzyme reaction is followed by a hyperbolic curve. As the concentration of casein was increased, the rate of reaction also increased until a point was reached where the enzyme was working as fast as it could; after that, it was transforming its maximum number of casein molecules each minute (White *et al.*, 1968). At this point, the enzyme was said to be saturated with substrate, and further increases in the concentration of the casein would not increase the rate of reaction. The enzyme could have worked no faster. For the more accurate estimation, K_m and V_{max} values were computed using statistical and various graphical methods (Figures 8 and 9), and the values are presented in Table 7.

Table 6. Relationship between Substrate Concentration and Velocity of Alkaline Protease-catalyzed Reaction

No.	[S]*×10^2 (g mL^{-1})	-[S] ×10^2 (g mL^{-1})	1/[S] ×10^{-2} (g^{-1} mL)	V×10^3 (mM min^{-1})	1/V×10^{-3} (mM^{-1} min)	V/[S] ×10^{-1} (mM min^{-1} g^{-1}mL)	[S]/V×10^1 (g mL^{-1} mM^{-1} min)
1	0.2	-0.2	5.00	13.644	0.073	68.220	0.014
2	0.4	-0.4	2.50	22.532	0.044	56.333	0.017
3	0.6	-0.6	1.67	28.925	0.034	48.208	0.020
4	0.8	-0.8	1.25	33.214	0.030	41.517	0.024
5	1.0	-1.0	1.00	35.942	0.027	35.942	0.027
6	1.2	-1.2	0.83	38.125	0.026	31.771	0.031
7	1.4	-1.4	0.71	39.763	0.025	28.402	0.035

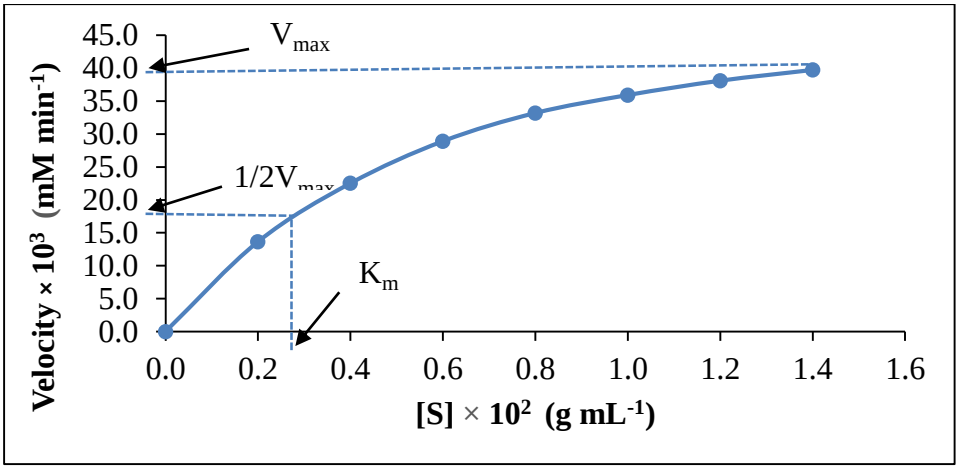

Figure 7. Michaelis-Menten plot of alkaline protease-catalyzed reaction

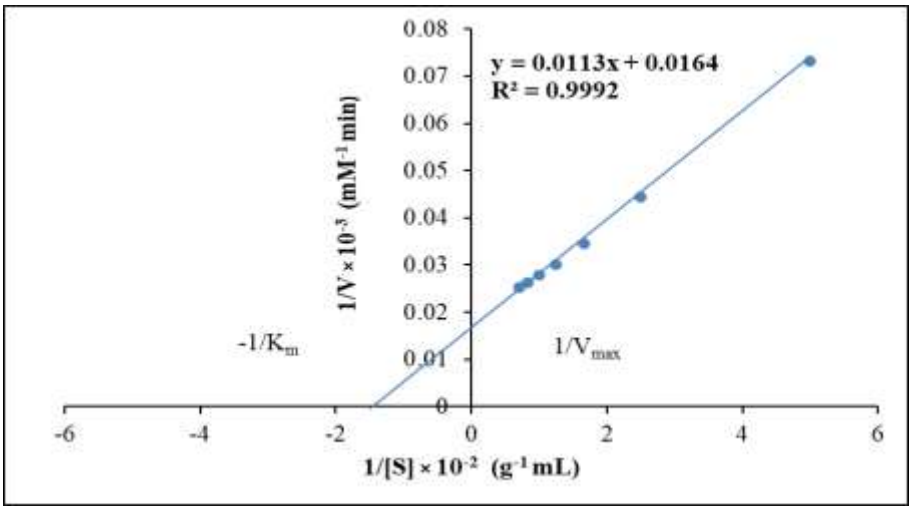

Figure 8. Lineweaver-Burk plot of 1/V vs. 1/[S] for alkaline protease-catalyzed reaction

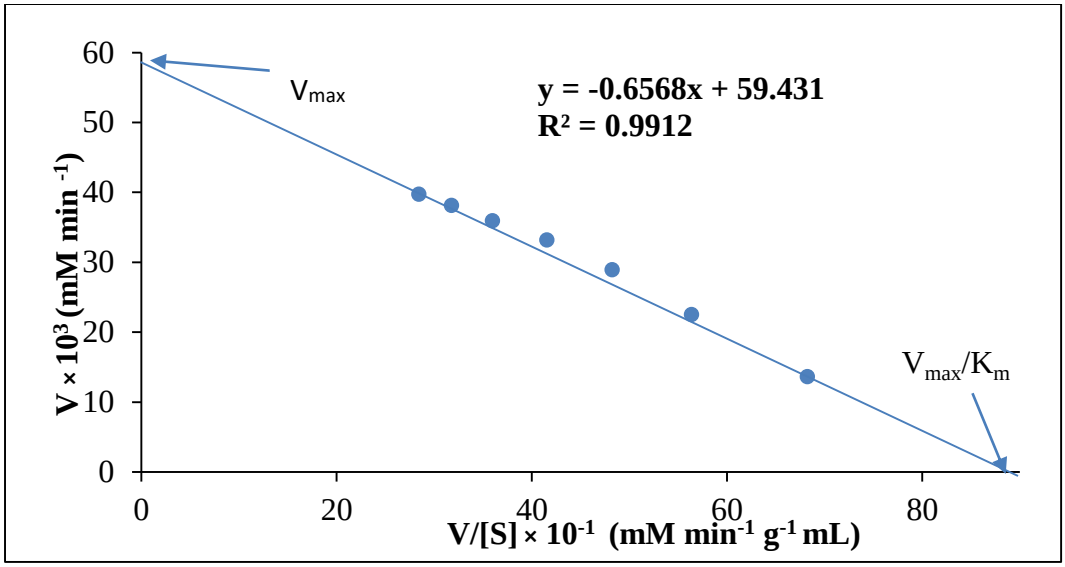

Figure 9. Eadie-Hofstee plot of alkaline protease-catalyzed reaction

Table 7. V_{max} and K_m Values of Alkaline Protease Enzyme using Statistical and Graphical Methods

Methods	Statistical		Graphical	
	$K_m \times 10^2$ (g mL^{-1})	$V_{max} \times 10^3$ (mM min^{-1})	$K_m \times 10^2$ (g mL^{-1})	$V_{max} \times 10^3$ (mM min^{-1})
Michaelis-Menten	-	-	0.33	39.76
Lineweaver-Burk	0.67	60.97	0.67	59.82
Eadie-Hofstee	0.66	59.43	0.66	59.62

Reaction Order on Alkaline Protease-catalyzed Reaction

A reaction specified by the transformation of one molecule of A to one molecule of B with no impact from any other reactant or solvent is a first-order reaction (Martin, 1993). In this study, the 'n' value was determined from the plot of Log V/ (V_{max} – V) *vs.* Log [S] for alkaline protease activity using the linear regression method (Table 8 and Figure 10). The reaction order (n) was observed to be a first-order reaction for the alkaline protease enzyme due to the evaluated value being 1.0437.

Washing Performance Test of Alkaline Protease Enzyme

In this present work, the detergent washing activity used 0.1 and 0.3 mL of enzyme solution and was compared with the control. In the case of removing protein stains from tea-mix-stained clothes, it was seen that the alkaline protease was able to remove tea-mix stains very easily. Tea-mix stains often contain tannins, proteins, and carbohydrates from tea or additives. The proteins in these stains bind to fabric fibers, making the stain difficult to remove with just water. The addition of protease in detergent formulation is effective in removing proteinaceous stained since it can breakdown the protein into smaller polypeptides and make it easier to be

removed (Indhumathi *et al*., 2023; Noor *et al*.,2020). The highest stain removal percentage (96.59%) was obtained from test sample-2 at 90 min. It was indicated that the higher the additive amount of enzyme, the higher the removal percentage of stains on the fabric (Table 9 Figure 11).

Table 8. Relationship between Log]S] and Log V/(V_{max}-V) for Alkaline Protease--Catalyzed Reaction

No.	Log [S]	Log V/(V_{max}-V)
1	-2.699	-0.5406
2	-2.398	-0.2319
3	-2.222	0.0498
4	-2.097	0.0779
5	-2.000	0.1571
6	-1.921	0.2221
7	-1.854	0.2729

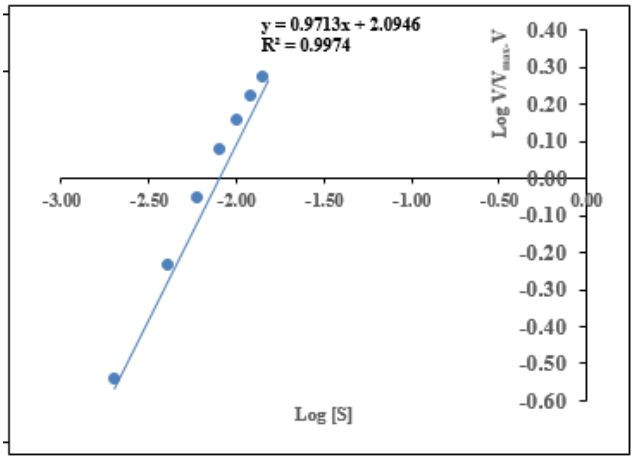

Figure 10. Plot of log V/V $_{max}$-V as a function of log [S] of alkaline protease-catalyzed reaction

Table 9. Stain Removal Percentage Using Alkaline Protease Enzyme in Wash Performance Test

Washing time (min)	Stain removal (%)		
	A	B	C
30	44.58	63.69	64.63
60	56.24	80.38	84.69
90	62.49	90.19	96.60

A = Control (without enzyme), B = Test sample-1 (with 0.1 mL of enzyme solution)

C = Test sample-2 (with 0.3 mL of enzyme solution)

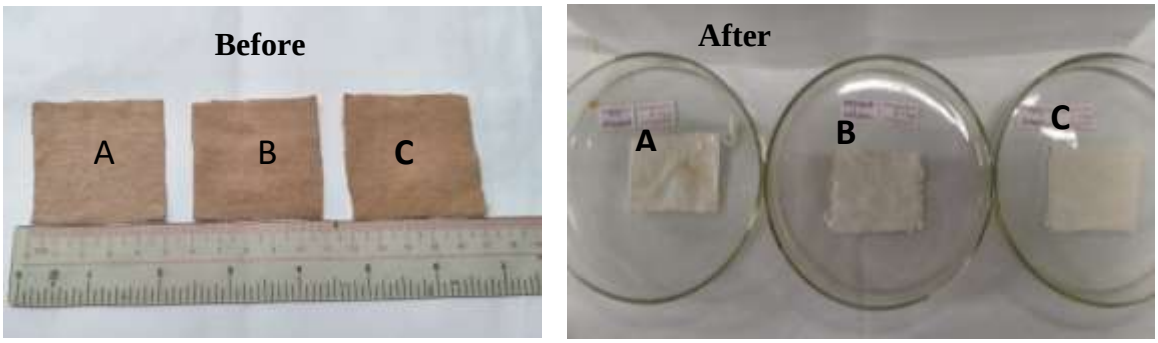

Figure 11. Washing performance on tea-stained fabric (5 × 5 cm) using alkaline protease enzyme; A = Control (without enzyme), B = Test sample-1 with 0.1 mL of enzyme solution), C = Test sample-2 (with 0.3 mL of enzyme solution)

Conclusion

In this research, alkaline protease enzyme was extracted from soybean. The alkaline protease enzyme was purified 3-fold over crude extract after gel filtration chromatography. The enzyme exhibited optimal activity at pH 9.0 and 55°C, with kinetic parameters K_m=0.67×10^{-2} g/mL and V_{max}=60.97×10^{-3} mM min^{-1}. The application of alkaline protease enzyme in laundry detergent was tested by using tea-stained fabric. The enzyme achieved a maximum stain removal efficiency of 96.60% within 90 min using 0.3 mL of the enzyme solution. These findings confirm that soybean-derived alkaline protease is an effective additive for laundry detergents, significantly enhancing their cleaning performance.

Acknowledgements

The authors would like to thank the Myanmar Academy of Arts and Science for giving permission to submit this paper and to Professor and Head, Dr Ni Ni Than, Department of Chemistry, University of Yangon, for her kind suggestion. Special thanks to the Department of Chemistry, University of Yangon, for providing the research and analytical facilities.

References

Adulyatham, P., and R. Owusu-Apenten. (2005). "Stabilization and Partial Purification of a Protease from Ginger Rhizome (*Zingiber officinale* Roscoe)". *Journal of Food Science*, vol.70, pp. 231-234.

Ahmad, N., H. Foo, B. Jamilah, and M. Hasanah. (2014). "Partial Characterization of an Enzymatic Extract from Bentong Ginger (*Zingiber officinale* var, Bentong). *Molecules*, vol.19, pp. 12336-12348.

Atkins, P. W. (1994). *Physical Chemistry*. New York: 5th Edition, Oxford University Press, pp. 899-910.

Bhaskar, N., N. Sachindra, V. Modi, P. Sakhare, and N. Mahendrakar. (2006). "Preparation of Proteolytic Activity Rich Ginger Powder and Evaluation of its Tenderizing Effects on Spent-hen Muscles". *Journal of Muscle Foods*, vol.17, pp. 174-184.

Dyson, H.J. and P. E. Wright. (2002). "Coupling of Folding and Binding for Unstructured Proteins". *Current Opinion in Structural Biology"*. vol.12(1), pp. 54-60.

Ibrahim, N.A., N. Ibrahim, N. S. R. Lizawardi, N. F. I. Fauzi, and S.M. Al-Amsyar. (2020). "Production and

Application of Thermostable Protease 50a as Liquid Protein Stain Remover". *IOP Conf. Series: Earth and Environmental Science*, vol. 596, pp.1-6.

Indhumathi, T., R. Mahavidhya, S. Mavuniq, and V.P. Shri. (2023). "Isolation of Alkaline Protease from Fruit Waste and its Application as Detergent". *Biosc.Biotech.Res.Comm*. vol.16(3), pp. 205-211.

Liu, S., L. Wang, and L. Yuan. (2012). "Purification and Characterization of an Alkaline Protease from *Bacillus alcalophilus*". *Applied Mechanics and Materials*, vol.192, pp. 285-288.

Lucey, J. A. (2002). "Formation and Physical Properties of Milk Protein Gels". *Journal of Diary Sci.*, vol 85(2), pp. 281-94.

Martin, D. W. (1993). *Harper's Review of Biochemistry*. California: Lange Medical Pub., pp. 81-90.

Sawhney, S. K. and Singh, R. (2000). *Introduction Practical Biochemistry*. New Delhi: Narosa Publishing House, pp. 88-96.

Walsh, E. O' F. (1968). *An Introduction to Biochemistry*. London: 2nd., Edition., The English Universities Press Ltd., pp.135-144.

White, A., P. Handler, and E. L. Smith. (1973). *Principles of Biochemistry*. New York: 5thEdition, McGraw-Hill, Inc.

Whitehurst, R.J. and Oort, M.V. (2010). *Enzymes in Food Technology*. Chichester, U.K. ,2nd., Edition, Blackwell Publishing Ltd, pp. 6-8.

INVESTIGATION OF BIOACTIVE CONSTITUENTS AND BIOLOGICAL ACTIVITIES OF THE RHIZOME OF *CURCUMA CAESIA* ROXB.

Htet Htet San[1], Kay Khaing Win[2]

Abstract

Curcuma caesia Roxb. commonly known as Sanwin tain pyar or black turmeric, is one of the important and endangered species in the genus of *Curcuma*. The present study aimed to conduct phytochemical screening, isolating some organic compounds and evaluating the biological activities of the Myanmar medicinal plant *C. caesia* rhizome, including antidiabetic and anti-inflammatory properties. The preliminary phytochemical screening of the rhizome of *C. caesia* showed the presence of alkaloids, glycosides, phenolic compounds, polyphenols, saponin and terpenoids. Five pure compounds (HHS-1, 2, 3, 4 and 5) were isolated from the *n*-hexane extract of *C. caesia* by using thin layer and column chromatographic separation methods. The isolated compound (HHS-1) was identified as zederone based on FT IR and UV-vis spectral data and melting point (152-153 ºC). Four extracts and the isolated HHS-1 compound were tested for antidiabetic activity using the Cirillo VP method (Glucose Uptake Capacity by Yeast Cells). The test revealed that the ethyl acetate extract and the HHS-1 compound exhibited the highest antidiabetic activity. Furthermore, the anti-inflammatory effect of the compound HHS-1 was determined by the Croton oil-induced ear oedema method**.** Topical application of the compound HHS-1 showed significant inhibition of the induced ear oedema (39 % for 0.75 mg/ear, 44 % for 1.5 mg/ear and 98 % for 2.25 mg/ear). This study will support further investigations on the pharmacological activity of medicinal plant species in Myanmar.

Keywords*:* *Curcuma caesia* Roxb., phytochemical screening, antidiabetic activity, anti-inflammatory activity

Introduction

Medicinal plants are a rich source of diverse bioactive compounds with many therapeutic properties. Myanmar has abundant plant resources and Myanmar people have used their traditional medicines to maintain their health and treat various ailments, including malaria, diarrhoea and fever over millennia of history (Aye *et al*., 2019). In Kachin State, Northern Myanmar, the people have a long history of the use of traditional plants for medicinal purposes (Aung *et al*., 2016). The use of herbal plants has gained interest from many sectors and in combating diseases because of their safety, availability, and low cost (Ibrahim *et al*., 2023).

Curcuma caesia has a bluish-black rhizome with a bitter taste and pungent smell and is widely used in treating haemorrhoids, leprosy, asthma, cancer, epilepsy, fever, wound, vomiting, menstrual disorder, anthelmintic, aphrodisiac, inflammation, and more. *C. caesia* is a family member of Zingiberaceae. *C. caesia* rhizome has been reported to exhibit various therapeutic activities including antioxidant, antibacterial, antipyretic, larvicidal, insecticidal, antimicrobial, wound healing and anti-hyperglycemic properties (Fatt *et al*., 2021). It is reported to be rich in major constituents of carbohydrates, proteins, amino acids, steroids, glycosides, flavonoids, alkaloids, tannins, and phenols (Ibrahim *et al*., 2023). Owing to its high medical and aromatic properties, it is widely cultivated as a medicinal plant in many Southeast Asian countries (Fatt *et al*., 2021). Recently, significant attention has been directed toward natural and synthetic glycation inhibitors to delay the onset or progression of diabetic complications. The potential for discovering and developing new anti-diabetic therapies from nature's pharmacy is vast and deserves corresponding consideration (Naila *et al.*, 2012). Furthermore, there is increasing interest in medicinal plant-based therapies to mitigate the inflammatory processes associated with

[1] Department of Chemistry, University of Mandalay
[2] Department of Chemistry, University of Mandalay

diseases and tissue damage (Padilla-Camberos *et al.*, 2021). According to the World Health Organization (WHO), over 80 % of the world's population relies on herbal and natural products for medicinal treatment (Ibrahim *et al.*, 2023). The present work aims to investigate bioactive constituents and biological activities of the rhizome of *C. caesia* (Figure 1).

Figure 1. Morphological characters of *C. caesia* (A) Habit (B) Rhizome

Materials and Methods

Collection of Plant Material and Preparation of Sample

The rhizome of *C. caesia* used in the present study was collected from Lamone Village, Tanai Township, Kachin State, Myanmar. The rhizome was further identified in the Department of Botany, University of Mandalay.

Phytochemicals Screening

The phytochemical screening of the selected sample was carried out according to the reported method (Harborne, 1998). The presence of different phytochemicals was analysed using different specific reagents.

Extraction from the Rhizome of *C. caesia*

The dried sample (700 g) was percolated with 95 % ethanol (a total of 9.0 L) twice, with each percolation lasting ten days. Then, the solution was filtered and the ethanol solvent was removed using a rotary evaporator. A total of 73.82 g of ethanol crude extract was obtained. A mixture of *n*-hexane and ethanol (1:1 v/v) (1 L) was added into 32.40 g of ethanol crude extract then it was partitioned by using a separating funnel. A total of 11.92 g of *n*-hexane extract, 7.90 g of ethyl acetate crude extract and 12.58 g of ethanol-water extract were obtained.

Isolation of Pure Compounds

The *n*-hexane crude extract 9.87 g was separated by column chromatography on silica gel with various solvent ratios of *n*-hexane: ethyl acetate from non-polar to polar. Totally 169 fractions were obtained. Every fraction was checked on TLC, UV detector and developing reagent. The fractions of the same R_f value were combined and then, 9 combined fractions were obtained. Combined fractions 9, 7 and 2 were rechromatographed by microcolumn. The combined fractions 9 and 7 were rechromatographed by microcolumn with the same adsorbent and eluent mentioned in the previous column. About 202.1 mg of pure compound HHS-1 was obtained from combined fraction 9. 147.3 mg of pure compound HHS-2, 13.4 mg of pure compound HHS-3 and 3.5 mg of pure compound HHS-4 were obtained from the combined fraction 7. The combined fraction 2 was rechromatographed by microcolumn on silica gel with various solvent ratios of *n*-hexane: chloroform from non-polar to polar. Totally 54 fractions were obtained. Every fraction was checked on TLC, UV detector and developing reagent. The fractions of the same R_f values were combined and then, 5 combined fractions (1-5) were obtained. Among them, combined fractions 2 was rechromatographed by microcolumn on silica

gel with various solvent ratios of *n*-hexane: ethyl acetate from nonpolar to polar. About 0.9 mg of pure compound HHS-5 was obtained from the combined fraction 2. The R_f values of these five isolated compounds were determined using *n*-hexane: ethyl acetate = 9:1 v/v solvent system.

Identification of the Isolated Compound HHS-1

Among five isolated compounds, compound HHS-1 was chosen to identify using FT IR and UV-Vis spectroscopic techniques, and comparing its melting point with the reported data.

The functional groups of isolated compound HHS-1 were assigned by FT IR spectra measured using a Fourier Transform Infrared Spectrophotometer (IR Prestige-21. Shimadzu, Japan) at the University Research Center, University of Mandalay. The UV-visible spectrum of pure compound HHS-1 was also measured at Mandalay University Research Center, University of Mandalay. It was taken using a UV-visible spectrophotometer (UV-1800 SHIMASZU) with a slit width of 2 nm, using a 10 mm cell at room temperature.

The melting point of pure isolated compound HHS-1 was measured using the Thiele tube method (Stuart SMP30 melting point apparatus) at Mandalay University Research Center.

Determination of Antidiabetic Activity of the Extracts and Isolated Compound HHS-1

This assay was performed according to the well-defined method of Cirillo, 1962. About 1 g of commercial Barker's yeast was dissolved in 100 mL of distilled water to prepare 1 % suspension. The suspension was kept overnight at room temperature (25 ℃). Then the yeast cell suspension was centrifuged at 4200 rpm for 5 minutes. The process was repeated by adding the distilled water to the pallet until a clear supernatant was obtained. Exactly 10 parts of the clear supernatant fluids were mixed with 90 parts of distilled water to get a 10 % v/v suspension of the yeast cells. Each of the 5 mg/mL of ethanol, ethanol-water, ethyl acetate and *n*-hexane extracts was mixed with 1 mL of dimethyl sulphoxide (DMSO) until fully dissolved to prepare the extract solutions. The pure compound HHS-1 was also prepared following the same procedure.

Each of the 500 µL of the extract solutions was mixed with 500 µL of various concentrations (5, 10 and 25 mM) of glucose solution and incubated for 10 min at 37 ℃. To initiate the reaction, 100 µL of yeast suspension was poured into the mixture of glucose and extract, vortexed and incubated for another 60 min at 37 ℃. After incubation, the tubes were centrifuged for 5 min at 3800 rpm and glucose was estimated by using UV-vis spectrophotometry at 520 nm. Glucose uptake capacity for pure compound HHS-1 was carried out by using the same procedure. Absorbance for the respective control was also recorded on the same wavelength. The percent increase in glucose uptake for each sample was calculated by the following formula:

$$\% \text{ increase in glucose uptake} = \frac{A_{\text{control}} - A_{\text{sample}}}{A_{\text{control}}} \times 100$$

where, A_{sample} = Absorbance of the sample

A_{control} = Absorbance of the control (solution having all reagents except test sample)

Determination of Anti-inflammatory Activity of the Isolated Compound HHS-1 by the Croton Oil-induced Ear Oedema Method

The *in vivo* anti-inflammatory activity of the pure compound HHS-1 was tested via the Croton oil-induced ear oedema method according to Manga *et al.*, 2004. The internal surface of the right ear of five groups of mice with a weight of 25-30 g was treated with 20 µL of 5 % croton oil (in ethanol) as an irritant to induce skin inflammation. The left ear remained untreated. The experimental mice were topically applied 0.75 mg/ear, 1.5 mg/ear and 2.25 mg/ear of pure compound HHS-1 before 30 min Croton oil application, and the positive control group received

0.50 mg/ear aspirin. Ear thickness was evaluated with a calliper 6 h after oedema induction. The mice were randomised into five groups, each of which included three mice. (1) negative control group: treated with 5 % Croton oil only, (2) positive control group: received aspirin (0.50 mg/ear), (3) Groups A, B and C: received 0.75 mg/ear, 1.5 mg/ear and 2.25 mg/ear of pure compound HHS-1. The percentage of oedema inhibition was defined with the control group, which received the Croton oil solution, according to the following formula:

$$\text{Inhibition \%} = \frac{(D_{\text{Control}} - D_{\text{Treated}})}{D_{\text{Control}}}$$

where D_{Control} is the difference in oedema thickness in the control group and $D_{\text{Treatment}}$ is the difference in oedema thickness for the treated groups.

Results and Discussion

Phytochemicals Present in the Rhizome of *C. ceasia*

Preliminary phytochemical screening was carried out to detect the presence of organic constituents in the rhizome of *C. caesia*. It indicated that the rhizome of *C. caesia* consists of alkaloids, glycosides, phenolic compounds, polyphenols, saponin and terpenoids.

Five pure compounds HHS-1, 2, 3, 4, and 5 were isolated from the chromatographic separation. The R_f values of these five compounds: HHS-1, 2, 3, 4 and 5 were observed as 0.35, 0.6, 0.27, 0.15, and 0.77, respectively, on silica gel (602 F_{254}) TLC chromatograms with n-hexane: ethyl acetate 9:1 v/v solvent system.

Identification of the Isolated Compound HHS-1

FT IR assignment of the isolated compound HHS-1

The FT IR spectrum of the isolated compound HHS-1 is shown in Figure 2. In this spectrum, the broad band which appears at 3016 cm^{-1} indicates the C-H stretching vibration of sp^2 hydrocarbon. The peaks at 2931 cm^{-1} and 2877 cm^{-1} indicate the asymmetric and symmetric C-H stretching vibration of sp^3 hydrocarbon. The peak at 1658 cm^{-1} gives C=O stretching vibration of the carbonyl group. The peak at 1527 cm^{-1} gives C=C stretching vibration of alkenic group. The peaks at 1458 cm^{-1} and 1234 cm^{-1} indicate C-H bending vibration of sp^3 hydrocarbon. The peaks at 1075 cm^{-1} and 1018 cm^{-1} give C-O-C stretching vibration of the ether group. The peaks at 925 cm^{-1} show C-H out-of-plane bending vibration of the trans or E alkenic group. The functional groups observed in the FT IR spectrum of pure compound (HHS-1) were compared by literature data of zederone (Prapapan *et al*., 2013) as tabulated in Table 1.

Table 1. FT IR Assignments of the Isolated Compound HHS-1

Wavenumber (cm^{-1})		Functional groups
HHS-1	**Literature ***	
3016	3017	C-H stretching vibration of sp^2 hydrocarbon
2931, 2877	2932, 2878	Asymmetric and symmetric C-H stretching vibration of sp^3 hydrocarbon
1658	1662	C=O stretching vibration of the carbonyl group
1527	1523	C=C stretching vibration of alkenic group

Wavenumber (cm^{-1})		Functional groups
HHS-1	**Literature ***	
1458, 1234	1427, 1232	C-H bending vibration of sp^3 hydrocarbon
1075, 1018	1066, 1020	C-O-C stretching vibration of the ether group
925	929	C-H out-of-plane bending vibration of trans or E alkenic group

* Prapapan *et al*., 2013

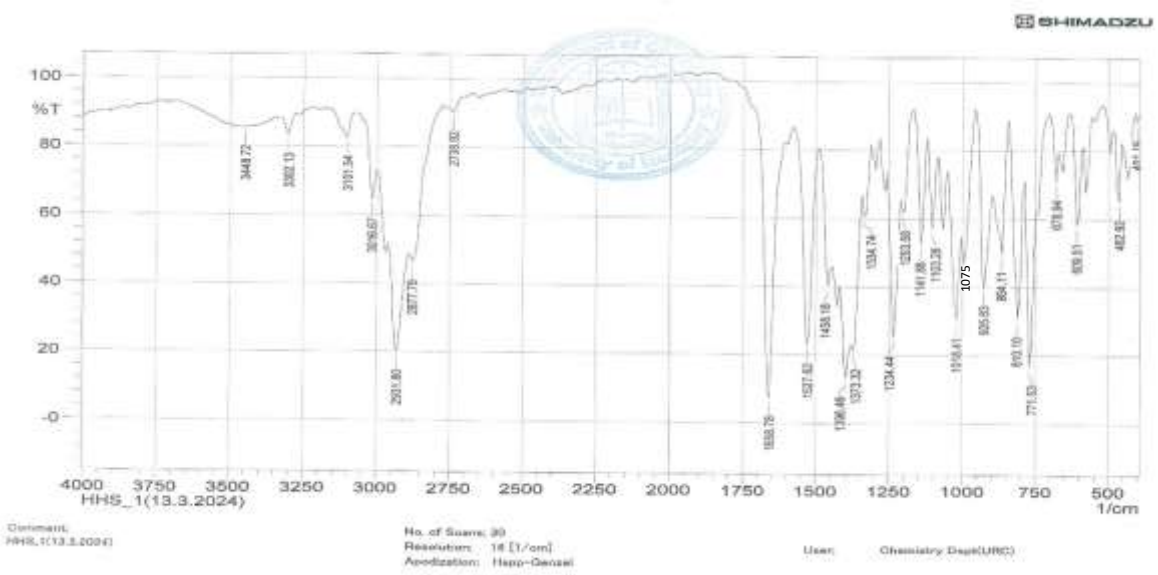

Figure 2. FT IR spectrum of the isolated compound HHS-1

UV-visible Spectroscopic Analysis of the Isolated Compound HHS-1

The UV-visible analysis was performed for the identification of compound HHS-1 containing σ-bonds**,** π-bonds, lone pairs of electrons, chromophores and aromatic rings. The UV-visible spectrum was taken at the wavelength of 200 nm to 700 nm due to the sharpness of the peaks and proper baseline. This profile (Figure 3) showed the peaks at λ_{max}^{MeOH}284 nm with an absorption of 1.242. The peak at 284 nm was characteristic of the carbonyl group corresponding to n $\rightarrow$ π^* transitions (Kania *et al*., 1983). The UV-visible spectral data of the pure compound HHS-1 was compared with literature data of zederone (Prapapan *et al*., 2013) and is shown in Table 2.

Table 2. UV-vis Spectral Data of the Isolated Compound HHS-1

Literature *	HHS-1 compound	Wavelength number (nm)	Absorbance	Remark
281	HHS-1	284	1.242	n $\rightarrow$ π^*

* Kania *et al*., 1983; Prapapan *et al*., 2013

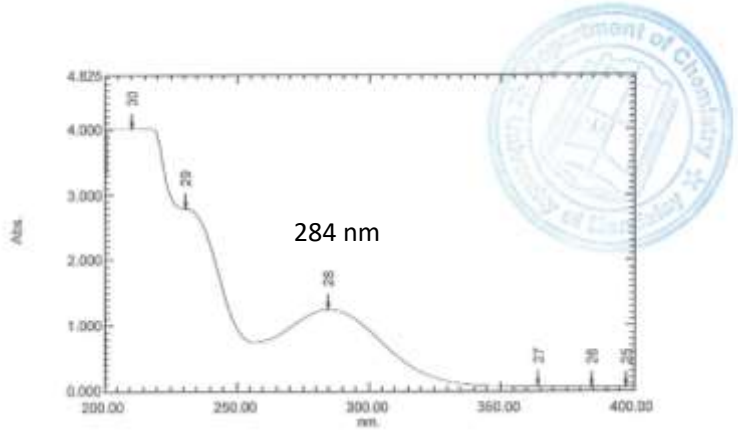

Figure 3. UV-vis spectrum of the isolated compound HHS-1 (in methanol)

Melting Point of the Isolated Compound HHS-1 and Visualization on TLC

The melting point of the isolated compound HHS-1 was found to be 152-153 °C and it is close to the melting point of zederone (153-154 °C) (Prapapan *et al*., 2013). Visualization of the compound HHS-1 on TLC sprayed with developing reagent (*p*-anisaldehyde, H_2SO_4 and EtOH) is identical to the literature (Gerard *et al.*, 2013) as shown in Table 3. Therefore, the isolated compound HHS-1 may be zederone, a sesquiterpene lactone. According to FT IR, UV-vis, melting point measurements and literature data, the isolated compound HHS-1 can be identified as zederone. The structure of zederone is shown in Figure 4.

Table 3. Visualization of the Isolated Compound HHS-1 on TLC Compared with Zederone

Isolated compound HHS-1	Literature *
	

*Gerard *et al.*, 2013; Prapapan *et al*., 2013

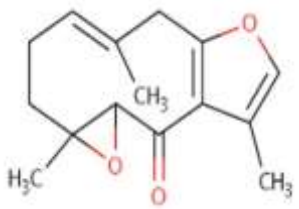

Figure 4. Structure of Zederone

Effects of Four Different Extracts and the Isolated Compound HHS-1 on Glucose Uptake Capacity by Yeast Cells

Four different extracts and the isolated compound HHS-1 showed antidiabetic activity. Among them, ethyl acetate extract showed the highest antidiabetic capacity than other extracts. Pure compound HHS-1 showed the highest antidiabetic capacity at 25 mM glucose concentration (Table 4 and Figure 5). When the percent increases in glucose uptake capacity, the antidiabetic activity shows. The glucose uptake capacity of four different extracts and the isolated compound HHS-1 were dependent on the use of glucose concentrations.

Table 4. The Glucose Uptake Capacity Determined by Yeast Cells Assay (Cirillo VP Method)

Sample	% increase in glucose uptake (Mean± SEM)		
	5 mM glucose	10 mM glucose	25 mM glucose
ethanol extract	68.13±0.61	52.73±3.42	42.79±1.82
ethanol-water extract	46.20±3.63	17.41±0.66	22.83±5.74
ethyl acetate extract	62.79±0.35	52.71±0.57	53.66±0.98
n-hexane extract	45.15±0.67	54.32±0.74	39.94±2.39
HHS-1	18.63±13.59	18.95±6.86	36.33±4.14
Metronidazole	52.69±2.08	55.39±1.72	55.53±3.71

5 mg/mL of each sample was used.

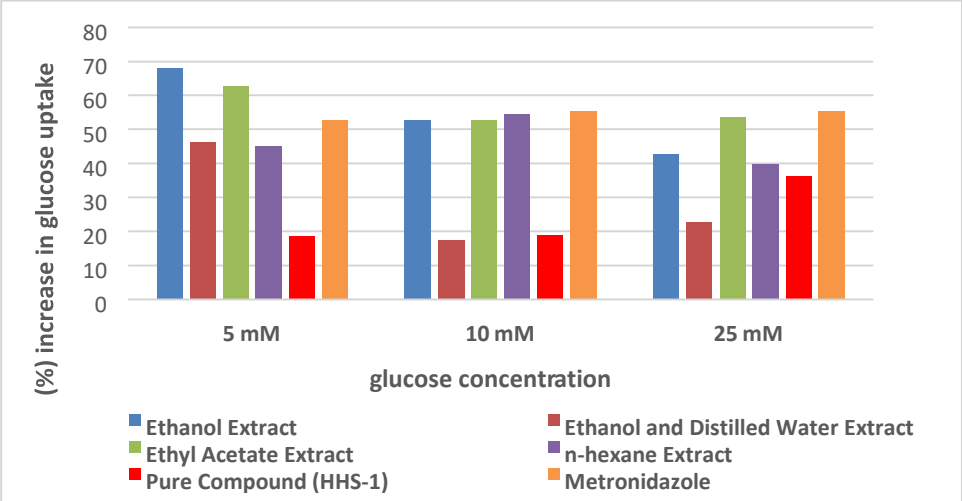

Figure 5. A bar graph of the plot of the concentration of glucose (mM) vs (%) increase in glucose uptake

Effects of the Isolated Compound HHS-1 on Croton Oil-induced Ear Oedema

The anti-inflammatory activity of the pure compound HHS-1 was evaluated with doses of 0.75 (Group A), 1.5 (Group B), and 2.25 mg/ear (Group C) resulting in 39 %, 44 %, and 98 %, respectively (Table 5 and Figure 6). These results indicate significant differences in the efficacy of the groups in reducing inflammation, with an increase in dosage leading to enhanced anti-inflammatory effects. The anti-inflammatory activity of groups A, B and C was compared with negative (treated only with Croton oil) and positive (treated with aspirin) groups how much they can reduce inflammation. Groups A, B and C show higher anti-inflammatory activity than the

negative group. Although groups A and B show less anti-inflammatory activity than the positive group, group C shows higher anti-inflammatory activity than the positive group. Notably, Group C (2.25 mg/ear) demonstrated exceptional efficacy, achieving a very high anti-inflammatory activity of 98 %. This suggests that group C was highly effective in reducing inflammation, almost completely inhibiting the inflammatory process. The significant difference between group C and the other two groups indicates that it could be a promising candidate for further development as an anti-inflammatory agent.

Table 5. The Effect of Isolated Compound HHS-1 on Croton Oil-induced Ear Oedema

Treatment	Dose	Thickness of ear oedema (mm)	Inhibition %
Negative control (Croton oil only)	20 µL/ear	4	-
Aspirin (Positive control)	0.5 mg/ear	2.03	49
Group A	0.75 mg/ear	2.45	39
Group B	1.5 mg/ear	2.25	44
Group C	2.25 mg/ear	0.07	98

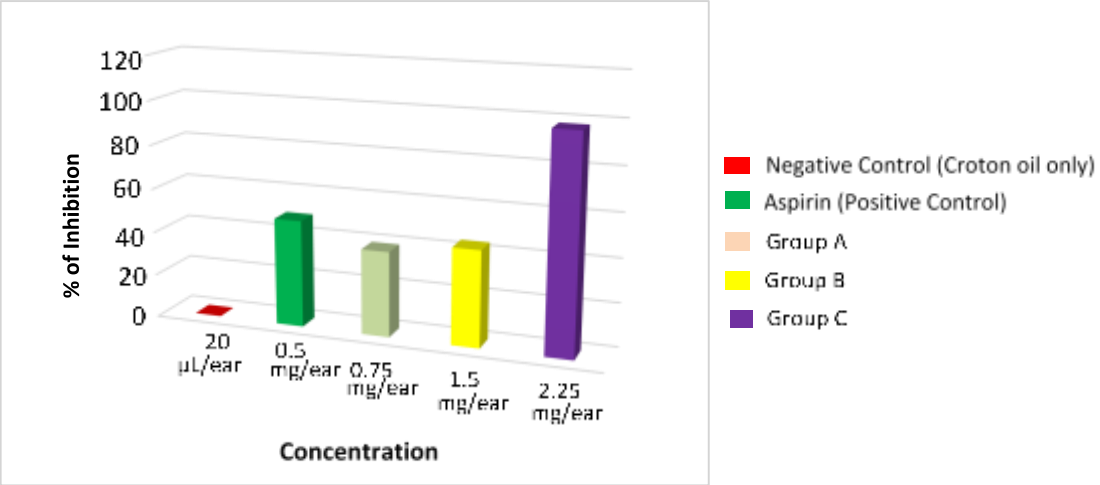

Figure 6. A bar graph of the plot of concentrations vs inhibition (%)

Conclusion

The rhizome of *C. caesia* was collected from Lamone Village, Tanai Township, Myanmar. According to the phytochemical screening, the rhizome of *C. caesia* contains alkaloids, glycosides, phenolic compounds, polyphenols, saponin and terpenoids. Five pure compounds (HHS-1, 2, 3, 4 and 5) were isolated from the *n*-hexane extract of *C. caesia* by using a thin layer and column chromatographic separation methods. Based on FT IR and UV-Vis spectroscopic analyses, as well as melting point determination and TLC visualization compared with reported data, the isolated pure compound HHS-1 (melting point: 152–153 °C) was identified as zederone (reported melting point: 153–154 °C).

Ethanol, ethanol-water, ethyl acetate and *n*-hexane extracts and the isolated zederone (HHS-1) demonstrated antidiabetic activity. Among these, the ethyl acetate extract exhibited the highest antidiabetic capacity. Notably, the isolated zederone (HHS-1) showed the strongest antidiabetic activity at a 25 mM glucose concentration. The comparative analysis of the anti-inflammatory activities at different doses on ear oedema mice demonstrated that a 2.25 mg/ear dose of zederone (HHS-1) was the most effective, achieving an activity rate of 98 %. This highlights its potential as a strong therapeutic candidate for treating diabetic and inflammatory conditions. However, *C. caesia* is a critically endangered species with remarkable medicinal properties, underscoring the urgent need for its conservation. Efforts must be made to value, protect, and sustainably maintain this plant for future generations.

Acknowledgements

I would like to express my thanks to Dr Thinn Myat Nwe, Professor and Head, Dr Tin Myo Thant, Associate Professor, Department of Chemistry, University of Mandalay for their permission to conduct this paper.

References

Aye, M.M., H.T. Aung, M.M. Sein, and C. Armijos. (2019). "A Review on the Phytochemistry, Medicinal Properties and Pharmacological Activities of 15 Selected Myanmar Medicinal Plants". *Journal of molecules,* vol.24(2), pp. 293.

Aung, H.T., M.M. Sein, M.M. Aye, and Z.M. Thu. (2016). "A Review of Traditional Medicinal Plants from Kachin State, Northern Myanmar". *Natural Product Communications*, vol.11(3), pp.353-364.

Cirillo, V.P., (1962). "Mechanism of glucose transport across the yeast cell membrane". *J Bacteriol,* vol.84(3), pp. 485-491.

Fatt, L.C., N.W.A. Rahman, M.A.A. Aziz, and K.M. Isa. (2021). "Identification of the chemical constituents of *Curcuma caesia* (Black Turmeric) hydrosol extracted by hydro-distillation method". *In IOP Conference Series: Earth and Environmental Science*, vol. 765, pp. 1-9.

Gerard, N., M. Urbanska, J. Nawrot, M.K. Bernard, and R. Dawid-Pac. (2013). "Color and Chemical Reactions of Selected Sesquiterpene Lactones and Ecdysones from Asteraceae on TLC Plate". *Journal of Planar Chromatography-Modern TLC,* vol.26(3), p. 289-293.

Harborne, J.B. (1998). *Phytochemical Methods: A Guide to Modern Techniques of Plant Analysis.* London: 5th Ed., Chapman and Hall Ltd, vol.3, pp. 54-84.

Ibrahim, N.N.A., W.A. Wan Mustapha, NS. Sofian-Seng, S.J. Lim, N.S. Mohd Razali, A.H. Teh, H.A. Rahman, and A.A. Mediani. (2023). "A Comprehensive Review with Future Prospects on the Medicinal Properties and Biological Activities of *Curcuma caesia* Roxb". *Journal of Evid Based Complement Alternat Med*, pp. 1-17.

Kania, L., K. Kamieńska-Trela, and M. Witanowski. (1983). "Structural increments in UV spectra of conjugated carbonyl compounds: Part I. The *α*alkyl substituted enaminones". *Journal of molecular structure*, vol.102(1-2), pp. 1-17.

Manga, H.M., D. Brkic, D.E.P. Marie, and J. Quetin-Leclercq. (2004). "In vivo anti-inflammatory activity of *Alchornea cordifolia* (Schumach. & Thonn.) Mull. Arg. (Euphorbiaceae)". *J Ethnopharmacol*, vol.92, pp. 209-214.

Naila, A.S., F. Hussain, T. Iqbal, and M.A. Sheikh. (2012). "Determination of in vitro antidiabetic effects of *Zingiber officinale* Roscoe". *Brazilian Journal of Pharmaceutical Sciences*, vol.48, pp. 601-605.

Padilla-Camberos, E., O.R. Torres-Gonzalez, I.M. Sanchez-Hernandez, N.E. Diaz-Martinez, O.R. Hernandez Perez, and J.M. Flores-fernandez. (2021). "Anti-inflammatory activity of *Cnidoscolus aconitifolius* (Mill.) ethyl acetate extract on croton oil-induced mouse ear oedema". *Journal of applied sciences*, vol.11(20), pp. 1-8.

Prapapan, P., K. Suksen, K. Somkid, R. Chokcharsiri, S. Jariyawat, A. Chuncharunee, A. Suksamrarn, and P. Piyachaturawat. (2013). "Zederone, a sesquiterpene from *Curcuma elata* roxb, is hepatotoxic in mice". *International Journal Toxicol*, vol.32(6), pp. 454-62.

COLORATION OF COTTON FABRIC WITH NATURAL COLORANT EXTRACTED FROM WASTE LEAVES OF INDIAN ALMOND (*TERMINALIACATAPPA* L.) *

Wai Wai Phyoe[1], Tin Moe Moe Myint Zaw[2], NguWah Htwe[3], Pyae Phyo San[4]

Abstract

Indian almond (*Terminaliacatappa*L.) leaves are the waste of Indian almondtree and the tannin compound present in the leaves extract can be an alternative colorant for synthetic dyes. Indian almondtrees are abundant and the extraction of colorant from leaves is an effective way to utilize the waste leaves as natural colorant. This research aims to extract the natural colorant from Indian almondleaves and the extracted colorant was utilized in the coloration of cotton fabric. The extraction applied in this study was solvent extraction method in which the leaf samples were extracted using ethanol. The colorant extracted from Indian almondleaves was characterized and identified by using UV-vis Spectrophotometry and FT-IR methods. The physico-chemical properties of extracted colorant were investigated. In this research, extracted colorant was applied in the coloration of cotton fabric with and without mordant. Before coloration, the types of mordant on the absorbance of extracted colorant was examined by using different mordants such as alum, $CuSO_4$, $FeSO_4$, $K_2Cr_2O_7$and CaO, respectively. The effect of mordanting methods on the color development of extract on dyed cotton fabric was determined by using three different methods like pre mordanting, post mordanting and combined mordanting. The analysis of dyeing time on the color development of extracted colorant on dyed cotton fabrics was performed. The high absorbance value (0.928) was observed using alum mordant. Among three different methods, the pre mordanting method was preferable because the color absorption on cotton fabric was great and obvious color change was not occurred. Dyeing time 40 minprovided the better color absorption and color remaining on cotton fabric. For mordanted and unmordanted cotton fabric, the color development of extracted colorant on the cotton fabric such as the color fastness test to sunlight, washing and wet rubbing test were carried out. The results indicated that the colorant extracted from Indian almondleaves could be utilized as natural colorant for the coloration of cotton fabric in the presence of mordant.

Keywords: Extracted Natural Colorant, Solvent Extraction, Coloration to Cotton fabric, Mordant

Introduction

Natural dyes from plant sources have been given much more interest in recent years due to threat raised and the harmfuleffects by synthetic dyes. The main idea of extracting dyes from plant (natural) sources is to avoid the environmental contamination. Natural dyes are hygienic, user friendly, permanentand environmentally friendly than other colorants. For this reason, colorants derived from natural sources have become an important alternative to unsafe synthetic dyes. Natural dyes/colorants derived from plants are believed to be safe because of its non-carcinogenic, biodegradable and nontoxic in nature. Natural dyes are nowadays in demand not only in cosmetics, leather, food and pharmaceutical industries but also in textile industry. Present days with global concern over the use of eco-friendly and biodegradable materials, considerable research work is being undertaken around the world on the application of natural dyes (Yogesh V. and Namrita K., 2017). The advantages of natural dyes compared with synthetic dyes mainly are that(1) the shades produced by natural dyes/colorants are soft and soothing to the human eye, (2) natural dyestuff can produce a wide range of colors by mix and match system including the use of different mordants which can shift the colors to a wide range, (3) natural dyestuff produce rare color ideas and are automatically harmonizing, (4) unlike non-renewable basic raw materials forsynthetic dyes, the natural dyes are renewable, being agro-renewable/vegetable based and at

---

* Special Award (2024)

[1] Department of Industrial Chemistry, West Yangon University
[2] Department of Industrial Chemistry, West Yangon University
[3] Department of Industrial Chemistry, West Yangon University
[4] Department of Industrial Chemistry, West Yangon University

the same time biodegradable, (5) in some case like indigo, the waste in the process becomes an ideal fertilizer for use in agricultural lands, (6) many dye plants thrive on wastelands, so there is no additional cost or effort required to grow it, and (7) application of natural dyes has potential to earn carbon credit by reducing consumption of petroleum based synthetic dyes (Herry P., et al., 2019). *Terminaliacatappa*L. is one of the sources of natural dye (Menna M.R., et al., 2022). The leaves are large, 15–25 cm (5.9–9.8 inch) long, 10–14 cm (3.9–5.5 inch) broad, ovoid, glossy dark green and leathery. Before falling, they turn pinkish-red or yellow-brown, due to pigments such as violaxanthin, lutein, and zeaxanthin. The leaves contain several flavonoids (like kaempferol or quercetin), several tannins (such as punicalin, punicalagin or tercatin), saponins and phytosterols (Yogesh V. and Namrita K., 2017). The main aim of this workis to studythe effective utilization of waste leaves in extracting natural colorant. The objectives of this research are to extract the natural colorant from Indian almond leaves, to characterize the extracted colorant, to utilize the extracted colorant in dyeing of cotton fabric and to study the color fastness of extracted colorant on the dyed cotton fabric.

Materials and Methods

Sample Collection

Indian almondleaves were collected from Ward 20, HlaingTharYar Township, Yangon Region**.**

Extraction of Natural Colorant from Indian AlmondLeaves

Indian almond leaves were washed with water to remove the dust and they were sun dried for 5 h. The dried leaves were cut into small pieces and ground into fine powder for efficient solvent extraction. 5g of the dried leaf powder sample was extracted using 50 mL of ethanol. The mixture was allowed to stand overnight. Then, the mixture was filtered using Whatman Filter Paper No. (4) to obtain clear colorant solution. Consequently, the filtrate was concentrated using distillation method. The dilute colorant solution was distilledat 60℃ until 10 mL of concentrated colorant extract was obtained.

Figure 1: Indian Almond Leaves

Figure 2: Indian Almond Dried Leaf Powder

Figure3: Extracted Colorant from Indian Almond Leaves

Figure 4: Dyed Cotton Fabric

Coloring Process

The white cotton fabric was cut into 1×1 inch and weighed. The preweighed cotton fabric was mercerized by using 20% (w/v) NaOH solution for 20 min. And then 10% (w/v) of mordant solution (45mL distilled water and 5g alum) was prepared and the white cotton fabric was soaked in mordant solution for 25 min at room temperature. After 25 min, the white cotton fabric was removed from mordant solution and immersed in the extracted colorant solution at 40℃ in a water bath for 40 min. Finally, the dyed cotton fabric was removed from the dye solution and rinsed with water and dried.

Color Fastness to Lighting

The cotton fabric sample (1×1 inch) was soaked in an extracted colorant solution for 60 min and dried at room temperature. After drying, the dyed cotton fabric was exposed to sunlight for 5 h. After exposure to sunlight, the change in color of cotton fabric was studied at oneday interval for one week. Then the color fastness to light of dyed cotton fabric was determined.

Color Fastness to Washing

1×1 inchin length cotton fabric sample was immersed in an extracted colorant solution for 40 min and dried at room temperature. After drying, the dyedfabric was washed with mild detergent solution. Then, dyed cotton fabric was rinsed with water and dried again.The color fastness to washing was determinedevery day for one week.

Color Fastness to Rubbing

The cotton fabric (1×1 inch) was dipped in an extracted colorant solution for 40 min and dried at room temperature. After drying, the dyed fabric wasrubbed by hand and washed with water. Then the color fastness to rubbing test was studied.

Results and Discussion

This study was intended to extract the natural colorant from Indian almond leaves and utilized in the dyeing of cotton fabrics. The identification of extracted colorant was carried out by using UV-vis spectrophotometer and FT-IR analyses. The results are indicated in Tables 1, and 2, and also in Figures 1 and 2. UV-vis spectrophotometry and FT-IR analysis are valuable devices for characterization and identification of compounds or functional groups present in a substance. UV-vis spectra obtained from extracted colorant exhibited that higher absorbance values were observed at wavelength between 400 and 406.5 nm. It confirmed the presence of tannin in extracted colorant from Indian almond leaves. According to the FT-IR results, the functional groups produced from extract of Indian almond leaves showed that the tannin compoundsare present in theIndian almond leaves extract. The results of this analysis are in accordance with the results of FT-IR spectrum analysis of tannin compounds from the previous study conducted by (Muhammadu A.B. et al., 2017). FT-IR spectra showed that -OH group was in the region of wavelength absorption 3387.06 cm^{-1} with a very strong and broad signal. C = C groups were in the area with a wavelength of 1614.45 cm^{-1}. In the region of 1448.57 cm^{-1} indicated the presence of C=C of aromatic group and the absorption band. 1238.32-1054.12 cm^{-1} indicated the presence of C-O groups.

The physico-chemical properties of extracted colorant were determined and the results are presented in Table 3. According to the results, pH of the extract was 5.5 and it was acidic. The color of the extract was reddish brown and the color density of extracted dye was 0.467.

Mordanting process plays an important role in the fabric dyeing using natural dyes. The effect of different mordants such as alum, $CuSO_4$, $FeSO_4$, $K_2Cr_2O_7$and CaO on the absorbance values of extracted colorant were studied and the results are shown in Table 4. The highest

absorbance value was obtained with alum. Moreover, the development of color on dyed cotton fabrics were observed by dyeing the cotton fabric with and without mordant and the results are presented in Table 5. Various colors were observed and the resulting color varied from yellow, reddish brown to brown, dark brown and light yellow.

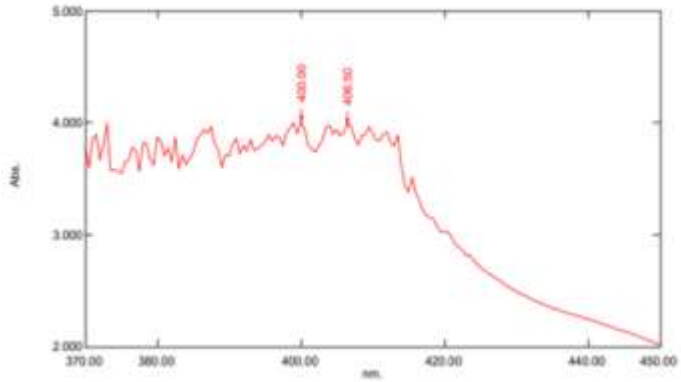

Figure 5: UV-Visible Analysis of Extracted Colorant

Table 1: UV-Visible Analysis Data of Extracted Colorant

Sr. No.	Wavelength (nm)	Absorbance
1.	406.5	3.977
2.	400.00	4.00

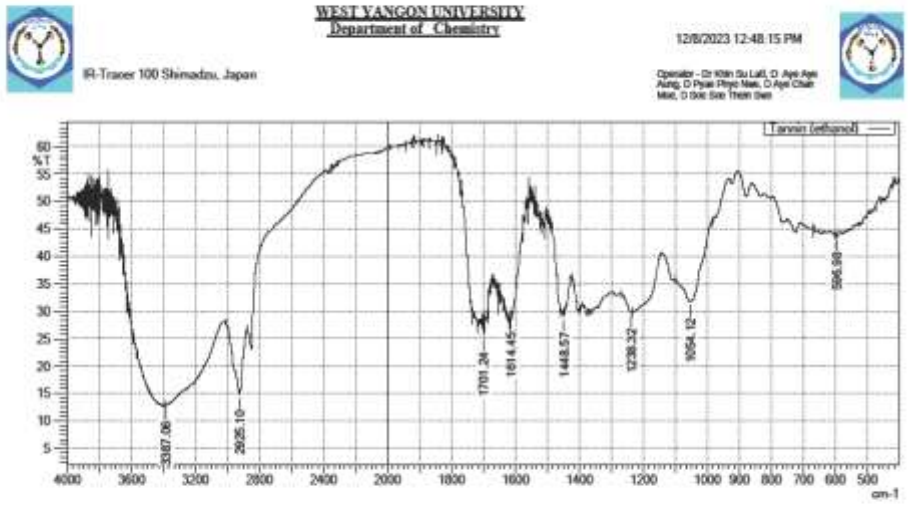

Figure 6: FT-IR Spectral Analysis of Extracted Colorant

Table 2: FT-IR Spectral Data of Extracted Colorant

Wave Number (cm^{-1})			Functional Group	Interpretation
Sr. No.	Observed Value	Literature Value*		
1.	3387.06	3406	ν_{-OH}	-OH bond stretching vibration

Wave Number (cm^{-1})			Functional Group	Interpretation
Sr. No.	**Observed Value**	**Literature Value***		
2.	2925.10	2950	ν_{-CH}	C-H bond extension stretching vibration
3.	1701.24	1713	$\nu_{-C=O}$	C=O bond stretching vibration
4.	1614.45	1613	γ_{-CH} $\nu_{-C=C}$	C-H bending, C=C aromatic stretching vibration
5.	1448.57	1446	γ_{-CH} $\nu_{-C=C}$	C-H bending, C=C alkene and aromatic stretching vibration
6.	1238.32	1227	ν_{-CO}	C-O stretching vibration
7.	1054.12	1066	ν_{-COC}	C-O-C linked symmetric stretching vibration

*****(Jag,2000)

Table 3: Physico-chemical Properties of Extracted Colorant

Sr. No.	Properties	Extracted Colorant
1.	pH	5.5
2.	Absorbance value at 405 nm	1.048
3.	Color Density	0.467
4.	Yield % (v/v)	20

Table 4: Effect of Different Mordant on Absorbance of Extracted Colorant

Sr.No.	Types of Mordant	Absorbance Value at 405 nm	pH
1.	Alum*	0.928	4.5
2.	$CuSO_4$	0.852	4.2
3.	$FeSO_4$	0.898	6.3
4.	$K_2Cr_2O_7$	0.905	5.7
5.	CaO	0.846	10.76

* The most suitable mordant

Table 5: Effect of Different Mordant on Color Development on Cotton Fabric

Sr. No.	Mordant	Extracted Colorant	Color Development
1.	Without Mordant	Ethanol	
2.	Alum*		
3.	$CuSO_4$		
4.	$FeSO_4$		
5.	$K_2Cr_2O_7$		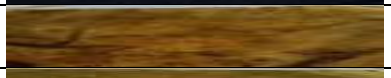
6.	CaO		

*The most favorable mordant for color development after application of color

The effect of dyeing method and dyeing time on the color development of dyed cotton fabrics and percent of dye on cotton fabrics were also investigated and the results are presented in Tables 6, 7 and 8. Different dyeing methods such as pre mordanting, post mordanting and combined mordanting were used to evaluate the color development of extracted colorant on dyed cotton fabric. For cotton fabric mordanted with alum, the pre mordanting method was preferable because the color retention on cotton fabric was acceptable and no obvious color change has occurred. The color obtained from these methods indicated that the pre mordanting method was effective in color absorption and its color retention on cotton fabric was preferable. The percent of dyeing and color development on dyed cotton fabric were determined by using various dyeing time such as 20 min, 40 min and 60 min. Dyeing time did not significantly affect the weight of dyebefore and after dyeing from Indian almond leaves while dyeing with 40 min exhibited better color absorption, uniform color dispersion and color retention on cotton fabric. The percent of dyeing on cotton fabric was 2.6%.

Table 6: Effect of Dyeing Method on Color Development on Cotton Fabric
Extract - Ethanol extract
Mordant - Alum

Sr.No.	Dyeing Method	Color Development
1.	Pre Mordanting*	
2.	Post Mordanting	
3.	CombinedMordanting	

*The most favorable method for mordanting

Table 7: Effect of Dyeing Time on Percent of Dyeing on Cotton Fabric
Extract - Ethanol extract
Mordant - Alum

Sr. No.	Dyeing Temp. (°C)	Dyeing Time (min)	Cotton Fabric			
			WeightBefore Dyeing (g)	Weight After Dyeing (g)	Percent of Dyeing (%)	Color
1.	40	20	0.04	0.048	2.5	Reddish brown
2.	40	40*	0.04	0.06	2.6	Reddish brown
3.	40	60	0.04	0.06	2.6	Reddish brown

Table 8: Effect of Dyeing Time on Color Development on Cotton Fabric
Extract - Ethanol extract
Mordant - Alum

Sr.No.	Dyeing Time (min)	Color Development
1.	20	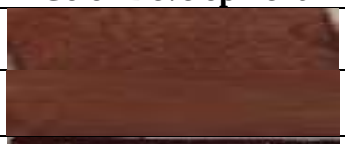
2.	40*	
3.	60	

* The most suitable dyeing time

The color fastness test to light, washing with mild detergent and wet rubbing were conducted and the results are presented in Tables 9, 10 and 11, respectively. Sunlight fastness test forunmordanted and mordanted dyed cotton fabric was conducted by exposing the dyed cotton to sunlight for one week. For cotton fabric mordanted with alum, color retention was found to be goodand the original color of extract on the cotton fabric did not obviously change after one week of exposure to sunlight. Washing fastness test of unmordanted and mordanted dyed cotton fabric was carried out by washing dyed fabric with mild detergent. Obvious color changes were observed for all dyed cotton fabric except for fabric mordanted with alum. The results obtained for wet rubbing fastness indicated that the color of dyed fabric before rubbing fastness were totally different from that of dyed fabric after rubbing fastness except mordanted fabric with alum. For unmordanted and mordanted fabrics with $CuSO_4$, $FeSO_4$, $K_2Cr_2O_7$, CaO, the color of the fabric after wet rubbing changed to grey and dark while in the case of mordanted fabric using alum, it was found that there wasno significant color change, and the color retention on the fabric was preferable. Therefore, alum was considered as an effective mordant and the best in color absorption.

Table 9: Color Fastness to Light for Dyed Cotton

Sr.No.	Mordant	Color Stability	
		(Before Light Testing)	(After Light Testing)
1.	Without Mordant	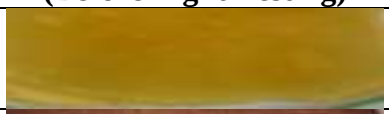	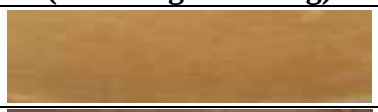
2.	Alum*	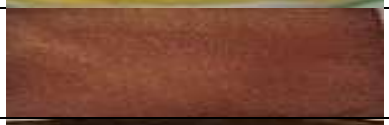	
3.	$CuSO_4$	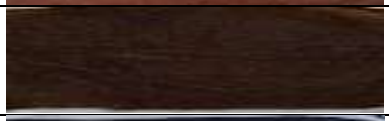	
4.	$FeSO_4$	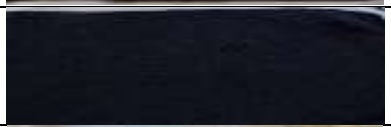	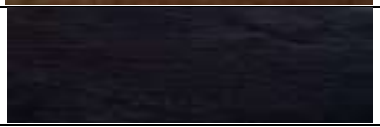
5.	$K_2Cr_2O_7$	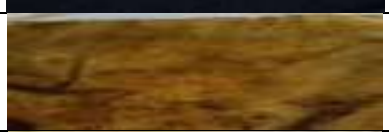	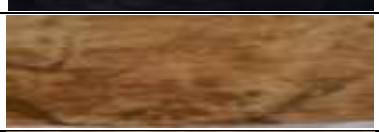
6.	CaO		

*The most favorable mordant for color stability

Table 10: Color Fastness to Washing for Dyed Cotton

Sr. No.	Mordant	Color of Dyed Cotton	
		Before Washing	After Washing
1.	Without Mordant		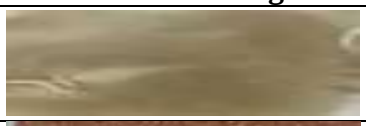
2.	Alum*	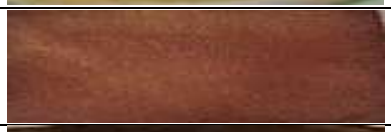	
3.	$CuSO_4$	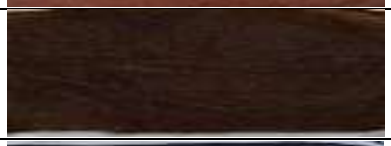	
4.	$FeSO_4$		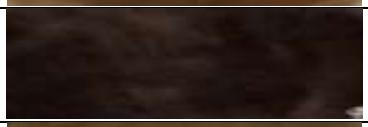
5.	$K_2Cr_2O_7$	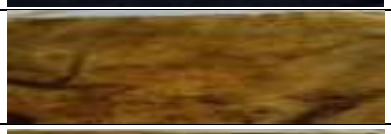	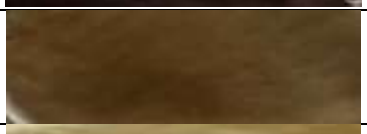
6.	CaO		

*The most favorable mordant for color stability

Table 11: Color Fastness to Rubbing for Dyed Cotton

Sr. No.	Mordant	Color of Dyed Cotton	
		Before Rubbing	After Rubbing
1.	Without Mordant	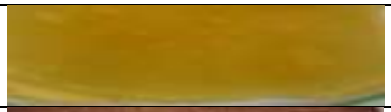	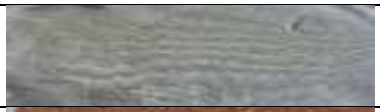
2.	Alum*	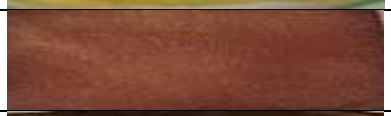	
3.	$CuSO_4$	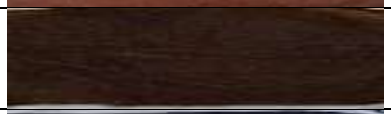	
4.	$FeSO_4$		
5.	$K_2Cr_2O_7$		
6.	CaO		

*The most favorable mordant for color stability

Conclusion

This research was carried out to extract the natural colorant from Indian almond leaves and its application on cotton fabric. The extracted colorant was characterized and identified by using UV-vis spectrophotometer and FT-IR method. Based on the UV-vis analysis, higher absorbance values were observed at wavelength between 400 and 406.5 nm and it confirmed the presence of tannin in Indian almond leaves extract. According to the FT-IR results, the functional groups produced from extract of Indian almond leaves verified that the tannin compounds were present in the extract of Indian almondleaves. The results of this analysis are in accordance with the results of FT-IR spectrum analysis of tannin compounds from literature value. Indian almondleaves could be utilized as natural dye source in fabric coloration in the presence of mordant. Alum was an effective mordant in color absorption and color retention on cotton fabric. Therefore, the colorant extracted from Indian almond leaves could be used to minimize the usage of synthetic dye and the extraction process in this study can be an effective way to advantageouslyutilize the forest waste in making valuable product.

Acknowledgements

The authors would like to express sincere thanks toDr.ThanZawOo, Rectorof West Yangon University.We are profoundly gratefulto Dr. Htate Tin Han and Dr. KhinNwet Aye, Pro-Rectors of West Yangon University. We would like to extend our gratitude to Dr. Thin ThinKhaing, Professor and Head of the Department of Industrial Chemistry, West Yangon University, for giving us permission to present this research paper at the Research Paper Reading Session organized by Myanmar Academy of Arts and Science.

References

Herry, P., E. Winyaand H. Nur, (2019) “Natural dye extraction from tropical almond (*Terminaliscatappa*Linn) leaves and its characterization”. Importance of Color Fastness” *Journal of Textiles*, Coloration and Polymer Science.19(2), pp.137-153.

Jag,M.,(2000)"Organic spectroscopy:principles and applications."ISBN 10: 8173192952,ISBN 13 : 9788173192951. Narosa Publishing House, New Dehli, 1-512.

Menna, M.R., G.H. Ahmed and A.O. Hanan, (2022) “An Overview of Natural Dyes Extraction Techniques for Valuable Utilization on Textile Fabrics”. *Journal of Textiles*, Coloration and Polymer Science, 19(2), pp.137-153.

Muhammadu, A.B., A. Hassan and R.M. Okezi, (2017) “Characterization of Colorant Extracted from Almond Leaves”. *Nigerian Journal of Chemical Research*, 22(2), 31-44.

Yogesh, V. andK. Namrita, (2017) “Natural Dyes Extracted from Waste Leaves of *TerminallaCatappa* Locally Known as Tropical Almond and Its Application on Silk Fabrics Pretreated with Eco friendly and Noneco-friendly Mordants”. *International Journal of Research Granthaalayah*, 5(5), 125-137.

HIGHLY EFFICIENT HYDROGEN EVOLUTION BY USING $Zn_{1-X}Cd_XS$ COMPOSITES DERIVED METAL ORGANIC FRAMEWORK UNDER VISIBLE LIGHT ILLUMINATION

Pyai Pyai Phyo[1], Tian Liang[2]

Abstract

Hydrogen production from water splitting under visible-light irradiation is considered as an ideal process to convert solar energy into renewable hydrogen energy and a promising technology to reduce fossil fuel consumption. In this research, $Zn_{1-X}Cd_XS$ derived metal organic framework was developed via an elementary hydrothermal method that was integrated with the calcination means. The different experimental parameters were employed to investigate the transformation of phase and morphology. The $Zn_{0.7}Cd_{0.3}S$ nano material exhibited the higher hydrogen production rate of 14.1 mmol $h^{-1}g^{-1}$ under cocatalyst-free and visible-light irradiation conditions. Furthermore, these ZnCdS nano materials showed excellent long-term stability, maintaining high photocatalytic activity for hydrogen evolution over a number of cycles. This research work represents a simple strategy to fabricate visible-light responded ZnCdS derived from zeolitic-imidazolate-framework-8 (ZIF-8) and highlights the critical role for developing Z-scheme photocatalyst in solar energy conversion.

Keyword: hydrothermal method, metal organic framework, hydrogen evolution, photocatalyst

Introduction

The problems of the global energy crisis and environmental pollution insist on clean and renewable energy alternatives. Photo-catalytic hydrogen evolution from water splitting by using sun light and a photocatalyst has been considered as an ideal process to convert solar energy into chemical energy and as a promising technology to reduce fossil fuel consumption. Photocatalytic water splitting is a process that requires only light energy, water and a catalyst for dissociation of water into hydrogen and oxygen. In particular, hydrogen production using solar energy has attracted significant attention as a key issue in the utilization of the sun as the most abundant renewable energy source. Hydrogen is a clean energy carrier when used in fuel cells because only water is emitted as an oxidation product.

Nowadays, numerous semiconductor-type photocatalysts (e.g., oxides, sulfides, and oxynitride semiconductors) are being explored as one class of the most promising low-cost catalysts for producing hydrogen energy under visible light irradiation ($\lambda > 420$ nm) (Y. J. Yuanet.al, 2016). The photocatalytic splitting of water into hydrogen and oxygen by using a powdered photocatalyst has become the subject of research, mainly focusing on the visible light sensitization of photocatalysts because visible light accounts for about 45 % of sunlight. In this research work, a ZnCdS rhombic dodecahedral structure by employing zeolitic-imidazolate-framework-8 (ZIF-8), a metal-organic frameworks (MOFs), which are constructed through coordination bonds between metal ions/clusters and organic ligands, an attractive nanoporous crystalline material for a variety of potential applications due to its unique structural and physicochemical properties. The as-prepared hollow ZnCdS cages showed significantly enhanced activity and durability in photocatalytic water splitting without any co-catalyst and photosensitizer under visible-light illumination. By adjusting the Cadmium (Cd) content of the

[1] Department of Industrial Chemistry, East Yangon University, Yangon.
[2] Department of Environmental Science and Chemical Engineering, Shanghai University, China.

$Zn_{1-X}Cd_XS$, the chemical composition of the $Zn_{1-X}Cd_XS$ catalysts can be fine-tuned to optimize the light absorption capacity, charge carrier separation efficiency and photocatalytic activity by controlling the conduction band edge of the catalyst (X. Zhao, 2018).

Materials and Methods

Chemicals

Zinc nitrate hexahydrate Zn $(NO_3)_2$. $6H_2O$, 2-methylimidazole ($C_4H_6N_2$), thioacetamide (TAA) and methanol were purchased from Sinopharm Group Chemical Reagent Co., Ltd, China. Cadmium acetate dihydrate Cd $(CH_3COO)_2.2H_2O$, ethanol and ethylene glycol from Adamas Reagent Co., Ltd, China.

Synthesis of ZIF-8 Nanoparticle

ZIF-8 nanoparticle was synthesized according to the method previously reported in literatures. Specific method is as follows: 1.8 g of zinc nitrate hexahydrate (Zn $(NO_3)_2.6H_2O$ containing Zinc (Zn, 6.05 mmol) and 3.96 g of 2-methylimidazole ($C_4H_6N_2$, 48.23 mmol) were separately dissolved in 67.8 g of methanol. The two solutions were rapidly mixed into a glass beaker (300 mL); then a white powdery solid was obtained after stirring for one hour at room temperature. The solid product was centrifuged (4000 rpm, 10 min) and washed with methanol for purification. This procedure was repeated twice. Finally, the resultant ZIF-8 powder was dried in a vacuum drying oven overnight at 80 ℃, then stored in a desiccator before using.

Preparation of the $Zn_{1-X}Cd_XS$ Nanomaterials

The hollow ZnCdS materials were obtained by using ZIF-8 as the precursor. Firstly, hollow ZnS was prepared by the sulfurization of ZIF-8. Briefly, thioacetamide (TAA) (500 mg) was dissolved in 10 mL ethanol. ZIF-8 was mixed with the above solution and treated at 40 ℃ for 24 h under stirring. Then, the obtained hollow ZnS and a certain amount of cadmium acetate dihydrate Cd $(CH_3COO)_2.2H_2O$ were added to 20 mL of ethylene glycol under continuous stirring. After 30 min of continuous stirring, the aqueous solution was transferred to a 100 mL Teflon-lined stainless-steel autoclave as shown in Figure (1) and heated at 160℃ for 4 h in the oven. The resulting hollow ZnCdS was collected via centrifugation, washed thoroughly with ethanol, and dried under vacuum at 40 ℃ for 12 h. By adjusting the amount of Cd $(CH_3COO)_2.2H_2O$, $Zn_{1-x}Cd_xS$ (x= 0, 0.1, 0.3, 0.5, 0.7, 0.9) nanomaterials can be obtained.

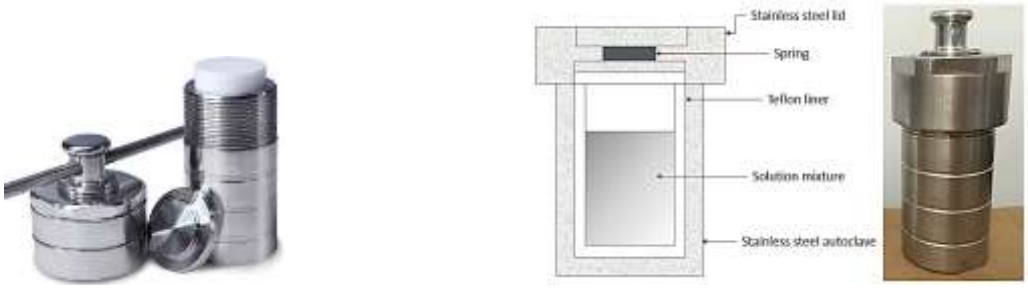

Figure 1: Teflon-lined Stainless-Steel Autoclave

Results and Discussion

Powder X-ray diffraction (XRD) patterns were collected by using by a Bruker D 8 advance X-ray diffractometer that used Cu K α radiation and the diffraction patterns were recorded over the 2θ range of 5-80° with scan rate of 5 min^{-1}. According to Figure 2 (a), the characteristic peak ZIF-8 almost corresponds with the stimulated data from the standard card JCPDS(No.864310).

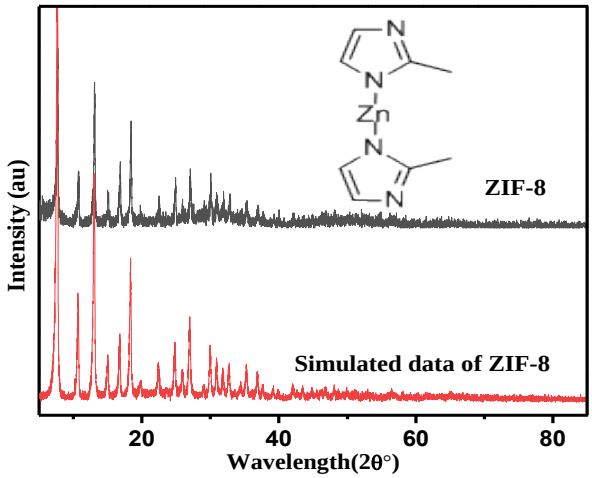

Figure 2: (a) XRD Patterns of ZIF-8

Furthermore, XRD patterns of the hollow $Zn_{1-x}Cd_xS$ with different metal ratios are shown in Figure 2 (b). The XRD pattern of Zn $_{1-x}Cd_xS$ in Figure 2 (b) is consistent with the standard card JCPDS NO.40-0985, indicating that the synthesized $Zn_{1-x}Cd_xS$ crystallinity is relatively high. As compared to the hollow ZnS, the XRD peak positions for $Zn_{1-x}Cd_xS$ were slightly shifted to lower degrees, i.e., from 39.5 to 35.2, 34.9, 33.9 and 33.6, respectively, as the content of Cd increased (x = 0.1, 0.3, 0.5, 0.7 and 0.9) and indicated that an expansion to a higher lattice parameter. This observation suggests the formation of solid solutions rather than simple physical mixtures of ZnS and CdS.

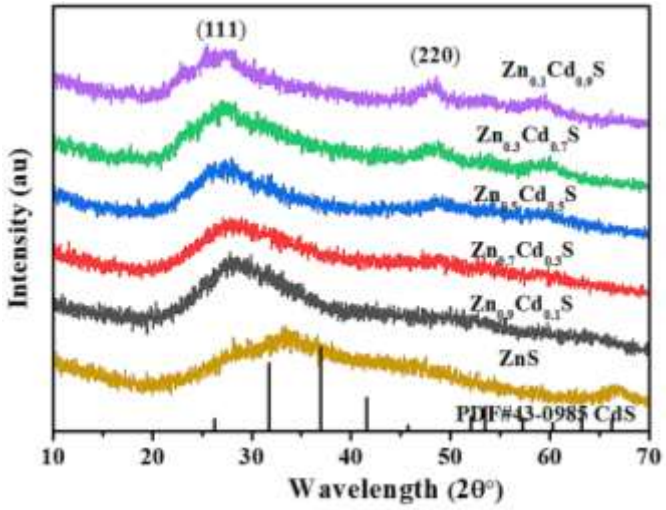

Figure 2: (b) XRD Patterns of the As-synthesized $Zn_{1-x}Cd_xS$ with Different Metal Ratios

The morphologies of the as-prepared ZIF-8 and hollow $Zn_{1-x}Cd_xS$ with different metal compositions were characterized by the SEM images which were performed on Hitachi FESEM-4800. Figures 4 (a) and (b) show the SEM images of ZIF-8 and Figures 4 (c) and 4 (d) are the composite of $Zn_{0.7}Cd_{0.3}S$. The SEM images of ZIF-8 showed highly uniform and well-dispersed rhombic dodecahedral particles. In Figures 4(c) and 4(d), the appearance of composite $Zn_{0.7}Cd_{0.3}S$ has a rhombic shape and the surface is rough and uneven.

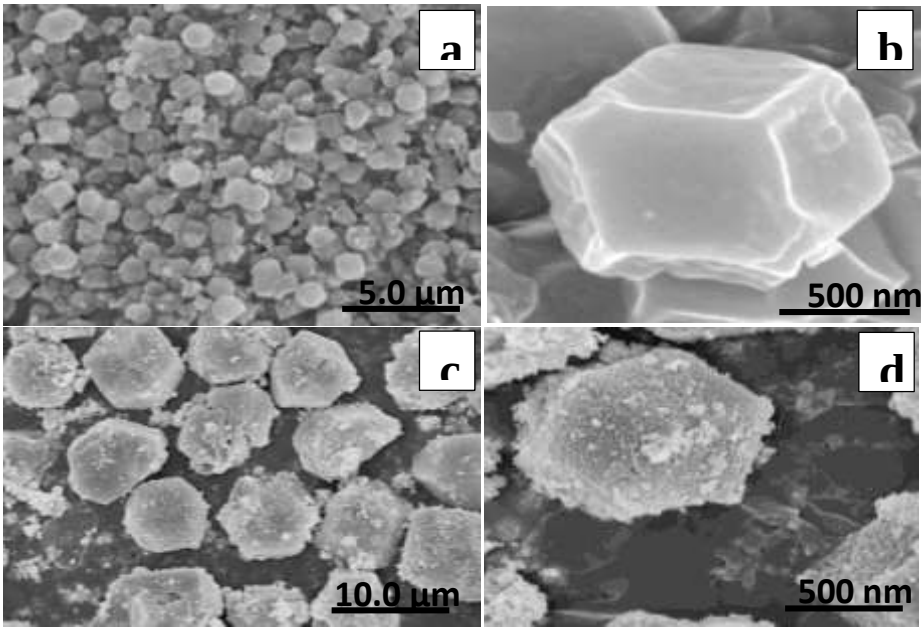

Figure 3: (a) and (b) SEM Images of ZIF-8
(c) and (d) SEM Images of $Zn_{0.7}Cd_{0.3}S$ Composites

Photocatalytic Tests

The photocatalytic hydrogen experiments were conducted in a gas-closed circulation system (CEL-SPH2N) and connected to an on-line gas chromatograph (GC-8A, CEALJ LIGHT) with a thermal conductivity detector (TCD) for fully automated hydrogen detection. The gas in the gas-closed circulation system is automatically extracted into the gas chromatograph system at a set interval, and the specific volume of the produced hydrogen gas can be determined by the peak area through the standard curves. According to a conventional method, 50 mg of the catalyst was weighed and added into a reactor containing 50 mL of deionized water containing 20 % CH_3OH that acts as a sacrificial agent, and continuously stirred by a magnetic stirrer. The low temperature condition of 20 ℃ is controlled by the cooling circulating water system. The light source system is a 300 W Xe lamp (CEL-HXF 300). The hydrogen production by photocatalysis in the laboratory is presented in Schematic Diagram of Figure (4).

Photocatalytic Performance

The photocatalytic hydrogen production experiment was carried out under a visible light irradiation ($\lambda > 400$ nm) with methanol as a sacrificial agent. As shown in Figure 5 (a), the hydrogen yield was negligible when pure ZnS was used as a photocatalyst, owing to its poor visible light absorption. After the introduction of Cd atoms, the activity of $Zn_{1-x}Cd_xS$ was dramatically enhanced. Moreover, the efficient hydrogen production ability of ZnCdS nanocomposites could be well controlled by changing the contents of Cd. The average hydrogen

evolution rate on 3 h for each composite as shown in figures 5 (a) and 5 (b). According to these results, $Zn_{0.7}Cd_{0.3}S$ represented the highest catalytic activity with an average H_2 production rate of 14.1 mmol h^{-1} g^{-1}, ranking among the reported ZnCdS photocatalysts under cocatalyst-free and visible light irradiation ($\lambda > 420$ nm) conditions. This superior photo-catalytic water splitting performance was even beyond that of some sulphide-based catalysts loaded with noble metals as co-catalysts.

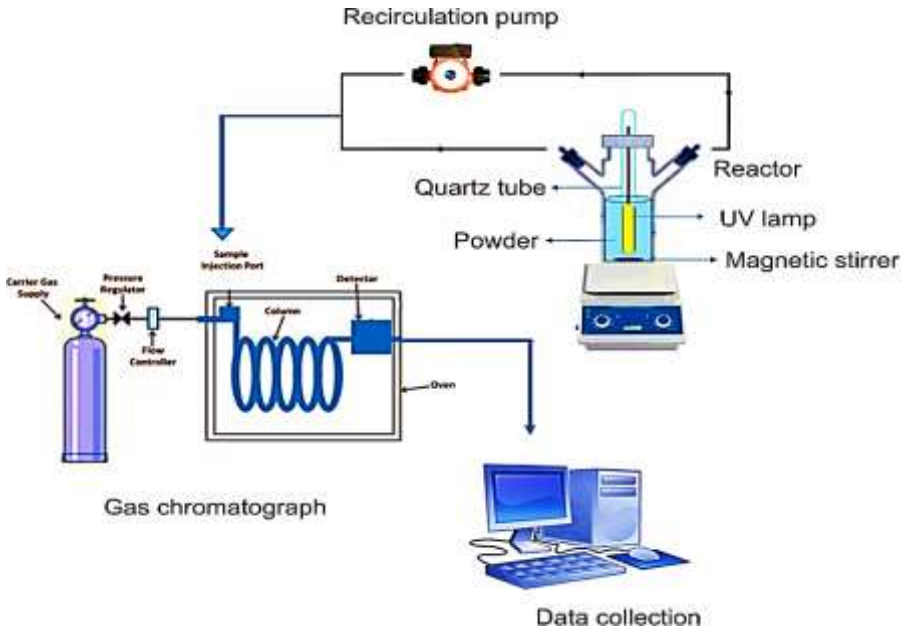

Figure 4: Schematic Diagram of the Reaction System for Hydrogen Production by Photocatalysis

The optical absorption capability of a photocatalyst may have essential impacts on its photocatalytic activity. In this regard, the optical properties of $Zn_{1-x}Cd_xS$ composites were investigated by solid UV-visible diffuse reflectance spectroscopy (UV-Vis DRS). As shown in Figure 6 (a), the as-prepared hollow ZnS cages represented a broad absorption band that extended from the ultraviolet to the near-ultraviolet range and a steep absorption edge. This result was indicative of high phase purity and crystallinity of the hollow material with a uniform structural morphology. The obvious shift of the absorption edges and a significant increase of the absorption intensity in the wavelength region shorter than 520 nm, could be detected with increasing Cd content in the $Zn_{1-x}Cd_xS$ composites.

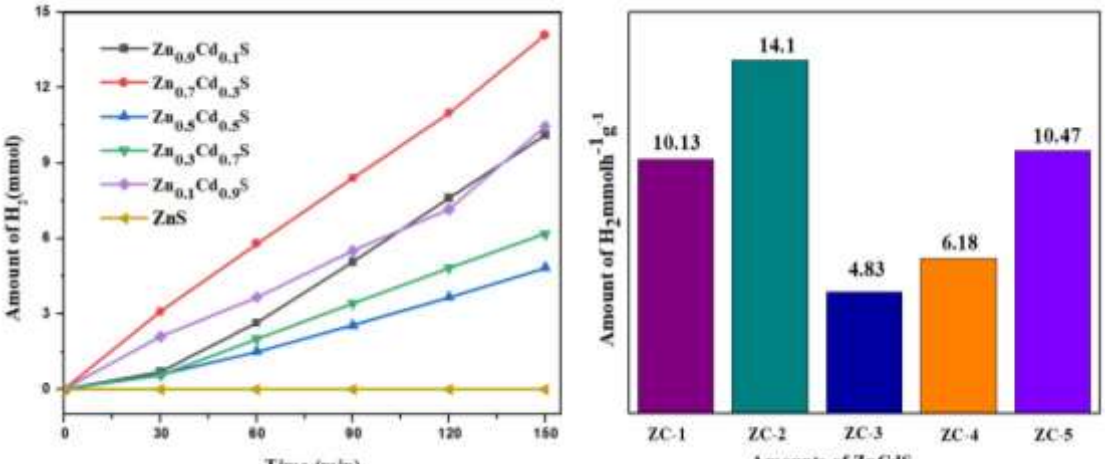

Figure 5: (a) Photocatalytic Hydrogen Generation of $Zn_{1-x}Cd_xS$ Composites (b) Average Hydrogen Evolution Rate of $Zn_{1-x}Cd_xS$ Composites for 3 h

The bandgap energy (Eg) of the as-synthesized ZnS and $Zn_{1-x}Cd_xS$ samples could be estimated from these spectra according to the Kubelka–Munk method using the following equation:

$$\alpha h\nu = A(h\nu - E_g)^{1/2}$$

where α is the absorption coefficient, A is a constant, *hν* is the photon energy and h is Planck's constant. (K. Zhang.et al., 2016). The results are shown in Table (1). The UV-Vis Absorption Spectrum of ZnS and E_g value (3.15eV) of ZnS is shown in Figure 6 (a) and (b). Furthermore, the E_g value of Zn $_{1-x}Cd_xS$ composites varied from 2.34 eV to 2.14 eV, representing mostly a decreasing trend by varying Cd content as shown in Figures 7 (a) and 7 (b). These results indicated that the introduction of Cd atoms into the ZnS structure could significantly lower the E_g values. The data represented that it is more effective harvest of visible light, consequently, implying that these MOF-derivatives might have good visible-light photocatalytic activities. The photocatalytic hydrogen production activity of the as-prepared $Zn_{1-x}Cd_xS$ and its related samples for control experiments were investigated under visible light irradiation (λ > 420 nm) for 3 h in the absence of any cocatalyst.

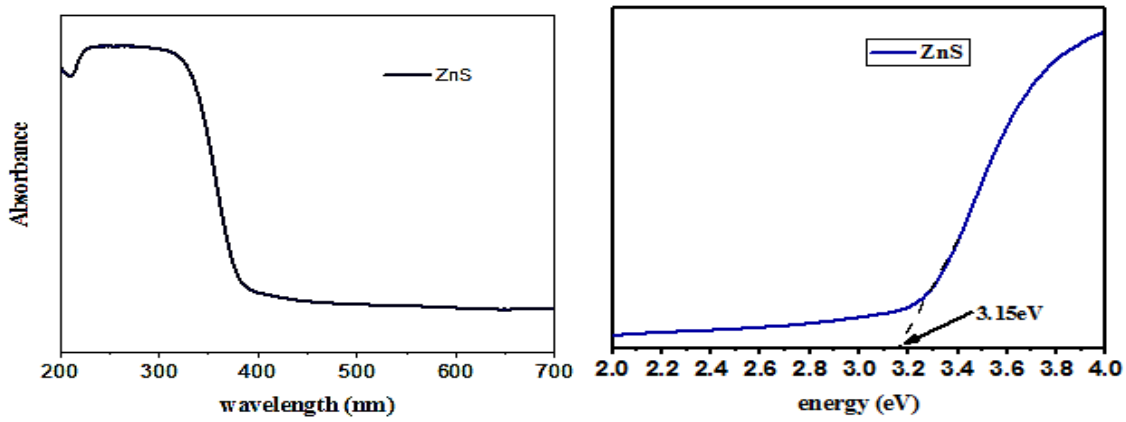

(a) (b)

Figure 6: (a) UV-Vis Absorption Spectrum of ZnS derived from ZIF-ʊ
(b) Curve of Kubelka-Munk Function Plotted Against the Photon Energy

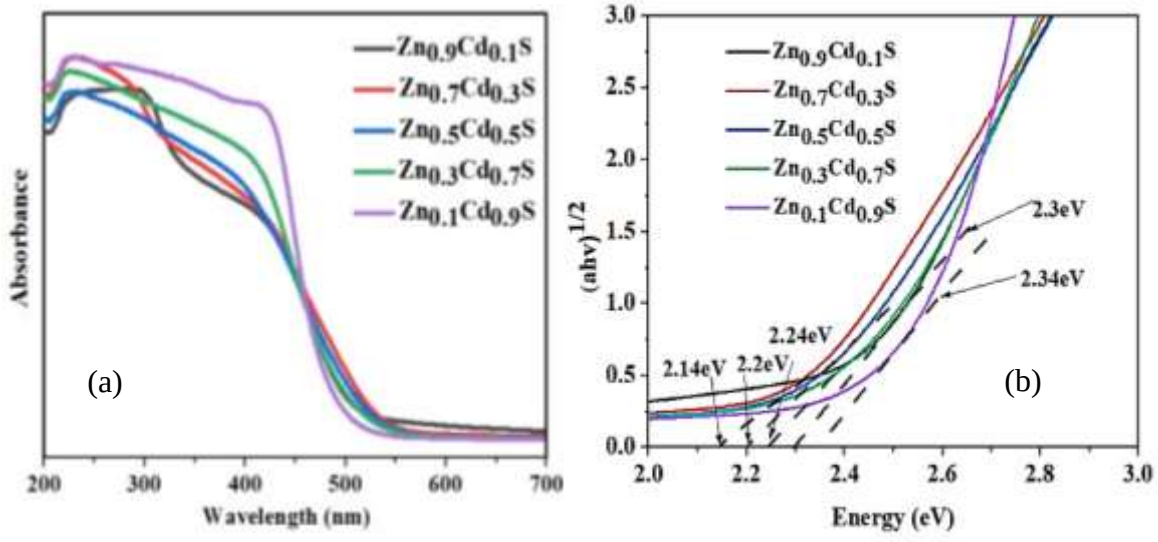

Figure 7: (a) UV-Vis Absorption Spectra of $Zn_{1-x}Cd_xS$ Nanocomposites
(b) Curve of Kubelka-Munk Function Plotted Against the Photon energy

Table 1. Properties of $Zn_{1-x}Cd_xS$ Composites

Sr.No	Catalysts	E_g(eV)	HER (mmol $g^{-1}h^{-1}$)
1.	ZnS	3.15	-
2.	$Zn_{0.9}Cd_{0.1}S$	2.3	10.13
3.	$Zn_{0.7}Cd_{0.3}S$*	2.34	14.1
4.	$Zn_{0.5}Cd_{0.5}S$	2.14	4.83
5.	$Zn_{0.3}Cd_{0.7}S$	2.24	6.18
6.	$Zn_{0.1}Cd_{0.9}S$	2.2	10.47

Conclusion

In conclusion, a metal–organic framework (MOF) template strategy with hydrothermal sulfidation and thermal annealing was successfully developed to fabricate $Znx_{-1}Cd_xS$ for photocatalytic H_2 evolution under visible light irradiation. Turnability of the $Zn_{x-1}Cd_xS$ energy band was realized via changing Cadmium (Cd) concentrations and the optimal photocatalytic activity is primarily influenced by structural and morphological superiorities. ZnCdS catalysts also showed excellent chemical and thermal stability and catalytic durability, suggesting that their great potential in practical applications. In addition, the construction of hollow ZnCdS cages by using MOFs as precursors might bring new opportunities in developing highly effective and durable photocatalysts for a wide range of photochemical applications.

Acknowledgements

I would like to express my profound gratitude to the Myanmar Academy of Arts and Science for permitting to publish this paper. I would first like to express my sincere gratitude to Dr. Nay Win Oo, Rector of East Yangon University, Dr. Aye Aye Ko, Dr. War War Lwin, Dr. Thida Aung, Pro-Rectors of East Yangon University and to professor Dr. Moe Theingi Hlaing, Head of Department of Industrial Chemistry, East Yangon University for their kind encouragement. I would like to express my deepest gratitude to Dr. Tian Liang, Professor, Department of Environmental Science and Chemical Engineering, Shanghai University, China for his suggestions and valuable advices as a supervisor.

References

C. Jianmin, Junying C. and Yingwei L. (2017) Hollow ZnCdS dodecahedral cages for highly efficient visible-light-driven hydrogen generation, Journal of Materials Chemistry A.

C. Xing, Zhang Y., Yan W. and Guo L., 2006, Band structure-controlled solid solution of $Cd_{1-x}Zn_xS$ photocatalyst for hydrogen production by water splitting, International Journal of Hydrogen Energy, Volume31.

E. Patterson, C. Shelden, B. Stockton, 2020, An Efficient and Stable $MoS_2/Zn_{0.5}Cd_{0.5}S$Nanocatalyst for Photocatalytic Hydrogen Evolution, Journal of chemistry in Europe, 26-53, 12206-12211.

K. Zhang, Wang L., and Park J. H., (2016) An order/disorder/water junction system for highly efficient co-catalyst-free photocatalytic hydrogen generation, Journal of Energy and Environmental Science, Issue 2.

K.S. Park, Ni Z., Côté A.P, Choi J.Y., R. Huang, O'Keeffe M.and Yaghi O.M., (2006), Exceptional chemical and thermal stability of zeolitic imidazolate frameworks, National Academic of Science U.S.A.

N. Serpone, D. Lawless, R. Khairutdinov, J.,1995, Size Effects on the Photophysical Properties of Colloidal Anatase TiO_2 Particles: Size Quantization Versus Direct Transitions in This Indirect Semiconductor, the Journal of Physical Chemistry,99,16646-16654.

X. Zhao, Jianrui F., Jing L., Wei S., Guangming Y., Gui-Chang W., and Peng C. (2018) An Efficient, Visible-Light-Driven, Hydrogen Evolution Catalyst $NiS/Zn_xCd_{1-x}S$ Nanocrystal Derived from a Metal–Organic Framework, Journal of German Chemical Society, Volume 57.

Yuan Y. J., Tu J. R., Ye Z. J., Huang Y. W., D. P. Cao, Z. T. Yu and Z. G. Zou, (2016), MoS_2-graphene/$ZnIn_2S_4$ hierarchical microarchitectures between light-harvesting semiconductor and cocatalyst for solar hydrogen generation Applied Catalysis B: Journal of Environmental Science. 188: pp. 13-22**.**

ASSESSMENT OF THE COLOUR DEVELOPMENT OF SHRIMP PASTE

Moe Theingi Hlaing[1]

Abstract

This work is to investigate the quality improvement of Myanmar shrimp paste and to determine the most suitable colorant for shrimp paste from natural sources as well as synthetic products. Natural food colorant, anthocyanin was extracted from purple corn (Tatkon Township, Mandalay Region). Both purple corn-cob and kernel were used for natural colorant. Effects of temperature, extraction time and solvents on the yield percent of anthocyanin were studied. Prepared anthocyanin compounds (cob and kernel) were identified by Fourier Transformed Infrared (FT-IR) Spectroscopy and Ultraviolet Visible (UV/VIS) Spectroscopy. From UV spectrum, corn-cob and kernel extracts are anthocyanidins and anthocyanins. The FT-IR spectrum of extracted compound indicated for hydroxyl group, methoxy group, carbonyl group and secondary alcohol. For synthetic food colorant, secondary permitted food colorants are used to prepare the tertiary color for shrimp paste. Different permitted food dyes were mixed in different ratios to prepare color, suitable for shrimp paste. The color stability of the shrimp paste produced by using natural or synthetic colorants was assessed during one year storage period. Color No.359 was almost identical to natural shrimp paste colour of the better quality and popular one. Synthetic food colorant mixture (Color No.359) was observed to be more attractive to the consumers than anthocyanin extract, although both colorants lasted for 8 months. This research work will support the need of shrimp paste dealers to attract customers.

Keywords: Anthocyanin, shrimp paste, natural or synthetic colorants, purple corn.

Introduction

Myanma Ngapi (Shrimp Paste) is an important source of low cost dietary protein. Ngapi means “Pressed fish”, named by its traditional processing technique. It can be classified into two groups: nga-ngapi (for fish) and hmyin- or seinsa ngapi (for shrimp). Shrimp paste or shrimp sauce, is a common ingredient used in Southeast Asian and Southern Chinese cuisine (Myint Myint Sein, 1999).

Ngapi in Myanmar is known as terasi in Indonesia, kapi in Thai, Khmer and Lao, belacan (also spelled *belachan*, *blachang*) in Malay, mắm ruốc, mắm tép and mắm tôm in Vietnam, bagoong alamang in Philippines, haam ha/ha jeung and hom ha/hae ko in Chinese. Shrimp paste can be used in most meals in Myanmar, Laos, Thailand, Malaysia, Singapore, Indonesia and the Philippines. It is often an ingredient in dipping sauce for fish or vegetables. Its colour ranges from light pink to dark brown.

Shrimp paste varies in forms, some are almost liquid or liquid, some are smooth or other consistencies of paste and some are used as air-dried block forms or powder, depending on the region of the production, or the end product and its uses. At the end of the manufacturing process, shrimp paste is usually dried to reduce the moisture content and to produce a semi-solid product. The paste of the product needs only a little amount of salt and it has a strong umami taste. The drying process and reduction of moisture also increase the shelf life and flavour intensity of the product; complete drying would prevent rancidity of the product (Pérez-Villarreal. B. and Pozo R.,1990).

The color of shrimp varies from yellowish white to pinkish according to the season. During the hot season, the shrimp is pinkish and shrimp paste produced from this kind of shrimp is purple pink and its taste is more delicious than the rest. Most shrimp paste consumers prefer such kind of purple pink shrimp paste. The role of natural or synthetic colorant becomes important for yellowish white shrimp to meet customers’ demand.

[1] Department of Industrial Chemistry, East Yangon University

Materials and Method

Materials

Zea mays L. purple corn, purchased from Tatkon Township, Naypyidaw Region and *Mysis diluviana* shrimp from Naukmee Village, Pyapon Township were used for this research. The certified colors of commercial grade, manufactured by the Ram Ratna International Co., Ltd. Ram Ratna House, Victoria Mill Compound, PB Marg, Worli, Mumbai 400 013 (India) were used for synthetic color.

Extraction of Anthocyanin from Purple Corn-Cob and Kernel

The purple corns were threshed and corn-cobs were air-dried for five days. Dried purple corn-cobs were crushed before milling in a grinder. The milled corn-cobs were screened and then stored in a desiccator for the extraction of anthocyanin. Dry corn-cob granules (50 g) were mixed with 30 mL of 95 % ethanol in a beaker, and warmed in a water bath at 40 °C for 5 h. The mixture was filtered and the filtrate was put into a round-bottomed flask and then distilled. During distillation, the pressure of the solution was reduced to about 140 mmHg by using a vacuum pump. At this pressure, the boiling point of ethanol was reduced from 78.8 °C to 60 °C and ethanol was quickly evaporated. The ethanol was collected as condensate and anthocyanin was left in the flask with a small amount of ethanol. After air drying, the dried anthocyanin was weighed and stored for further analysis.

Purple corns were threshed and corn kernels were air-dried for five days and stored in a desiccator for the extraction of Anthocyanin 1 (c). The extractions were conducted as previously described and the results are shown in Tables 2, 3 and 4.

(a) **(b)** **(c)**

Figure 1: (a) Purple Corn
(b) Purple Corn Plant
(c) Purple Corn Maize

(a) **(b)**

Figure 2: (a) Purple Corn Cob (b) Extracted Anthocyanin from Purple Corn Cob

Effect of Extraction Temperature, Time and Solvents on the Yield of Anthocyanin

The extractions were conducted at different extraction temperature of 30 °C, 40 °C, 50 °C, 60 °C and 70 °C, with different extraction times of 3 h, 4 h, 5 h and 6 h at 60˚C, using different solvents such as distilled water, 95 % ethanol and ethanol acidified with 1 % citric acid. The results are shown in Tables 1, 2 and 3.

Table 1: Effect of Temperature on Extraction of Anthocyanin from Purple Corn

Sr. No	Extraction Temperature (°C)	Weight of Corn Cob/Kernel (g)	Anthocyanin Yield	
			Cob % (w/w)	Kernel % (w/w)
1.	30	50	0.5682	0.0825
2.	40	50	0.7218	0.0922
3.	50	50	0.8064	0.1143
4.	60*	50	0.9658	0.1592
5.	70	50	0.9826	0.1659

*60˚C is the most suitable extraction temperature.

Table 2: Effect of Extraction Time on Extraction of Anthocyanin from Purple Corn

Sr. No	Extraction Time (h)	Weight of Corn Cob/Kernel (g)	Anthocyanin Yield	
			Cob % (w/w)	Kernel % (w/w)
1.	3	50	0.7152	0.0967
2.	4	50	0.7966	0.1348
3.	5*	50	0.9658	0.1582
4.	6	50	0.9686	0.1631

*5 hr is the most suitable extraction time

Table 3: Effect of Solvents on Extraction of Anthocyanin from Corn Cob and Kernel

Sr. No	Solvents	Weight of Corn Cob/Kernel (g)	Anthocyanin Yield	
			Cob % (w/w)	Kernel % (w/w)
1.	Water	50	0.6532	0.0654
2.	95 % ethanol	50	0.9658	0.1582
3.	ethanol acidified with 1% citric acid *	50	0.9972	0.1865

* ethanol acidified with 1% citric acid is the most suitable solvent for extraction of anthocyanin.

Analysis of Extracted Anthocyanin

Identification of Anthocyanin by Ultraviolet Spectroscopy

Anthocyanin exhibits very high extinction coefficients between 270 - 280 nm and 465 - 560 nm wavelengths. Prepared Anthocyanins were identified by Ultraviolet Visible (UV/VIS) Spectroscopy [Figures 5 and 6 and Table 6].

Identification of Anthocyanin by Infrared (IR) Spectroscopy

Prepared anthocyanins (cob and kernel) were identified by Infrared (IR) Spectroscopy Figures 7 and 8, Tables 7 and 8.

Application of Prepared Anthocyanin on Shrimp Paste

About 100 g of shrimp from Pyapon Township was washed and weighed. Prepared natural food colorant, anthocyanin 0.01 % (w/w) was added to the shrimp before mixing with salt to prepare shrimp paste.

Preparation of Mixed Synthetic Food Colourants for Shrimp Paste

The most suitable food colorant for shrimp paste was produced by mixing 50 % of grape purple, 25 % of raspberry red and 25 % of bright red colors, known as color number 359.

Table 4: Properties of Certified Colors for Food Products

Sr. No.	Colour Name	Commercial Name	C.I. No*	Colour	pH	Density
1.	Bright red (E124)	Ponceau 4R	16255	Bright red colour	6-8	0.8
2.	Grape purple	(Brilliant Blue +Ponceau 4R) Blended Colour	75300 + 16255	Purple	6.5-8	0.7
3.	Raspberry red (E122)	Carmoisine	14720	red	6-8	0.7
4.	Strawberry red	Blended Colour	-	Strawberry	6-8	0.7

* C.I. No = Colour Index Number

Application of Synthetic Food Colourants on Shrimp Paste

About 100 g of shrimp from Pyapon Township, Naukmee village was washed, weighed and mixed with synthetic colorants. Each synthetic food colorant of 0.01 % (w/w) and 0.005 % (w/w) of prepared synthetic colorants mixture were used for coloring shrimp to produce shrimp paste.

(a) **(b)** **(c)**

Figure 3. (a) Mixed Permitted Color Solution for Shrimp Paste
(b) Suitable Permitted Color for Shrimp Paste
(c) Shrimp Paste with Certified Synthetic Colour

Results and Discussion

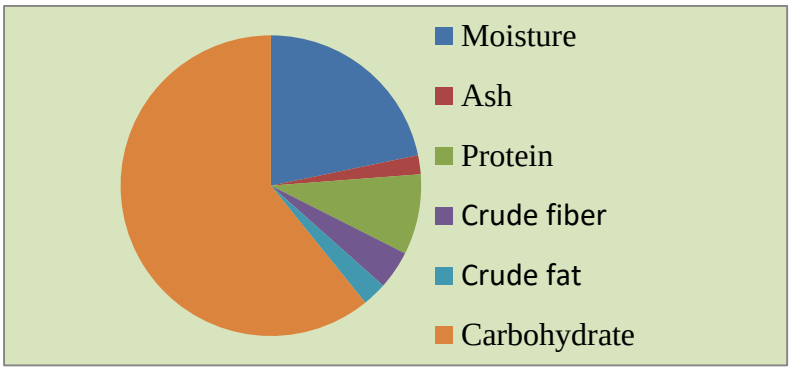

Figure 4: Nutritional facts of purple corn kernel

Nutritional values such as protein, ash, moisture content, crude fiber and crude fat (ether extract) of purple corn kernel were analyzed and results are shown in Figure (4).

The effects of extraction temperature, extraction time and nature of solvents on the yield of anthocyanin from purple corn cob and kernel are described in Tables (1) to (3) and. The most suitable extraction temperature was 60°C, extraction time was 5 hours and ethanol acidified with 1% citric acid was the best solvent for maximum yield of anthocyanin in this research work.

The UV spectrum of extracted anthocyanin from purple corn cob [Figure (5) and Table (6)] showed the flavonoid band I and band II in methanol at 531.2 nm and 278 nm. These absorption bands match with that of anthocyanins and anthocyanidins (Band I 465-560 nm; Band II 270-280 nm) (Markhan, 1982). Therefore, from UV spectrum, it can be concluded that corn cob extracts are anthocyanidins and anthocyanins.

The UV spectrum of extracted anthocyanin from purple corn kernel [Figure 6 and Table 6] showed the flavonoid band I and band II in methanol at 526.2 nm and 284.4 nm. These absorption bands match with that of anthocyanins and anthocyanidins (Band I 465-560 nm; Band II 270-280 nm) (Markhan, 1982). So, from UV spectrum, it can be said that corn kernel extracts are anthocyanidins and anthocyanins.

The FT-IR spectrum of extracted anthocyanin [Figure 7 and Table 7] indicated the stretching -OH group at 3392 cm^{-1} for the hydroxyl group. The absorption band at 2926 cm^{-1} due to CH_3, indicated the methoxy group. The absorption band at 1726 cm^{-1} is due to C=O, indicated

the carbonyl group. The stretching for C=C unsaturated cyclic ring is at 1631, 1514 cm^{-1}. The in-plane bending - OH at 1383, 1332 cm^{-1} was the hydroxyl group. The stretching C-O at 1267, 1211, 1076 and 1055 cm^{-1} is stretching C-O. The absorption band at 611 cm^{-1} detected the out-of-plane bending -CH.

The FT-IR spectrum of extracted compound [Figure 8 and Table 8] indicated the stretching-OH group at 3383 cm^{-1} for hydroxyl group. The absorption band at 2926, 2852cm^{-1} due to CH_3 indicated the methoxy group. The absorption band at 1718 cm^{-1} due to C=O, indicated the carbonyl group. The stretching for C=C unsaturated cyclic ring is at 1641 cm^{-1}. The in-plane bending -OH at 1408 cm^{-1} directed the hydroxyl group. The stretching C-O at 1269, 1078 and 1045 cm^{-1} is arc -OH and secondary alcohol. The absorption band at 570 cm^{-1} detected the out-of-plane bending -CH.

Shrimp paste prepared with natural and synthetic colorant was stored for one year and their color stability was assessed [Table 6]. Anthocyanin colorant gave delicate pink color although the color itself was bright. The shrimp paste using synthetic colorant was brighter than the common shrimp paste color. It is found that their color intensity was not suitable for shrimp paste. The color of shrimp paste using the synthetic color retained up to six months. There is neither color irregulation nor color changes of shrimp paste during six months. After six months, the shrimp paste with the synthetic pink color gradually changed into brown.

Shrimp paste sample with mixed synthetic food colourant known as colour number 359 (colourant mixture) is shown in Figure [3 (c)]. Most of the shrimp paste processors concluded that color No.359 is almost identical to the color of natural shrimp paste of better quality and popular one. Synthetic food colorant mixture (Color No.359) was observed to be more attractive to consumers than anthocyanin, although both colorants lasted for 8 months. These certified colorants are the ones that FDA Myanmar permitted for food preparation. These colors have no adverse effect on the human health. This research work gave useful information to improve the quality of Myanmar shrimp paste. This food permitted synthetic color from Ram Ratna International Co., Ltd. solved the problems for shrimp paste. This colour can be used to substitute the hazardous chemical dyes that were previously used in shrimp paste. This work also participates correct usage to produce the marine-based foods.

Table 5: Effect of Natural and Synthetic Color on Shrimp Paste

Sr. No.	Name of Colourant	Type of Colourant	Amount of Colourant % (w/w)	Colour of Shrimp Paste	Intensity of Colour
1.	Anthocyanin	Natural	0.01	Pinkish brown	Last for 8 months
2.	Raspberry red	Synthetic	0.01	Deep red	Last for 8 months
3.	Bright red	Synthetic	0.01	Bright red	Last for 8 months
4.	Strawberry red	Synthetic	0.01	Pinkish red	Last for 8 months
5.	Mixed colour suitable for shrimp paste	Synthetic	0.005	Purple pink	Last for 6 months

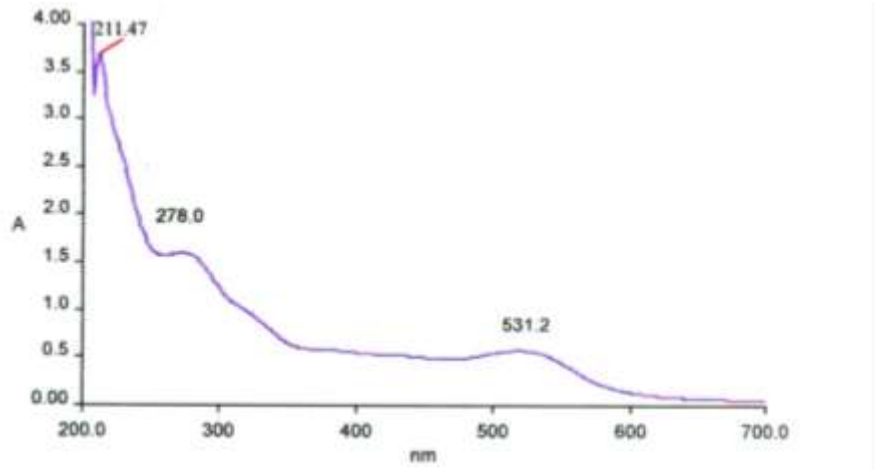

Figure 5: UV Spectrum of Extracted Anthocyanin (Corn Cob)

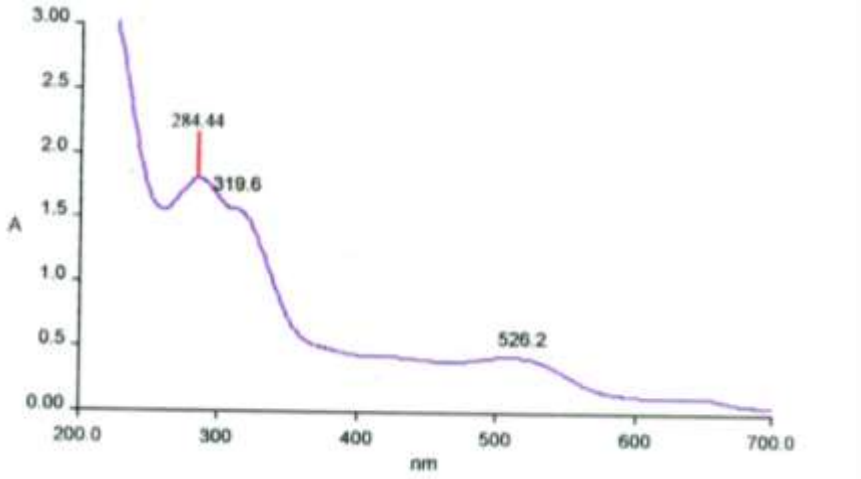

Figure 6: UV Spectrum of Extracted Anthocyanin (Corn Kernel)

Table 6: UV/VIS Data of Extracted Anthocyanin (Corn Cob & Corn Kernel)

Wave Number (nm)		**Assignment**	**Remarks**
Observed	**Literature***		
278	270-280	Band Π ππ*	Flavonoids compounds are anthocyanins and anthocyanidins (Conjugated double bonds are present)
531.2	465-560	Band I n-π*	
284.4	270-280	Band Π π -π*	Flavonoids compounds are anthocyanins and anthocyanidins (Conjugated double bonds are present)
526.2	465-560	Band I n-π*	

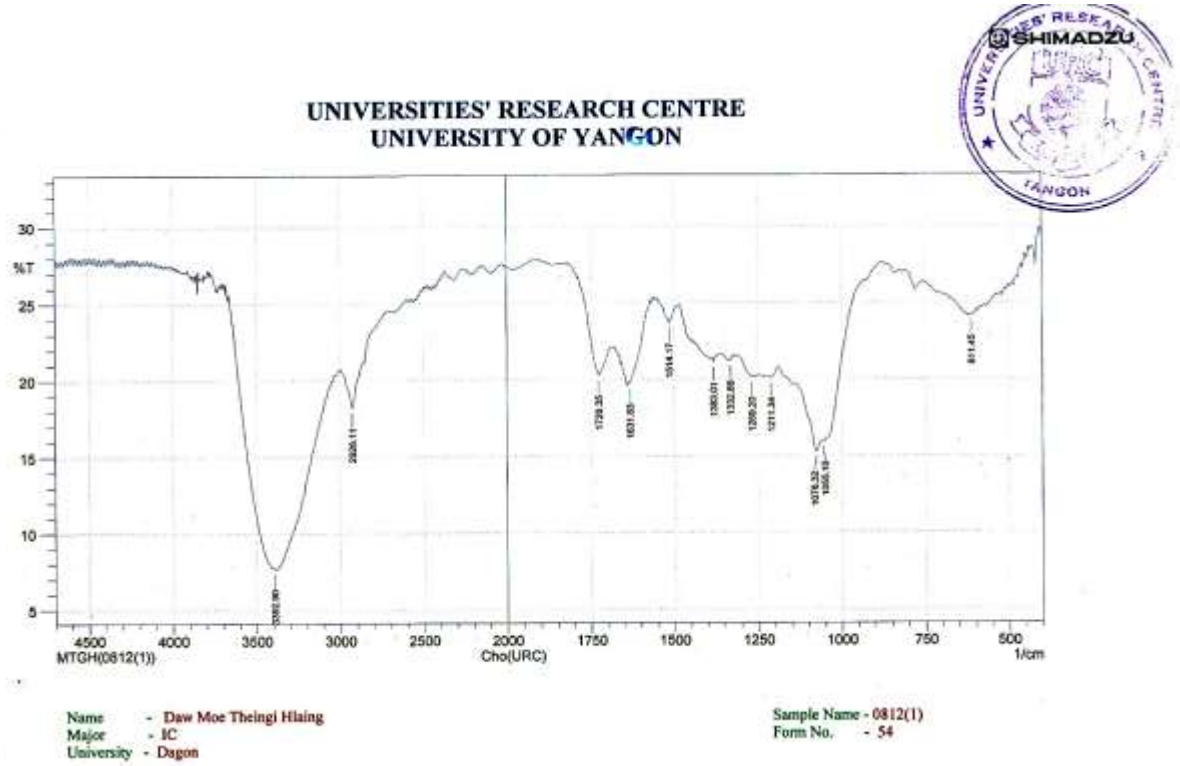

Figure 7: FT-IR Spectrum of Extracted Anthocyanin (Corn Cob)

Table 7: FT-IR Data of Extracted Anthocyanin (Corn Cob)

No.	Wave number, cm^{-1}		Functional Group	
	Observed	Literature*		
1.	3392	3550-3300	$\upsilon_{=OH}$	OH, stretching for alcohol or phenolic compound
2.	2926	~2800	$\upsilon_{=CH3}$	stretching vibration of methoxy group
3.	1726	~1700	$\upsilon_{C=O}$	stretching vibration of carbonyl group
4.	1631,1514	~1600	$\upsilon_{C=C}$	C = C stretching for unsaturated cyclic ring
5.	1383,1332	~1400	δ_{sCH}	C-H symmetric bending vibration
6.	1269,1211 1076,1055	1200-1000	$\upsilon_{c=O}$	stretching vibration of CO group
7.	611	900-450	δ_{CH}	C-H out of plane bending vibration

* Mohan 2000

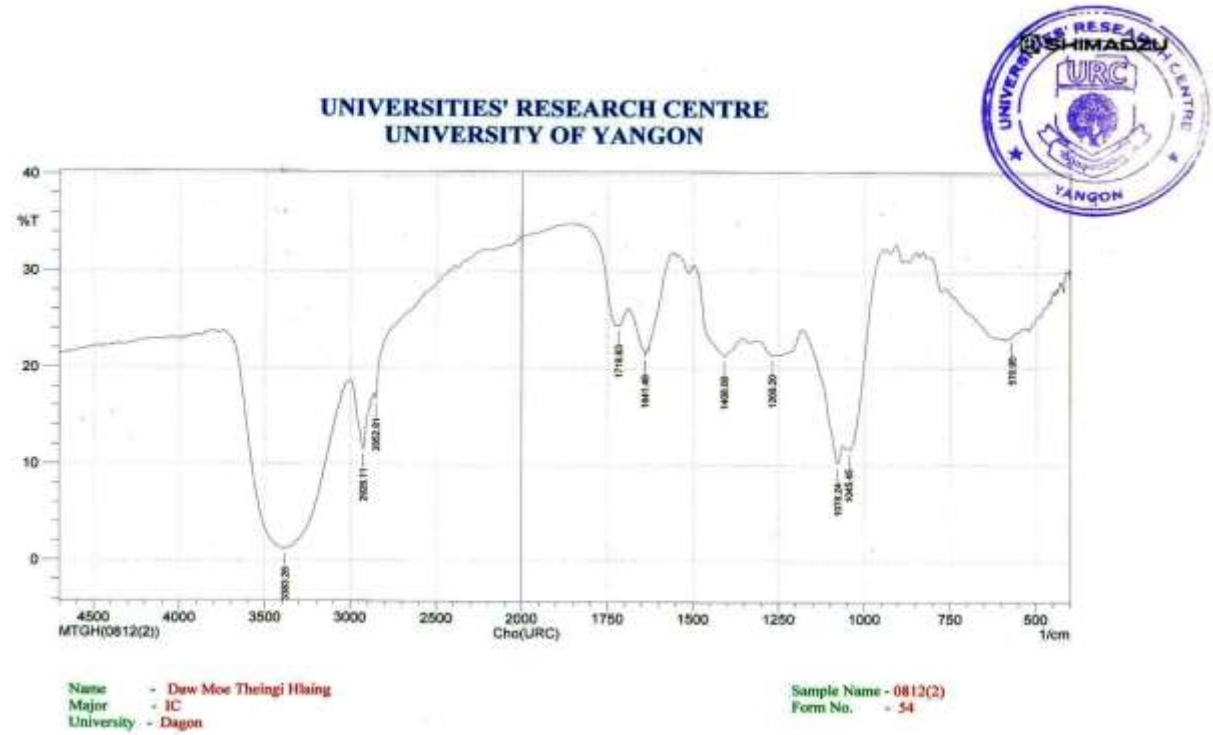

Figure 8: FT-IR Spectrum of Extracted Anthocyanin (Corn Kernel)

Table 8: FT-IR Data of Extracted Anthocyanin (Corn Kernel)

No.	Wave N		Functional group	
	Observed	Literature*		
1.	3383	3550-3300	$\upsilon_{=OH}$	OH, stretching for alcohol or phenolic compound
2.	2926,2852	~2800	$\upsilon_{=CH3}$	stretching vibration of methoxy group
3.	1718	~1700	$\upsilon_{C=O}$	stretching vibration of carbonyl group
4.	1641	~1600	$\upsilon_{C=C}$	C = C stretching for unsaturated cyclic ring
5.	1408	~1400	δ_{sCH}	C-H symmetric bending vibration
6.	1269,1078,1045	1200-1000	$\upsilon_{c=O}$	stretching vibration of CO group
7.	570	900-450	δ_{CH}	C-H out of plane bending vibration

* Mohan 2000

Conclusion

The IR spectra of extracted anthocyanin samples show the possible functional groups for characteristic absorption peaks of IR spectra. Based on these results, it can be concluded that the samples contain anthocyanin. Anthocyanins from purple corn are water-soluble pigments that may appear red, purple, or blue colours depending on pH.

The valuable anthocyanin extract can be used as natural colorant for shrimp paste. The optimum conditions for the extraction of anthocyanin from purple corn are, extraction temperature 60 °C and extraction time 5 h to give a yield of 0.9658 % w/w. The solvent which should be used is ethanol acidified with 1 % citric acid.

On the other hand, extracted anthocyanin gives light color on shrimp paste and the resultant color was not satisfactory for shrimp paste processors. The synthetic mixed colorant, color number 359 gave the most suitable color on shrimp paste. Both of their stabilities overcome the need of shrimp paste dealer.

Acknowledgements

I am grateful to Dr Nay Win Oo, Rector and Dr Aye Aye Ko, Dr Wah Wah Lwin and Dr Thida Aung, Prorectors of East Yangon University for giving permission to submit this paper. I would like to express my deepest gratitude to Dr Khin Thet Ni, Head of Department of Industrial Chemistry (Retd.), University of Yangon, and Professor Dr Cho Cho Oo, Head of Department of Industrial Chemistry, (Retd.), University of Yangon, for giving permission to perform this research and advice throughout this research work.

References

Faithong N., Benjakul S., Phatcharat S., Binsan W, 2010, (133-140) Chemical composition and antioxidative activity of Thai traditional fermented shrimp and krill products. Food Chemistry 119 (133–140)

FDA, 2001, Fish and Fishery Products Hazards and Controls Guidance, Scombrotoxin (Histamine Formation),3rd Edition

Hajeb. P, Jinap S.,2013, Umami taste components and their sources in Asian foods. Crit Rev Food Sci 8:1102–1115

Hajeb and Jinap, J Nutr Food Sci., 2012, Fermented Shrimp Products as Source of Umami in Southeast Asia

Haras, Alina, OvidiuToma, 2007, Determination of total proteins in some products

Harborne, J. B, 1973, Phytochemical Methods: A Guide to Modern Technique of Plant Analysis, Chapman and Hall, London

HPLC Basics, Fundamentals of Liquid Chromatography (HPLC), Courtesy of Agilent Technologies, Inc

Ishige N.,1993, Cultural aspects of fermented fish products in Asia. Fish fermentation technology, United Nations University Press

Malle and Poumeyrol, M.1989. A new chemical criterion for the quality control of fish; Trimethyl amine/Total volatile basic Nitrogen (%). Journal of food protection, 52(6):419-423

Markhan, K R. 1982, Techniques of Flavonoid Identification, Academic Press Inc., London New York

Mohan. J, 2000, Organic Spectroscopy: Principles and Applications, Narosa Publishing House, New Delhi

Myint Myint Sein, 1999, The mode of fermentation of shrimp paste, Chemistry, Ph D dissertation, Yangon University

Ogunwande, Dr. I.A., 2011, Colour Chemistry and Technology

Orella. C.J. and D.J. Kirwan, 1989, The Solubility of Amino Acids in Mixtures of Water and Aliphatic Alcohol Peralta E.M. et al, 2008, Food Chemistry 111,72-77

Pérez-Villarreal B. and Pozo R., 1990, Chemical composition and ice spoilage of albacore *(Thunnus alalunga) Journal of Food Science,* 55 678-682

Yoshida Y.1998, Umami taste and traditional seasonings. Food Rev Int 14: 213 246

http://purple-corn.html {Accessed August 2012}

www.purple-corn- drink html {Accessed August 2012}

Anthocyanin.htm {Accessed August 2012

PROCESSING AND CHARACTERIZATION OF FERMENTED FOODS FROM LOCALLY AVAILABLE GREENGAGE PLUM

Ei Thu Zar Naing[1], Mon Mon Maung[2]

Abstract

Fermented foods have been produced from all manner of plant materials and not only from fruits. The conversion of raw food materials into finished fermented products is considered to be one of the best examples of "value added" processing. This research focused on the preparation of fermented food from locally available greengage plums and on the effects of sugar, yeast, fermentation and storage time on the properties of fermented food over a 1-year fermentation period. Firstly, characteristics of greengage plum were studied and greengage plum wine was processed with variations in sugar, yeast and fermentation period; the properties of the prepared wines were also analysed. The effects of these on the product's characteristics were investigated. Secondly, greengage plum syrup was prepared by fermenting greengage plums with varying sugar levels and storage times. The color of fermented foods was determined by UV Spectrophotometer, and the acceptability of experimental fermented foods was perceived by sensory evaluation using 9-Point Hedonic Scale Rating Test. The most suitable greengage plum syrup was obtained at the ratio of greengage plum to sugar (1:1). The highest alcohol content 10 % (v/v) in prepared greengage plum wine was formed with 1: 0.75 greengage plums to sugar ratio after seven weeks of fermentation period.

Keywords: greengage plum, fermented food, fermentation

Introduction

Fermented foods and alcoholic beverages have long been an important part of the human diet in nearly every culture on every continent. These foods are often well-preserved and serve as stable, significant sources of protein, vitamins, minerals, and other nutrients. Despite these standard features, there are many differences in substrates and products, and the types of microbes involved in the manufacture of fermented foods and beverages produced worldwide. Fermented foods and beverages depend on dietary comsumers' habits, as well as regional agricultural conditions and resources availability (Kamboj, Gupta, Bandral and Gandotra & Anjum, 2020).

The greengage plum is an important and widely cultivated temperate fruit crop with attractive colour and flavour. It is a highly perishable fruit with a shelf life of 3-4 days at ambient temperature and 1-2 weeks in cold storage. Production of alcoholic beverages from this fruit is a profitable alternative. It has demonstrated its potential for the preparation of alcoholic beverages, including wine and vermouth (Rastogi & Shukla, 2013).

Fruit syrups or fruit molasses are concentrated fruit juices used as sweeteners. Some foods are made using fruit syrups or molasses. In modern industrial food production, they are often made from less expensive fruits (such as apples, pears, or pineapples) and used to sweeten more expensive fruits or products and to extend their quantity. Wine may be defined as the usually fermented juice of a plant product (as a fruit) used as a beverage. To make a wine of acceptable quality, several approaches have been used, including yeast, dilution with water, and blending with low-acid juices. Besides, the sugar used to improve the must for fermentation to produce wine with a desirable alcoholic content profoundly influences on wine quality (Vyas & Joshi, 1982).

The term *fermentation* refers to microbial cell growth and the production of products under aerobic, microaerobic, or anaerobic conditions. The secretion of metabolites from the inside of microbial cells to the surrounding medium, and their accumulation in the medium,

[1] Department of Industrial Chemistry, University of Mandalay
[2] Department of Industrial Chemistry, University of Mandalay

occur as a consequence of the oxidation of monosaccharides, particularly glucose, under both aerobic and anaerobic conditions (Bisson, Butzke, and Ebeler, 1995). The main objective of this research was to prepare the fermented foods from greengage plum and to enrich food substrates with protein, essential amino acids, and vitamins. The specific objectives of this study were to study the characteristics of the greengage plum to prepare the fermented food from the greengage plum, and to analyse the properties of processed greengage plum syrup and wine.

Materials and Methods

Materials

Raw materials for the processing of fermented foods (syrup and wine) and greengage plums were collected from Wundwin Township, Mandalay Region. Sugar was purchased from Ocean Supermarket, Chan Mya Thar Si Township, Mandalay Region. The needed chemicals for processing were purchased from Wine Making Supplies & Equipment, Kywal Sal Kan 10th, between 78th and 79th, Mandalay.

Methods

Processing of Greengage Plum Syrup

Greengage plums were washed, drained and thoroughly dried. Any stems including the stubs near the stem, were removed. Alternating layers of sugar and plums were placed in a glass bottle. The glass bottle was covered and left in a cool place for 90 days. After 90 days, the plums with seeds were removed, and the syrup was stored at room temperature.

Processing of Greengage Plum Wine

Greengage plums were pitted, cut into pieces, and frozen overnight in a glass fermenter. After defrosting, three quarts of boiling water were poured over the plums. Once cooled, pectic enzyme, yeast nutrient, lemon juice, and wine yeast were added. The fermenter was loosely covered, and the mixture was fermented for five days. To prepare the sugar syrup, sugar was dissolved in boiling water to achieve 30 °Brix, then cooled and filtered to obtain a clear syrup. This syrup was added to the fermenting mixture, and additional water was added as needed. The must was stirred twice daily during fermentation. When fermentation ceased and no bubbles appeared in the airlock for at least five minutes, the fruit mash was strained through cheesecloth. The resulting wine was racked three times for clarification, then stored in sterilized wine bottles.

Characterization

The physicochemical characteristics of greengage plum, syrup, and wine were determined. Moisture content, ash content, fibre content, protein content, fat content, and carbohydrate content were analyzed using AOAC methods. pH and soluble solids (°Brix) were measured using a pH meter and a refractometer, respectively. To determine the alcohol content, the specific gravity of each sample was first measured and then converted to the corresponding alcohol percentage (% v/v) using the Standard Alcohol Density Table. Colour (absorbance) was measured using a UV spectrophotometer (UV-1800 Shimadzu). Reducing sugar was determined by the Lane-Eynon method. A sensory evaluation (organoleptic properties) of greengage plum syrup and wine was also conducted, based on colour, taste, odour, and overall acceptability, using a panel of 15 semi-trained panelists. The scoring was based on a 9-point Hedonic Scale, where: 9 = like remarkably, 8 = like very much, 7 = like moderately, 6 = like slightly, 5 = neither like nor dislike, 4 = dislike slightly, 3 = dislike moderately, 2 = dislike very much, and 1 = dislike immensely. Overall acceptability was calculated as the average score of all these organoleptic attributes.

Results and Discussion

Fermented food preparation serves not only as an example of value-added processing, but also as an ancient technology. Fermentation is highly effective method for preserving foodstuffs at industrial level. This paper provides a general overview of the production of greengage plum syrup and wine, with a particular emphasis on the quality of fruit used for food processing.

The physicochemical characteristics of the greengage plum were determined for pH, acidity, soluble solids, moisture content, ash content, fibre content, protein content, fat content, carbohydrate content, and compared with the literature values. Moisture content, ash content, fibre content, protein content, fat content, carbohydrate content of greengage plum were 4.89, 0.33, 1.25, 0.65, 0.25, and 10.8 respectively, which were higher than the literature values. The soluble solids (°Brix), pH, acidity, reducing sugar content of greengage plum were 9.77, 2.61, 2.47, and 7.19 respectively, and were nearly similar to the literature values. The quality of fruit could also be affected by the cultivation method, e.g., organic or conventional.

Table 1: Effect of Volume of Sugar Syrup on the Characteristics of Prepared Greengage Plum Wine

Weight of Greengage Plum - 2000 g

Weight of Yeast - 3 g

Fermentation Period - Seven Weeks

Sr. No.	Sugar Syrup (mL)	Characteristics of Prepared Greengage Plum Wine				
		pH	Acidity	Soluble Solids (°Brix)	Specific Gravity	Alcohol Content % (v/v)
1.	0	3.55	0.69	12	1.0731	6
2.	500	3.68	0.65	13	1.0653	7
3.	1000	3.71	0.54	16	1.0534	9
4.	1500*	3.85	0.53	18	1.0458	10
5.	2000	3.91	0.49	15	1.0613	8

* The most suitable condition

Effects of volume of sugar syrup and weight of yeast on the characteristics of prepared greengage plum wine were analysed and are shown in Tables 1 and 2, respectively. Acidity is an important factor, as it contributes directly and indirectly to wines quality (Clarke & Baker, 2004). The pH of the prepared wine increased gradually as the acidity decreased with increasing volume of sugar syrup. Soluble solids (°Brix) and alcohol content of prepared wine were also increased but the specific gravity of prepared wine was decreased. The alcohol content of wines depended on the amount of sugar used in wine making. Soluble solids (°Brix) of prepared wine were also an important quality parameter and an indicator of the stability and completeness of fermentation. After 7 weeks of fermentation, the highest alcohol content of 10 % (v/v) was obtained using 3 g of yeast in wine making. If there was too much yeast during wine fermentation, it caused off-flavours and a shortened wine shelf life. Yeast affected not only the alcohol content of prepared wine, but also its aroma, character, mouthfeel, and flavor.

Table 2: Effect of Weight of Yeast on the Characteristics of Prepared Greengage Plum Wine

Weight of Greengage Plum - 2000 g
Volume of Sugar Syrup - 1500 mL
Fermentation Period - Seven Weeks

Sr. No.	Yeast (g)	Characteristics of Prepared Greengage Plum Wine				
		pH	Acidity	Soluble Solids (°Brix)	Specific Gravity	Alcohol Content % (v/v)
1.	1	3.53	0.69	11	1.0623	6
2.	2	3.65	0.65	12	1.0552	7
3.	3*	3.83	0.54	18	1.0458	10
4.	4	3.84	0.51	15	1.0523	9
5.	5	3.89	0.48	14	1.0535	8

* The most suitable condition

Table 3: Effect of Fermentation Period on the Characteristics of Prepared Greengage Plum Wine

Weight of Greengage Plum - 2000 g
Volume of Sugar Syrup - 1500 mL
Weight of Yeast - 3 g

Sr. No.	Fermentation Period (Weeks)	Characteristics of Prepared Greengage Plum Wine				
		pH	Acidity	Soluble Solids (°Brix)	Specific Gravity	Alcohol Content % (v/v)
1.	1	3.87	0.51	11	1.0675	6
2.	3	3.85	0.52	13	1.0573	8
3.	5	3.84	0.55	15	1.0465	9
4.	7*	3.83	0.54	18	1.0451	10
5.	9	3.63	0. 69	17	1.0451	10

* The most suitable condition

Table 4: Effect of Fermentation Period on the Yield of Alcohol Content in Greengage Plum Wines

Fermentation Period (Weeks)	Yield of Alcohol, % (v/v)				
	Greengage Plum:Sugar Syrup (1:0)	Greengage Plum:Sugar Syrup (1:0.25)	Greengage Plum:Sugar Syrup (1:0.5)	Greengage Plum:Sugar Syrup (1:0.75)	Greengage Plum:Sugar Syrup (1:1)
1	0	1	3	4	2
2	1	2	4	5	3
3	2	3	5	7	5
4	3	4	7	8	6
5	5	6	8	9	7
6	6	7	9	10	8
7*	6	7	9	10	8

FP = Fermentation Period

* The most suitable condition

The effect of the fermentation period on the characteristics of prepared greengage plum wine was studied, as shown in Table 3. The pH, acidity, soluble solids (°Brix), specific gravity, and alcohol content of the prepared wines were measured every two weeks. The pH values of the wines decreased slightly over time, ranging from 3.87 to 3.63. Acidity increased from 0.51 % to 0.69 %. The primary non-volatile acids—tartaric, citric, and malic acids—are crucial components in wine, as they influence both taste and color. As the soluble solids (°Brix) of the wine increased, the alcohol content also increased. The alcohol content remained relatively stable during the final weeks of fermentation. These results are presented in Table 4.

All greengage plum wine samples exhibited pH values of 3.0-4.0 and acidity values of 0.3-0.7 throughout the study. Soluble solids (˚Brix), specific gravity, and alcohol content were 10-20 (˚Brix), 1.01-1.09, and 5–10 % (v/v), respectively. All these results are shown in Table 5. The acidity of the prepared wines increased as fermentation progressed, due to the formation of organic acids by-products. The increase in acidity may be due to the increased alcohol production from the high initial sugar concentration (Attri, 2009). The fermentation period affects wine pH; as fermentation proceeds, pH decreases which is desirable because it inhibits their growth of microorganisms. Low pH and high acidity give good fermentation in natural environments. The decrease in soluble solids (°Brix) content of wine indicates the utilization of the sugar present in the must during fermentation. Alcohol was the most abundant volatile compound in wines and helped improve their sensory properties and acceptability. Ethanol was the most important alcohol in wine and an indicator of wine quality. Increasing fermentation time increases the alcohol concentration but decreases the wine's specific gravity. The decrease in the specific gravity of prepared wine during storage with varying amounts of yeast and sugar, may be due to the type of yeast used in wine production.

Table 5: Effect of Fermentation Period on the Properties of Prepared Greengage Plum Wine

Sr. No.	Properties	Fermentation Period (Week)						
		1	**2**	**3**	**4**	**5**	**6**	**7***
1.	pH	3.98	3.95	3.92	3.87	3.85	3.83	3.83
2.	Acidity, % (w/v)	0.35	0.39	0.46	0.49	0.52	0.54	0.54
3.	Specific Gravity	1.0653	1.0613	1.0534	1.0514	1.0438	1.0451	1.0451
4.	Alcohol Content, % (v/v)	4	6	7	8	9	10	10
5.	Soluble Solids, °Brix	25	23	22	20	19	18	18
6.	Reducing Sugar, %	0.25	0.28	0.29	0.31	0.32	0.33	0.33
7.	Colour (Absorbance)	0.04	0.05	0.09	0.17	0.11	0.15	0.15

* The most suitable condition

Table 6: Comparison between the Properties of Prepared Greengage Plum Wine and Commercial Wine

Sr. No.	Properties	Prepared Greengage PlumWine	Commercial Plum Wine
1.	pH	3.85	3.78
2.	Acidity, % (w/v)	0.52	0.49
3.	Specific Gravity	1.0731	0.994
4.	Alcohol Content, % (v/v)	10	10.0
5.	Soluble Solids, °Brix	18	6.5
6.	Reducing Sugar, %	0.33	0.67
7.	Colour (Absorbance)	0.15	0.19

The properties of the prepared greengage plum wine were compared with those of commercial plum wine, and the results are shown in Table 6. Although the pH, acidity, specific gravity, and alcohol content of the prepared wine were nearly similar, other properties were significantly different. Color is an essential physical factor that affects consumers' acceptability of a product. The colour of prepared wine and commercial wine had 0.15 and 0.19 colour (absorbance) in the visible region (wavelength 520 nm) and were clear and transparent, without sediments or cloudiness.

Sensory evaluation (organoleptic properties) of greengage plum wine included appearance, colour, taste, and aroma, and these results are shown in Table 7. In this table, panelists gave the highest preference to all sensory attributes of sample (3), followed by sample (4), sample (2), sample (1), and sample (5). Sample (3) was recorded as having the highest overall acceptance in the sensory evaluation (7.18) and the highest mean scores for appearance (7.15), colour (6.98), taste (7.26), and aroma (7.32). The sample with the least preference for all sensory attributes recorded the lowest overall acceptance in the sensory evaluation (5.15). The colour of the prepared wine changed from pale yellow to red during storage. As the wine appropriately aged, the harsh taste and yeasty odour diminished, and a smooth, mellow flavor and clean odour emerged.

Table 7: Sensory Evaluation of Prepared Greengage Plum Wine

Organoleptic Properties	**Panelist Hedonic Rating**				
	Sample (1)	**Sample (2)**	**Sample (3)***	**Sample (4)**	**Sample (5)**
Appearance	5.43	6.20	7.15	6.91	5.00
Colour	5.74	6.33	6.98	6.75	5.25
Taste	5.82	7.12	7.26	6.67	5.33
Aroma	5.87	6.67	7.32	7.11	5.00
Overall Acceptance	5.72	6.58	7.18	6.86	5.15

* The most suitable condition

Table 8: Effect of Ratio of Greengage Plum to Sugar on the Characteristics of Prepared Greengage Plum Syrup

Weight of Greengage Plum - 1200 g

Weight of Sugar - 400 g, 800 g, 1200 g, 1600 g, 2000 g

Storage Period - Three Months

Sr. No.	**Greengage Plum:Sugar**	**Characteristics of Prepared Greengage Plum Wine**				
		Soluble Solids (°Brix)	**Acidity % (w/v)**	**Reducing Sugar (%)**	**Non-Reducing Sugar (%)**	**Total Sugar (%)**
1.	1 : 033	52	1.49	1.65	68.31	69.96
2.	1 : 0.67	54	1.32	1.98	67.75	69.73

Sr. No.	Greengage Plum:Sugar	Characteristics of Prepared Greengage Plum Wine				
		Soluble Solids (°Brix)	Acidity % (w/v)	Reducing Sugar (%)	Non-Reducing Sugar (%)	Total Sugar (%)
3.	1 : 1*	56	1.36	2.48	67.69	70.17
4.	1 : 1.33	58	1.38	2.82	66.54	69.36
5.	1 : 1.67	60	1.42	2.95	66.47	69.42

* The most suitable condition

The ratio of plums to sugar was important for preparing good plum syrup. The basic ratio was 1:1, but it was increased 1:2 depending on the plums' size and juiciness of the plums. More sugar was added to achieve a good plum syrup, and less sugar resulted in mold or sourness rather than sweetness. The type of sugar also has an effect on the quality of the syrup. White sugar intensified the plum fragrance in the syrup. Brown sugar which contained a molasses-like substance in addition to sugar, diminished the flavor and fragrance of the greengage plums. Prepared greengage plum syrup with the ratio of plum to sugar (1:1), containing soluble solids 56 (°Brix), 1.36 (%w/w) acidity was found to be the best according to organoleptic evaluation, as shown in Table 8.

Table 9: Effect of Storage Period on the Characteristics of Prepared Greengage Plum Syrup

Weight of Greengage Plum - 1200 g

Weight of Sugar - 1200 g

Sr. No.	Storage Period (Months)	Characteristics of Prepared Greengage Plum Wine				
		Soluble Solids (°Brix)	Acidity % (w/v)	Reducing Sugar (%)	Non-Reducing Sugar (%)	Total Sugar (%)
1.	1	53	1.26	1.78	68.36	70.14
2.	2	55	1.29	1.96	67.39	69.35
3.	3*	56	1.36	2.48	67.69	70.17
4.	4	58	1.38	2.96	67.88	70.84
5.	5	59	1.4	3.2	67.98	71.18

* The most suitable condition

The soluble solids, acidity, reducing sugars, and total sugars increased, whereas non-reducing sugars decreased during storage in bottles. The syrup stored up to 3 months at ambient storage temperature in bottles is of acceptable quality. During storage, changes in soluble solids,

acidity, reducing sugar, non-reducing sugar, and total sugar were recorded monthly and are described in Table 9.

Comparative studies were conducted on the properties of prepared greengage plum syrup and commercial syrup, and the results are shown in Table 10. Properties of prepared syrup, like pH, reducing sugar, non-reducing sugar, and total sugar, were almost identical to those of commercial plum syrup. It was found that other properties of the prepared syrup and the commercial syrup were totally different.

Table 11 shows that sample 3 has the highest overall acceptance in the sensory evaluation (7.68) and the highest mean scores for appearance (7.45), colour (7.58), taste (8.00), and aroma (7.67). The least preference sample was recorded as having the lowest overall acceptance in the sensory evaluation (5.24). The overall acceptability of greengage plum syrup depended on its organoleptic properties.

Table 10: Comparison of the Properties of Prepared Greengage Plum Syrup and Commercial Syrup

Sr. No.	Properties	Prepared Greengage Plum Syrup	Commercial Plum Syrup (Royal Kalaw, Myanmar)
1.	pH	3.5	3.36
2.	Acidity (%w/v)	1.36	0.98
3.	Soluble solids (°Brix)	56	69
4 .	Reducing sugar (%)	2.48	2.36
5.	Non-reducing sugar (%)	67.69	65.48
6.	Total Sugar (%)	70.17	67.48
7.	Colour (Absorbance)	0.19	0.21

Table 11: Sensory Evaluation of Prepared Greengage Plum Syrup

Organoleptic Properties	Panelist Hedonic Rating				
	Sample (1)	Sample (2)	Sample (3)*	Sample (4)	Sample (5)
Appearance	6.54	6.53	7.45	6.24	5.49
Colour	6.42	5.64	7.58	6.35	5.36
Taste	6.55	6.92	8.00	7.00	5.00
Aroma	6.17	4.87	7.67	6.67	5.12
Overall Acceptance	6.42	5.99	7.68	6.57	5.24

* The most suitable condition

Conclusion

In this research, value-added fermented foods were prepared from locally available greengage plums. All prepared fruit syrups are free of pathogenic and aerobic bacteria, and only yeast contributes to the fermentation process. The use of unripe fruits for the preparation of fruit syrups, along with longer fermentation times, and whole-fruit sources, increases the functional properties and contributes to the unique flavor and taste of fruit syrups. Fruits, both in fresh and in processed forms, not only improve the quality of our diet but also provide essential ingredients like vitamins, minerals, carbohydrates, etc. The nutritive value of wine is increased due to the release of amino acids and other nutrients from yeast during fermentation.

Acknowledgements

I am grateful to Dr Tin Tun, Rector, University of Mandalay, and Dr Thu Nandar and Dr Ye Ye Cho, Pro-Rectors, University of Mandalay, for their permission to submit this article. I would like to express my deepest appreciation to Dr Khin Mar Hlaing, Professor and Head, Department of Industrial Chemistry, University of Mandalay, for her permission to submit this research paper, for reviewing the manuscript, and for her suggestions.

References

Attri, B. L. (2009) Effect of initial concentration on the physicochemical characteristics and sensory qualities of cashew apple wine. Indian Journal of Natural Products and Resources, 8: 374- 379.

Bisson L F, Butzke C E and Ebeler S E, (1995), The role of moderate ethanol consumption in health and human nutrition, Amer J Enol Vitic, 48(4), 449-460.

Clarke, R. J. and Bakker, J. (2004) Volatile components. In: Wine flavour chemistry. Blackwell Publishing Limited, Oxford, UK, pp. 120- 188.

Kamboj, S., Gupta, N., Bandral, J., Gandotra, G., & Anjum, N. (2020). Food safety and hygiene: A review. International Journal of Chemical Studies, *8*, 358– 368.

https://doi.org/10.22271/chemi.2020.v8.i2f.8794

Rastogi, D. A., & Shukla, S. (2013). Amaranth: A New Millennium Crop of Nutraceutical Values. Critical Reviews in Food Science and Nutrition, *53*,109–125.

https://doi.org/10.1080/10408398.2010.517876

Vyas K K and Joshi V K, (1982), Plum wine making: Standardization of a methodology, Indian Food Packer, 36, 80-86.

OPTIMIZATION OF TANNIN EXTRACTION FROM TAMARIND SEED TESTA AND ITS APPLICATION

Sandar Win[1], Shwe Zin Mon[2]

Abstract

Tamarind (*Tamarindus indica* L.) is abundantly found in Myanmar and is also a commercially used plant. In natural dyeing tannins play an important role as a mordant and have an affinity to cellulose as well as to protein fiber. This study is aimed to the extraction of natural tannin from tamarind seed testa and application of cotton and silk fabric as natural mordant. The color compounds present in tamarind seed testa were identified by phytochemical tests. The mineral content of tamarind seed testa was analyzed by Energy Dispersive X-ray Fluorescence (EDXRF) spectroscopy. Tannin was extracted from tamarind seed testa using ethanol-water mixture by simple distillation method. The effects of extraction temperature, time and ethanol-water ratio on the yield percent of tannin powder were investigated. In the extraction with 95 % ethanol-water mixture, ethanol-water ratio (35:15), extraction time 60 min and temperature 50 °C were suitable conditions for the preparation of extracted tannin. The functional groups present in extracted tannin was determined by using FTIR spectrometer. The extracted tannin powder was applied as a natural mordant alone and the tannin treated fabric was further mordanted with copper sulphate for dyeing of cotton and silk fabrics. The washing and rubbing fastness of dyed fabrics were tested by grey scale.

Keywords: tamarind seed, simple distillation, tannin, mordant, fastness

Introduction

Tannins are polyphenolic compound that bind and precipitate proteins, amino acids and alkaloids. Tannins are present in almost every part of plants, such as leaves, barks, wood, roots, fruits, and seeds. They are widely used in the production of cationic dyes, ink, clarifying agents in wine, textile dyes, fruit juice antioxidants, and coagulants in the production of rubber (Khanbabaee and Van Ree, 2001). They are able to combine with various substances and precipitate in aqueous solution (Lokeswari and Sujatha, 2011). In natural dyeing they take part an important role as a mordant. They are easy to extract with warm water and have an affinity to cellulose as well as to protein fiber. Tannins can also form complexes with metal ions such as copper, lead, zinc, cadmium, and manganese, which are insoluble compounds. Formation of the tannin complexes with metal compound is important in the mordanting of cellulose fiber. Tannic acid is also a specific commercial form of tannin.

Tamarind tree (*Tamarindus indica* L.) trees are abundant in Africa and Southeast Asia. These trees contain several brown pods with dark brown seeds bounded by a gummy pulp that dries naturally to a sticky paste. Tamarind fruits have outer-shell, pulp and the seeds. The seeds have about 25 % testa and 75 % kernel. Testa is of brown colour and kernel is of light cream. The seeds are used in the textile industry as a sizing substance as well as a source of polysaccharide, glue oil, and tannin for different industrial applications. They are primarily used in the preservation of leather glues, stains and mordants (Swarna et al., 2009). Meanwhile, some of the natural fibres such as cotton have very low affinity for most of the natural dyes. The tannins serve as an important role in cotton dyeing to retain colouring matter permanently. The ultimate aim, the purpose of preparing the natural fibers with tannin is not so much to fix the colouring matter, as to fix certain metallic salts such as copper, iron, potassium etc., in the form of insoluble tannates. The metal tannates present on the material forms insoluble lakes with the natural dyes during the dyeing process and results in improved fastness properties (Gulrajani, 1992).

[1] Department of Industrial Chemistry, Dagon University
[2] Department of Industrial Chemistry, University of Yangon

In textiles dyeing industry, most of the dyes employed are the synthetic azo dyes of which the azo bond cleavage brings about aromatic amines. These synthetic azo dyes may be harmful to human health and environment although they can greatly reduce the cost and enhance certain application and wear characteristics. For these reason, natural dyes are among the promising options for the waste. After the dyeing process, they are easily absorbed by the soil (Seiko Akiyama, 1996). The main objective of the mordant when used with adjective dye is to open up the pores so that the dye can penetrate the fibres, thereby supporting in the fixation of the dyestuffs on the substrate. However, mordants can also be used with dyes which may be applied directly to the fiber. In this case the function of the mordant is to form an insoluble compound with the dyestuff within the fiber itself, thereby improving the fastness properties of the dyed material (Patel, 2011).

The objective of this work was to extract tannin from tamarind seed testa. The specific objectives of this study were to study the suitable extraction conditions by using different extraction temperatures, time and ethanol-water ratios on yield percent of tannin powder, to study the absorbance value of extracted tannin solution by UV spectrophotometer and to evaluate the fastness properties of dyed cotton and silk fabrics.

Materials and Methods

Materials

Tamarind seeds were collected from Nyaung Oo Township, Mandalay Region. The required chemicals for processing were purchased from Able Teaching Aids, at the corner of 35th street and 85th street, Maha Aung Mye Township, Mandalay Region. Cotton and silk fabrics were purchased from the Saunders Weaving and Vocational Institute (SWVI), Amarapura Township, Mandalay Region.

Methods

Preparation of Tamarind Seed Testa Powder

The tamarind seeds were rinsed with water to remove impurities. The seeds were dried in hot air oven at 120 °C for 45 min and the testa were removed by crushing and then grinding into powder form. The tamarind seed testa powder was sieved through a 40-mesh screen and stored in an airtight container at room temperature for further use.

Phytochemical Screening of Tamarind Seed Testa

Before the extraction of natural dyestuff, phytochemical investigation was carried out to study the organic compounds which are present or absent in the tamarind seed testa. The experiments were conducted according to the procedures mentioned in “A Guide to Modern Techniques of Plant Analysis” (Harbone, 1984).

Determination of Mineral Contents of Tamarind Seed Testa

The quantitative analysis of tamarind seed testa was carried out by using Shimadzu EDX-700 spectrometer, Japan. The resultant EDXRF spectrum is illustrated in Figure 1 and the relative abundance of the elements found in tamarind seed testa are described in Table 2. EDXRF analysis was carried out at Laboratory of Chemistry Department, University of Mandalay.

Extraction of Tamarind Seed Testa Tannin using Ethanol-Water Mixture

Tamarind seed testa powder 5 g, 35 mL of ethanol and 15 mL of water were added to a 500 mL 3-neck round bottom flask. The round bottomed flask was fitted with condenser and the extraction was carried out at 50 °C for 60 min. Afterwards, the extract solution 50 mL was cooled and filtered through a filter paper and collected. The residue was extracted again with 50 mL of the same ratio of ethanol -water mixture at the same temperature and time. The filtrate 100 mL was cooled, filtered again and ethanol was removed by distillation. The total extract was cooled and tannin was separated with petroleum ether by using a separating funnel. The maximum absorbance value (optical density) of a tannin extract was measured by UV-Vis spectrophotometer (Model-PD-303S, APEL) at a wavelength of 725 nm (Elgailani and Ishak, 2014). Then the extracted tannin solution was concentrated and dried at 60˚C for 6 h in an oven.

The experiments using the same procedures as mentioned above were conducted by using different extraction temperatures (40 °C, 60 °C, 70 °C), extraction time (30 min, 90 min, 120 min) and ethanol-water ratios (15:35, 25:25, 45:5).

Identification of Extracted Tamarind Seed Testa Tannin by FT-IR Spectrophotometer

The chemical characteristic profiles and identification of functional groups of the tamarind seed testa tannin was determined by SHIMADZU FT-IR spectrophotometer.

Qualitative Analysis of Tamarind Seed Testa Tannin

The qualitative analysis was carried out to find the class of tannin obtained from tamarind seed testa. The experiments were carried out by treating 0.5 % solution of the extracted tannin with various reagents such as 2 % gelatin, 5 % aqueous ferric chloride, 10 % lead acetate, copper sulphate solution, dilute hydrochloric acid solution and dilute sulfuric acid solution. The change in color of the tannin solution was observed after the addition of the reagents.

Dyeing Process of Fabrics using Coconut Husk

Preparation of Coconut Husk Dye Liquid

For the preparation of coconut husk extract, 30 g of coconut husk powder (mesh no. 20) and 1200 mL of water were mixed in a stainless-steel pot and heated at 90 °C for about 45 min resulting in a final dye solution volume of 600 mL. After that, the dye solution was cooled, filtered and stored at room temperature for dyeing of cotton and silk fabrics.

Mercerization of Cotton Fabric

Mercerization was done according to the standard procedures (Seiko Akiyama, 1992). To prepare mercerized cotton fabrics, 1 yard of cotton (about 100 g) fabric was scoured using a solution of 5 g caustic soda in two litres of warm water. And then, the cotton fabrics was simmered in this solution for 1 h. After completion of this step, the fabric was put into vinegar solution (4 mL acetic acid to one litre of water) to neutralize it. Then, the fabric was rinsed with water and then dried at room temperature.

Mordanting of Cotton Fabrics by Pre-Mordanting Method

In this method, mordant solution was prepared by heating 1 g (0.5 % w/v) of tamarind seed testa tannin with 200 mL of water. This solution was heated to a temperature of 80 °C in a water bath and 7 g (25 cm × 25 cm) of cleaned fabric was simmered in solution for about 45 min. During mordanting, the fabric was frequently stirred with a glass rod to obtain good penetration of mordant into the cotton fabric. Then the mordanted cotton fabric was rinsed with water and allowed to air dry.

The other mordant solution was prepared by heating 0.1 g (0.05 % w/v) of copper sulphate with 200 mL of water and the tannin treated fabrics were simmered in this solution for about 45 min. The remaining procedures were carried out as mentioned above.

Dyeing of Mordanted Cotton Fabrics

After mordanting, 200 mL of prepared concentrated dye was heated at 80°C and mordanted fabric was simmered in this solution for 60 min. After that, the dyed fabric was rinsed with water and allowed to air dry. The colour developed on dyed cotton fabrics are shown in Figure 4.

Dyeing Process of Silk Fabrics

In this method, 3 g (25 cm × 25 cm) of cleaned silk fabric was simmered in 200 mL of warm water for about 1 h. After that, mordant solution was prepared by heating 1 g of the tamarind seed testa tannin with 200 mL of water. The remaining procedures were the same as mentioned in mordanting of cotton fabrics. The dyeing procedures were the same as mentioned above. The colour developed on dyed silk fabrics are shown in Figure 4.

Testing the Colour Fastness of Dyed Fabrics

After the dyeing process, testing the colour fastness of dyed fabrics such as washing fastness and rubbing fastness were determined.

Washing Fastness

Launder Meter washing machine, Model L-4 (containing 4-rack testing bottle) washing machine was used and Test No. 2 of ISO 105 was used to assess the colour fastness to washing. 2 g/L of soap solution was added to the jar (material to liquor ratio of 1:50) and the soap solution was preheated to 50˚C. Then the composite sample was placed in the jar and treated at 50 ˚C for 45 min. After washing, the fabrics were rinsed with water for 3 times and dried at room temperature.

Rubbing Fastness

The rubbing fastness of dyed fabric was determined by JIS STDL–0241 Rubbing Tester Machine. The test specimen (25 cm × 5 cm) and a piece of white bleached cotton fabric about (5 cm × 5 cm) were cut parallel to the warp direction for the rubbing fastness test. In dry rubbing fastness test, the test specimen was mounted on the white bleached cotton cloth and placed on the rubbing tester. The test specimen was rubbed with 500 g load at the speed of 30 circles per minute for about 100 times.

In this study, both dry and wet rubbing fastness tests were carried out. In wet rubbing fastness test, the rubbed fabric was wetted with water and the amount of water was two times of the fabric weight. The fabric was finally dried at room temperature. The color stained on bleached cotton fabrics were compared by grey scale for staining and the degree of fastness rating was determined.

Results and Discussion

Table 1 shows the results of phytochemical screening of tamarind seed testa. According to the results obtained from this test, it can be seen that the colour compounds such as phenolic, tannins, flavonoids, glycosides, saponins, alkaloids and polyphenols are present in the tamarind seed testa.

Table 1: Phytochemical Screening of Tamarind Seed Testa

Sr. No.	Tests	Extract	Reagents	Observation	Inference
1.	Phenolics	Distilled Water	1 % $FeCl_3$	Violet Color	+
2.	Tannins	Distilled Water	1 % $FeCl_3$	Deep Blue Precipitate	+
3.	Flavonoids	95 % Ethanol	Conc: HCl + Mg	Pink Color	+
4.	Glycosides	Distilled Water	10 % $FeCl_3$	Purple colour	+
5.	Saponins	Distilled Water	$NaHCO_3$	Frothing	+
6.	Alkaloids	1 % HCl	Dragendroff"s Reagent	Orange Precipitate	+
7.	Polyphenols	95 % Ethanol	1 % $FeCl_3$ + 1 % $K_3Fe(CN)_6$	Greenish Blue Color	+

Note: (+) = present, (-) = absent

According to the results of Table 2 and Figure 1, the elements found from tamarind seed testa powder were calcium, potassium, sulphur, aluminium, silicon, phosphorus and chlorine. Among them, calcium is the most abundant element and contains 0.544 %.

Table 2: Relative Abundance of Elements in Tamarind Seed Testa

Sr. No.	Symbols	Elements	Concentration (%)
1.	Ca	Calcium	0.544
2.	K	Potassium	0.0820
3.	S	Sulphur	0.0678
4.	Al	Aluminium	0.0666
5.	Si	Silicon	0.0471
6.	P	Phosphorus	0.0283
7.	Cl	Chlorine	0.0263

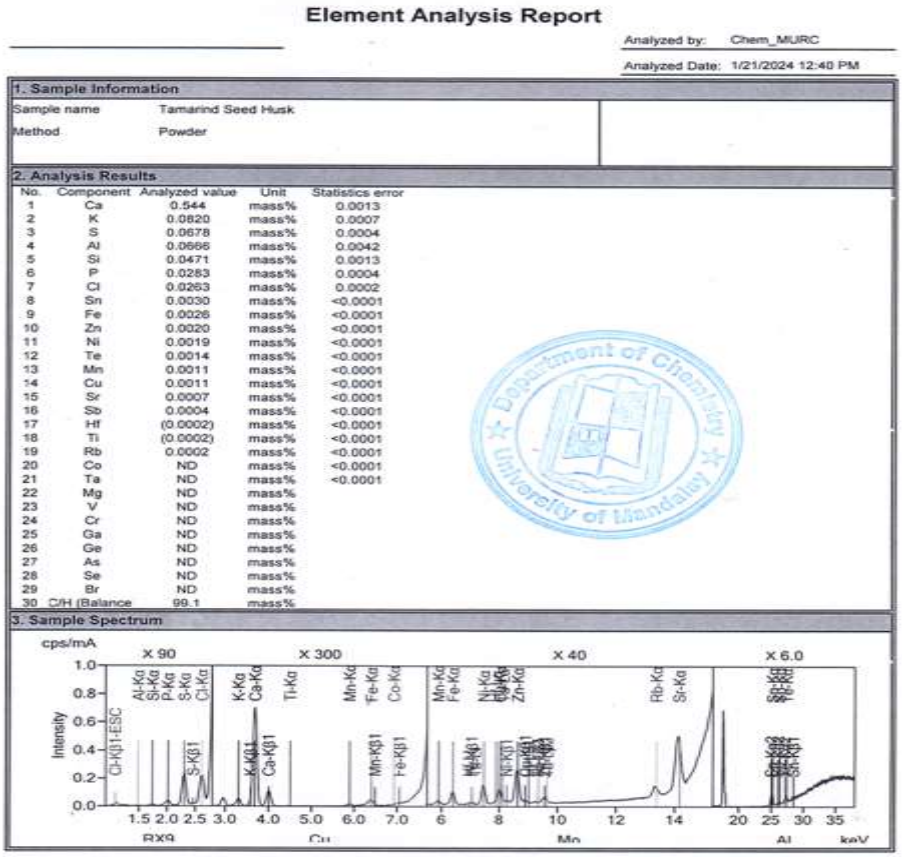

Element Analysis Report

Analyzed by: Chem_MURC
Analyzed Date: 1/21/2024 12:40 PM

1. Sample Information

Sample name	Tamarind Seed Husk
Method	Powder

2. Analysis Results

No.	Component	Analyzed value	Unit	Statistics error
1	Ca	0.544	mass%	0.0013
2	K	0.0820	mass%	0.0007
3	S	0.0678	mass%	0.0004
4	Al	0.0666	mass%	0.0042
5	Si	0.0471	mass%	0.0013
6	P	0.0283	mass%	0.0004
7	Cl	0.0263	mass%	0.0002
8	Sn	0.0030	mass%	<0.0001
9	Fe	0.0026	mass%	<0.0001
10	Zn	0.0020	mass%	<0.0001
11	Ni	0.0019	mass%	<0.0001
12	Te	0.0014	mass%	<0.0001
13	Mn	0.0011	mass%	<0.0001
14	Cu	0.0011	mass%	<0.0001
15	Sr	0.0007	mass%	<0.0001
16	Sb	0.0004	mass%	<0.0001
17	Hf	(0.0002)	mass%	<0.0001
18	Ti	(0.0002)	mass%	<0.0001
19	Rb	0.0002	mass%	<0.0001
20	Co	ND	mass%	<0.0001
21	Ta	ND	mass%	<0.0001
22	Mg	ND	mass%	
23	V	ND	mass%	
24	Cr	ND	mass%	
25	Ga	ND	mass%	
26	Ge	ND	mass%	
27	As	ND	mass%	
28	Se	ND	mass%	
29	Br	ND	mass%	
30	C/H (Balance	99.1	mass%	

3. Sample Spectrum

Figure 1: EDXRF Spectrum of Tamarind Seed Testa Powder

According to the Beer-Lambert law, absorbance value is directly proportional to the concentration of solution and the extraction of tannin solution at 50°C for 60 min was more suitable than the other conditions because of the maximum absorbance value and yield percent of 0.3344 and 33.6 % at 725 nm. The results are shown in Table 3. It can also be clearly seen that the increase in extraction temperature above 50 °C gave decrease in absorbance value and yield percent of tannin powder.

Table 3: Effect of Extraction Temperature on the Absorbance Value and Yield Percent of Tamarind Seed Testa Tannin

Weight of Tamarind Seed Testa Powder = 5 g

Ethanol: Water = 25 : 25

Wavelength = 725 nm

Sr. No.	Extraction Temp. (˚C)	Extraction Time (min)	Volume of Solvent (mL)	Absorbance Values	Extracted Powder (g)	Yield % (w/w)
1.	40	60	50	0.16	1.18	23.6
2.	50*	60	50	0.334	1.68	33.6
3.	60	60	50	0.169	1.67	33.4
4.	70	60	50	0.180	1.4	28

*The most suitable condition

According to the results of Table 4, maximum absorbance value and yield percent of tannin powder was observed with 60 min extraction time but after that the absorbance value was decreased from 0.334 to 0.176.

Table 4: Effect of Extraction Time on the Absorbance Value and Yield Percent of of Tamarind Seed Testa Tannin

Weight of Tamarind Seed Testa Powder = 5 g

Ethanol: Water = 25 : 25

Wavelength = 725 nm

Sr. No.	Extraction Time (min)	Extraction Temperature (˚C)	Volume of Solvent (mL)	Absorbance Values	Extracted Powder (g)	Yield % (w/w)
1.	30	50	50	0.168	0.94	18.8
2.	60*	50	50	0.334	1.67	33.4
3.	90	50	50	0.224	1.42	28.4
4.	120	50	50	0.176	1.39	27.8

*The most suitable condition

Table 5 tabulates the effect of ethanol- water ratio on maximum absorbance value and yield percent of tannin powder. According to the results, it was clearly seen that ethanol: water ratio of 35:15 was more suitable than other conditions because of the absorbance value and yield percent of 1.7 and 34 %.

Table 5: Effect of Ethanol -Water Ratio on the Absorbance Value and Yield Percent of Tamarind Seed Testa Tannin

Weight of Tamarind Seed Testa Powder = 5 g

Wavelength = 725 nm

Sr. No.	Solvent Ratio Ethanol: Water	Extraction Time (min)	Extraction Temp. (˚C)	Absorbance Values	Extracted Powder (g)	Yield % (w/w)
1.	15 : 35	60	50	0.212	1.43	28.6
2.	25: 25	60	50	0.334	1.67	33.4
3.	35: 15*	60	50	0.601	1.7	34
4.	45: 5	60	50	0.156	1.56	31.2

*The most suitable condition

Figure 2: Tamarind Seed Testa Tannin

Figure 3 shows the FT-IR spectrum of tamarind seed testa tannin powder extracted by 95 % ethanol-water mixture. Stretching band of alkenes group was found at 771.53 cm^{-1}. Alcohol and phenol group gave the absorption band at 1249.87 cm^{-1}, 1203.58 cm^{-1}, 1103.28 cm^{-1} and 1056.99 cm^{-1}. The absorption bands at 1280.73 cm^{-1} and 1365.60 cm^{-1} was attributed to CH symmetric bending vibration. CH asymmetric bending vibration was found at 1442.75cm^{-1}. The band at 1519.91 cm^{-1} and 1604.77 cm^{-1} were characteristics of stretching region of aromatic groups. The peak at 1604.77 cm^{-1} showed the characteristics of condensed tannin and these values were in agreement with the range of literature value reported by (Sirisangsawang and Phetyim, 2023). The stretching vibration of carbonyl group was found at 1732.08 cm^{-1}. In addition, absorption band at 3356.14 cm^{-1}, 3317.56 cm^{-1} and 3232.70 cm^{-1} indicated the presence of amines group.

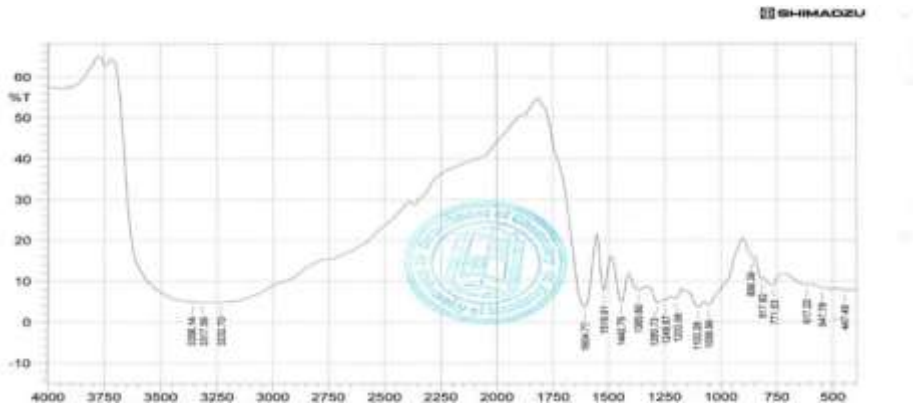

Figure 3: FTIR Spectrum of Tamarind Seed Testa Tannin

From the results of Table 6, the tamarind seed testa gave identical colour and precipitation reaction when compared with the phlobatannins or condensed tannins as mentioned in the literature (Russell, 1935). It produced a dark green precipitate with aqueous ferric chloride and dark red solids with dilute HCl solution. It clearly confirms that tamarind seed testa extract is of condensed tannins.

Table 6: Qualitative Analysis of Tamarind Seed Testa Tannin

Sr. No.	Reagents	Observations
1.	10 % Lead acetate	Pinkish precipitate
2.	2 % Gelatin	Dirty white precipitate
3.	5 % Aqueous Ferric chloride	Dark green precipitate
4.	10 % $CuSO_4$ solution	Faint green
5.	HCl (dil)	Dark red solids
6.	H_2SO_4 (dil)	Flesh-coloured precipitate

The characteristics of tamarind seed testa tannin are shown in Table 7. According to the results, the moisture content extracted by ethanol-water mixture are moisture content 7.6 %, total solids 92.4 % and pH 5.11.

Table 7: Characteristics of Tamarind Seed Testa Tannin

Sr. No.	Characteristics	Prepared Sample	Literature Value*
1.	Moisture Content, % (w/w)	7.6	8.40
2.	Total Solids Content, % (w/w)	92.4	91.60
3.	pH	5.11	4.57

* Nyaga et al., 2023

From the results of Table 8, cotton fabrics mordanting with 0.5 % tamarind seed testa tannin was found to be more suitable due to its good wet rubbing fastness grade of 4. According to the results of silk fabrics, it was demonstrated that mordanting with 0.5 % tamarind seed testa tannin gave very poor in change of shade mark than other conditions. It was also found that mordanting with tannin gave poor fastness in change of shade mark and dark brown colour on dyed fabrics mordanting with tamarind seed testa tannin and $CuSO_4$.

Table 8: Effect of Mordants on Color Fastness of Fabrics Dyeing by Pre-Mordanting Method

Coconut Husk Dye Powder = 10 g
Mercerized Fabric = 25 cm × 25 cm
Mordanting Temperature and Time = 80 °C, 45 min
Dyeing Temperature and Time = 80 °C, 60 min
Volume of Dye Solution = 200 mL

Sr. No.	Sample Code	Washing Fastness (60 ºC, 30 min)			Rubbing Fastness (500 g, 100 Times)	
		Change of Shade	Staining on Cotton		Dry	Wet
			Cotton	p/c		
1.	*C_1	2	4	4	4	4
2.	C_2	2	4	4	4	3
3.	S_1	1	4	4	4	4
4.	*S_2	2	4	4	4	4

*The most suitable condition

Notes: C_1 = Dyed Cotton fabrics Mordanting with 0.5 % Tamarind seed testa tannin
C_2 = Dyed Cotton fabrics Mordanting with 0.5 % Tamarind seed testa tannin and 0.05%$CuSO_4$
S_1 = Dyed Silk fabrics Mordanting with 0.5 % Tamarind seed testa tannin
S_2 = Dyed Silk fabrics Mordanting with 0.5 % Tamarind seed testa tannin and 0.05% $CuSO_4$
5 = excellent, 4 = good, 3 = fair, 2 = poor, 1 = very poor, p/c = polyester + cotton (Lye, Siegert, 1977)

Sr. No.	Sample Code	Original Sample	Washing Fastness (I.S.O Test No.2) (50 °C, 45 min)	Rubbing Fastness (500 g, 100 Times)	
				Dry mark	Wet mark
1.	C_1				
2.	C_2				
3.	S_1				
4.	S_2				

Figure 4: Colour Fastness of Fabrics Dyeing with Coconut Husk

Conclusion

In this research work, natural tannin was extracted from tamarind seed testa using ethanol due to its polar nature, which allows tannin to effectively dissolve, and it is also a safe and relatively inexpensive solvent. According to the results of phytochemical tests, it was found that the colour compounds such as phenolic compounds, tannins, flavonoids, glycosides, saponins, alkaloids and polyphenols were present in tamarind seed testa. From the results of EDXRF analysis, the relative abundance is found to be 0.544% Ca, 0.0820 % K, 0.0678 % S, 0.0666% Al, 0.0471 % Si, 0.0283 % P and 0.0263 % Cl. In addition, the most suitable conditions for extraction of tannin from tamarind seed testa were ethanol-water ratio (35:15), extraction temperature 50°C and extraction time 60 min according to the results of absorbance value 0.601 and yield percent of 34.

It was evident that prepared tamarind seed testa tannin is of condensed tannins according to the qualitative analysis and the results of FTIR analysis. The cotton fabrics dyeing by pre-mordanting method with 0.5 % tannin gave attractive colour and acceptable wet rubbing fastness

of 4 (Good). It was observed that the fastness results of silk fabric mordanting with 0.5 % tannin and 0.05% copper sulfate was found to be more suitable when compared with tannin alone.

Acknowledgements

I would like to express my greatest appreciation to the Myanmar Academy of Arts and Science for allowing me to submit this paper.

References

Gulrajani, M. L. (1992). Introduction to Natural dyes, India Institute of Technology, New Delhi.

Harbone, J. B. (1984). Phytochemical Methods,2nd Edition, Ruhard Clay Ltd., Great Britain.

Khanbabaee, K., and van Ree, T. (2001). Tannins: Classification and definition. *National Product Reports* 18(6), 641-649. DOI: 10.1039/B101061L.

Lokeswari, N., and Sujatha, P. (2011). Isolation of tannins from *Caesalpinia coriaria* and effect of physical parameters. *International Research Journal of Pharmacy* 2(2), 146-152.

Lyle, Dorothy Siegert. (1977). Performance of Textile, United States of America.

Nyaga M., Tanui P, Njenga S. (2023). Evaluation of Tamarindus indica L. Seed Tannins, Textiles &Leather Review,6 ,373-386.

Patel, B. H. (2011). Handbook of textile and industrial dyeing, vol 1, UK, Woodhead Publishing Limited, pp. 412.

Russell, A. (1935). The Natural Tannins. Chemical Review 17(2),155-186

Seiko Akiyama. (1996). The Dye Plants of AWA: The Colour of Tears, Dai-Ichi Co. Inc, Tolushima, Japan.

Sirisangsawang R., Phetyim N. (2023). Optimization of tannin extraction from coconut coir through response surface methodology, doi: 10.1016/ j. heliyon.2023e13377.

Swarna (2009). R. Venba, B. Madhan, N.K. Chandrababu, S. Sadulla Cleaner tanning practices for tannery pollution abatement: role of enzymes in eco-friendly vegetable tanning. *Journal of Cleaner Production*, 17 (2009), pp. 507-515

INSTRUCTIONS TO AUTHORS

Presentation: Manuscripts (MS) should be typed on one side of **quarto or A4 size paper**. Typing should be single spaced, with a one-inch margin all around. A CD of the paper should be submitted together with two print-outs. In general, the text should be organized according to the following outline:

(i) Title
(ii) Abstract
(iii) Materials & Methods/ Premises / Hypotheses
(iv) Results / Findings
(v) Discussion
(vi) Summary/ Conclusion
(vii) Acknowledgements
(viii) References

The body of the text should be printed in **font size 12**, and those of the Abstract, Acknowledgement and References should be printed in **font size 10.** The relative importance of the **headings** in the text should be indicated as follows:

First Order	-	CENTRE HEADING, All Capitals
Second Order	-	Centre Heading, Capitals & lower case
Side Heading	-	Capitals & lower case, not indented (bold – faced)
Run-in heading	-	Capitals & lower case, indented (bold-faced)

Title. The title should describe the contents of the article adequately and concisely and should be typed in **font size 14.**

Author's name. Capital & lower case. The designation of the first author and email (where the number of authors is more than two) and the name of the institution where the work was carried out should be given at the bottom of the title page; but academic degree of the author is not necessary.

Abstract. The main points of the paper, including its findings and conclusions, should be highlighted in the abstract; it should not contain more than 300 words. Add email address for making further contact with the author; evaluation of the paper should be typed in **font size 10**.

Keywords: Between 3-7 keywords highlighting the main points should be listed below the abstract.

References. References should be presented in alphabetical order, beginning with the surname first for the senior author and surname last for the other authors, followed by the year of publication. Examples of references are given below:

To a paper: Rabinowitz, A., Than Myint, email, Tun Khaing, and S. Rabinowitz, (1999)"Description of the Leaf Deer (*Muntiacus Putaoensis),* a New Species of Muntjac from Northern Myanmar" *Journal of Zoology,* London, vol.249, pp.427-435.

To a book: Corbet, G.B., & J.E. Hill, (1992) *The mammals of the Indomalayan Region.* Oxford, Oxford University Press.

To a thesis: May Soe Thu (1995) *Taxonomy of Offshore Fishes Caught by Bottom Trawl Operations in Myanmar Waters.* M.Sc. Thesis Zoology Department, Yangon University (Unpublished).

N.B. If the manuscript submitted is from a thesis, its format should be revised to conform to the instructions of the Myanmar Journal of Arts & Science presented here. **Pagination** should commence from the title page except when they are used to identify the affiliated instructions, and cite unpublished material. **Footnotes** should be avoided wherever possible. The MS, including illustrations and references, should not exceed **15 pages** for Arts and related subjects and **10 pages** for Science in length. Please kindly follow this limit in your final manuscript.

MYANMAR ACADEMY OF ARTS AND SCIENCE
EXECUTIVE COMMITTEE

President : Dr Thet Lwin

Vice-Presidents : Dr Maung Kyaw, Dr U Win

Secretary : Dr Win Tun

Joint Secretaries: Dr Tin Maung Tun, Dr Aye Aye Khaing, Dr Tin Tin Htwe

Executive Members

Dr Myo Thant Tyn
Dr Tin Nyo
Dr Khin Than Oo
Dr Hla Pe
Dr Maung Thin
Dr Daw Than Nwe
Daw Carole Ann Chit Tha
Daw Khin Lat

Publication Committee

Dr Thet Lwin	(Chairman)	Dr Maung Kyaw	(Vice-Chairman)
Dr Tin Nyo	(member)	Daw Carole Ann Chit Tha	(member)
Daw Khin Lat	(member)	Dr Hla Pe	(member)
Dr U Win	(member)	Dr Maung Thin	(member)
Dr Daw Than Nwe	(member)	Dr Khin Than Oo	(Joint Secretary)
Dr Myo Thant Tyn	(Secretary)		

Editorial Board

Dr Maung Kyaw	(Chairman)	Dr Daw Than Nwe	(member)
Dr Myo Thant Tyn	(member)	Dr Khin Than Oo	(member)
Dr Tin Nyo	(member)	Dr Hla Pe	(member)
Daw Khin Lat	(member)	Dr Aye Aye Khaing	(member)
Dr Maung Thin	(member)	Daw Carole Ann Chit Tha	(Joint Secretary)
Dr U Win	(Secretary)		

Coordinators for International Academies

Daw Carole Ann Chit Tha
Dr Myo Thant Tyn
Dr Tin Nyo
Dr Tin Tin Htwe
Dr Maung Kyaw
Dr Daw Than Nwe
Dr Tin Maung Tun